RESEARCH ONLINE

University of Wollongong
Research Online

University of Wollongong Thesis Collection

University of Wollongong Thesis Collections

2012

A novel anatomical lung phantom and its applications in lung perfusion scans for pulmonary embolism diagnosis

Norlaili Ahmad Kabir
University of Wollongong

Recommended Citation

Kabir, Norlaili Ahmad, A novel anatomical lung phantom and its applications in lung perfusion scans for pulmonary embolism diagnosis, Doctor of Philosophy thesis, Faculty of Engineering, University of Wollongong, 2012. http://ro.uow.edu.au/theses/3659

Research Online is the open access institutional repository for the University of Wollongong. For further information contact the UOW Library: research-pubs@uow.edu.au

RESEARCH ONLINE

UNIVERSITY OF WOLLONGONG

COPYRIGHT WARNING

You may print or download ONE copy of this document for the purpose of your own research or study. The University does not authorise you to copy, communicate or otherwise make available electronically to any other person any copyright material contained on this site. You are reminded of the following:

Copyright owners are entitled to take legal action against persons who infringe their copyright. A reproduction of material that is protected by copyright may be a copyright infringement. A court may impose penalties and award damages in relation to offences and infringements relating to copyright material. Higher penalties may apply, and higher damages may be awarded, for offences and infringements involving the conversion of material into digital or electronic form.

A NOVEL ANATOMICAL LUNG PHANTOM AND ITS APPLICATIONS IN LUNG PERFUSION SCANS FOR PULMONARY EMBOLISM DIAGNOSIS

A thesis submitted in fulfilment of the

requirements for the award of the degree

DOCTOR OF PHILOSOPHY

from

UNIVERSITY OF WOLLONGONG

by

NORLAILI AHMAD KABIR, BSc (Hons), MSc

CENTRE FOR MEDICAL RADIATION PHYSICS,

ENGINEERING PHYSICS, FACULTY OF ENGINEERING

(2012)

Thesis Certification

I, Norlaili Ahmad Kabir, declare that this thesis, submitted in partial fulfilment of the requirements for the award of Doctor of Philosophy, in the Centre for Medical Radiation Physics, University of Wollongong, is wholly my own work unless otherwise referenced or acknowledged. The document has not been submitted for qualifications at any other academic institutions.

Norlaili A. Kabir

31st March 2012

Contents

Thesis Certification 2

Contents 3

List of figures 7

List of tables 14

Abstract 15

Acknowledgement 17

List of abbreviations 19

1. Introduction 22

1.1 Summary 22

1.2 Aims 25

1.3 Original contributions 26

1.4 Publications 26

1.5 Presentations 27

2. Background 29

2.1 Nuclear medicine imaging phantoms in general 29

2.2 Available physical lung phantoms 31

2.3 Pulmonary embolism 33

2.4 Diagnostic algorithm for pulmonary embolism 35

2.5 Lung perfusion and ventilation scans 41

2.6 Comparison between planar imaging and SPECT imaging for pulmonary embolism diagnosis 43

2.7 Interaction of photons with matter 44

2.8 Nuclear medicine imaging 47

2.9 ImageJ software 51

3. Design and development of an anatomical lung phantom 52

3.1 Introduction 52

3.2 Concept 52

3.3 Limitations 53

3.4 Lung anatomy 53

3.5 The anatomical lung phantom components 56

3.6 Assembly of the lung phantom 64

3.7 Imaging protocols 66

4. Characteristics of the anatomical lung phantom 71

4.1 The lung phantom size 71

4.2 Hounsfield units 75

4.3 Count rate stability of the phantom 78

4.4 Radioactivity distribution 83

4.5 Anatomical properties 88

4.6 Reproducibility 95

5. Quality assurance study 103

5.1 Abstract 103

5.2 Introduction 105

5.3 Materials and methods 110

5.4 Results 117

5.5 Discussion 121

5.6 Conclusion 125

6. A lung perfusion imaging atlas 126

6.1 Abstract 126

6.2 Introduction 128

6.3 Materials and methods 129

6.4 Results 133

6.5 Discussion 152

6.6 Conclusion 155

7. Water bath attenuation effects on lung phantom planar acquisition 157

7.1 Introduction 157

7.2 Materials and methods 160

7.3 Results 161

7.4 Discussion 163

7.5 Conclusion 163

8. Conclusion 165

8.1 Review of the thesis 165

8.2 Future work 167

9. References 168

10. Appendixes 191

List of figures

Figure 2.1: Diagnosis algorithm for PE at the Department of Pulmonary Medicine and Internal Medicine, Institute of Medical Education and Research Sector, India, 2009 (40). 36

Figure 2.2: Algorithm suggested by the EANM (published in 2009) for diagnostic imaging of patients with suspected acute PE (41). V/Q = lung perfusion and ventilation scan. PA = contrast-enhanced pulmonary angiography. 37

Figure 2.3: The PE diagnosis algorithm suggested by Hogg et al. (published in 2006) (42). 39

Figure 2.4: Diagnostic algorithm for suspected PE recommended by Kuriakose et al. (published in 2010) (44). HP = High Probability. 40

Figure 2.5: This schematic diagram illustrates steps in a normal diagnostic imaging process. The first three steps are performed by the imaging modality. The last three steps are part of visual psychophysical process (quantitative in nature) and are performed by a radiologist (69). 47

Figure 2.6: The picture illustrates components of nuclear medicine imaging system (63, 70). 49

Figure 3.1. **a** The right lung (lateral view). **b** The right lung (medial view). **c** The left lung (lateral view). **d** The left lung (medial view). **e** Segmental bronchi. Each segmental bronchus was numbered corresponding to its matching bronchopulmonary segment (29). 55

Figure 3.2: The reference lung model (American 3B Scientific, Atlanta, USA). The model is made of 18 colour coded bronchopulmonary segments, with all segments attached elastically. 56

Figure 3.3: **a** The left lung cavity. **b** The left lung cavity and the left lung reference model. **c** The right lung cavity. **d** The right lung cavity and the right lung reference model. 58

Figure 3.4: **a** The left lung cavity filled with EPS beads, with a valve shown in green colour. **b** The lid for the left lung cavity. **c** The right lung cavity filled with EPS beads, with a valve is shown in green colour. **d** The lid for the right lung cavity. 58

Figure 3.5: **a** The anatomical bronchopulmonary segments of the reference lung model. **b** The perfusion defect inserts for the lung phantom. 60

Figure 3.6: **a** All the perfusion defect inserts for the right lung attached together. **b** The perfusion defect inserts for the right upper lobe: comprising apical, posterior and anterior segments. **c** The perfusion defect inserts for the right middle lobe: comprising medial and lateral segments attached together **d** The perfusion defect inserts for the right lower lobe: comprising superior, medial basal, anterior basal, lateral basal and posterior basal segments. 61

Figure 3.7: The perfusion defect inserts for the left lung. **a** Apical and posterior segments (commonly referred to as a single segment). **b** Anterior segment. **c** Lingular superior segment **d** Lingular inferior segment. **e** Superior segment. **f** Medial basal and anterior basal segments (usually considered as a single segment). **g** Lateral basal segment. **h** Posterior basal segment. 62

Figure 3.8: The steps taken to prepare the phantom for a perfusion scan. **a** The left lung lower lobe posterior basal defect insert was fitted into the left cavity at its anatomical position. The green cap on the picture is the filling and draining valve for the cavity **b** Magnified view of the image **a**. **c** The cavity is filled with EPS beads. **d** Silicone sealant is piped around the cavity. **e** The lid is attached to the cavity. Coloured water is then poured into the cavity **ei** The perfusion defect area is free of coloured water (dotted

circle). **f** Appropriate activity of ^{99m}Tc solution is added to the assembled phantom, leaving the phantom ready for a planar or SPECT scan. 65

Figure 3.9: The lung phantom while on a scan procedure at Department of Nuclear Medicine, Wollongong Hospital, NSW, Australia. 67

Figure 3.10: Planar perfusion images of a simulated lung perfusion event at six different views. The arrow shows the perfusion defect within the left lung lower lobe posterior basal segment. 68

Figure 3.11: SPECT perfusion tomographic slices of the right upper lobe defect. **a** Selected coronal slices from anterior to posterior show a clear defect in the right upper lobe. **b** Selected sagittal slices from right to left show sharp edges of the right upper lobe defect. **c** Selected transverse slices from head to feet show the defect in the right upper lobe. 70

Figure 4.1: The dimensions of the anatomical lung phantom. **a** The right lung. **b** The left lung. 72

Figure 4.2: **a** The A, B, and C points are the perimeter points measured on the left lung. Line 1 is the height of the left lung. Line 2, line 3, and line 4 are the transverse measurements of the left lung. **b** The D, E, and F points are the perimeter points measured of the right lung. The line 5 is the height of the right lung. Line 6, line 7, and line 8 are the transverse measurements of the right lung. 73

Figure 4.3: **a** The CT scan image (axial plane) of the lung phantom with a perfusion defect insert fitted in the left lung. **b** Schematic diagram of the lung phantom in a water-filled container. 76

Figure 4.4: Mean values and standard deviation bars of time taken to reach maximum counts for each planar view of lung scans in Population 1. 81

Figure 4.5: Mean values and standard deviation bars of time taken to reach maximum counts for each planar view of lung scans in Population 2. 81

Figure 4.6: Mean values and standard deviation bars of time taken to reach maximum counts for each planar view of lung scans in Population 3. 82

Figure 4.7: Selection maps drawn on the lung images (anterior view) using the selection tool of the ImageJ software 84

Figure 4.8: Distribution plots of pixels' intensities on a 0-255 greyscale of 18 Selection Maps. The plots were generated using the ImageJ software. 86

Figure 4.9: Lung perfusion images of three clinical conditions simulated using the lung phantom. Six planar views were acquired for each scan. Clinical condition 1 = lung perfusion without deficiency; Clinical condition 2 = lung perfusion with the left lung upper lobe apical-posterior deficiency; and Clinical condition 3 = lung perfusion with the right lower lobe lateral basal deficiency. 90

Figure 4.10: The chart shows the mode scores of the image quality of lung images in Figure 4.9. 93

Figure 4.11: Three lung perfusion scans of lung perfusion Condition 1. Each scan was acquired independently. 97

Figure 4.12: Three lung perfusion scans of lung perfusion Condition 2. Each scan was acquired independently. 98

Figure 4.13: Three lung perfusion scans of lung perfusion Condition 3. Each scan was acquired independently. 99

Figure 4.14: The chart shows mode scores of the reproducibility questionnaire survey's results. 101

Figure 5.1: Lung perfusion images of six embolic events modelled using the anatomical lung phantom. 113

Figure 5.2: Planar images show lung perfusion defects image sets of six embolic events. All lung perfusion defects were assumed mismatch defects.

The lung scans were acquired at six planar projections: anterior (A); posterior (P); left anterior oblique (LAO); left posterior oblique (LPO); right posterior oblique (RPO); and right anterior oblique (RAO). 116

Figure 5.3: The horizontal hierarchy shows the blind test's answer sheet. Nuclear Medicine physicians were required to report: **i** number of visible mismatch defects on each embolic event; **ii** size the mismatch defects based of the PIOPED criteria; and **iii** probability of PE based on the revised PIOPED criteria. PE = pulmonary embolism; and NMP = nuclear medicine physician. 117

Figure 5.4: Lung perfusion images of Embolic event 1, Embolic event 2, and Embolic event 3, were simulated twice: at moderate size; and at large size (for the benefit of the reader). The first column contains lung perfusion images with moderate size defects according to the revised PIOPED criteria (25-75% of a bronchopulmonary segment). The second column contains lung perfusion images with large size defects according to the revised PIOPED criteria (>75% of a bronchopulmonary segment). 119

Figure 5.5: Number of Nuclear Medicine physicians that have made correct and incorrect interpretation on: **i** number of present mismatch defects; **ii** size of mismatch defects; and **iii** probability of PE on based on the revised PIOPED criteria. The bar charts were created based on the nuclear physician answers to the blind test questions. 120

Figure 5.6: The bar chart illustrates number of the Nuclear Medicine physicians whom had correctly and incorrectly categorised (according to the revised PIOPED (59-60, 119) criteria) the V/Q mismatch defects shown in Figure 5.1..... 121

Figure 6.1: Planar and SPECT images of a perfusion defect within the apical segment of the right upper lobe. 133

Figure 6.2: Planar and SPECT images of a perfusion defect within the posterior segment of the right upper lobe. 134

Figure 6.3: Planar and SPECT images of a perfusion defect within the anterior segment of the right upper lobe. 135

Figure 6.4: Planar and SPECT images of perfusion defect within the lateral segment of the right middle lobe. 136

Figure 6.5: Planar and SPECT images of a perfusion defect within the medial segment of the right middle lobe. 137

Figure 6.6: Planar and SPECT images of a perfusion defect within the superior segment of the right lower lobe. 138

Figure 6.7: Planar and SPECT images of a perfusion defect within the medial basal segment of the right lower lobe. 139

Figure 6.8: Planar and SPECT images of a perfusion defect within the anterior basal segment of the right lower lobe 140

Figure 6.9: Planar and SPECT images of a perfusion defect within the lateral basal segment of the right lower lobe. 141

Figure 6.10: Planar and SPECT images of a perfusion defect within the posterior basal segment of the right lower lobe. 142

Figure 6.11: Planar and SPECT images of a perfusion defect within the apical and posterior segment of the left upper lobe. 143

Figure 6.12: Planar and SPECT images of a perfusion defect within the anterior segment of the left upper lobe. 144

Figure 6.13: Planar and SPECT images of a perfusion defect within the lingular superior segment of the left upper lobe. 145

Figure 6.14: Planar and SPECT images of a perfusion defect within the lingular inferior segment of the left upper lobe. 146

Figure 6.15: Planar and SPECT images of a perfusion defect within the superior segment of the left lower lobe..... 147

Figure 6.16: Planar and SPECT images of a perfusion defect within the medial and anterior basal segment of the left lower lobe..... 148

Figure 6.17: Planar and SPECT images of a perfusion defect within the lateral basal segment of the left lower lobe..... 149

Figure 6.18: Planar and SPECT images of a perfusion defect involving the posterior basal segment of the left lower lobe..... 150

Figure 6.19: The chart shows mode scores of the survey..... 151

Figure 7.1: **a** Experimental set-up: the anthropomorphic lung phantom submerged in water (red) on the gamma camera bed. **b** Dimensions of the water bath..... 160

Figure 7.2: **a** The planar posterior view of the anatomical lung phantom scanned without the water bath. **b** The planar posterior view of the anatomical lung phantom scanned with the water bath..... 161

Figure 7.3: **a** ROI1 is the edge of planar perfusion image of the lung phantom without water-filled container. ROI2 is the edge of planar perfusion image of the lung phantom with water-filled container. **b** Frequency distribution of pixel value intensities (0-255) in ROI1. **c** Frequency distribution of pixel value intensities (0-255) in ROI2..... 162

List of tables

Table 4.1: Measurements of the lung phantom at several points (see Figure 4.2). Line 1 and line 5 are height measurements of the left lung and the right lung respectively. Line 2, line 3, and line 4 are transverse measurements of the left lung. Line 6, line 7, and line 8 are transverse measurements of the right lung..... 74

Table 4.2: HU numbers of the anatomical lung phantom. Material numbers are listed as illustrated in Figure 4.3 76

Table 4.3: Radioactivity of ^{99m}Tc solution in each lung cavity..... 80

Table 4.4: The table lists number of pixels, mean intensity of the pixels and its standard deviation, and skewness of the selection maps. 87

Table 4.5: The Likert-scale score values of the quality of planar perfusion images generated using the anatomical lung phantom..... 92

Table 4.6: List of questions incorporated in the questionnaire survey 92

Table 4.7: The Likert-scale score values of reproducibility quality of planar perfusion images generated using the anatomical lung phantom 100

Table 5.1: The revised PIOPED criteria(59-60). 108

Table 5.2: This table lists Nuclear Medicine physicians' answers to the blind test study. The physicians were asked to categorise the mismatch defects size in Figure 5.1 according to the revised PIOPED (59-60, 119) criteria..... 118

Table 6.1: Nuclear Medicine physicians were required to score each question using the four-points Likert-scale as shown in the table 131

A NOVEL ANATOMICAL LUNG PHANTOM AND ITS APPLICATIONS IN LUNG PERFUSION SCANS FOR PULMONARY EMBOLISM DIAGNOSIS

Norlaili A. Kabir

A Thesis for Doctor of Philosophy

Centre for Medical Radiation Physics, Engineering Physics

University of Wollongong

Abstract

Numerous commercial and non-commercial nuclear medicine imaging phantoms are used for quality assurance studies, teaching, training, and research. Commercially available phantoms are sometimes not applicable in specific medical studies. As non-commercial phantoms are not easily accessible, many researchers have chosen to construct their own distinct phantom. This thesis describes the design, development and characteristics of a novel anatomical lung phantom. The phantom was uniquely developed to model perfusion conditions of patients with suspected pulmonary emboli. Two imaging modalities were chosen in this study: planar imaging and Single Photon Emission Computed Tomography (SPECT) imaging.

Applications of the phantom as a quality assurance (QA) device and as a training and teaching tool were studied. The phantom was used as a QA tool to compare the interpretations of Nuclear Medicine physicians on lung perfusion and ventilations scans using the revised Prospective Investigation of Pulmonary Embolism Diagnosis (PIOPED) criteria. The studies showed both the correct and incorrect diagnosis of pulmonary embolism by the physicians. A comprehensive lung perfusion imaging atlas is also included in the thesis. A close ended Likert-scale survey was carried out to study the significance of the imaging atlas to Nuclear Medicine physicians. Nuclear Medicine physicians acknowledged the ability of the atlas to help in training new Nuclear Medicine physicians. The atlas was classified as an adequate teaching material for the physicians who are developing experience to diagnose lung perfusion and ventilation scans. In summary, the thesis demonstrates an original contribution to the nuclear medicine imaging field through the development of the novel anatomical lung phantom.

Keywords: Planar, SPECT, Lung perfusion, Phantom, Pulmonary Embolism

Acknowledgement

It is a great pleasure to thank the many people and institutions that have made this thesis possible.

I would like to express my deep and sincere gratitude to my primary PhD adviser and my clinical supervisor, Dr. Steven Harvey, Physicist and Manager of the Department of Nuclear Medicine, Wollongong Hospital. The journey in obtaining my PhD would not have been possible without his supervision, assistance, encouragement and motivation. I appreciate his knowledge and skill in nuclear medicine imaging, and his assistance in my clinical studies.

I am extremely grateful to my second thesis adviser, Professor Anatoly Rosenfeld, Director of Centre for Medical Radiation Physics, University of Wollongong. I am thankful for his support and guidance in my research. He was always an attentive supervisor and was always approachable. Professor Rosenfeld also provided me with facilities and resources during my research at the University of Wollongong.

I must acknowledge Ministry of Higher Education, Malaysia, for the scholarship which enabled me to undertake a PhD course at the University of Wollongong, Australia. I am also thankful to the Universiti Sains

Malaysia, Malaysia, that had granted me three and half years paid study leave.

I would like to thank Nuclear Medicine physicians Professor Judith Freund, Dr. Ian Swanson, Dr. Lily Shen, and Dr. Lyn Chan, who participated in the survey studies. The quality of their responses has enriched the content of the thesis.

I am grateful to David Wilkinson, Belinda Fletcher, and the other technologists at the Department of Nuclear Medicine, Wollongong Hospital for their valuable time assisting me in my clinical works. I also thank A/Prof Barry Elison, Director of Nuclear Medicine at Wollongong Hospital, for supporting this research by permitting me to use the departmental resources and equipment.

I wish to thank my dear officemate, Dr. Jeannie Wong, for the friendship and for all the motivational talks. I am thankful to Veronica for her assistance in helping me get through the difficult times in my PhD journey. To John Canadi, thank you for your love and your support, and for all the terrific camping trips.

Lastly, and most importantly, I am sincerely thankful to my loving mother, Siti Maryam, for the moral support through out my PhD journey. To her, I dedicate this thesis.

List of abbreviations

^{99m}Tc	Technetium
A	Anterior
AIHW	Australian Institute of Health and Welfare
BCE	Before the Common Era
CT	Computed Tomography
CTPA	Computed Tomography Pulmonary Angiogram
DTPA	Pentetic Acid or Diethylene Triamine Pentaacetic Acid
DVT	Deep Vein Thrombosis
EANM	European Association of Nuclear Medicine
EPS	Expanded Polystyrene Beads
FBP	Filtered Back-Projection
HU	Hounsfield Unit
keV	kilo Electronvolt
kVp	kilovolt Peak
LAO	Left Anterior Oblique
LL	Left Lung
LPO	Left Posterior Oblique
LS	Lung Scan
M	Mean
MAA	Macro Aggregated Human Serum Albumin
MBq	Megabecquerel
MDCT	Multidetector Computed Tomography

MeV	Mega Electronvolt
ml	millilitre
MS	Mode Score
N	Neutron Number
NaI(Tl)	Sodium Iodide doped with Thallium
NIH	National Institute of Health
NMP	Nuclear Medicine physician
NSW	New South Wales
OSEM	Operating System/Environment Manager
P	Posterior
PAAP	IQ and SNM's Practitioner Acquisition Assessment Program
PACS	Picture Archiving Communication System
PE	Pulmonary Embolism
PET	Positron Emission Tomography
PIOPED	Prospective Investigation of Pulmonary Embolism Diagnosis
QA	Quality Assurance
RAO	Right Anterior Oblique
RL	Right Lung
ROI	Region of Interest
RPO	Right Posterior Oblique
SD	Standard Deviation
SNM	Society Nuclear Medicine

SPECT	Single Photon Emission Computed Tomography
SS	Sample Size
USA	United States of America
V/Q	Perfusion and Ventilation
^{133}Xe	Xenon
Z	Atomic Number
Z_{eff}	Effective Atomic Number

1. INTRODUCTION

1.1 Summary

This thesis seeks to offer the nuclear medicine imaging field a novel anatomical lung phantom and a variety of its possible applications. In particular, this thesis describes the development process to manufacture and test the anatomical lung phantom to exclusively model lung perfusion conditions of suspected pulmonary embolism (PE) patients. The thesis introduces applications of the anatomical lung phantom as a quality assurance device, and as a reference tool (lung perfusion imaging atlas) using planar and SPECT imaging. The lung phantom is considered an original and valuable knowledge contribution to the field. The thesis is divided into eight chapters:

Chapter 1

The chapter establishes aims and original contributions of the thesis to the nuclear imaging field.

Chapter 2

The chapter gives an overview of literature review of the relevant and important literature on the conducted research. The reviews are based on journal articles, books, thesis, and conference papers.

Chapter 3

The chapter explains in detail methods to develop the lung phantom. Elaborate instructions on how to use the phantom in clinical studies are included in the chapter. This chapter is an extended version of a journal article written by the author and two co-authors. The article was entitled 'Design and fabrication of pulmonary embolism phantom for planar and SPECT V/Q imaging quality assurance'.

Chapter 4

The chapter describes size, Hounsfield unit values, stability, radioactivity distribution properties, anatomical properties, and reproducibility characteristics of the anatomical lung phantom. In this chapter, two surveys in close ended format were used as research instruments.

Chapter 5

The chapter contains reports on a small scale QA study on Nuclear Medicine physicians' interpretations accuracy in diagnosing lung perfusion images using the PIOPED criteria. Two journal articles were written based on the findings of this chapter. The articles have been submitted to peer reviewed scientific journals (The Journal of Medical Imaging and Radiation Oncology, and Canadian Association of Radiologist Journal) for consideration for publication. The two articles are currently under peer review.

Chapter 6

The chapter shows the application of the anatomical lung phantom as a reference and as a teaching tool. A lung perfusion imaging atlas was constructed. A survey study was conducted to study the significance of the atlas to Nuclear Medicine physicians. The chapter was written in a form suitable for publication in scientific journals. The manuscript has been submitted and currently under review by Nuclear Medicine Communications Journal.

Chapter 7

The chapter explains the effect of uniform water bath as an alternative attenuation material to the lung phantom. The phantom was immersed in a water bath prior planar scans. The scanned images were compared to the images modelled using the lung phantom without water bath.

Chapter 8

The chapter summarises the current works and future works of the author.

1.2 Aims

The primary aim of the thesis is to describe methods to design and develop a novel anatomical lung phantom to simulate lung perfusion conditions of suspected pulmonary embolism patients via planar and SPECT imaging. The specific aims of the thesis are:

1. to summarise the main findings and reviews of subjects related to the research,
2. to describe, in detail, the materials and the methods needed to develop the anatomical lung phantom,
3. to give an explanation on instructions for using the lung phantom to model lung perfusion conditions of suspected pulmonary embolism patients with planar and SPECT imaging,
4. to compare the size of the lung phantom to the size of the human lung,
5. to characterise the Hounsfield units of the phantom materials,
6. to describe the radiation distribution properties, anatomical properties and reproducibility properties of the lung phantom,
7. to report a small scale QA study using the lung phantom as the main tool,
8. to construct a novel lung perfusion planar and SPECT lung perfusion imaging atlas,

9. to study the water bath attenuation effects on the lung phantom planar acquisitions.

1.3 Original contributions

The original knowledge contributions of this thesis are:

1. A novel anatomical lung phantom exclusively designed to model the lung perfusion conditions of suspected pulmonary embolism patients.

2. A reference resource and a teaching tool consisting of a lung perfusion imaging atlas. The atlas is an informative teaching resource and reference tool for inexperienced Nuclear Medicine physicians that are developing experience in diagnosing lung perfusion and ventilation scans.

3. Original methods to perform a QA study of the interpretation accuracy in diagnosing lung perfusion images modelled using the anatomical lung phantom.

1.4 Publications

Peer reviewed journal

Kabir, N. A., Harvey, S. B. & Rosenfeld, A. 2010. Design and fabrication of pulmonary embolism phantom for planar and SPECT V/Q imaging quality

assurance. *Australasian Physical & Engineering Sciences in Medicine,* 33**,** 271-277.

Peer reviewed scientific meetings (abstract only)

Kabir, N. A., Harvey, S. B. & Rosenfeld, A. 2009. A methodology for manufacturing a QC phantom for ventilation and perfusion (V/Q) lung scans. *Internal Medicine Journal,* 39**,** A105-A135.

Kabir, N. A., Harvey, S. B. & Rosenfeld, A.2010. An anatomical lung phantom for quality assurance in V/Q imaging. *Internal Medicine Journal,* 40**,** s2**,** 1-36.

Kabir, N. A., Harvey, S. B. & Rosenfeld, A. 2011. Pulmonary Embolism Diagnosis – An Atlas of planar and SPECT perfusion images. *Internal Medicine Journal,* 41**,** 20-45.

1.5 Presentations

Kabir, N. A., Harvey, S. B. & Rosenfeld, A. 2009. A methodology for manufacturing a QC phantom for ventilation and perfusion (V/Q) lung scans. *Australian and New Zealand Society of Nuclear Medicine 39th Annual Scientific Meeting.* Sydney, Australia.

Kabir, N. A., Harvey, S. B. & Rosenfeld, A. 2009. Pulmonary Embolism Phantom: Segmental Embolus. *MedPhys09*, Sydney, Australia.

Kabir, N. A., Harvey, S. B. & Rosenfeld, A.2010. An anatomical lung phantom for quality assurance in V/Q imaging. *Australian and New Zealand Society of Nuclear Medicine 40th Annual Scientific Meeting*. Auckland, New Zealand.

Kabir, N. A., Harvey, S. B. & Rosenfeld, A. 2011. Pulmonary Embolism Diagnosis – An Atlas of planar and SPECT perfusion images. *Australian and New Zealand Society of Nuclear Medicine 41st Annual Scientific Meeting*. Darwin, Australia.

2. BACKGROUND

2.1 Nuclear medicine imaging phantoms in general

Phantoms are applicable for many uses in the field of nuclear medicine imaging. Phantoms offer a practical approach to test and evaluate imaging techniques, and to evaluate comparison in imaging systems (1). Phantoms have also been developed as an examination tool for medical physicist accreditation examinations (2). Device characterisation and method testing of SPECT imaging and Positron Emission Tomography (PET) imaging can be done using a phantom (3). More commonly, phantoms are used in medical imaging for quality assurance, calibration, research and teaching (4-6). A phantom can also be used to as a training tool for nuclear medicine practitioners (7). Phantoms are also used to verify simulated data, planning radionuclide treatments, and demonstrating the quality of imaging instruments (8).

Most physical phantoms used for PET and SPECT imaging are based on either of two designs: **i** fillable cylinders containing either radioactive or non-radioactive inserts; or **ii** complex geometry that is represented by multiple distinct slices or sheets (9). In contrast to physical phantoms, some researchers have developed digital phantoms (10-11). Monte Carlo simulation is one of computational algorithms used to simulate radionuclide distribution in virtual phantoms (12-13).

A high quality phantom should mimic as closely as possible the imaging routine of a patient (14). A phantom that mimics a region of the human anatomy is called an anthropomorphic phantom (15). Constructing such phantoms is always challenging. The phantoms must be built of tissue equivalent materials to represent true clinical conditions (16). To find tissue substitute materials is a great concern in designing anthropomorphic phantoms (17). The attenuation properties of the tissue substitute materials linearly depend on the effective atomic number of the substances (18). The anthropomorphic phantoms should consist of homogenous material in where test subjects are embedded (19).

There are many commercial anthropomorphic phantoms that are able to closely resemble the attenuating properties of human tissue. In these phantoms construction is always of utmost quality with a wide range of applications. Commercial phantoms are not applicable when a higher level of reproducibility; higher level of anatomical accuracy; or other qualities are required in clinical studies (20). To overcome these limitations, many researchers have designed unique phantoms to fully fulfil their study needs (20).

In this thesis, a reusable semi-anthropomorphic lung phantom comprising anatomically correct structures was constructed. The term ‘semi’ is used to indicate that the breathing dynamic of the human lung was not considered

while developing the phantom. Also, the semi-anthropomorphic lung phantom did not carry the same attenuation properties as the human lung. Throughout the thesis, the phantom is referred to as an anatomical lung phantom.

2.2 Available physical lung phantoms

A group of researchers (21) have developed an anatomically realistic lung phantom to compare nuclear imaging quality in Finland. Plastic plates were used to create the lung cavities. The cavities were filled with plastic pallets to resemble lung tissue. A wax and plastic pellet mixture were used to model lung perfusion defects in the cavities. The lung phantom needed to be filled with ^{99m}Tc solution and water prior any clinical studies. The lung tissue has -616 HU (Hounsfield Unit) value and the perfusion defect insert has -488 HU value. The lung phantom was not reusable. Five pairs of the lung phantom were constructed for the study (21).

A research group from Michigan extended the existing lung insert of a thoracic phantom (RS-330, Radiology Support Devices, Long Beach CA) to create a deformable phantom for dynamic modelling in radiation therapy. The extension was constructed using high density foam. The foam was infused with iodine to better mimic lung attenuation at diagnostic imaging kV. The reconstructed lung phantom has HU value -800 to -600. Tumor inserts were embedded into the lung phantom for clinical studies. The

phantom was classified as simple, efficient and viable by the researchers (22).

A Lung-Spine SPECT phantom is a commercially available phantom supplied by BIODEX (Shirley, New York). The left lung insert volume is approximately 0.9 litre; and 1.1 litre of the right lung. Styrofoam beads and water can be used to mimic lung tissue (with a density of approximately 0.3gm/cm^3). The phantom is able to evaluate non-uniform attenuation and scatter compensation methods.

A multipurpose novel anthropomorphic plastinated lung phantom has also been designed using a pig's lung. The lung was extracted from a pig's thorax; inflated; and fixed using formalin and silicone rubber. The lung was then left to dehydrate in cold acetone. Finally, the phantom was leave to soak in a curable silicone polymer (together with a curing agent). The phantom retains major anatomical and imaging characteristics of an in-vivo lung. The phantom was used in an imaging system comparison study, lung tomosynthesis study and many other studies (23).

The IQ and SNM's Practitioner Acquisition Assessment Program (PAAP) designed a 3-D lung perfusion phantom. This phantom can be used to detect the location, extent, and significance of simulated perfusion abnormalities. The phantom is suggested to be an appropriate tool to

assess the ability of nuclear medicine staff, and nuclear medicine equipment (24).

2.3 Pulmonary embolism

Venous thromboembolic disease was first discovered by an Ayurveda physician and surgeon, Susruta, (circa 600-1000 BCE). In his medical manuscript, he describes a patient who had a swollen and painful leg which was difficult to treat (25-26). A French pathologist, Jean Cruveilheir, in his book proposed the reasons for venous inflammation and thrombosis in all disease conditions. Rudolph Virchow further investigated Cruveilheir proposal and developed the relationship between venous thrombosis with obstruction of the pulmonary arteries (pulmonary embolism) (25).

A blood clot (thrombus) is formed of platelets and fibrin. A thrombosis occurs when too many (or too large) thrombi forms rapidly (27). Small thrombi regularly clear themselves from the circulation (28). Thromboses in the legs or pelvic veins (deep vein thrombosis); or in the lung vessels (pulmonary embolus) carry a high risk factor (27-28). A deep vein thrombosis is rarely fatal but can lead to long term morbidity (27).

A pulmonary embolus usually originates from a deep vein thrombosis (28). Larger or multiple thrombi (from deep vein thrombosis) may travel to the heart, then on to the pulmonary arteries (28-29). Pulmonary embolism

occurs when a thrombus partially or completely blocks a pulmonary artery (30). The affected region of the lung will be ventilated but not perfused. This may cause abnormalities of blood gases, pulmonary infraction and, when extensive, can be fatal (31-32).

PE is the third most commonly occurring acute cardiovascular disease after cardiac ischemic syndrome and stroke (33). PE will be fatal in up to 25% of patients that have been through diagnosis but are left untreated (34). It is a life threatening disease (35). The rate of PE is higher in women (60 cases/100 000 women) than in men (42 cases/100 000 men) (36-37).

Australian Institute of Health and Welfare (AIHW) estimated that there were approximately 14716 cases of venous thromboembolism in Australia in 2008 (38). The AIHW report stated that venous thromboembolism is a bigger killer than bowel or breast cancer (38). Of the cases, 8253 cases were estimated PE and 6462 cases were estimated DVT (deep vein thrombosis) (38). The figure shows that PE is one of major health concerns in Australia.

Until 1998, in the United States of America (USA) approximately 200 000 deaths were recorded from PE, with 11% of patients dying in the first hour and 38% within two hours (39). In 2006, 247 000 adults were hospitalised in the USA with acute pulmonary embolism (36). These figures displayed a general overview of PE in a country other than Australia.

The work undertaken in this thesis concerns the quality assurance of PE diagnosis via lung perfusion and ventilation (V/Q) scans. Also included in the thesis is a lung perfusion imaging atlas to help new Nuclear Medicine physicians diagnose PE via lung perfusion and ventilation scans. The results of this thesis are expected to make an original knowledge contribution to the pulmonary embolism research field.

2.4 Diagnostic algorithm for pulmonary embolism

PE diagnosis varies from one nuclear medicine department to another. The following are diagnosis algorithms for PE in several departments.

Figure 2.1 shows diagnostic algorithm at the Department of Pulmonary Medicine and Internal Medicine, Institute of Medical Education and Research Sector, India (40). In the algorithm, lung perfusion and ventilation is opted when Computed Tomography Pulmonary Angiogram (CTPA) reports a non-diagnostic PE or when CTPA is unavailable.

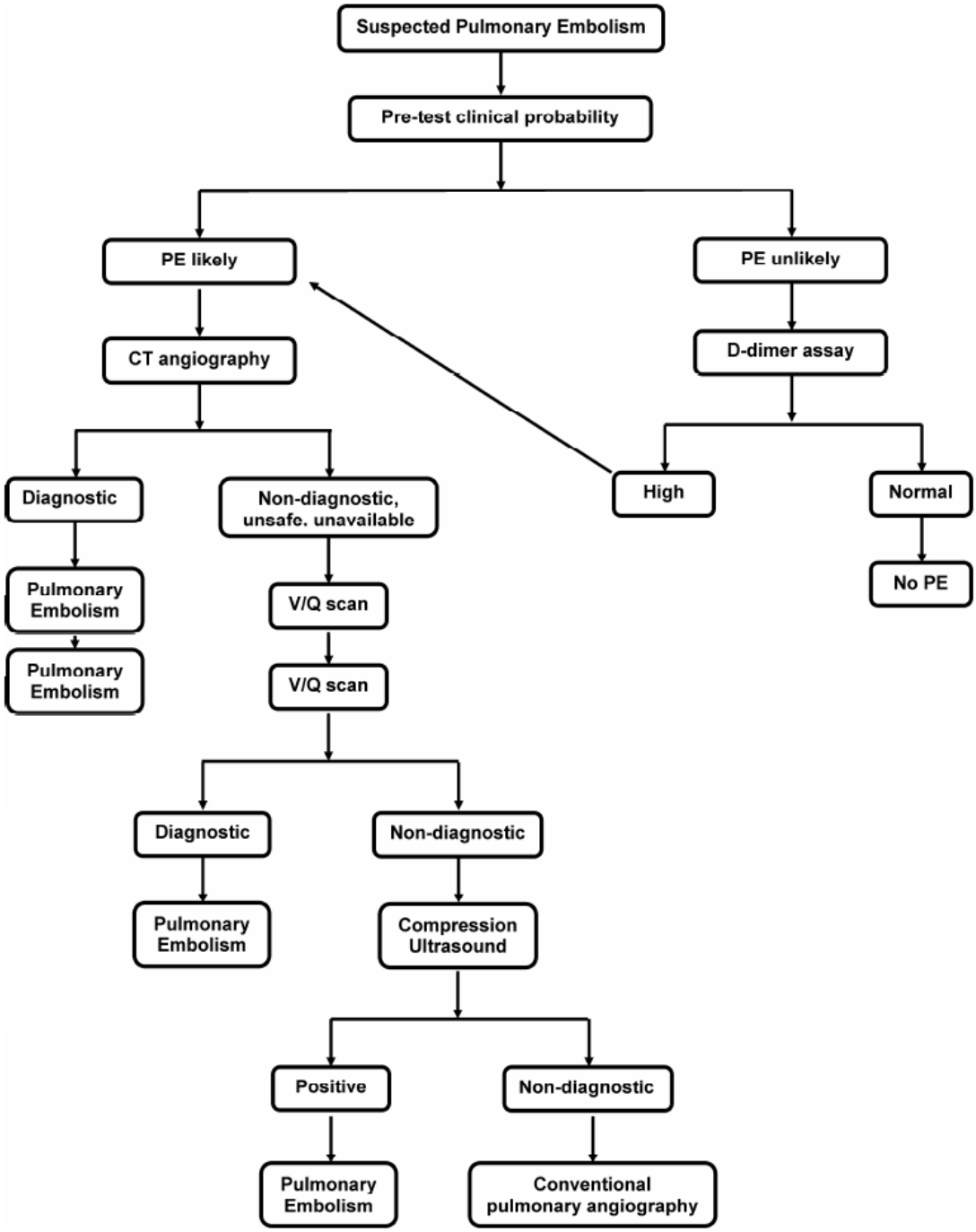

Figure 2.1: Diagnosis algorithm for PE at the Department of Pulmonary Medicine and Internal Medicine, Institute of Medical Education and Research Sector, India, 2009 (40).

The European Association of Nuclear Medicine (EANM) suggested conducting lung perfusion and ventilation scans using SPECT imaging as a first-line procedure to diagnose pulmonary embolism, compared to Multidetector Computed Tomography (MDCT). The lung perfusion and ventilation scan using SPECT imaging should be widely implemented where the modality is available, according to the EANM. The algorithm for diagnostic imaging of suspected PE patients as suggested by the EANM is shown in *Figure 2.2* (41).

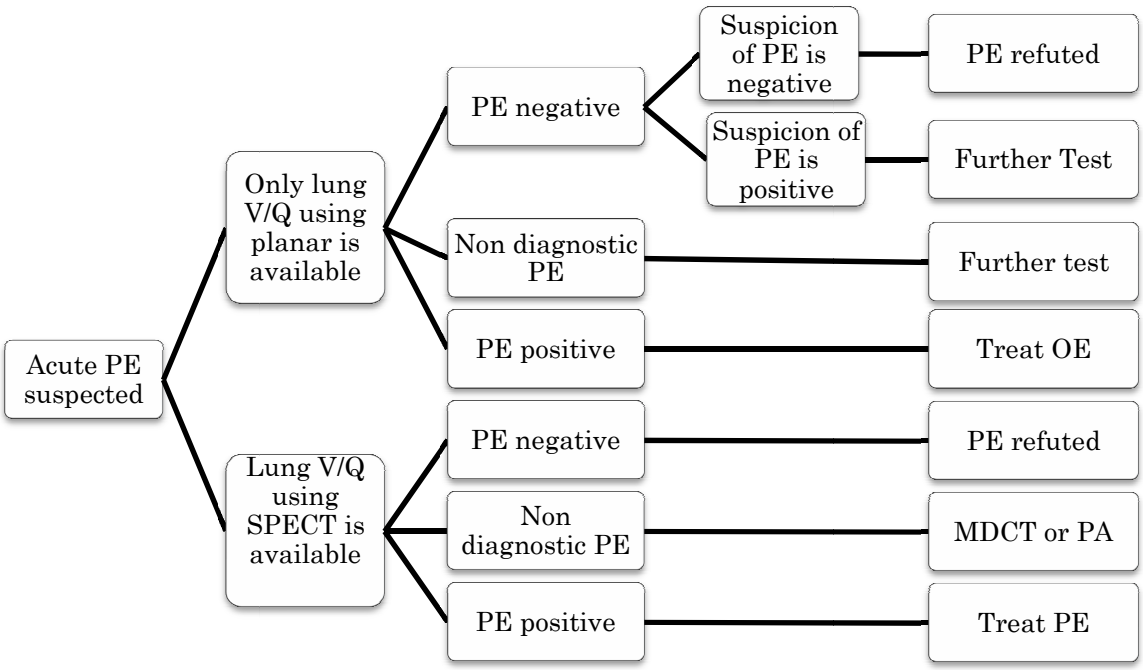

Figure 2.2: Algorithm suggested by the EANM (published in 2009) for diagnostic imaging of patients with suspected acute PE (41). V/Q = lung perfusion and ventilation scan. PA = contrast-enhanced pulmonary angiography.

Figure 2.3 shows the diagnostic algorithm for PE suggested by Hogg K. et al. (42). The lung perfusion and ventilation scan is a following procedure after moderate or high D-dimer blood test result. The lung perfusion and ventilation scan is to be interpreted using the Prospective Investigation of Pulmonary Embolism Diagnosis (PIOPED) criteria (43).

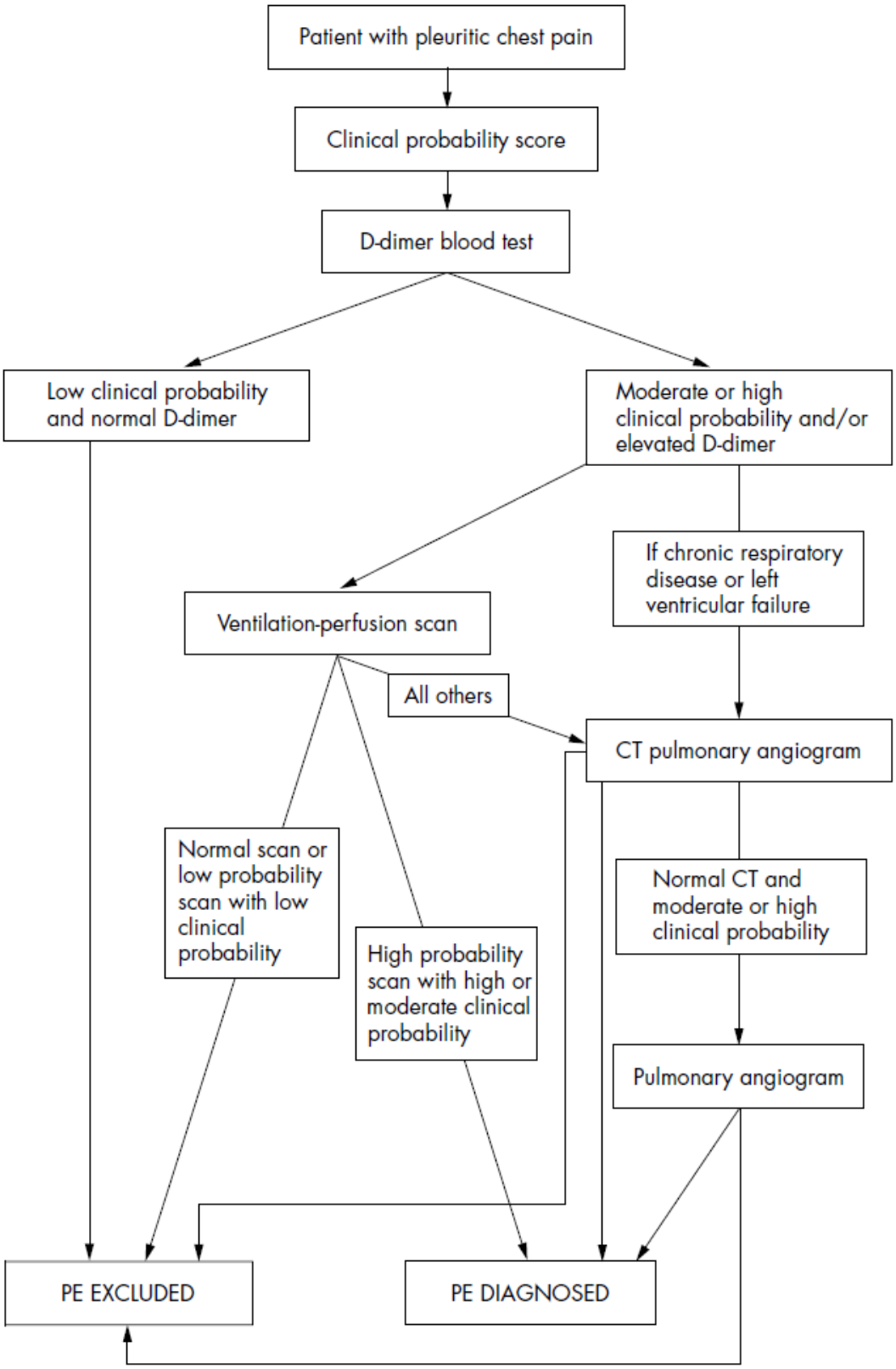

Figure 2.3: The PE diagnosis algorithm suggested by Hogg et al. (published in 2006) (42).

Kuriakose et al., suggested a diagnostic algorithm for suspected PE based on the clinical probability of disease in patients. Lung perfusion and ventilation scan is recommended for patients with a normal chest X-ray (44).

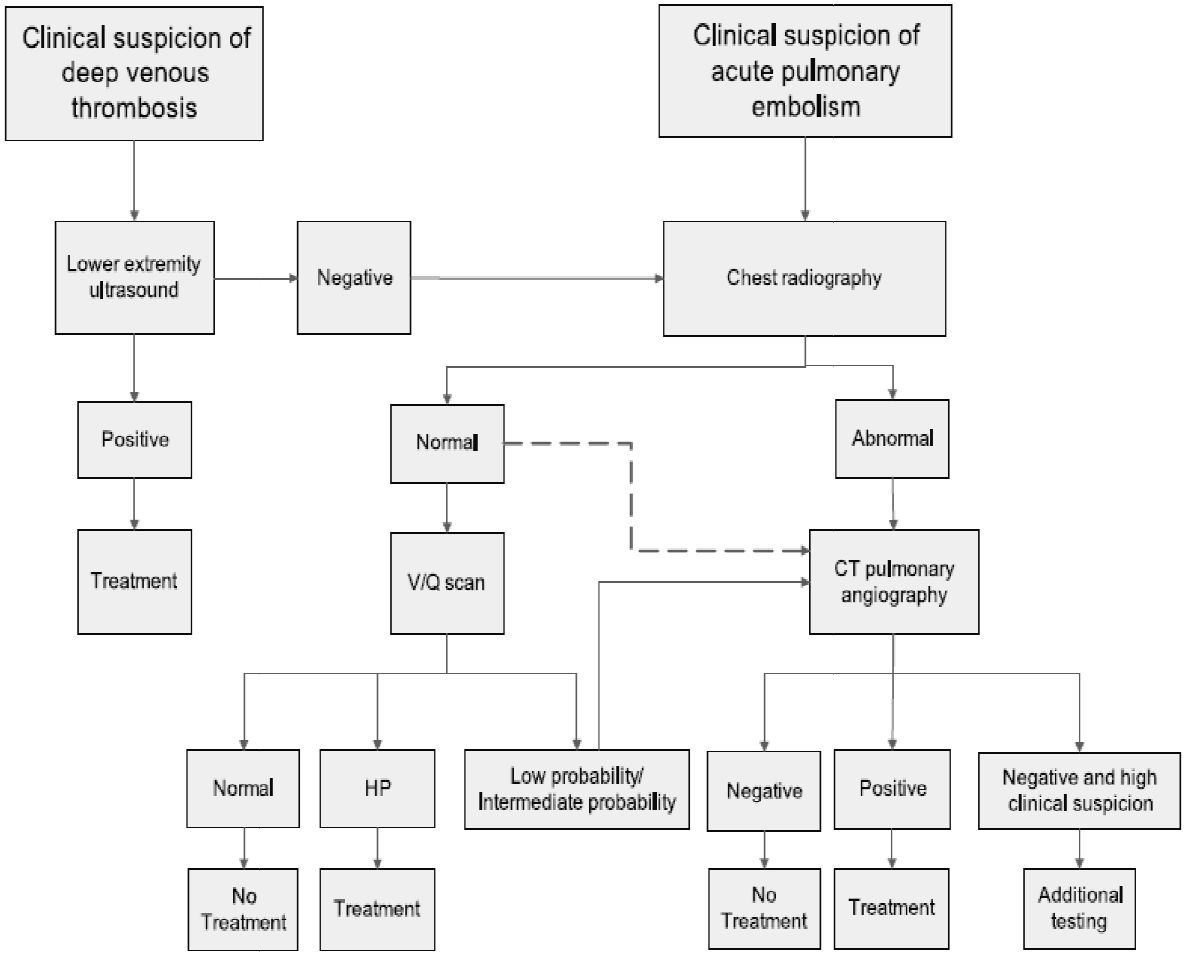

Figure 2.4: Diagnostic algorithm for suspected PE recommended by Kuriakose et al. (published in 2010) (44). HP = High Probability.

The four examples of diagnostic algorithm of PE as described above demonstrate the significance of lung perfusion and ventilation scans to diagnose pulmonary embolism.

2.5 Lung perfusion and ventilation scans

Lung perfusion and ventilation scans have been a preferred medical imaging procedure for suspected PE for the past 30 years (45). The ventilation scan is often performed by administering a mixed radioactive gas (46) (a mixture of oxygen and nitrogen containing small amounts of radioactive ^{133}Xe or ^{99m}Tc) by inhalation. Diethylenetriaminepentaacetic acid (DTPA) labelled with ^{99m}Tc (radioaerosol) is also used in lung ventilation scans. The perfusion scan is undertaken by injecting a solution of macro aggregated human serum albumin (MAA) labelled with a radionuclide (usually ^{99m}Tc) into a peripheral vein. An uptake of the tracer will only occur in the lung units that are perfused by blood (46-47).

The planar ventilation and perfusion scans are normally obtained in a minimum of six to maximum eight views. The views are: **i** anterior (A); **ii** left anterior oblique (LAO); **iii** left posterior oblique (LPO); **iv** posterior (P); **v** right posterior oblique (RPO); **vi** left lateral; **vii** right lateral and **viii** right anterior oblique (RAO) (46). Then, the planar perfusion and ventilation images are compared to assess mismatch or to assess match visible defects in the images (48). The areas of lung that are ventilated but

not perfused (termed mismatch defects) are suggestive of the presence of pulmonary embolism. The defect conditions basically defined by lung perfusion and ventilation scans are: normal or near normal; non diagnostic; very low probability; low probability; intermediate probability; or high probability for PE (49).

Palmer et al., published comprehensive standard acquisition parameters for lung perfusion and ventilation scans. In their study a large field-of-view, dual head gamma camera was used. The activity of ^{99m}Tc recommended for the ventilation scan is 30 MBq, and for perfusion scan is 100 MBq. The suggested SPECT acquisition protocols were: 64 x 64 matrix zoomed at 6.8 mm pixel size; 128 projections over 360°; each projection at 10 s for ventilation studies and 5 s for perfusion studies. The patient inhales the ^{99m}Tc-DTPA (TechneScan DTPA: Mallinckrodt Medical BV, Peten, Holland) while in the supine position. The patient is then transferred to the SPECT table to complete the ventilation acquisition. At the completion of the ventilation acquisition, ^{99m}Tc-MAA was injected immediately without moving the patient. The perfusion acquisition was then performed on the patient. To process the reconstructed SPECT images any focal ^{99m}Tc-DTPA depositions (hot spot) were removed. Then, a contour was drawn individually for each lung (the left and the right lung). The ^{99m}Tc clearance correction was performed to produce two corrected projection sets: one assuming constant clearance and the other allowing variable clearance. Finally, transverse slices were reconstructed using

Operating System/Environment Manager (OSEM) with eight subsets and two iterations. The resulting multi transverse slice set was normalised to contain the same number of voxels (50).

2.6 Comparison between planar imaging and SPECT imaging for pulmonary embolism diagnosis

PE diagnosis via lung perfusion and ventilation SPECT has better diagnostic performance than using planar imaging (51-53). SPECT has demonstrated better sensitivity and accuracy compared to planar imaging for the detection of small lesions in the lungs (50, 53). SPECT imaging is a better modality to detect subsegmental lung perfusion defects (54). Magnussen et al., reported that SPECT images make viewing of the right lung lower lobe medial basal segment easier (55). In addition SPECT offers the advantage of tomographic planes and 3-D viewing (56). Lung perfusion and ventilation scans done with SPECT imaging provide better image quality than planar scans, thereby increasing the interpretive confidence amongst Nuclear Medicine physicians (57).

Despite the advantages of SPECT, interpreting SPECT images of lung perfusion and ventilation scans remain challenging for many Nuclear Medicine physicians. Many physicians are more comfortable, and more familiar with 2-D planar images of lung perfusion and ventilation scans (58). Most importantly, planar imaging has established interpretative

criteria from the PIOPED investigation team (59-60), the Hull criteria (61) and the Gestalt interpretation (62). SPECT imaging does not offer strong evidence-based research or criteria to help Nuclear Medicine physicians diagnose PE via SPECT images (58). There are many cases when planar imaging is preferred as it is widely available and easy to perform (54).

In summary, both (planar and SPECT) are currently relevant and significant imaging modalities to acquire lung perfusion and ventilation images. Planar imaging is a currently relevant method to acquire lung perfusion and ventilation images. SPECT imaging is viewed as the preferred method to acquire lung perfusion and ventilation images in the future. More literature reviews and research on lung perfusion and ventilation scans undertaken with SPECT imaging will establish a comprehensive guide to help Nuclear Medicine physicians diagnose pulmonary embolism.

2.7 Interaction of photons with matters

The nuclear composition of an isotope of an element may have a different number of neutrons (N) to the element, but the same number of protons (atomic number = Z) as the element (63). Some isotopes are not stable. These isotopes will disintegrate spontaneously to reach a stable state by emitting radiation (63-64). Three kinds of the emitted radiation are alpha particles (α), beta particles (ß), and gamma radiation (γ) (65).

Gamma emission is dissimilar to alpha and beta emissions. Gamma radiation is emitted by a nucleus with stable neutron to proton ratio but having a greater nuclear energy that its resting level (excited state). Gamma radiation is a photon (quanta of energy) emitted by an excited nucleus. Gamma radiation is an uncharged and short wave length electromagnetic radiation with typical energies from 0.1 to 3 MeV (in radioactive decay) (63).

Gamma radiation interacts with atoms as it passes through matter. Its photon intensity is attenuated through the interaction (65). Types of photon interactions in matter (within nuclear medicine practice) are photoelectric absorption, Compton scattering and pair production (66). The interactions are a function of the energy of the photons and the atomic number, Z, of the matter (63).

Compton scattering is an interaction of photon energy with orbital electrons that are usually at outer shells or free electrons, producing scattered photons and recoil Compton electrons. The scattered photons emerge at angle, θ, relative to the initial photons' trajectory. The energy of scattered photons is smaller than the initial photons. The recoil Compton electron is ejected from the atom with a particular kinetic energy (67). Compton scattering is the dominant interaction of photons in materials with low atomic number such as human tissue (weighted average Z=7.5).

This interaction is the most common type of interaction of photons in the energy range from 100 keV to 10 Mev (63).

The interaction of photons with K or L shell electrons is called the photoelectric effect. In this interaction, energy of the photons is absorbed completely and the orbital electron is ejected. This interaction is dominant in photons with energy of approximately 100 keV or less (65). The ejected orbital electron is referred as a photoelectron (67). The photoelectric effect is a dominant interaction in material with higher atomic number such as lead, Z= 82, (63) at lower energies. The photoelectric effect decreases rapidly with increasing photon energy. The interaction is proportional to the atomic number (Z^3) of the attenuator material (68).

Pair production interaction occurs only with high photon energies (greater than 1020 keV). When a photon with energy in excess of 1020 keV passes through an attenuator it transforms into two anti particles (negatron and positron). The positron soon losses its energy and annihilates, to combine with negatron. This annihilation produces two photons moving in opposite direction each with energy 0.511 MeV (65, 68).

As gamma radiation passes through matter, the photon spectra can be modified and the intensity of gamma radiation is attenuated (through the interactions described above). The attenuation of the photons largely

depends on: the thickness of the attenuator material; atomic number of the attenuator material; and the initial photon energy (65).

2.8 Nuclear medicine imaging

Diagnostic imaging was invented about 110 years ago, after the first x-ray image was recorded by Wilhelm C. Roentgen (69). The goal of diagnostic imaging is a better understanding of the anatomy, physiology; and pathology of the human body in improving medical prevention, diagnosis and therapy (70). The overview of diagnostic imaging is best described by *Figure 2.5*.

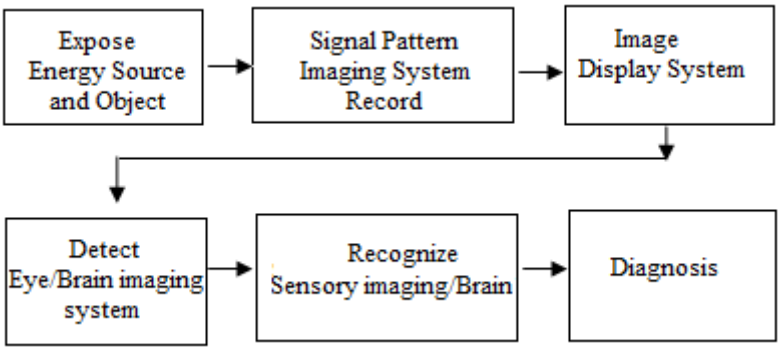

Figure 2.5: This schematic diagram illustrates steps in a normal diagnostic imaging process. The first three steps are performed by the imaging modality. The last three steps are part of visual psychophysical process (quantitative in nature) and are performed by a radiologist (69).

The purpose of an imaging device is to produce 2-D or 3-D images of an object. The objective of diagnostic imaging is to detect a lesion. The image

production using imaging devices are affected by contrast, resolution, noise and sensitivity (69).

The fundamental concept of nuclear medicine imaging is based on the external detection of biodistributed radiotracers that have been administered to patients. Physiological uptake, distribution, and excretion allow clear understanding of the presence or absence of disease in the patient. Nuclear medicine reflects the biodistribution of radiopharmaceuticals and therefore the physiology, anatomy, pathology, and artefact overlays of a patient present at the time of imaging. Usually a radioisotope is combined with a physiological compound to create a radiopharmaceutical. Radiopharmaceuticals can be administered to patients via intravenous; oral; or injection (71).

Gamma camera

Gamma cameras are stationary imaging devices that are commonly used in nuclear medicine. These cameras are able to detect radiation across the entire field of view. Gamma cameras are capable of recording dynamic as well as static images of the area of interest in the patient.

The basic design of most gamma camera is based on the Anger camera (72) The basic components of a gamma camera are: **i** collimator; **ii** NaI(Tl) detector; **iii** photomultiplier tubes; **iv** preamplifier; **v** amplifier; **vi** X, Y positioning circuit; **vii** summing circuit; **viii** pulse height analyser; **ix** and

viii computer unit (72). *Figure 2.6* illustrates a basic gamma camera configuration.

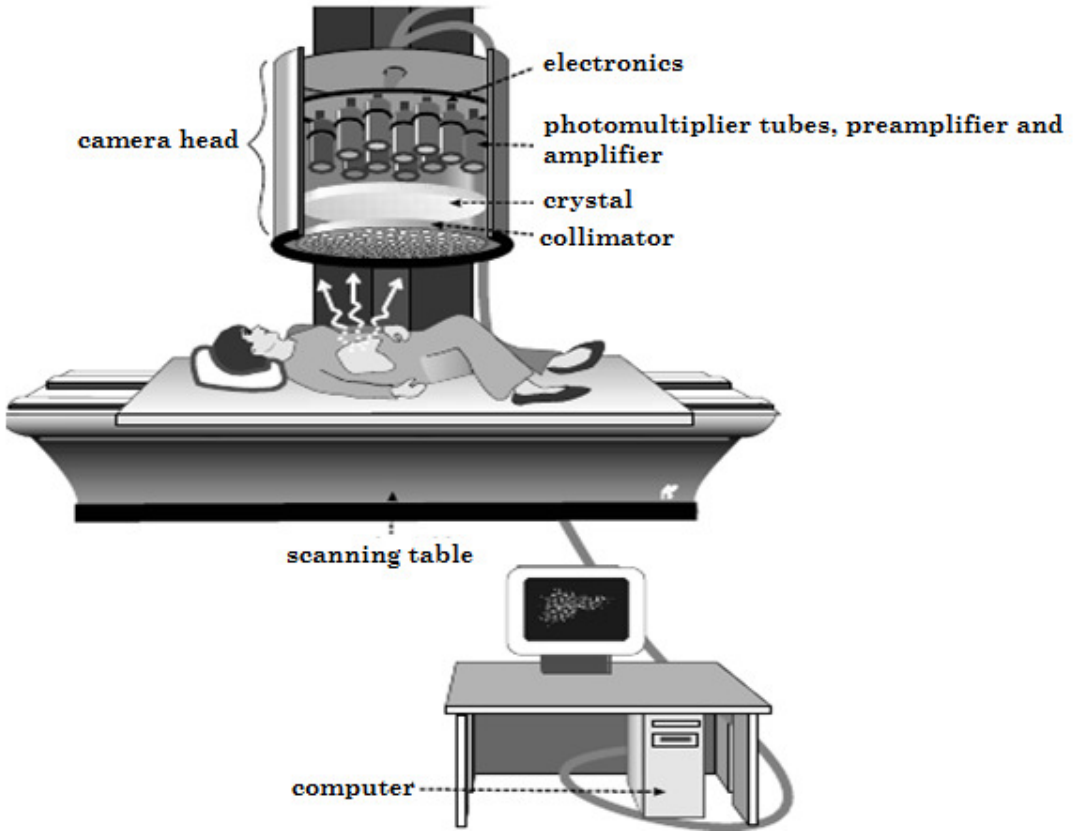

Figure 2.6: The picture illustrates components of nuclear medicine imaging system (63, 70).

There are many types of collimator for different photon energies and for many imaging qualities (63). The collimator is attached to the NaI(Tl) detector to limit the field of view so that gamma (γ) radiations from outside the field of view are prevented from reaching the detector (72). Photons emitted from other directions will be absorbed by the collimator septa (63). Parallel collimators are the most commonly used type in nuclear medicine procedures (72).

The NaI(Tl) detector is a clear crystal in which gamma radiation interacts, thereby converting the radiation to light photons. Photomultiplier tubes generate a pulse in response to the light photons. Each γ radiation interaction generates a pulse projected at the X, Y coordinate point of interaction of the γ radiation (72). A preamplifier amplifies the pulse to allow it to be transmitted through a cable to the main amplifier for further amplification (63). X, Y positioning circuits correlate the X, Y coordinate on the image to the X, Y coordinate at the point of interaction of the γ radiation. A summing circuit provides summed pulses, and creates Z (energy) pulses (72). A pulse height analyser analyses the amplitude of Z pulse. The computer of a gamma camera imaging system is used for acquisition, storage and data processing (63, 70).

Single photon emission computed tomography (SPECT)

A typical SPECT system consists of gamma detectors (one; two; or three) mounted on a rotating gantry (72). A computer for acquisition and processing data; and a display system are normally included in the system. The detectors rotate at a small angular increments (3° – 10°) until a full 360° rotation is completed. Data collected at each rotation are recorded for later reconstruction (72). Images in the transverse, sagittal, and coronal planes are generated from the collected data using image reconstruction software (72). SPECT imaging allows the localisation of radiation signals

from complex organ structures for critical patient diagnosis and management (73).

2.9 ImageJ software

ImageJ is an open source software developed by the National Institute of Health (NIH), Bethesda, Maryland. The software is able to display, edit, analyse, process, save and print 8-bit, 16-bit, 32-bit images. The analysis tools allow area and pixel calculation of an image. The software is also able to measure distance and angles of pixels. Statistical programs are included in the software package. It also supports standard image processing functions such as contrast manipulation, sharpening, smoothing, edge detection and median filtering. The software is usually used in microscopy, gel, astronomy and medical imaging fields (74). The software package was used for image analysis in this thesis.

3. DESIGN AND DEVELOPMENT OF AN ANATOMICAL LUNG PHANTOM

3.1 Introduction

This chapter consists mainly of previously published article by the author and two co-authors in the Australasian Physical & Engineering Sciences in Medicine Journal (48). Also, the chapter contains material previously presented as posters at the 39th and the 40th Annual Scientific Meeting of the Australian and New Zealand Society of Nuclear Medicine. Abstracts of the posters have been published in the Internal Medicine Journal (75-76).

3.2 Concept

The fundamental phantom design focuses on its ability to model anatomical lung perfusion defects of patients suspected having pulmonary embolism. The basis for the phantom's development was to assess quality assurance in diagnostic imaging. The phantom was also built as a teaching tool and reference resource for Nuclear Medicine physicians.

Steps taken to manufacture the phantom were carefully planned to ensure its ability to achieve the research objectives. The essential characteristics of the phantom are: **i** reusable; **ii** water tight; **iii** stable; and **iv** easy to handle. One other key features of the phantom is its approximate anatomical resemblance to the human lungs. These characteristics

facilitate the application of the phantom to the generation of lung perfusion images as depicted in lung perfusion and ventilation scans.

3.3 Limitations

The phantom does have some limitations. For instance it does not share the exact tissue textures and mechanical properties of human lungs. Also, the distribution of radioactivity in the phantom does not exactly resemble the distribution of pulmonary blood flow. These characteristics were omitted in order to minimise cost and lessen the development time.

Normally, to diagnose the probability of pulmonary embolism, both lung ventilation and perfusion images are compared. The areas of lung that are ventilated but not perfused are suspected of having pulmonary emboli (termed mismatch defects) (48, 77). In this thesis however, lung ventilation scans will not be simulated or modelled. Lung ventilation is assumed to be perfect in this research. Therefore, all lung perfusion deficiencies modelled using the lung phantom will be considered as V/Q mismatch defects.

3.4 Lung anatomy

The lung phantom was constructed to duplicate the anatomical structures of human lungs as closely as possible. To ensure anatomical similarity, the anatomy of human a lung was studied prior to manufacturing the phantom.

The lungs are comprised of two tree-like structures: the vascular tree and the airway tree. Arteries, veins and capillaries comprise the vascular tree. The airway tree consists of series of hollow branching "pipelines" that decrease in diameter at each division. The airway tree begins at the trachea, which divides into two bronchi, the right bronchus and the left bronchus. Each bronchus enters a lung and then splits and sub-splits numerous times forming bronchioles. Terminal bronchioles are the smallest airways in the tree. The terminal bronchioles lead the airway path into the respiratory zone. This zone consists of alveolar ducts and alveolar sacs that eventually terminate at the alveoli. There are millions of clustered alveoli occupying spaces in the lungs. Thus, the lungs are actually air spaces interspersed with lung tissue (78).

As the trachea divides, the bronchi diverge at greater angles to reach the left and right lung tissues. The right lung has three lobes; upper lobe, middle lobe and lower lobe. Each lobe is supplied by an individual lobar bronchus. The right lobar bronchi are further divided into ten segmental bronchi. The left lung has two lobes: upper lobe and lower lobe. Each lobe has its own bronchus (lobar bronchus). The left lobar bronchi are further divided into ten segmental bronchi. Each segmental bronchus of the left lung and the right lung is occupied with clustered alveoli; forming a functional bronchopulmonary segment *Figure 3.1* (79).

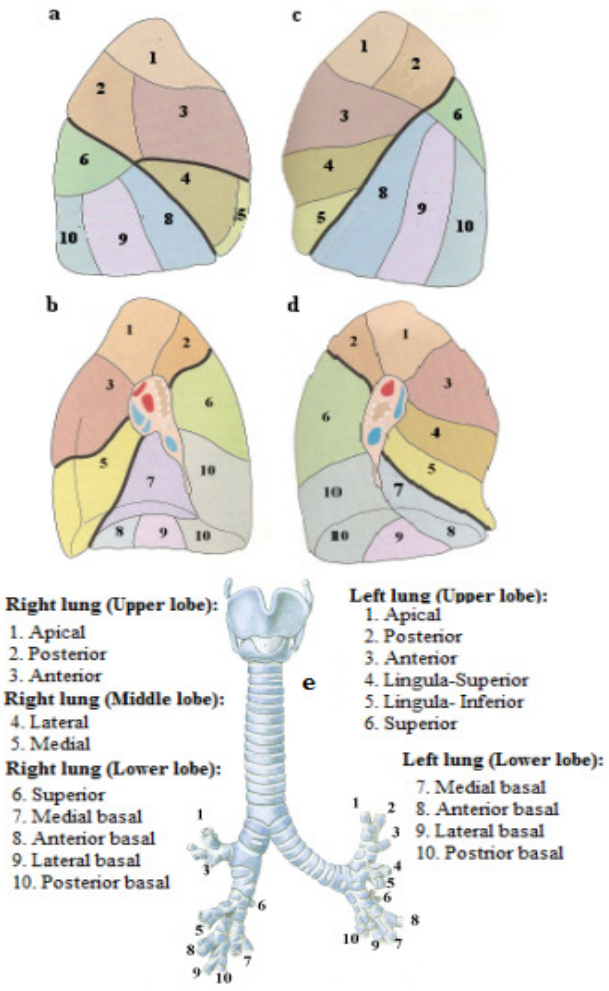

Figure 3.1. ***a*** *The right lung (lateral view).* ***b*** *The right lung (medial view).* ***c*** *The left lung (lateral view).* ***d*** *The left lung (medial view).* ***e*** *Segmental bronchi. Each segmental bronchus was numbered corresponding to its matching bronchopulmonary segment (29).*

An anatomical human lung model (*Figure 3.2*) (American 3B Scientific, Atlanta, USA) was used as a reference model throughout the manufacturing process. The model was cast from an actual human lung with representation of bronchial tree, bronchioles and alveoli. It has 18 segments held together elastically which allows easy viewing of the lung structures; ten bronchopulmonary segments of the right lung and eight

bronchopulmonary segments of the left lung. Commonly, the apical and the posterior segments of the left upper lung lobe are regarded as a single segment (referred as apicoposterior segment). Also, the medial basal and the anterior basal segments left lower lung lobe are frequently fused and considered as a single segment (80). These combinations result in eight instead of ten bronchopulmonary segments of the left lung.

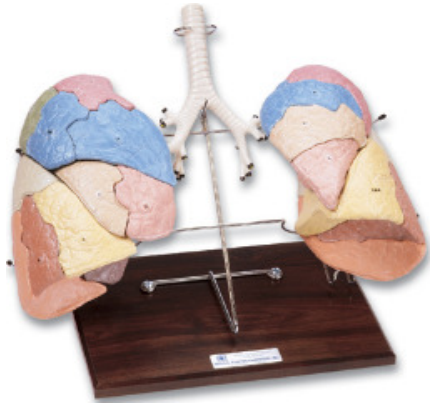

Figure 3.2: The reference lung model (American 3B Scientific, Atlanta, USA). The model is made of 18 colour coded bronchopulmonary segments, with all segments attached elastically.

3.5 The anatomical lung phantom components

The anatomical lung phantom consists of two hollow anatomical lung cavities, perfusion defect inserts and lung tissue. The following describes the process to manufacture all the phantom's components.

The right lung cavity and the left lung cavity

Polymorph (Nucletron Pty. Ltd, Newtown, Australia) plastic sheets were used to manufacture the two lung cavities. These plastic sheets are a

specially formulated rigid low melting temperature thermoplastic for bolus applications in radiation oncology. This material is available in a pre-cut sheet, 60 cm long and 45 cm wide, with a thickness of 2mm.

Two plastic sheets were used to manufacture the lung cavities, one for each cavity. Each sheet was cut into three pieces. The plastic sheets were placed in a water bath at a temperature of 65°C. A nylon mesh was placed into the water bath to prevent the material from sticking to the metal parts of the bath. The polymorph plastic material softens and becomes transparent on heating. One of the polymorph plastic pieces was moulded against the reference lung model (the left lung), creating the first part of the cavity. This was then removed from the model. These steps were repeated for the other two pieces of the polymorph plastic sheets, creating the second and third parts of the left lung cavity. The edges of the first and second parts were attached to each other, creating the left lung cavity. The third part of the cavity became the lid of the left lung cavity. All of the above steps were repeated in order to create the right lung cavity. A valve was installed on each lung cavity in such a way as to facilitate the filling and draining of water and ^{99m}Tc solution. Overall, dimensions of the cavities varied by ± 2 mm compared to the reference lung model.

Figure 3.3 and Figure 3.4 show the right and the left lung cavities, photographed next to the reference lung model. The figures show that the cavities were manufactured with a shape of the reference lung model.

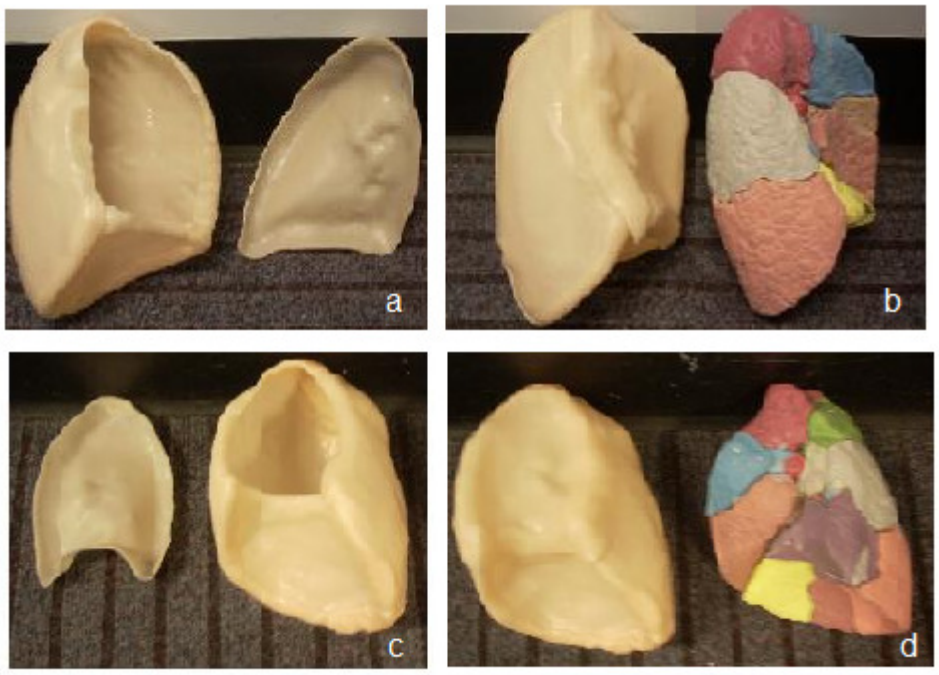

Figure 3.3: ***a*** *The left lung cavity.* ***b*** *The left lung cavity and the left lung reference model.* ***c*** *The right lung cavity.* ***d*** *The right lung cavity and the right lung reference model.*

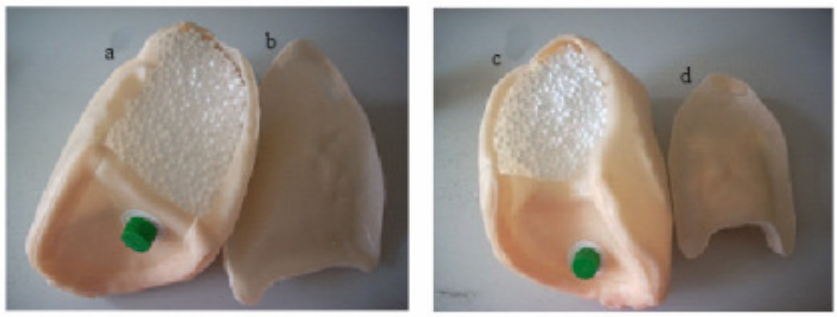

Figure 3.4: ***a*** *The left lung cavity filled with EPS beads, with a valve shown in green colour.* ***b*** *The lid for the left lung cavity.* ***c*** *The right lung cavity filled with EPS beads, with a valve is shown in green colour.* ***d*** *The lid for the right lung cavity.*

Perfusion defect inserts

The reference lung model (*Figure 3.2*) was also used as an anatomical reference to manufacture the perfusion defect inserts. The perfusion defect inserts manufacturing process began by creating negative moulds for the perfusion defect inserts. A chromatic dental alginate (Adelaide Moulding & Casting Supplies, Adelaide, Australia) was used to create the moulds. Equal amounts of water and alginate powder (1 : 1 ratio) were mixed in a container, forming an alginate solution. A single bronchopulmonary segment of the reference lung model was immersed into the alginate solution. The alginate solution firmed up after 1-2 minutes. The bronchopulmonary segment was then gently removed from the alginate, producing a negative mould.

Polyester resin (Solid Solutions, East Bentleigh, Australia) with a few drops of Methyl Ethyl Ketone Peroxide (MEKP) catalyst (Solid Solutions, East Bentleigh, Australia) were used to manufacture the positive structure (perfusion defect inserts) of the negative moulds. Approximately 29 drops of MEKP catalyst was needed for every 100 ml of polyester resin. The polyester resin and MEKP catalyst mixture was poured into the alginate negative moulds and left for up to five days to cure. The cured polyester surface was sticky, and a post-curing process (air exposure at room temperature) was carried out in order to fully cure the polyester. The fully cured polyester took on the impression of the bronchopulmonary segment of the reference lung model. Several of the manufactured perfusion defect

inserts are shown in *Figure 3.5*. Each perfusion defect insert in *Figure 3.5* were photographed next to its reference bronchopulmonary segment, in order to show the anatomical similarity shared between the two objects.

Figure 3.5: ***a*** *The anatomical bronchopulmonary segments of the reference lung model.* ***b*** *The perfusion defect inserts for the lung phantom.*

The polyester casting process was repeated to produce ten anatomical perfusion defect inserts for the right lung cavity and eight anatomical perfusion defect inserts for the left lung cavity. For the right lung cavity, the manufactured perfusion defect inserts were termed apical, posterior, anterior, medial, lateral, superior, medial basal, anterior basal, lateral

basal and posterior basal segments. For the left lung cavity, the defects were termed apical-posterior (commonly referred to as a single segment), anterior, lingular superior, lingular inferior, superior, medial basal-anterior basal (commonly referred to as a single segment), lateral basal and posterior basal segments.

Silicon sealant was used to separate and attach the perfusion defect inserts together; corresponding to any the clinical lung perfusion defect requirements (single segmental perfusion defect or multi-segmental perfusion defects). *Figure 3.6* shows the perfusion defect inserts for the right lung cavity. In *Figure 3.6,* silicone sealant was used to attach the perfusion defect inserts to make the right upper lobe; the right middle lobe; and the right lower lobe. *Figure 3.7* shows the perfusion defect inserts for the left lung cavity.

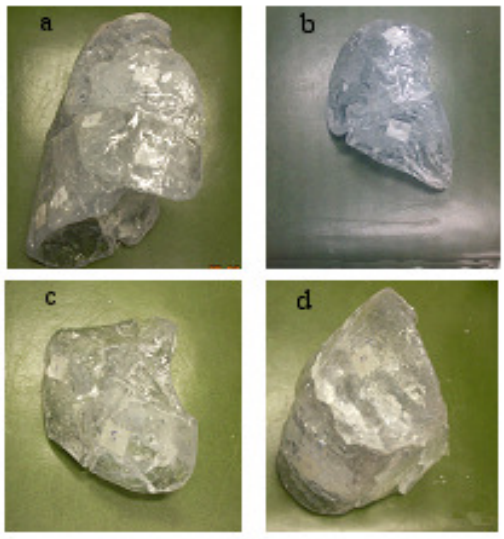

Figure 3.6: ***a*** *All the perfusion defect inserts for the right lung attached together.* ***b*** *The perfusion defect inserts for the right upper lobe: comprising*

apical, posterior and anterior segments. ***c*** *The perfusion defect inserts for the right middle lobe: comprising medial and lateral segments attached together* ***d*** *The perfusion defect inserts for the right lower lobe: comprising superior, medial basal, anterior basal, lateral basal and posterior basal segments.*

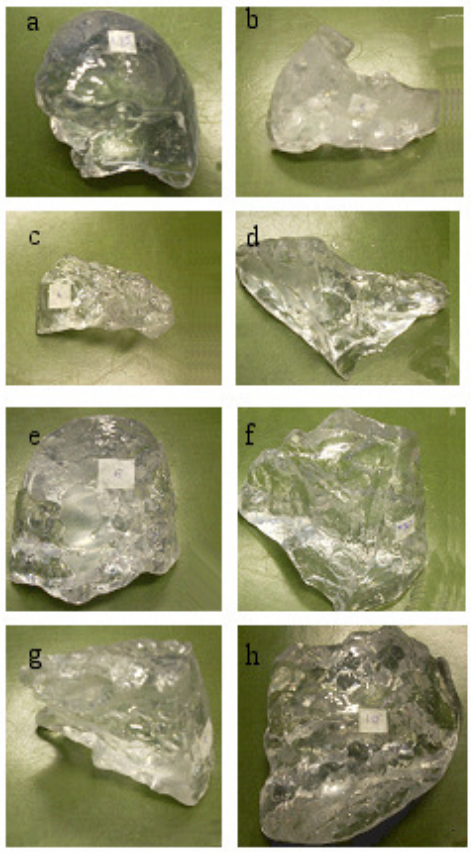

Figure 3.7: The perfusion defect inserts for the left lung. ***a*** *Apical and posterior segments (commonly referred to as a single segment).* ***b*** *Anterior segment.* ***c*** *Lingular superior segment* ***d*** *Lingular inferior segment.* ***e*** *Superior segment.* ***f*** *Medial basal and anterior basal segments (usually considered as a single segment).* ***g*** *Lateral basal segment.* ***h*** *Posterior basal segment.*

Lung tissue

Expanded polystyrene beads, EPS, $(C_8H_8)n$ were used to simulate lung tissue (with efficient lung perfusion) in the lung cavities (see *Figure 3.4*). Polyester $(C_{10}H_8O_4)n$ resin was used to manufacture the lung perfusion defect inserts. These inserts were employed to simulate areas of deficient lung perfusion. Attenuation responses of the 140keV of ^{99m}Tc solution differ within the lung tissue simulated by EPS beads and within the lung area simulated by perfusion defect inserts.

The effective atomic number, $Z_{eff,}$ of a compound can be calculated using Equation 1 (81).

$$\sqrt[3]{(a_1 {Z_1}^3 + a_2 {Z_2}^3 + a_3 {Z_3}^3 + \ldots\ldots\ldots)} \quad \text{Equation 1}$$

where:

a_i: Fractional content of element of the i^{th} element.

*Z*i: Atomic number of the i^{th} element.

The Z_{eff} of EPS beads is 5.7 while for the polyester resin it is 6.6, as calculated using Equation 1. Mass attenuation coefficient is highly dependent on the atomic number of the absorbing material (63) Mass

attenuation is fraction of photon absorbed or scattered from monoenergetic beam. The mass attenuation coefficient is independent of density (82).Consequently, the mass attenuation coefficient, μ/ρ, is higher for the perfusion defect inserts, as it has higher Z_{eff}, compared to the EPS beads. Furthermore, the perfusion defect inserts are relatively thicker than the EPS beads. Thus, the resulting attenuation in the solid defects is higher than in the EPS, resulting in non-uniform attenuation in the lung cavities.

The density of the perfusion defects of the lung phantom does not resemble the density of lung tissue. This is because the realistic density property of the phantom has been compromised to accommodate better anatomical features of the phantom. The polyester resin was chosen to manufacture the perfusion defect inserts because the material was able to better hold lung shapes and features. In this thesis, the lung phantom was manufactured with the aim of resembling the human lung as close as possible. Anatomical resemblance to a human lung is important for later studies (Chapter 5 and Chapter 6).

3.6 Assembly of the lung phantom

The anatomical lung phantom is reusable. The following are the steps required to model a lung perfusion defect as depicted in lung perfusion and ventilation scans.

To use the phantom, one or more perfusion defect inserts are placed into the lung cavities in the correct anatomical positions. Silicon sealant is used to seal the bronchopulmonary segments into the lung cavities. The lung cavities are then filled with EPS beads. Next, the lung lids are attached to the cavities, and the lids sealed to the cavities using silicone sealant. Finally, through the lung cavities' valves, the lung cavities are filled with water and an appropriate activity of ^{99m}Tc solution. *Figure 3.8* shows the step-to-step procedure to prepare the phantom with a perfusion defect in the left lung lower lobe posterior basal segment.

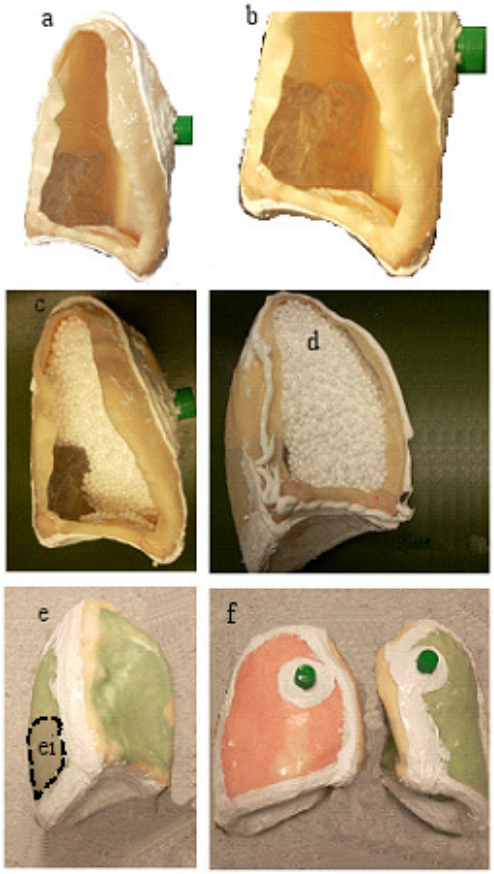

Figure 3.8: The steps taken to prepare the phantom for a perfusion scan. ***a*** *The left lung lower lobe posterior basal defect insert was fitted into the left cavity at its anatomical position. The green cap on the picture is the filling*

and draining valve for the cavity ***b*** *Magnified view of the image* ***a****.* ***c*** *The cavity is filled with EPS beads.* ***d*** *Silicone sealant is piped around the cavity.* ***e*** *The lid is attached to the cavity. Coloured water is then poured into the cavity* ***ei*** *The perfusion defect area is free of coloured water (dotted circle).* ***f*** *Appropriate activity of* ^{99m}*Tc solution is added to the assembled phantom, leaving the phantom ready for a planar or SPECT scan.*

3.7 Imaging protocols

In this thesis, all planar and SPECT scans were acquired with the same imaging protocols as at the Department of Nuclear Medicine, Wollongong Hospital, NSW, Australia. A dual head gamma camera 'Philips ADAC Forte' with a Low Energy High-Resolution (LEHR) collimator was used for all acquisitions. *Figure 3.9* shows the phantom being scanned using the dual head gamma camera. To begin the planar or the SPECT perfusion scans, an appropriate activity (approximately 40-50 MBq) of ^{99m}Tc solution, was added into the assembled phantom (*Figure 3.8*). The usual dosage of ^{99m}Tc-MAA for lung perfusion imaging recommended by the Society of Nuclear Medicine (SNM) is 40-150 MBq (83).

Conventionally, lung perfusion images are compared with lung ventilation images to observe perfusion-ventilation mismatch or match patterns within bronchopulmonary segments (54). This comparative step was omitted in

this study because the research was aimed at only studying lung perfusion defects.

Figure 3.9: The lung phantom while on a scan procedure at Department of Nuclear Medicine, Wollongong Hospital, NSW, Australia.

Planar acquisition

In each planar scan, six planar views were acquired in a 256 x 256 matrix: anterior (A), posterior (P), left anterior oblique (LAO), left posterior oblique (LPO), right posterior oblique (RPO) and right anterior oblique (RAO). The planar perfusion scans were acquired at a 140 keV photopeak. The planar perfusion image set was then printed on x-ray film and also stored

electronically in the hospital PACS (Picture Archiving and Communication System). *Figure 3.10* shows an example of planar perfusion images modelled using the phantom.

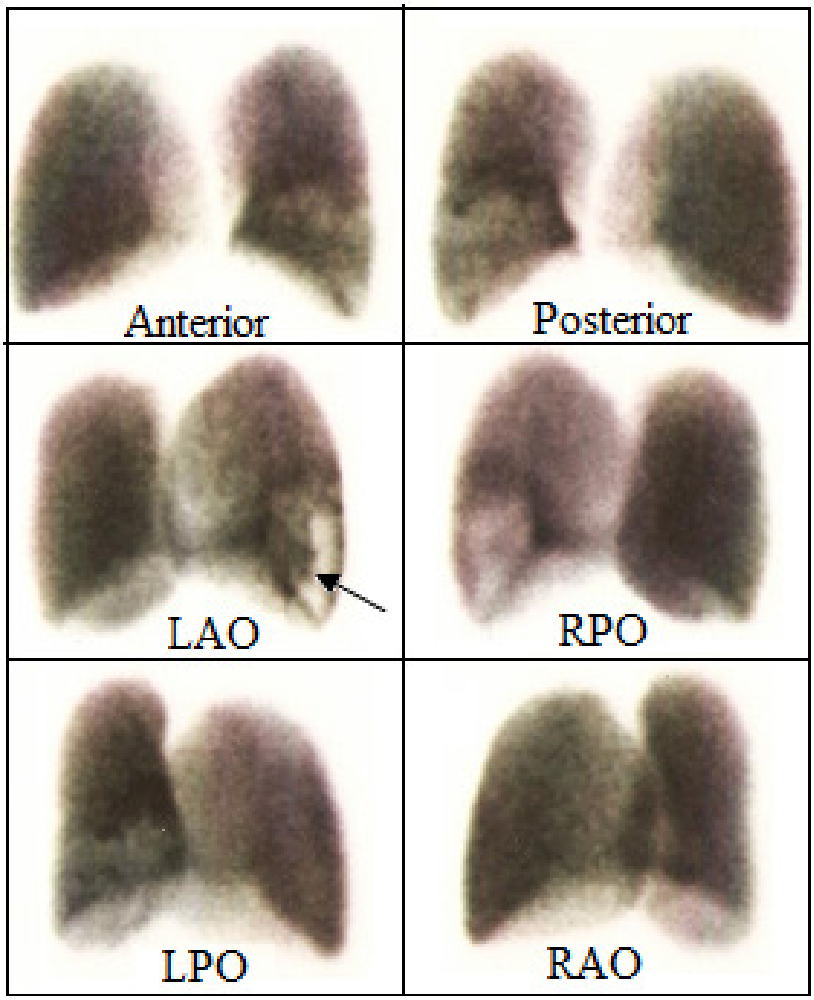

Figure 3.10: Planar perfusion images of a simulated lung perfusion event at six different views. The arrow shows the perfusion defect within the left lung lower lobe posterior basal segment.

At the Nuclear Medicine Department, Wollongong Hospital, planar lung perfusion acquisition time (on a dual head camera) is about 10 to 15 minutes. In this research, planar lung phantom perfusion acquisition time

is approximately 12 minutes (when administrated ^{99m}Tc activity into the lung phantom cavities is approximately 40-50 MBq).

SPECT acquisition

In each SPECT scan, a step-and-shoot protocol of 12 s/3°step for a total of 60 views per camera head was used. Images were collected at the 140keV energy window immediately after the planar acquisition. The lung SPECT image set was reconstructed using a HERMES workstation (Hermes Medical Solutions, Stockholm, Sweden). Reconstruction of coronal, sagittal and transverse slices were done using filtered back-projection (FBP) with a Butterworth cut off value of 0.4. The raw and reconstructed images were stored in digital format on the hospital PACS. Reconstructed SPECT images were viewed on the HERMES workstation and also printed on x-ray film. *Figure 3.11* shows an example of SPECT perfusion images modelled using the phantom.

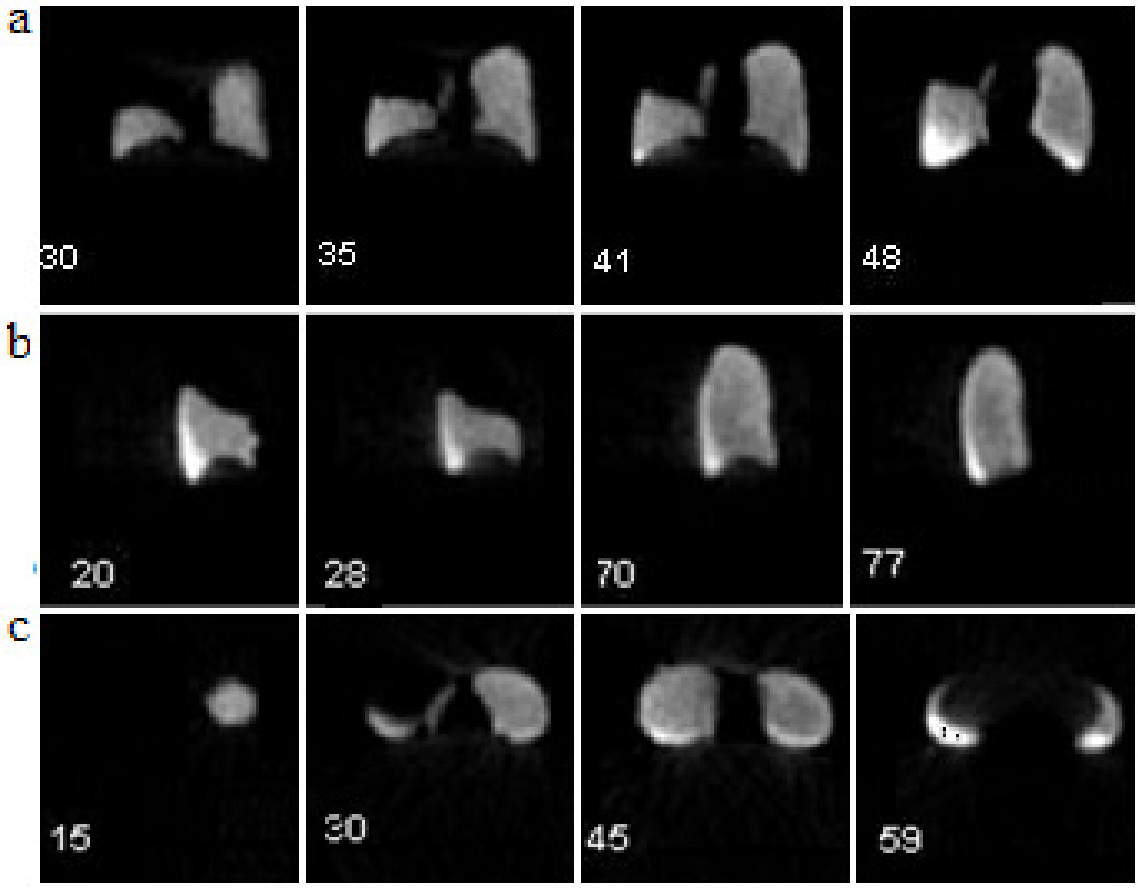

Figure 3.11: SPECT perfusion tomographic slices of the right upper lobe defect. ***a*** *Selected coronal slices from anterior to posterior show a clear defect in the right upper lobe.* ***b*** *Selected sagittal slices from right to left show sharp edges of the right upper lobe defect.* ***c*** *Selected transverse slices from head to feet show the defect in the right upper lobe.*

4. CHARACTERISTICS OF THE ANATOMICAL LUNG PHANTOM

4.1 The lung phantom size

The anatomical lung phantom (48) design was based on a reference anatomical human lung model (American 3B Scientific, Atlanta, USA). The reference model was cast from an actual human lung. The reference lung model was used to ensure that the phantom mimicked the physical dimensions of the human lung.

The anatomical lung phantom was manufactured to closely represent the shapes and the size of the human lung. The lung phantom dimensions are: 23 cm height; 28 cm width; 13.7 cm depth (see *Figure 4.1*). The human lungs vary in size and formation. Miller, in his book, reported the average height of the right lung and the left lung in a group of males are 27.1 cm and 29.8 cm respectively and in a group of females are 21.6 cm and 23 cm respectively (84). Average depth measurements at the base of the right lung were 13.5 cm in a group of males and 12.2 cm in a group of females, and of the left lung were 12.9 cm in a group of males and 10.8 cm in a group of males (84). The height and depth measurements of the manufactured lung phantom are considered within acceptable ranges of height and depth measurements of the human lung.

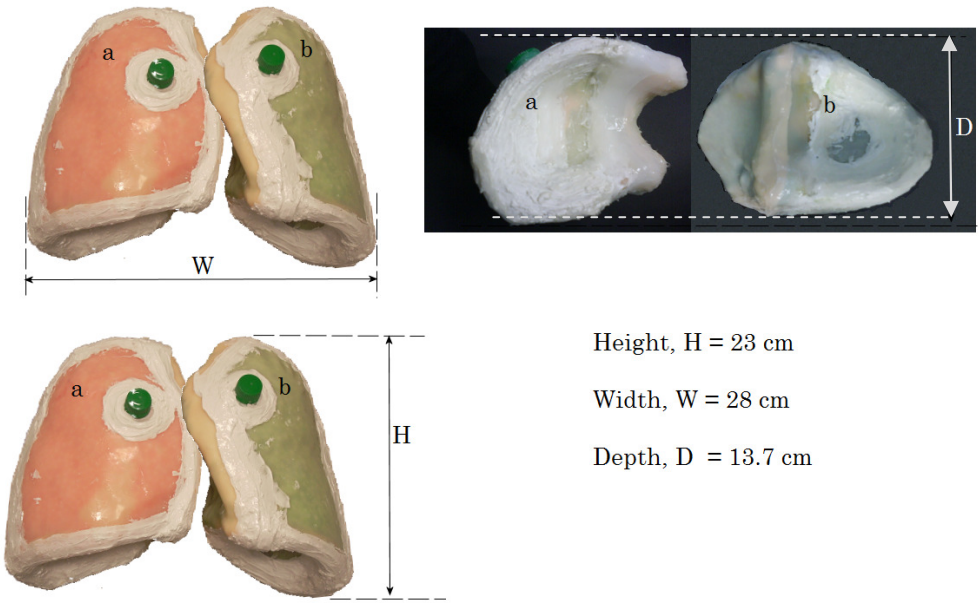

Figure 4.1: The dimensions of the anatomical lung phantom. ***a*** *The right lung.* ***b*** *The left lung.*

Height, width, depth, perimeter and length measurements of the phantom were measured at several points as depicted in *Figure 4.1* and in *Figure 4.2*. The measurements are shown in *Table 4.1*.

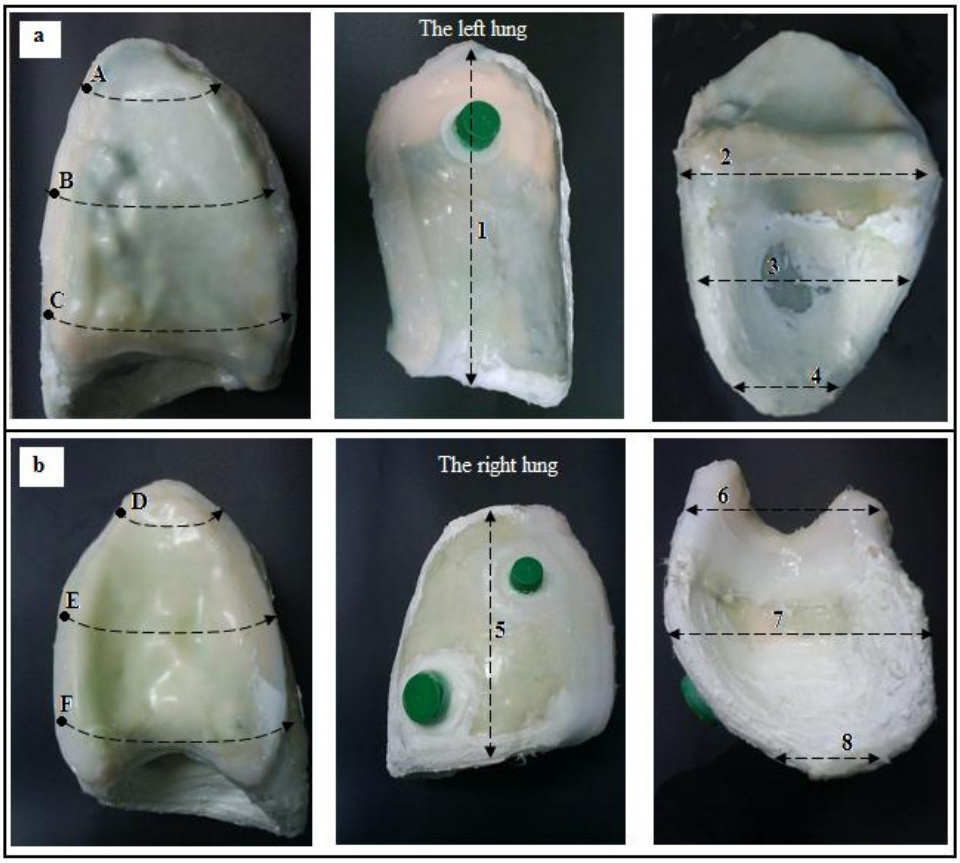

Figure 4.2: ***a*** *The A, B, and C points are the perimeter points measured on the left lung. Line 1 is the height of the left lung. Line 2, line 3, and line 4 are the transverse measurements of the left lung.* ***b*** *The D, E, and F points are the perimeter points measured of the right lung. The line 5 is the height of the right lung. Line 6, line 7, and line 8 are the transverse measurements of the right lung.*

Table 4.1: Measurements of the lung phantom at several points (see Figure 4.2). Line 1 and line 5 are height measurements of the left lung and the right lung respectively. Line 2, line 3, and line 4 are transverse measurements of the left lung. Line 6, line 7, and line 8 are transverse measurements of the right lung.

Perimeter		**Length**	
Point	Perimeter (cm)	Line	Length (cm)
A	28.5	1	23.0
B	45.5	2	13.6
C	46.8	3	13.0
D	34.0	4	8.3
E	61.0	5	20.6
F	59.5	6	11.8
		7	13.7
		8	4.6

The height of the left lung (line 1) and the right lung (line 5) are 23.0 cm and 20.6 cm respectively. The transverse measurement at the base of the left lung (line 3) and the right lung (line 7) are 13 cm and 13.7 cm respectively. Miller in his book reported that the right lung is shorter and broader than the left lung (84). Measurements of the anatomical lung phantom follow the measurement pattern reported by Miller in his book (84). These measurements were taken to confirm that the manufactured lung phantom size is approximately as the size of the human lungs.

4.2 Hounsfield units

Computed tomography (CT) scanners associate gray value scale value of a material produced during CT scanning with its attenuation value in Hounsfield units (HU). The HU range of CT scanners is from +1000 (cortical bone) to -1000 (air); with water having a HU value of 0 (85). Dense materials (for example muscle tissue, liver, and bone) that attenuate x-ray more than water have positive HU values. Less dense materials (for example lung and adipose tissue) have negative HU values, attenuate x-ray lesser than water (69). By definition,

$$HU\ value = \frac{\mu_m - \mu_w}{\mu_w} \ . \ 1000 \quad (Equation\ 2)$$

where μ_m is the linear attenuation coefficient (measured in cm^{-1}) for the object being scanned and μ_w is the linear attenuation coefficient (measured in cm^{-1}) for water (86).

In this thesis, the HU values of the anatomical lung phantom were identified. The lung phantom was submerged in a water-filled container, then scanned using a CT scanner. *Figure 4.3* shows the CT image and corresponding schematic diagram of the lung phantom. The scan was acquired at a setting of 120 kVp. HU numbers of the lung phantom materials are listed in *Table 4.2*.

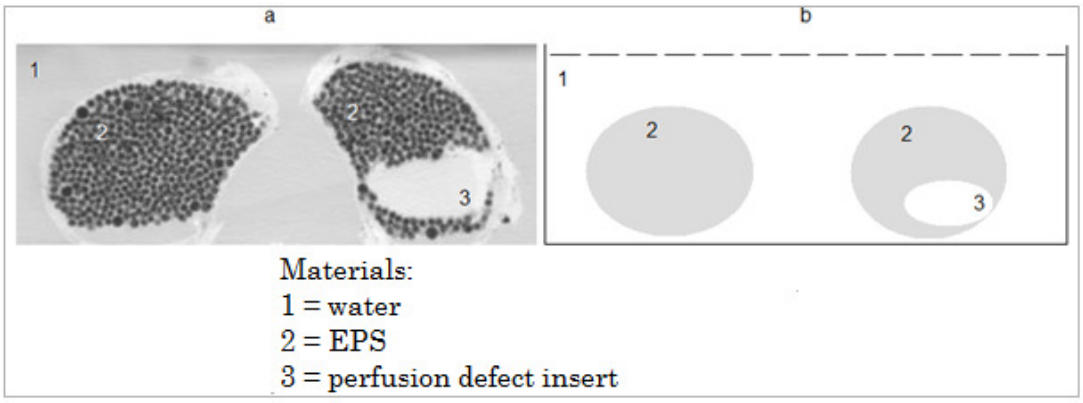

Figure 4.3: ***a*** *The CT scan image (axial plane) of the lung phantom with a perfusion defect insert fitted in the left lung.* ***b*** *Schematic diagram of the lung phantom in a water-filled container.*

Table 4.2: HU numbers of the anatomical lung phantom. Material numbers are listed as illustrated in Figure 4.3

Material Number	Material	HU Number
1	Water	0
2	EPS beads with water	-578
3	Perfusion defect insert	114

The HU values in *Table 4.2* were compared to published HU values of lung tissues. The anatomical lung phantom (lung tissue and perfusion inserts) has higher HU values compared to human lungs. Benseler, in his book recorded a HU value of lung as -903.5 (85). For non-smokers the lung HU

value range is reported as being from -720 to -880 (87). A study by Ezra et al. reported a mean HU value of females' lungs as -722 (SD=44) and of males' lungs as -746 (SD=42) (88). A study reported -648 ± 27 (mean ± SD) HU value of subjects' lung after strenuous, prolonged exercise (89).

CT images display gray shades of attenuated x-rays within the corresponding voxel (90). X-ray attenuations values measured by CT scanners are expressed in Hounsfield Units (90) (see Equation 2). Materials that attenuate x-ray more than water have positive HU values, while materials with less attenuation than water have negative HU values (69). The EPS beads with water that are used to resemble lung tissue within the efficient lung perfusion area have less attenuation than the perfusion defect inserts (that are used to resemble lung tissue within the deficient lung perfusion are). As explained in Chapter 3, the realistic density property of the phantom has been compromised to accommodate better anatomical features of the phantom. The specific materials were chosen to fabricate the phantom as they simplified the moulding process of the phantom. The chosen materials effectively maintained the anatomical shape of the human lungs. This was a key point in ensuring the phantom's ability to be used in our later clinical studies.

4.3 Count rate stability of the phantom

Pulmolite (Pharmalucence, Massachusetts, USA) is a kit for the preparation of ^{99m}Tc MAA used at the Department of Nuclear Medicine, Wollongong Hospital. The kit preparation instructions suggest an intravenous dose range for the average patient (70kg) of 37 to 148 MBq of ^{99m}Tc MAA.

The lung perfusion scan protocol at the Department of Nuclear Medicine, Wollongong Hospital requires 600 000 counts for each planar projection. In this thesis, a trial and error procedure was applied which determined that the radioactivity of the ^{99m}Tc solution should be maintained at 40-50 MBq for each lung phantom scan. The trial started by administrating 2ml of 20 MBq ^{99m}Tc solution into each lung cavity. The radioactivity of ^{99m}Tc solution was adjusted to achieve 600 000 counts per planar view at an appropriate acquisition time. The trials ended after the sixth trial with a radioactivity of a 2 ml ^{99m}Tc solution of 60 MBq. After discussion and consultation with the medical physicist and technologists, the radioactivity of ^{99m}Tc solution was restricted to 40 - 50 MBq for each lung cavity. The specified activities of ^{99m}Tc were chosen for the lung phantom in order to closely mimic a patient planar lung perfusion acquisition time at the Wollongong Hospital (refer to Sub-chapter 3.7). One of the purposes of the lung phantom is to be used as a teaching tool. A good quality of teaching phantoms should be able closely mimic scan acquisitions of actual patients. It was considered necessary for the lung phantom to closely mimic patient

acquisition time as it purpose as a teaching aid was taken into consideration.

A study was carried out to investigate the lung phantom's stability in relation to the time taken for each acquisition to reach the maximum counts per planar view. Three lung perfusion defect cases (Case 1, Case 2 and Case 3) were selected for the study, with each case being repeated three times, making a total of nine lung planar perfusion scans. The names of planar perfusion scans were: **Case 1** for Lung Scan 1, Lung Scan 2 and Lung Scan 3; **Case 2** for Lung Scan 4, Lung Scan 5 and Lung Scan 6; and **Case 3** for Lung Scan 7, Lung Scan 8 and Lung Scan 9. These scans made up the three statistical populations of measurements:

1. Population 1 (consists of Lung Scan 1, 2, and 3),
2. Population 2 (consists of Lung Scan 4, 5, and 6), and
3. Population 3 (consists of Lung Scan 7, 8, and 9).

Population 1 consists of planar perfusion scans of the lung phantom with a non-existent perfusion defect. Population 2 consists of planar perfusion scans of the lung phantom with a perfusion defect in the left lung upper lobe apical-posterior area. Population 3 consists of planar perfusion scans of the lung phantom with a perfusion defect within the right lung lower lobe lateral basal segment. The left lung and the right lung cavities were loaded with 2 ml of ^{99m}Tc solution (40 - 50 MBq) for each planar perfusion

scan. The mean values and one standard deviation values of ^{99m}Tc radioactivity of each statistical population were calculated and listed in *Table 4.3.*

Table 4.3: Radioactivity of ^{99m}Tc solution in each lung cavity.

Administered ^{99m}Tc radioactivity (MBq)									
	Population 1			Population 2			Population 3		
Lung Scan	LS[1] 1	LS 2	LS 3	LS 4	LS 5	LS 6	LS 7	LS 8	LS 9
The RL[2] cavity	42.7	42.7	43.6	41.2	43.2	44.7	42.5	49.3	43.8
The LL[3] cavity	43.1	41.0	42.9	44.0	39.1	42.0	40.7	48.0	39.9
M ± SD[4] of administrated radioactivity	42.7 ± 0.9			42.4 ± 2.1			44± 3.9		

Six planar views (A, LAO, LPO, P, RPO, and RAO) were acquired for all scans in Population 1, Population 2, and Population 3. The time taken for each planar projection to reach 600 000 counts was recorded. The end to end distances from the lung phantom to the camera for all six views were not the same. This distance affects the time required to complete each planar projection. Also, the volume of the lung perfusion defects affects the time taken to reach 600 000 counts per planar view. The mean and standard deviation of the time taken to reach the maximum counts at each

[1] LS = Lung scan
[2] RL = Right lung
[3] LL = Left lung
[4] M ± SD = Mean ± one standard deviation

planar view (for all lung scans) are shown in the bar charts of *Figure 4.4*, *Figure 4.5*, and *Figure 4.6*.

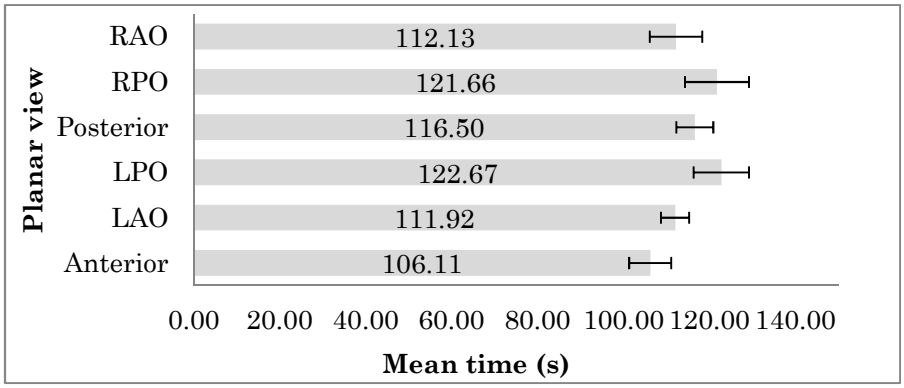

Figure 4.4: Mean values and standard deviation bars of time taken to reach maximum counts for each planar view of lung scans in Population 1.

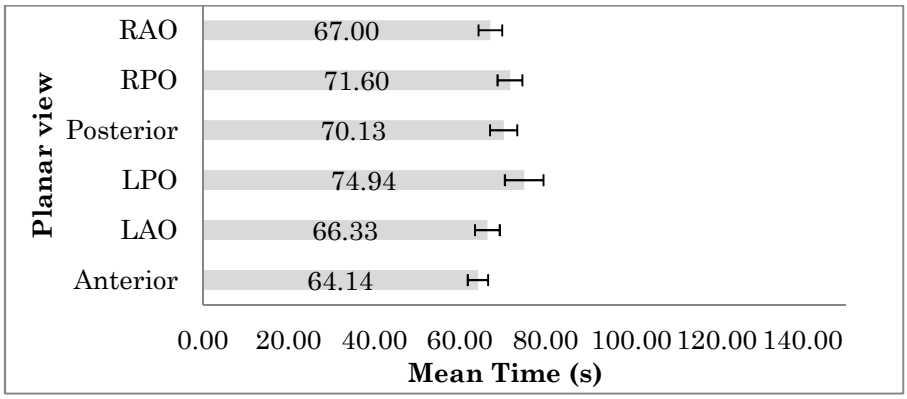

Figure 4.5: Mean values and standard deviation bars of time taken to reach maximum counts for each planar view of lung scans in Population 2.

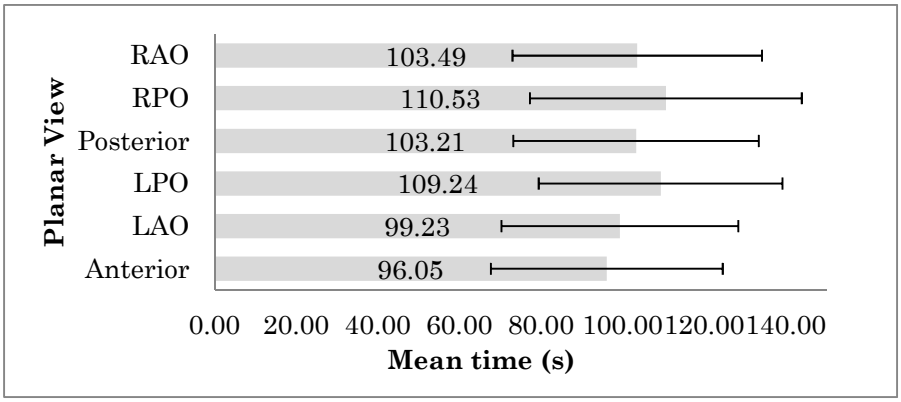

Figure 4.6: Mean values and standard deviation bars of time taken to reach maximum counts for each planar view of lung scans in Population 3.

The bar chart in *Figure 4.6* illustrates higher standard deviations of times taken to reach the maximum counts for all planar views in Population 3, when compared to Population 2 and Population 1. The possible explanations behind the situations are the end to end distance of the lung phantom to the camera at each acquisition in population 3 differs greatly from one to another. Radioactive decay was not considered as a factor because the ^{99m}Tc solutions in the phantom decayed with the same half-life (6.6 hour) in all scans. The end to end distance of the lung phantom to the camera was observed of all acquisitions in later clinical studies. The action was taken to ensure similar times will be taken to reach maximum counts for two or more scans acquired with the same acquisition parameters. Also, the action contribute towards improving reproducibility quality of the phantom

4.4 Radioactivity distribution

Planar and SPECT imaging allows the visualisation of the distribution of radioactivity within the human body (91). The imaging reveals the structure, and physiology of organs' functions. Most nuclear medicine departments have imposed quality assurance and quality control procedures to ensure high quality imaging. One of most applied methods to perform quality assurance and quality control in diagnostic nuclear medicine is by using phantoms. It is recommended that the phantoms are filled with the same radiopharmaceutical as applied to a patient (92). The radioactive solution (^{99m}Tc) has to be equally and homogeneously distributed throughout the lung phantom cavities.

To study the lung phantom's homogeneity, three conditions of planar perfusions were modelled. Each planar perfusion condition scan was repeated three times, making at total of nine lung scans for the study. All the acquired planar scans are in fact the same planar perfusion images *Section 4.3*.

The homogeneity properties of the phantom were studied using the ImageJ software (National Institutes of Health, USA). Pixel intensities of any planar images acquired using the phantom were assumed to have a linear relationship with the radioactivity concentration of ^{99m}Tc solution. The intensity of each pixel recorded using ImageJ is a reconstructed intensity of its corresponding voxel.

The first step to study the homogeneity of the radioisotope distribution was convert the planar image an 8-bit image with 0 - 255 grayscale shades (black = 0 and white = 255). Next, a selection tool was used to draw selection maps (yellow circles) on the lung images (*Figure 4.7)*. There are two selection maps drawn on each planar image; making a total of 18 selection maps all together. Each map was carefully drawn, where all voxels within the map are at similar length (similar thickness). This step was taken into consideration as the thickness of the lung phantom varies.

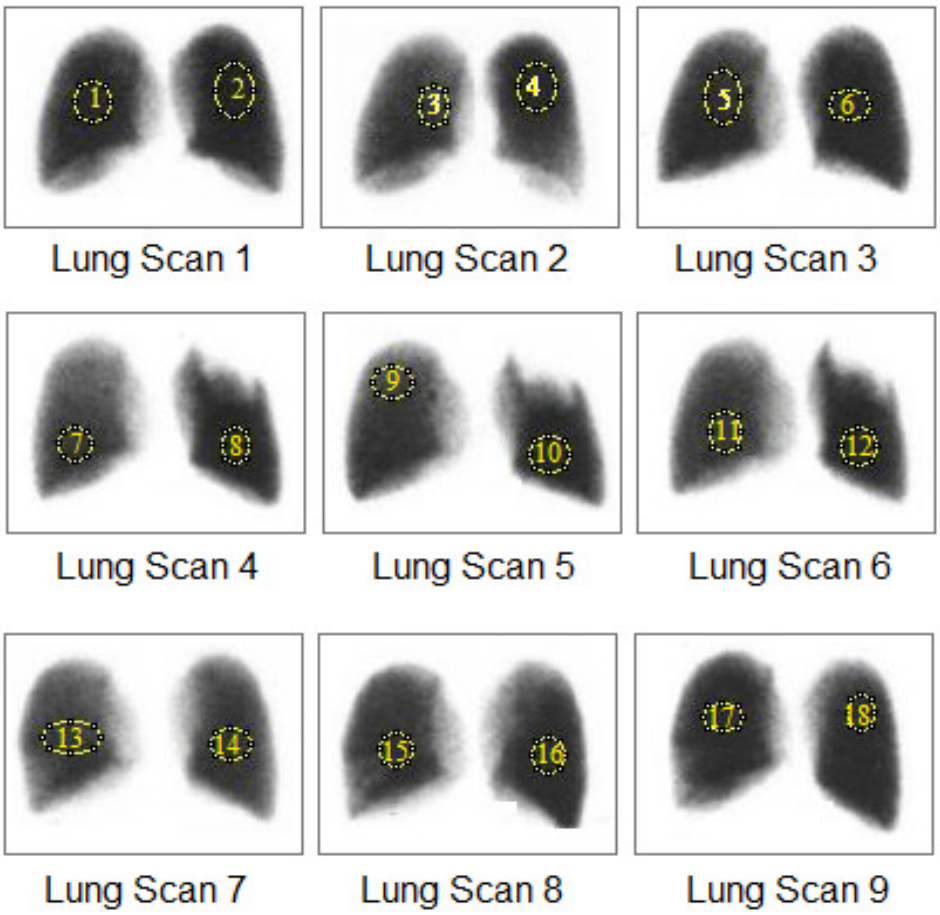

Figure 4.7: Selection maps drawn on the lung images (anterior view) using the selection tool of the ImageJ software

The regions of interest within the selection maps were then analysed using the 'analyse' tool of the software. The analysis reported a mean and standard deviation of the pixels' intensities within each selection map. Then the distribution of pixel intensities in each selection map was plotted using the software. Finally the skewness of the distribution plots of all selection maps were calculated using the software.

Skewness is the third order moment about the mean (74). For a sample size of *n,* the skewness would be:

$$\text{Skewness} = \frac{n}{(n-1)(n-2)} \frac{\sum_{i=1}^{n}(X_i - X_{\text{avg}})^3}{s^3} \qquad \text{(Equation 3)}$$

where:

n : sample size

s : sample standard deviation

X_{avg} : mean value

X_i : each value in the sample

These distribution plots are shown in *Figure 4.8.* The number of pixels in each selection map, the mean, standard deviation and skewness of the pixels' intensities of each selection map are listed in *Table 4.4.*

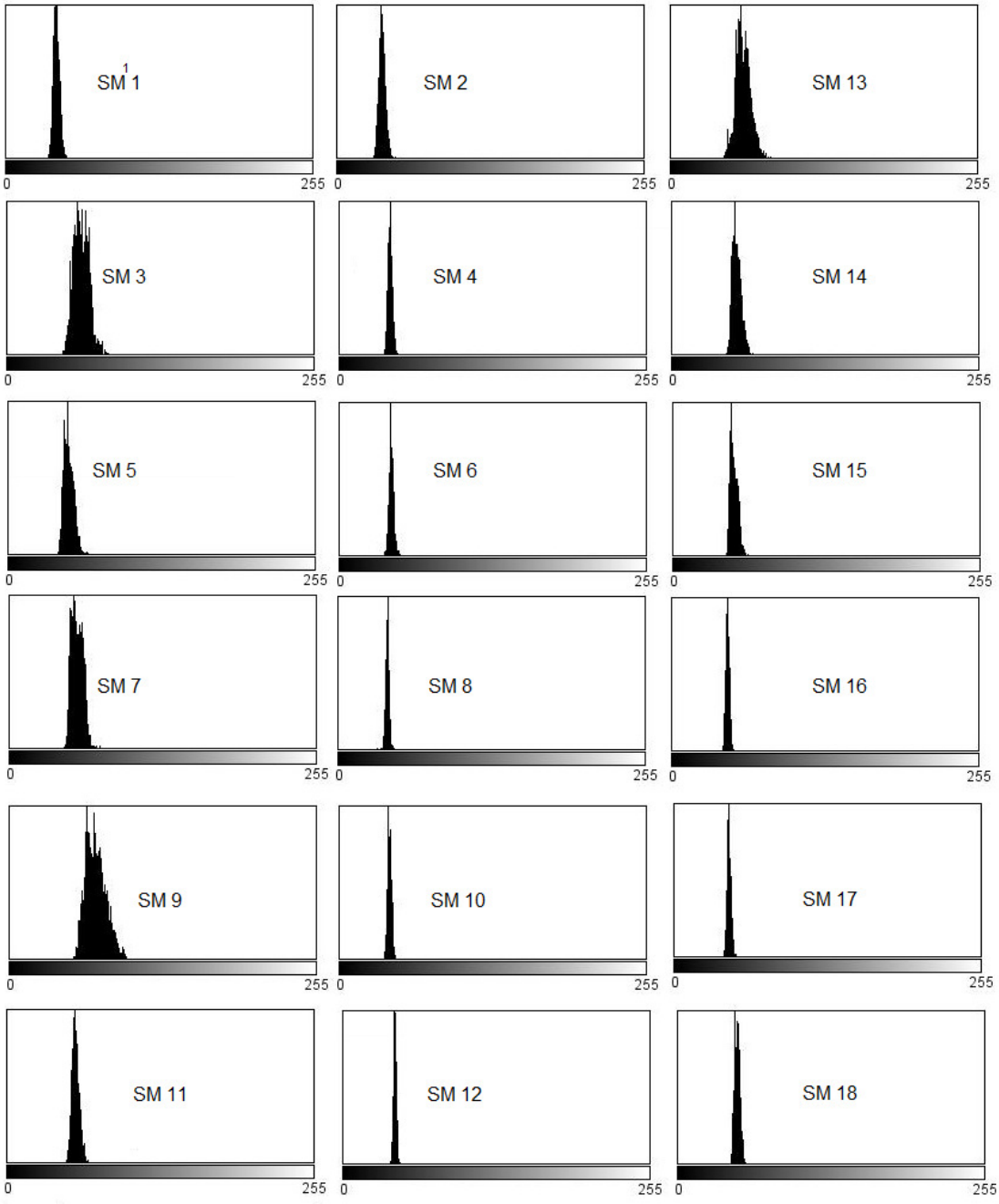

Figure 4.8: Distribution plots of pixels' intensities on a 0-255 greyscale of 18 Selection Maps[5]. The plots were generated using the ImageJ software.

Distribution plots of the 18 selection maps in *Figure 4.8* are moderately skewed but each distribution has a unimodal mode. Unimodal is one of the normal distribution properties (93). Most of the selection map distributions

[5] SM = Selection maps

have skewness values close to zero. A skewness statistic in the range of ±1 is usually acceptable to conclude that the distribution fits a normal distribution pattern (94-95). Therefore, all 18 selection maps are normally distributed.

Table 4.4: The table lists number of pixels, mean intensity of the pixels and its standard deviation, and skewness of the selection maps.

Selection map	Number of pixels	Mean intensity	SD	Skewness
1	2072	41.58	2.66	0.28
2	2724	37.04	2.85	0.34
3	1672	61.40	6.46	0.31
4	2376	41.67	1.99	0.25
5	2638	49.88	4.24	0.58
6	1565	42.71	2.09	0.36
7	1490	55.96	4.84	0.34
8	1310	40.42	1.74	0.29
9	1724	71.41	8.45	0.46
10	1928	41.22	1.77	0.23
11	1650	56.61	3.15	0.41
12	1803	42.72	1.34	0.00
13	2482	60.02	6.28	0.35
14	1690	53.61	3.90	0.83
15	1490	50.24	3.25	0.60
16	1576	45.97	1.64	0.10
17	1444	45.17	1.78	0.32
18	1310	48.96	2.34	0.21

The mean is usually the best measure of the central tendency of normally distributed data (96). In a normal distribution, 68% of the data will lie within ± 1 standard deviations (SD) of the mean.

The intensity of each pixel represents the radioactivity concentration at where the pixel is located on planar image. Standard deviation of pixels values are small (Table 4.4) for most parts of the phantom during three independent charging with ^{99m}Tc. Therefore, the ^{99m}Tc concentration was quite uniformly distributed within one piece in the lung phantom for a particular part charged with ^{99m}Tc. Uniform distribution of the ^{99m}Tc is expected only within a particular part (within a selection map) of the phantom. Uniform distribution of ^{99m}Tc are not expected the same pixel value (apparent activity) for different parts (different selection maps) of the phantom, as they are different in shape and can have different uptake of ^{99m}Tc.

4.5 Anatomical properties

Quality control and quality assurance measurement programs used in clinical practice are optimal when they mimic the complete medical imaging process including interpretation of the images by a radiologist (16, 98).

Anthropomorphic phantoms are able to provide physical representations and attenuation properties of human anatomy in nuclear medicine studies. These phantoms are designed to radiologically mimic body components (shape) and materials composition (structure) (99-100). In this thesis, a reusable semi-anthropomorphic lung phantom comprising anatomically

correct lung structure was developed. The term ‘semi’ was used because the breathing (ventilation) dynamics of the human lung was not considered while developing the phantom.

Three lung perfusion defect conditions (Clinical condition 1; Clinical condition2; and Clinical condition 3) were simulated using the anatomical lung phantom. The first clinical condition was lung perfusion without deficiency; the second clinical condition was lung perfusion with the left lung upper lobe apical-posterior deficiency; and the third clinical condition was lung perfusion with the right lower lobe lateral basal deficiency. The lung phantom was scanned at six planar views. These planar images are shown in *Figure 4.9*.

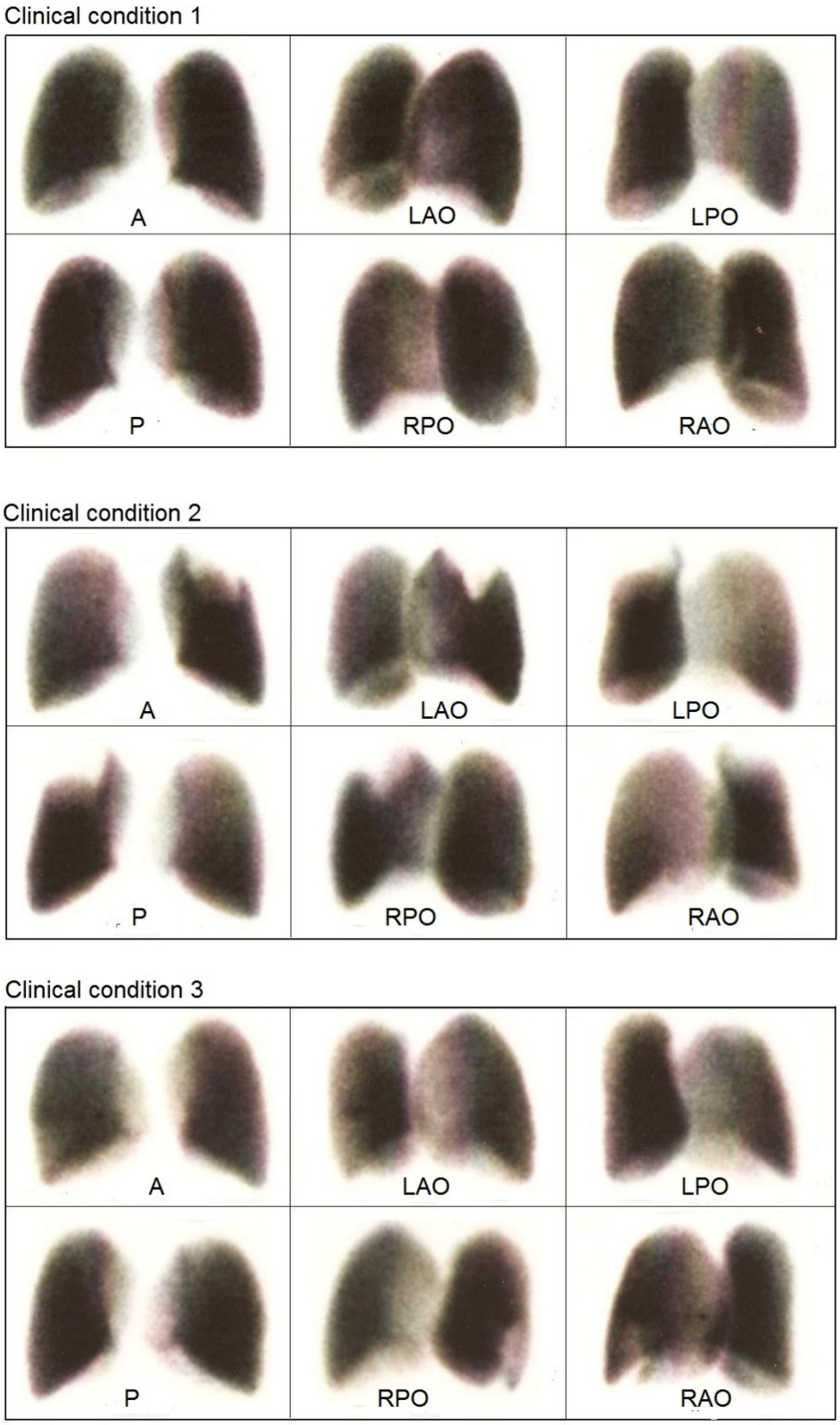

Figure 4.9: Lung perfusion images of three clinical conditions simulated using the lung phantom. Six planar views were acquired for each scan.

Clinical condition 1 = lung perfusion without deficiency; Clinical condition 2 = lung perfusion with the left lung upper lobe apical-posterior deficiency; and Clinical condition 3 = lung perfusion with the right lower lobe lateral basal deficiency.

A close-ended Likert-scale survey (see Appendix A) was conducted to gauge the image quality of the planar perfusion images generated using the phantom. Ten Nuclear Medicine physicians from various institutions[6] participated in the study. The survey was conducted on a paper-based format and on an online-based format[7]. Participants were required to score each question with a suitable score value as listed in *Table 4.5*. The score values are the same as used by Heikkinen et al. in their published article (101). The questions of the questionnaire survey are as listed in *Table 4.6*.

[6] The institutions are: Wollongong Hospital, Australia, St Vincent's Private Hospital, Australia, Peter McCallum Cancer Care Centre, Australia, Theranostics Centre for Molecular Radiotherapy and Molecular Imaging, Germany, Hospital Universiti Sains Malaysia, Malaysia, Hospital Kuala Lumpur, Malaysia, and Pusat Perubatan Universiti Malaya, Malaysia.

[7] http://booroo.com/app/rendersurvey.asp?sid=bj5jya9iebg5xg031784

Table 4.5: The Likert-scale score values of the quality of planar perfusion images generated using the anatomical lung phantom

Score	Image quality	Specification
1	Poor	Not adequate for clinical application.
2	Average	Barely adequate for limited clinical application.
3	Satisfactory	Adequate for clinical but not for exact scientific application.
4	Good	Adequate for clinical and exact scientific application.
5	Excellent	Excellent for clinical and scientific application.

Table 4.6: List of questions incorporated in the questionnaire survey

Number	Question
Question 1	How well do the lung perfusion images sets (*Figure 4.9*) represent actual **anatomical orientation** of a lung perfusion planar image set of a suspected PE patient with the indicated clinical condition?
Question 2	How well do the lung perfusion image sets (*Figure 4.9*) represent actual **anatomical location** of a lung perfusion planar image set of a suspected PE patient with the indicated clinical condition?
Question 3	How well do the lung perfusion image sets (*Figure 4.9*) represent actual **anatomical shape** of a lung perfusion planar image set of a suspected PE patient with the indicated clinical condition?

According to Jamieson, Likert-type rating scales fall within the ordinal level of measurement (102). The median or mode shall be used as a 'measure of central tendency' of ordinal data (102). Therefore, mode scores were chosen as a measure of central tendency' in this part of the study. The mode scores of the study are shown in *Figure 4.10*.

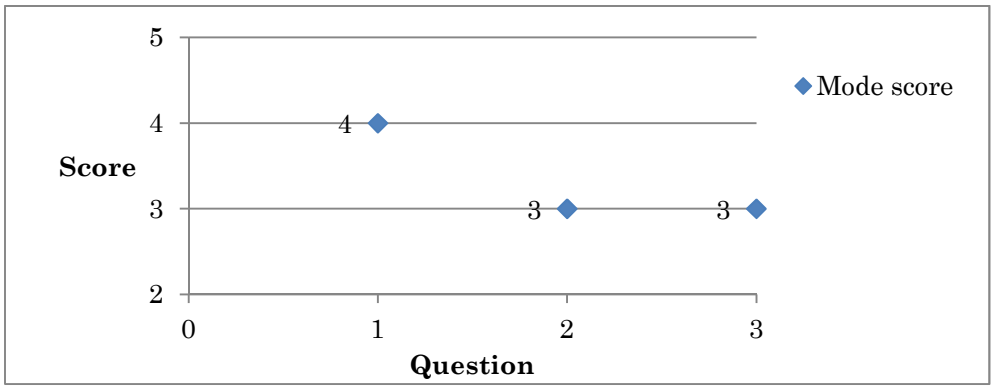

Figure 4.10: The chart shows the mode scores of the image quality of lung images in Figure 4.9.

A small sample size (SS=10) generates a large margin of error (104-105). Certainly, the statistical power of the study is low. Nevertheless, the survey results provide a valuable snapshot of Nuclear Medicine physicians' perspective of the lung phantom. The project was not aimed to be conducted as clinical trials with enrolment of large number of Nuclear Medicine physicians. The study was conducted to investigate the quality of end products of the phantom (lung scan images). Completion of the survey indicates that Nuclear Medicine physicians are able to identify lung perfusion defects modelled using the phantom.

The mode scores were used to summarise the central tendency of responses in this study. The higher the mode score (MS), the better quality is the lung perfusion image set. It must be noted that results are more likely to contain bias data as a result of using small a sample size.

The mode score of Question 1 was calculated based on the Nuclear Medicine physicians' responses to the **anatomical orientation** of the planar perfusion Clinical condition 1 image set; the planar perfusion Clinical condition 2 image set; and the planar perfusion Clinical condition 3 image set. The result of this question defines the ability of the anatomical lung phantom to simulate the exact anatomical orientation of lung perfusion scans of patients suspected having pulmonary embolism. The mode score, MS, was 4 on a scale of 1 (poor) to 5 (excellent). The mode score shows that the anatomical orientation of planar images generated using the phantom are at high quality to be used for clinical studies or for scientific studies.

The mode score of Question 2 was calculated based on the Nuclear Medicine physicians' responses to the **anatomical location** of the planar perfusion Clinical condition 1 image set; the planar perfusion Clinical condition 2 image set; and the planar perfusion Clinical condition 3 image set. The result of this question defines the ability of the anatomical lung phantom to simulate the accurate **anatomical location** of a particular lung perfusion deficiency. The mode score, MS, was 3 on a scale of 1 (poor)

to 5 (excellent). The mode score shows that the quality of anatomical location of a particular lung perfusion deficiency event (cold spot) simulated using the phantom is at medium quality to be used for clinical studies or for scientific studies.

The Question 3 mode score was calculated based on the Nuclear Medicine physicians' responses to the **anatomical shape** of the planar perfusion Clinical condition 1 image set; the planar perfusion Clinical condition 2 image set; and the planar perfusion Clinical condition 3 image set. The shapes shall resemble planar perfusion scan images of patients suspected with pulmonary embolism. The mode score, MS, was 3 on a scale of 1 (poor) to 5 (excellent). The mode score shows that the anatomical shapes of planar perfusion images simulated using the phantom are at medium quality to be used for clinical studies, not for exact scientific studies.

4.6 Reproducibility

Accuracy and reproducibility are very important characteristics of phantoms used for clinical studies (106). One of the thesis goals was to evaluate the reproducibility of lung perfusion images generated using the anatomical lung phantom. To do this, three lung perfusion defect conditions were simulated using the phantom. The first condition (Condition 1) was lung perfusion without deficiency; the second condition (Condition 2) was lung perfusion with the left lung upper lobe apical-

posterior deficiency; and the third clinical condition (Condition 3) was lung perfusion with the right lower lobe lateral basal deficiency. Three planar perfusion scans were acquired for each condition, allowing repetition. Repetition of the acquisition allows a comparison to be made between planar perfusion image sets having the same lung perfusion condition. All planar images are shown in Figure 4.11 to Figure 4.13.

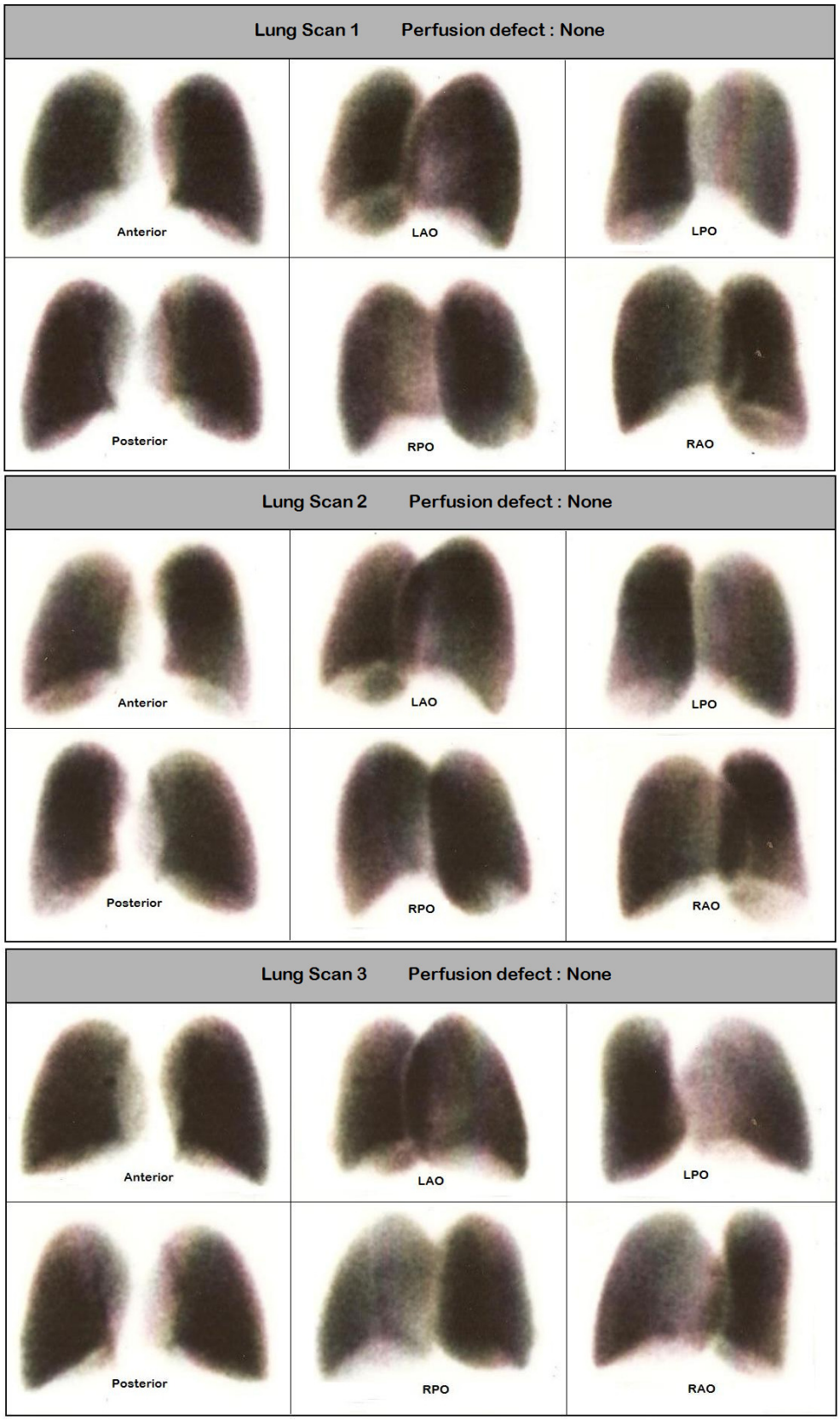

Figure 4.11: Three lung perfusion scans of lung perfusion Condition 1. Each scan was acquired independently.

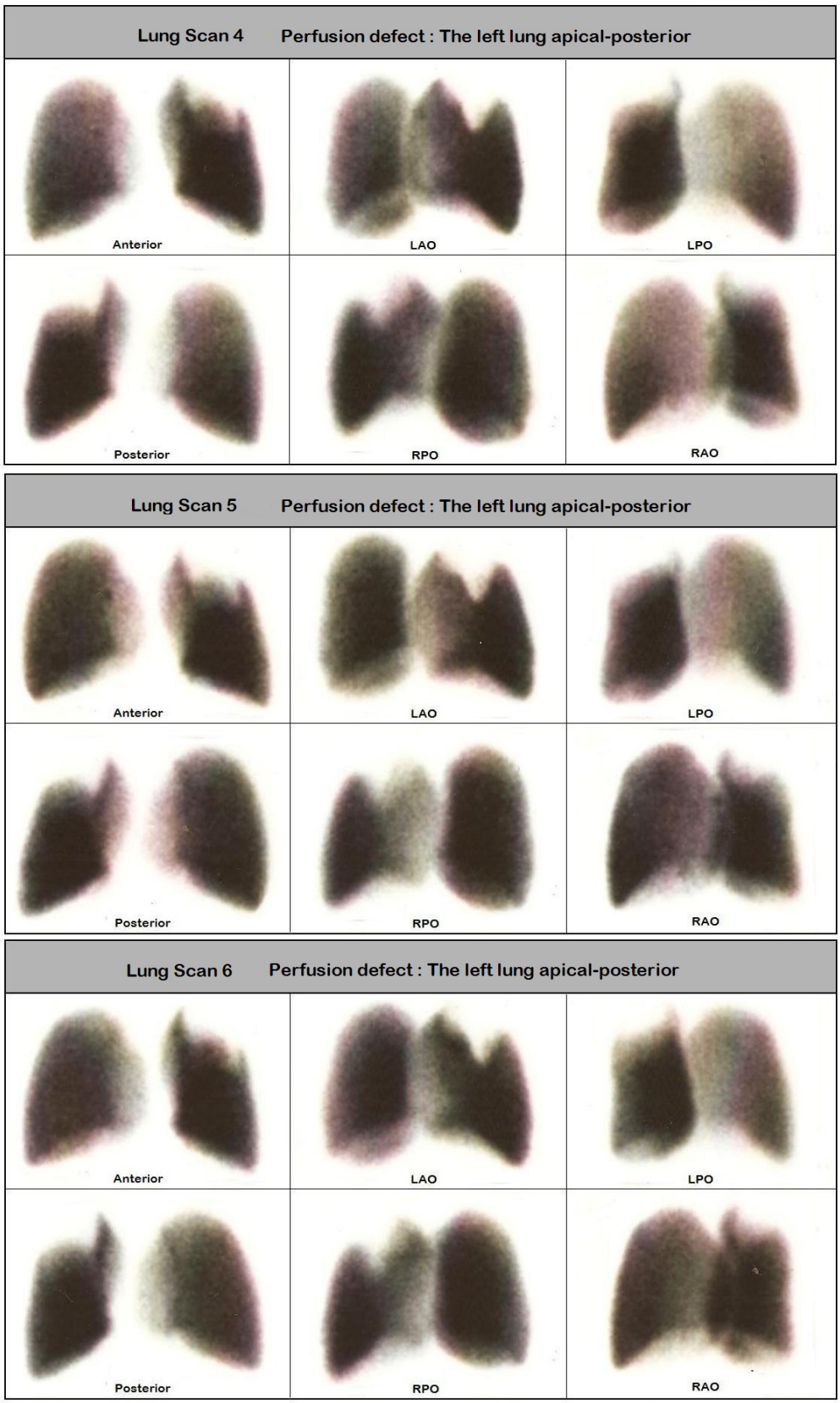

Figure 4.12: Three lung perfusion scans of lung perfusion Condition 2. Each scan was acquired independently.

Figure 4.13: Three lung perfusion scans of lung perfusion Condition 3. Each scan was acquired independently.

A close-ended Likert-scale (see Appendix B) survey was conducted to study the reproducibility quality of the planar perfusion images generated using the phantom (*Figure 4.11* to *Figure 4.13*). Participants of the survey were required to rate the reproducibility quality of the phantom based on the ranking scales in Table 4.7. The score values were re-modelled score values as used by Heikkinen et al. in their published article (101). The results are shown in *Figure 4.14*. Ten Nuclear Medicine physicians from various institutions[8] participated in this study. The survey was conducted on a paper-based format and on an online-based format[9].

Table 4.7: The Likert-scale score values of reproducibility quality of planar perfusion images generated using the anatomical lung phantom

Score	Image quality	Specification
1	Poor	The results show an inadequate reproducibility standard of lung perfusion imaging.
2	Average	The results show an acceptable reproducibility standard of lung perfusion imaging.
3	Satisfactory	The results illustrate an adequate reproducibility standard of lung perfusion imaging.
4	Good	The results show a precise reproducibility standard of lung perfusion imaging.
5	Excellent	The results show an outstanding reproducibility quality of lung perfusion imaging.

[8] The institutions are: Wollongong Hospital, Australia, St Vincent's Private Hospital, Australia, Peter McCallum Cancer Care Centre, Australia, Theranostics Centre for Molecular Radiotherapy and Molecular Imaging, Germany, Hospital Universiti Sains Malaysia, Malaysia, Hospital Kuala Lumpur, Malaysia, and Pusat Perubatan Universiti Malaya, Malaysia.

[9] http://booroo.com/app/rendersurvey.asp?sid=bj5jya9iebg5xg031784

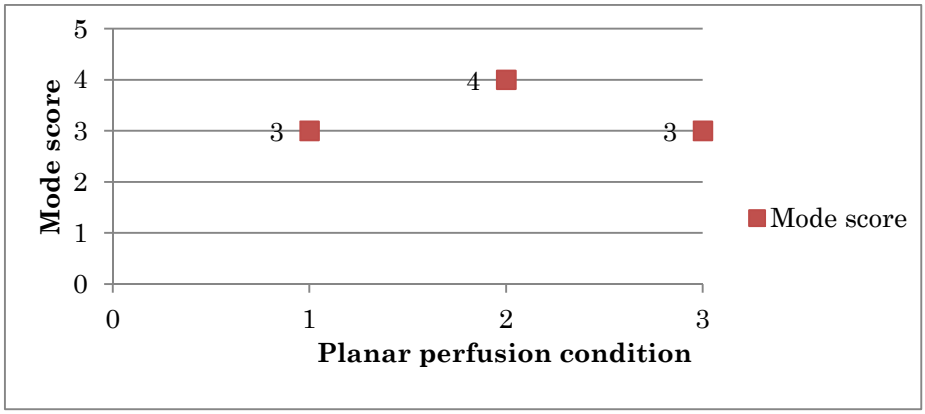

Figure 4.14: The chart shows mode scores of the reproducibility questionnaire survey's results.

As discussed earlier (see Section 4.5), according to Jamieson, Likert-type rating scales fall within the ordinal level of measurement (102). Median or mode shall be used as a 'measure of central tendency' of ordinal data (102). Therefore, mode scores were chosen as a 'measure of central tendency' in this part of the study.

The higher the mode score (MS), the better the quality of the lung perfusion image set. Thus, a 'poor' statement is responding to an unfavourable reproducible quality and an 'excellent' statement is responding to a favourable reproducible quality. The participants were required to score the five points Likert-style questions on scale 1 (poor) to 5 (excellent). Sample size, SS = 10 is acceptable in this study as it was not conducted as clinical trials with enrolment of large number of Nuclear Medicine physicians. The survey was conducted with aim to investigate

Nuclear Medicine physicians' overview of reproducibility quality of the phantom.

The reproducibility is an important criteria used to quantify the degree that the repeated acquisition process produced identical results (i.e., planar perfusion images). The phantom reproducibility quality is medium (MS = 3) when it was used to generate three planar perfusion image sets with Condition 1. The reproducibility quality is above medium-to-nearly high (MS = 4) when it was used to simulate three planar perfusion image sets with Condition 2. The phantom reproducibility quality is medium (MS = 3) when it was used to generate three planar perfusion image sets with Condition 3. As a conclusion, the anatomical lung phantom was able to reproduce planar perfusion images at the least in medium reproducibility quality.

5. QUALITY ASSURANCE STUDY

In this chapter, the study's findings were presented in a journal article format. Two manuscripts were prepared using materials from this chapter. The two manuscripts entitled: '*The use of revised PIOPED criteria in reporting probability of PE of phantom's generated planar perfusion images*'; and '*Interpretation of mismatch defect size of phantom-generated planar lung perfusion images by Nuclear Medicine physicians,* are currently under review by two peer reviewed journals.

5.1Abstract

Quality assurance in nuclear medicine imaging is essential to ensure a reliable imaging diagnosis. Nuclear Medicine physicians' interpretation of medical images must be of a consistently high quality as physicians make initial treatments on the basis of the imaging interpretation.

In this work, a quality assurance study was conducted to assess diagnostic accuracy in suspected PE by Nuclear Medicine physicians based on the revised Prospective Investigation of Pulmonary Embolism Diagnosis (PIOPED) criteria. An anatomical lung phantom with 18 separable lung perfusion inserts manufactured at the University of Wollongong, NSW was used to model lung perfusion images of patients suspected with pulmonary embolism. A blinded quality assurance test was conducted to compare

Nuclear Medicine physicians' interpretations of the acquired lung perfusion images. Ten Nuclear Medicine physicians participated in study. Each acquired planar lung perfusion image set containing one or more segmental defects. There were a number of incorrect diagnoses made by the Nuclear Medicine physicians. The interpretation criteria have thin probability borderlines (low probability borderline *to* intermediate probably borderline *to* high probability borderline) of PE. Nuclear Medicine physicians are more cautious when interpreting lung perfusion and ventilation scans that fall close to these borderlines.

Keywords: Lung perfusion, Quality assurance, Pulmonary Embolism.

5.2Introduction

Overview

The lung perfusion and ventilation scans is one of many diagnostic imaging methods available for use in PE management (107). Lung perfusion and ventilation planar imaging remains a significant pathway in PE management in many nuclear medicine departments (26, 57, 107-109), as it is considered less expensive than other methods (110).

PE is not always diagnosed because the condition can cause vague and non specific symptoms (111). Mountain et al. reports that many Nuclear Medicine physicians express a fatalistic approach managing pulmonary embolism. At Mountain et al. institution, less than 50% of 400 reviewed cases had a definitive diagnosis, with each case diagnosed after an initial PE test (112). In their article, the authors reported that complete investigations to confirm or exclude the PE diagnosis often do not occur. The authors also stated that over three decades 70% of patients who died of PE were misdiagnosed (112).

Quality assurance in medical imaging is implemented to ensure that radiology examinations are appropriate, that necessary image is obtained, that the correct interpretation is made, and that radiation cost and exposure are minimal (113). A quality assurance program depends on all members of the facility staff: imaging physician; medical physicist;

technologist; clerical personnel; nurses and other employees (114). Testing of misinterpretation of medical images has been suggested as part of the medical imaging quality assurance process (115).

Magnussen et al., reported in their article that there are limited investigations carried out to study the accuracy of lung scintigraphy interpretation (116). In the article, they reported that the accuracy of lung scan reporting is a difficult goal to achieve in vivo because a real gold standard for this does not exist (116). They have created a virtual scintigraphic model of the segmental anatomy of the human lungs. The model has precise defect size and location. The model was used a tool to investigate accuracy and intraobserver agreement in reporting lung scintigraphy defect size (116).

A study was conducted to evaluate the accuracy of Nuclear Medicine physicians' sensitivity:

1. to the number of mismatch defects present on lung scans;
2. to the size of mismatch defects according to the revised PIOPED criteria;
3. to probability of PE according to the revised PIOPED criteria.

The revised PIOPED criteria

A European Association of Nuclear Medicine (EANM) report suggested that interpretation of lung V/Q SPECT and lung V/Q planar images should

be based on: basic reference criteria, experience of the interpreter according to the principle of "Gestalt" (62) and pretest probability with the principle of Holistic interpretation (54). There are a number of lung perfusion and ventilation planar interpretation reference criteria sets: the revised PIOPED criteria (59-60), the Hull criteria (61) and the Gestalt interpretation (62). In Gestalt interpretation, expert Nuclear Medicine physicians interpret lung scans accurately based on their experience (62). The Hull criteria and the revised PIOPED criteria have major differences in terms criteria to classify probability of PE. In this study, the revised PIOPED criteria was used to study Nuclear Medicine physicians' interpretations of lung perfusion scans for PE diagnosis. The revised PIOPED criteria are presented as a summary in *Table 5.1*.

Table 5.1: The revised PIOPED criteria(59-60).

High probability	≥ 2 large[10] mismatch defects
	or
	1 large mismatch defect and ≥2 moderate mismatch defects
	or
	≥ 4 moderate[11] mismatch defects
Intermediate probability	1 large mismatch defect ± 1 moderate mismatch defect
	or
	1-3 moderate mismatch defects
	or
	1 mismatch defect with normal X-ray[12]
Low probability	≥ 1 perfusion defect (match defect) with «[13] X-ray defect
	or
	Perfusion defects due to pleural effusion, cardiomegaly, enlarged aorta, hilum, mediastinum and elevated diaphragm.
	or
	≥ 1 small[14] perfusion defect with normal X-ray
	or
	≥ 2 mismatch defects with normal X-ray and some areas of normal perfusion in lung
Normal probability	No perfusion defect. Perfusion outlines exactly the shape of the lung as seen on the chest radiograph.

Quality assurance: Size of V/Q mismatch defect

The size of V/Q mismatch defects is used within the revised PIOPED interpretation criteria to assess the probability of pulmonary embolism. According to the criteria, the size of mismatch defects are classified as

[10] Large = mismatch defect ≥ 75% of a bronchopulmonary segment volumetric size
[11] Moderate = mismatch defect = 25% to 75% of a bronchopulmonary segment volumetric size
[12] X-ray = Radiographic abnormality in region of perfusion abnormality
[13] « = with a lot less
[14] Small = mismatch defect ≤ 25% of bronchopulmonary segment volumetric size

small (<25% of a bronchopulmonary segment), moderate (25%-75% of a bronchopulmonary segment), or large (>75% of a bronchopulmonary segment). In the revised PIOPED criteria, a single large defect is considered as one segmental mismatch defect; a single moderate defect is equivalent to 0.5 segmental mismatch defect (60, 117). The segmental equivalent of any mismatch defects is an important concept in the revised PIOPED criteria. Any size of mismatch defects are added together to increase the probability of PE (118).

The PIOPED investigator team reported majority of patients with PE do not have high probability lung scans (119). A reason for that might be underestimate size of mismatch defects by interpreter while reading lung scans (120). The revised PIOPED criteria is a little complicated to use as certain bronchopulmonary segments are smaller (in term of volumetric size) than others. All bronchopulmonary segments of the left lung and the right lung are not equal in size (volumetric) (121). The size of mismatch defects on lung scans may not be consistent to true bronchopulmonary segments' natural size (120). Therefore, a mismatch defect that has been interpreted as a small mismatch defect might in fact being one large mismatch defect, or vice versa.

Quality assurance: Probability of pulmonary embolism

It is essential to accurately confirm or exclude the diagnosis of PE in its management. This has been reportedly missing in PE diagnosis via lung

scintigraphy because the method does not exclude or confirm the diagnosis of PE in the majority of suspected patients (122). Murchison et al. stated in their published article that several studies have shown that there are a significant number of lung scintigraphy scans (39% in the PIOPED study) where PE is either diagnosed or excluded (123). In the revised PIOPED criteria, number of present mismatches defects has a significant impact on the probability of pulmonary embolism. As the number of present mismatch defects increase, the probability of PE increases accordingly (refer the revised PIOPED criteria) (60).

5.3Materials and methods

Quality assurance: Size of mismatch defect

A similar study as published by Magnussen et al., (116, 124) was conducted. The purpose of this study was to evaluate the Nuclear Medicine physician diagnosis interpretations of mismatch defect size according to the revised PIOPED criteria. In this study, different materials and methods were employed compared to the study published by Magnussen et al.

In this study, an anatomical lung phantom was used to generate lung perfusion images (48). The phantom was specially designed to model lung perfusion defects circumstances depicted in lung perfusion scans. The phantom consists of two lung cavities; and 18 perfusion defect inserts (48). The perfusion defect inserts are complete bronchopulmonary segments of

the human lungs. These inserts were employed as perfusion defects; simulating perfusion absence in lung perfusion scans. The manufactured phantom is able to simulate segmental lung perfusion deficiencies (vascular segmental deficiencies) depicted in a typical lung perfusion scan of patients with suspected pulmonary embolism.

Additional perfusion defect inserts with size 25-75% of a bronchopulmonary segment were manufactured for this study. The additional perfusion defect inserts were manufactured using the same negative moulds (refer section 3.5) created to manufacture the initial perfusion defect inserts. Each mould was filled with water to identify its volume in millilitre. The moulds were then filled with polyester resin up to 25-75% of its volumetric capacity, created perfusion defect inserts with size 25-75% of a bronchopulmonary segment.

To generate planar lung perfusion images, a perfusion defect insert was fitted into the lung phantom. Next, an appropriate activity (approximately 40-50 MBq) of ^{99m}Tc solution was added into the assembled phantom. Then, the phantom was scanned using planar imaging. The planar perfusion was acquired at the 140 keV photopeak. In each planar scan, six planar views were acquired in a 256 x 256 matrix: anterior (A), posterior (P), left anterior oblique (LAO), left posterior oblique (LPO), right posterior oblique (RPO) and right anterior oblique (RAO). The planar perfusion image set

was then printed on a film. Then, the phantom was disassembled-then-assembled to prepare it for another planar scan.

Six perfusion defects at varied sizes were modelled using the anatomical lung phantom with planar imaging. The lung perfusion defect images generated using the phantom were assumed as V/Q mismatch defects as depicted in lung scintigraphy. The lung scans that were presented to the Nuclear Medicine physicians are shown in *Figure 5.1*. The six planar perfusion events are:

1. **Embolic event 1:** Moderate mismatch defect within the right lung upper lobe posterior segment.
2. **Embolic event 2:** Moderate mismatch defect within the left lung lower lobe posterior basal segment.
3. **Embolic event 3:** Moderate mismatch defect within the left lung lower lobe lateral basal segment.
4. **Embolic event 4:** Large mismatch defect within the left lung lower lobe superior segment.
5. **Embolic event 5:** Large mismatch defect within the left lung upper lobe anterior segment.
6. **Embolic event 6:** Large mismatch defect within the left lung upper lobe lingular superior segment.

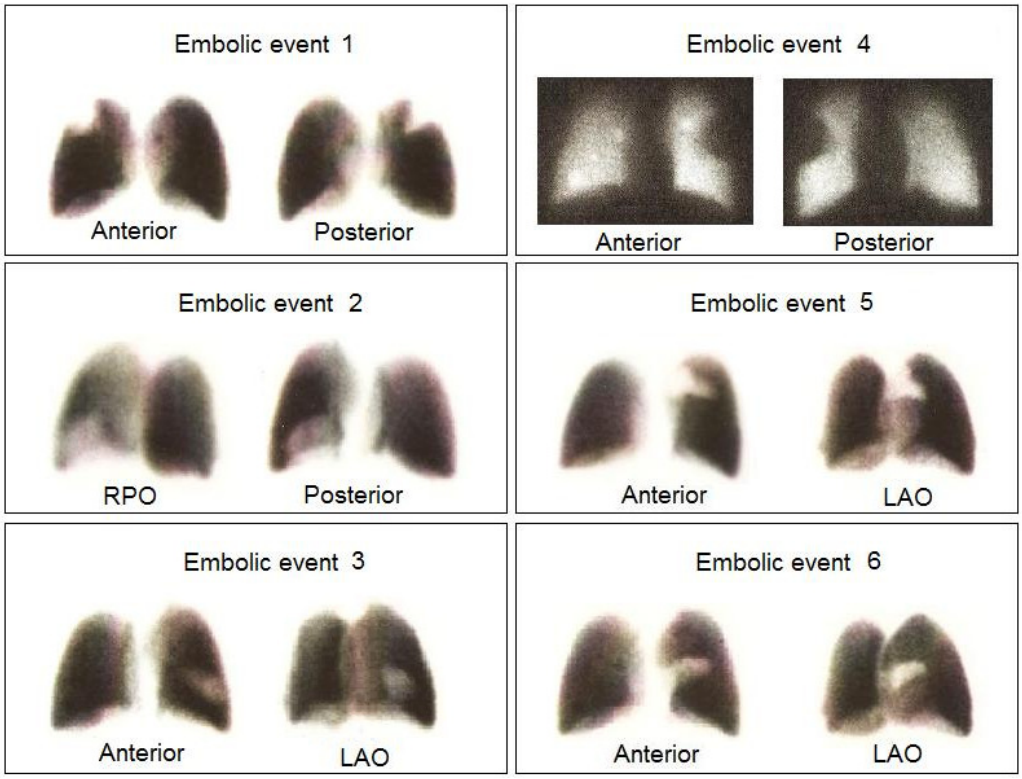

Figure 5.1: Lung perfusion images of six embolic events modelled using the anatomical lung phantom.

A blind test (see Appendix C) was conducted to compare Nuclear Medicine physicians' interpretations of mismatch defects' size on the planar lung perfusion images. All of the obtained images were presented to ten experienced Nuclear Medicine physicians. Details of the mismatch defects were not disclosed to the physicians. The physicians were asked to categorise the mismatched defects based on its size; **i** small (<25% of a bronchopulmonary segment); **ii** (25-75% of a bronchopulmonary segment); or **iii** (>75% of a bronchopulmonary segment). These are the categories used in the revised PIOPED criteria (59-60, 119).

Quality assurance: Probability of pulmonary embolism

The anatomical lung phantom was also used to model lung perfusion images for this quality assurance test (48). A blind test (see Appendix D) was conducted to study the accuracy of Nuclear Medicine physicians' interpretations of lung perfusion scan for PE diagnosis using the revised PIOPED criteria. Six lung perfusion conditions were modelled using the anatomical lung phantom with planar imaging. The planar perfusion images of C 1 – C 6 are shown in *Figure 5.2*. There perfusion conditions are:

1. **C 1:** Lung perfusion defect within the left lung upper lobe anterior segment (large defect).
2. **C 2:** Lung perfusion defect within the left lung upper lobe anterior segment (large defect) and lingular inferior segment (large defect).
3. **C 3:** Lung perfusion defect within the right lung upper lobe lateral segment (large defect) and posterior segment (moderate defect).
4. **C 4:** Lung perfusion defect within the left lung lower lobe lateral basal segment (large defect).
5. **C 5:** Lung perfusion defect within the right lung upper lobe anterior segment (large defect);
6. **C 6:** Lung perfusion defect within the whole right lung upper lobe.

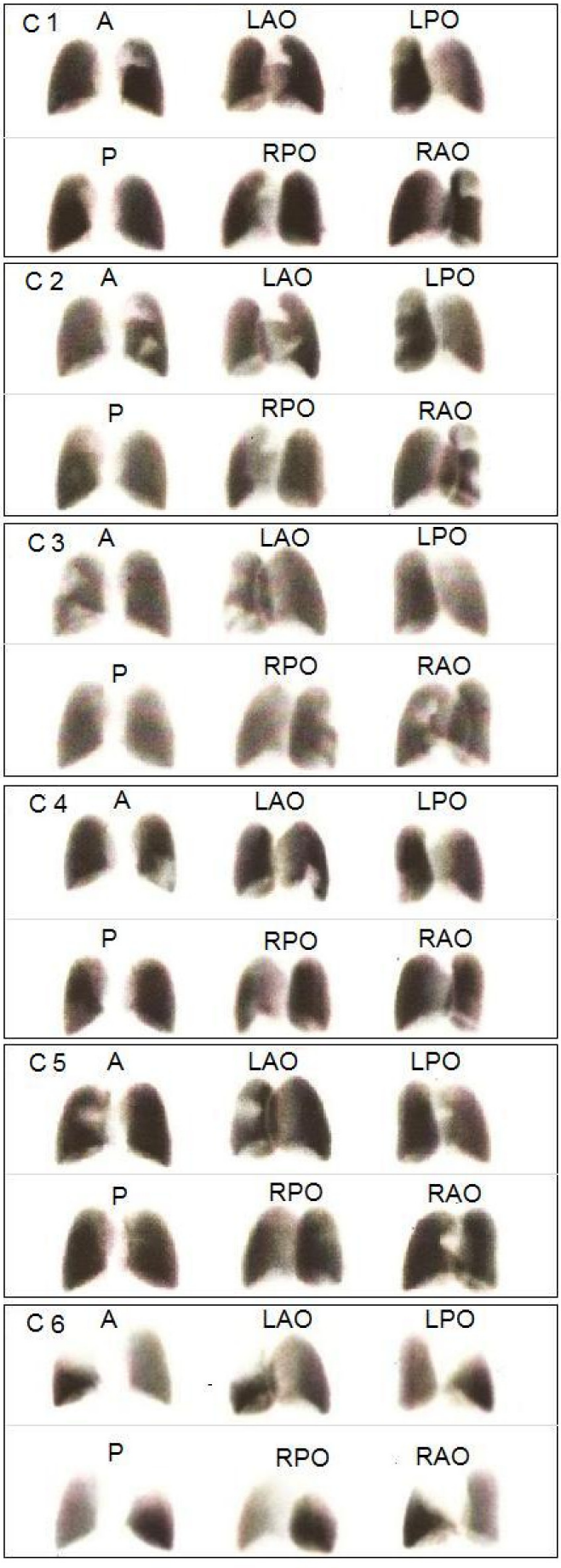

(caption is on the next page)

Figure 5.2: Planar images show lung perfusion defects image sets of six embolic events. All lung perfusion defects were assumed mismatch defects. The lung scans were acquired at six planar projections: anterior (A); posterior (P); left anterior oblique (LAO); left posterior oblique (LPO); right posterior oblique (RPO); and right anterior oblique (RAO).

The perfusion defect inserts used to model segmental defects are components of the lung phantom (48). Nuclear Medicine physicians were informed that all the visible lung perfusion defects were in fact V/Q mismatch defects associated with a normal X-ray (in the region of perfusion abnormality). Other information regarding the lung perfusion image sets were not provided to the Nuclear Medicine physicians. The physicians were given: **i** six lung perfusion image sets; **ii** the revised PIOPED criteria; and **iii** an answer sheet. The answer sheet (see *Figure 5.3*) contains series of questions with empty spaces to be filled by the physicians. The answer sheet provided in this chapter is a simplified version of the answer sheet provided to the physicians. The physicians were instructed to fill in the answer sheet based on: **i** the revised PIOPED criteria; and **ii** their experience as Nuclear Medicine physicians. There were ten Nuclear Medicine physicians from various institutions[15] involved

[15] The institutions are: Wollongong Hospital, Australia, St Vincent's Private Hospital, Australia, Peter McCallum Cancer Care Centre, Australia, Theranostics Centre for Molecular Radiotherapy and Molecular Imaging, Germany, Hospital Universiti Sains Malaysia, Malaysia, Hospital Kuala Lumpur, Malaysia, and Pusat Perubatan Universiti Malaya, Malaysia.

in this study. The study was conducted on a paper-based format and on an online-based format[16].

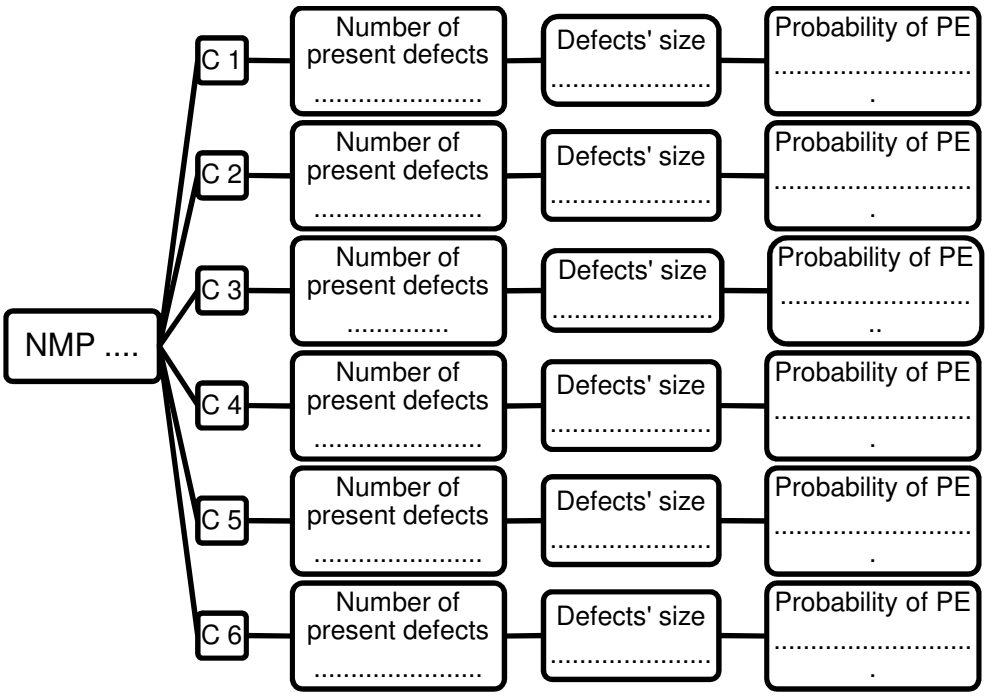

Figure 5.3: The horizontal hierarchy shows the blind test's answer sheet. Nuclear Medicine physicians were required to report: ***i*** *number of visible mismatch defects on each embolic event;* ***ii*** *size the mismatch defects based of the PIOPED criteria; and* ***iii*** *probability of PE based on the revised PIOPED criteria. PE = pulmonary embolism; and NMP = nuclear medicine physician.*

5.4 Results

Quality assurance: Size of V/Q mismatch defect

[16] http://booroo.com/app/rendersurvey.asp?sid=bj5jya9iebg5xg031784

The planar views selected for the study were selected at where the mismatch defects are at its largest (120). The physicians were informed that lung perfusion defects (see *Figure 5.1*) generated using the phantom were assumed as V/Q mismatch defects. The results of the blind test are listed in *Table 5.2*.

Table 5.2: This table lists Nuclear Medicine physicians' answers to the blind test study. The physicians were asked to categorise the mismatch defects size in Figure 5.1 according to the revised PIOPED (59-60, 119) criteria.

	EE[17] 1	EE 2	EE 3	EE4	EE5	EE 6
EE actual size	Moderate	Moderate	Moderate	Large	Large	Large
NMP[18] 1	Moderate	Large	Moderate	Large	Moderate	Large
NMP 2	Moderate	Large	Moderate	Moderate	Small	Moderate
NMP 3	Large	Large	Moderate	Large	Large	Moderate
NMP 4	Moderate	Moderate	Moderate	Large	Moderate	Small
NMP 5	Moderate	Moderate	Moderate	Large	Large	Large
NMP 6	Moderate	Moderate	Moderate	Large	Large	Moderate
NMP 7	Moderate	Large	Moderate	Large	Moderate	Moderate
NMP 8	Large	Large	Moderate	Large	Moderate	Large
NMP 9	Large	Large	Moderate	Large	Moderate	Small
NMP 10	Moderate	Moderate	Moderate	Moderate	Large	Moderate

The planar perfusion scans of Embolic event 1, Embolic event 2, and Embolic event 3 were repeated with defects equal to 100% of a single bronchopulmonary segment. This was done to give readers a clear view on how size of perfusion defect affects the scan outcome (planar perfusion images). The comparison of perfusion defects' size of Embolic event 1,

[17] EE = Embolic Event
[18] NMP=Nuclear Medicine physician's answer

Embolic event 2, and Embolic event 3 are shown in *Figure 5.4*. Please note, in this study, *Figure 5.4* was not presented to the Nuclear Medicine physicians.

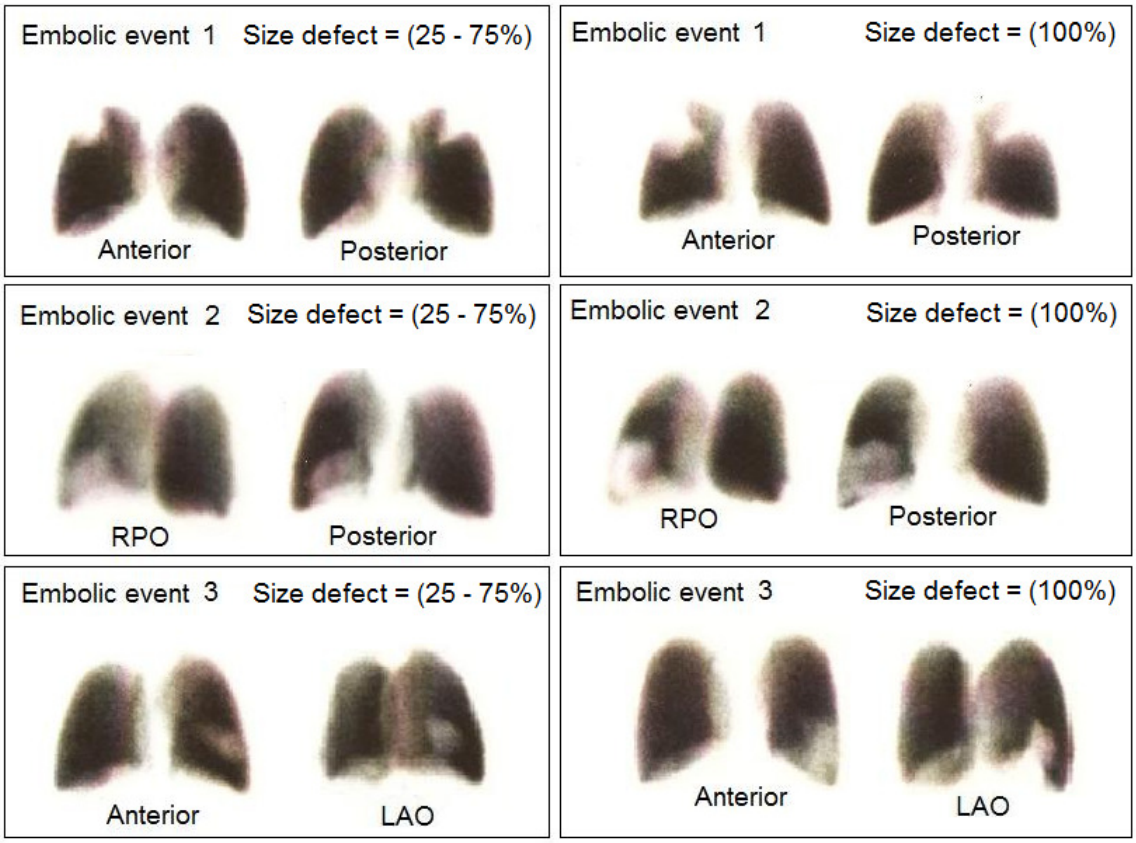

Figure 5.4: Lung perfusion images of Embolic event 1, Embolic event 2, and Embolic event 3, were simulated twice: at moderate size; and at large size (for the benefit of the reader). The first column contains lung perfusion images with moderate size defects according to the revised PIOPED criteria (25-75% of a bronchopulmonary segment). The second column contains lung perfusion images with large size defects according to the revised PIOPED criteria (>75% of a bronchopulmonary segment).

Quality assurance: Probability of pulmonary embolism

Each planar perfusion image set in *Figure 5.2* contains one or more segmental perfusion defects. The answers to the blind test questions were summarised, shown in *Figure 5.5*.

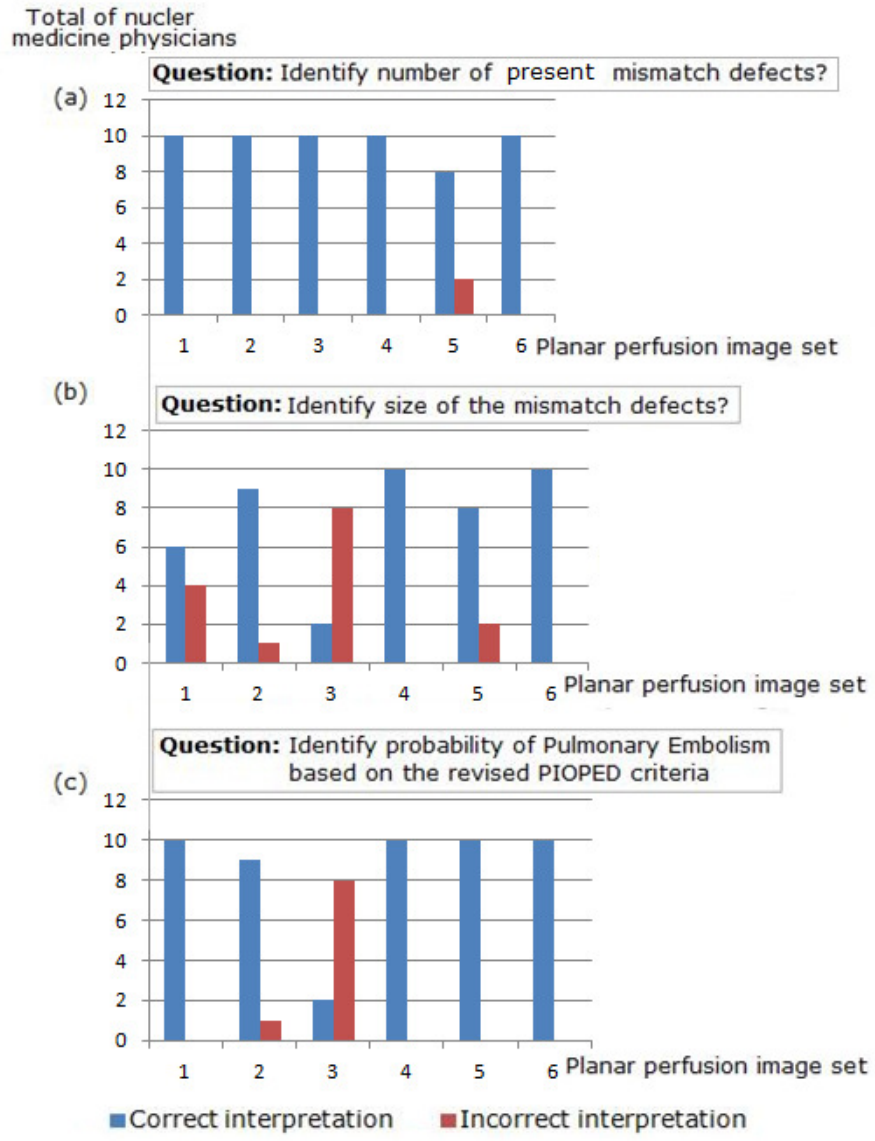

Figure 5.5: Number of Nuclear Medicine physicians that have made correct and incorrect interpretation on: ***i*** *number of present mismatch defects;* ***ii*** *size of mismatch defects; and* ***iii*** *probability of PE on based on the revised*

PIOPED criteria. The bar charts were created based on the nuclear physician answers to the blind test questions.

5.5 Discussion

Quality assurance: Size of mismatch defect

The accuracy of mismatch defect size categorisations by the physicians were summarised, shown in *Figure 5.6*.

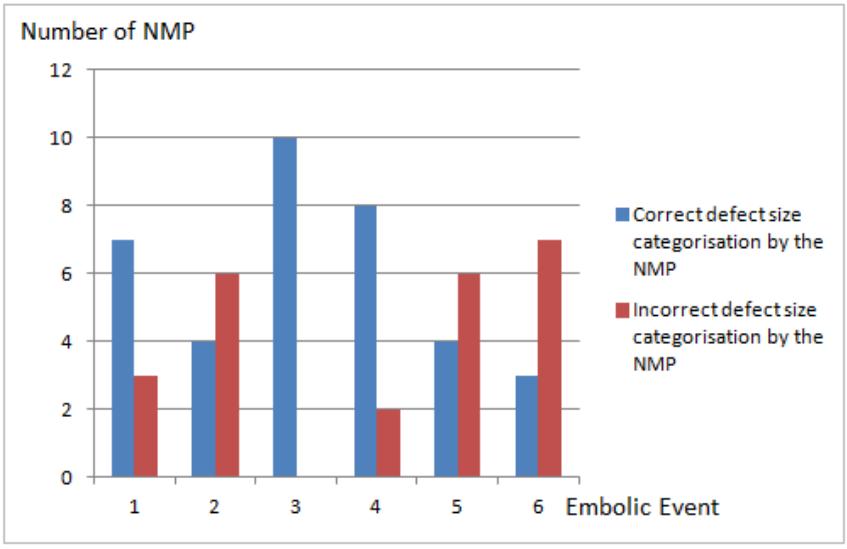

Figure 5.6: The bar chart illustrates number of the Nuclear Medicine physicians whom had correctly and incorrectly categorised (according to the revised PIOPED (59-60, 119) criteria) the V/Q mismatch defects shown in Figure 5.1

Size of the mismatch defect in embolic event 2 and embolic event 5 were categorised incorrectly by six Nuclear Medicine physicians. Three of the Nuclear Medicine physicians incorrectly categorised the size of mismatch defect of embolic event 1. Two Nuclear Medicine physicians have

incorrectly categorised the size of mismatch defect of embolic event 4. Seven Nuclear Medicine physicians incorrectly categorised the size of mismatch defect of embolic event 6. All Nuclear Medicine physicians have correctly categorised the mismatch defect size of embolic event 3. The number of incorrect mismatch defect size categorisations by nuclear medicine physician is an interesting outcome. Correct size categorisation of mismatch defect is essential in the revised PIOPED criteria (59-60, 119).

This study confirms Magnussen et al. works that segmental defect sizes are sometime underestimated (116, 124). Nuclear Medicine physicians are expected to familiarise themselves with the nature and size of bronchopulmonary segments in order to diagnose PE from lung scintigraphy. Accurate interpretation is an essential skill for these physicians (125).

Quality assurance: Probability of pulmonary embolism

The bar chart in *Figure 5.5*(a) shows that two Nuclear Medicine physicians made an incorrect interpretation on the number of mismatch defects seen on C 5. However, all the Nuclear Medicine physicians had correctly diagnosed the probability of PE on C 5.

The bar chart in *Figure 5.5*(b) shows ten Nuclear Medicine physicians have made incorrect interpretations on the size of mismatch defects seen on C 1.

However the probability of PE of C 1 was correctly diagnosed by all the Nuclear Medicine physicians.

The bar chart in *Figure 5.5*(b) shows that two Nuclear Medicine physicians made incorrect interpretations on the size of mismatch defects seen on C 5. Yet, probability of PE of C 5 was correctly diagnosed by all the Nuclear Medicine physicians.

Eight Nuclear Medicine physicians had incorrectly categorised the size of one of the defects on C 3. There are two defects on planar image C 3: **i** a large perfusion defect within the right lung upper lobe lateral segment; and **ii** a moderate perfusion defect within the right lung upper lobe posterior segment. The physicians categorised the moderate perfusion defect on C 3 as one large perfusion defect. This mistake lead to the incorrect evaluation of probability of PE of C 3 based on the revised PIOPED criteria. Eight physicians had incorrectly categorised the probability of PE of C 3 (see *Figure 5.5*(c)).

The study was conducted to evaluate the quality assurance of Nuclear Medicine physicians' interpretations of lung perfusion images based on the revised PIOPED criteria. The results show that Nuclear Medicine physicians had occasionally made incorrect interpretations on a number of present mismatch defects and their size on lung perfusion image sets.

These interpretations are important in the revised PIOPED criteria, in order to correctly categorise the probability of PE.

Two of the physicians had correctly categorised the probability of PE of C 5, with incorrect justification on a number of present mismatch defects seen on the planar perfusion image set. The two physicians had correctly categorised the probability of PE of C 5, accompanied by a poor justification on size of the present mismatch defects. Ten of the physicians had correctly diagnosed PE probability of C 1 even though prior to the diagnosis, they had incorrectly interpreted the size of the present mismatch defects seen on the planar perfusion image set.

This quality assurance study shows that Nuclear Medicine physicians may correctly categorise the probability of PE, even though the justifications that grounded the diagnosis are poor. This is mainly because, the revised PIOPED criteria have thin probability borderlines (low probability borderline *to* intermediate probably borderline *to* high probability borderline) of PE. Nuclear Medicine physicians that are using the revised PIOPED criteria should be more cautious in interpreting lung V/Q scans that fall close to the borderlines. This is to ensure strong justifications support each PE diagnosis that is being made based on the revised PIOPED criteria.

5.6 Conclusion

Quality assurance: Size of mismatch defect

The study was conducted to evaluate the accuracy of Nuclear Medicine physician's diagnosis on V/Q mismatch defect size based on the revised PIOPED criteria. The results show that a few Nuclear Medicine physicians had underestimated the size of mismatch defects. Morrell et al. suggested that scoring criteria based on segmental size should be done with caution (120). This will ensure the high quality of PE diagnosis via lung perfusion and ventilation scans.

Quality assurance: Probability of pulmonary embolism

In the revised PIOPED criteria, the number of present mismatch defects has a significant impact on the probability of PE. As the number of present mismatch defects increases, the probability of PE increases (60). Also, the criteria emphasises the significance of mismatch defects' size in assessing the probability of PE of any lung V/Q scans (59-60, 117, 119). Any size of mismatch defects are to be added together to increase the probability of PE (118).

6. A LUNG PERFUSION IMAGING ATLAS

The findings of this chapter were previously presented as a poster in the 40th Annual Scientific Meeting of the Australian and New Zealand Society of Nuclear Medicine. The abstract of the presentation was published in the Internal Medicine Journal (126).This chapter was written in a journal article format. This chapter was revised and edited creating a manuscript entitled '*Lung Perfusion Imaging Atlas for PE Diagnosis via Lung Perfusion and Ventilation Scan'*. The manuscript is currently under review by a peer reviewed journal.

6.1 Abstract

Objective: A lung perfusion imaging atlas was manufactured at the Department of Nuclear Medicine, Wollongong Hospital, NSW, Australia. The atlas was developed with the aim of being used as a teaching aid; and as a reference resource aid in interpreting lung perfusion and ventilation scans. Nuclear Medicine physicians are expected to be the primary users of the imaging atlas.

Methods: The anatomical lung phantom consists of two lung cavities and 18 separable lung perfusion inserts, and was used to develop the imaging atlas. Single segmental perfusion defects depicted in lung perfusion scans were modelled using the phantom with planar imaging and SPECT imaging. Segmental perfusion defects were simulated by means of 18

insertable bronchopulmonary segments of the human lungs. A questionnaire survey was conducted to study Nuclear Medicine physicians' opinions on the imaging atlas.

Results: Planar and SPECT images were gathered in the compilation of the lung perfusion imaging atlas. This atlas demonstrates the precise appearance of segmental defects on a lung scan. All Nuclear Medicine physicians agreed that the imaging atlas was a good teaching aid and a reference resource for inexperienced Nuclear Medicine physicians who are developing experience in the diagnosis of PE on lung perfusion and ventilation images.

Conclusions: We hope that the atlas will increase new Nuclear Medicine physicians understanding of lung bronchopulmonary segmental anatomy in lung scans.

Keywords: Planar, SPECT, Lung perfusion, Imaging atlas, Pulmonary Embolism

6.2 Introduction

PE is one of commonly clinically misdiagnosed diseases in the United States of America (127). Howarth et al. reported in their article that there is, in general, poor understanding of the test results among referring physicians (128). The fundamental rules of thumb to diagnose PE via lung perfusion and ventilation scan are to identify lobar, segmental, subsegmental perfusion and ventilation mismatch defects on lung perfusion and ventilation image sets (54). All segmental and subsegmental perfusion defects are considered significant at a minimum of 25% volumetric size of a lung bronchopulmonary segment (60, 128). With all the established methods to diagnose PE via lung scans, the disease remains challenging to diagnose, resulting in many nonconclusive diagnoses (129). Experienced Nuclear Medicine physicians were reported having difficulty in identifying the size of particular lung perfusion defects (120). Underestimation of lung perfusion defects size may lead to incorrect PE diagnosis. Therefore, this study was carried out to introduce an imaging atlas as a reference resource and a teaching aid for interpreting lung perfusion and ventilation scans. The atlas was generated with the hope of assisting Nuclear Medicine physicians in diagnosing PE via lung perfusion and ventilation scans.

6.3 Materials and methods

An anatomical lung phantom (48) was used throughout this study. The phantom was uniquely developed to model the lung perfusion conditions of patients with suspected pulmonary embolism. The phantom consists of 18 perfusion defect inserts. These inserts are complete bronchopulmonary segments of the human lungs. They were employed as perfusion defects simulating perfusion absence in lung perfusion scans. On the whole, the manufactured phantom is able to simulate segmental lung perfusion deficiencies (vascular segmental deficiencies) depicted in typical lung perfusion scans of patients with suspected pulmonary embolism.

The study was carried out to model single segmental perfusion defects (100% volumetric size) of lung bronchopulmonary segments of the human lungs. To generate the atlas, individual perfusion defect inserts were fitted into the lung phantom. Then an appropriate activity (approximately 40-50 MBq) of ^{99m}Tc solution was added to the assembled phantom. Next, the phantom was scanned using planar imaging and SPECT imaging. Then, the phantom was disassembled-then-re-assembled to prepare it for further planar and SPECT scans. The process was repeated until 18 planar and SPECT scans (of all 18 bronchopulmonary segments) were completed.

The atlas development process took approximately 13 weeks. The lung phantom was scanned using a dual head gamma camera (Philips ADAC Forte) at the Department of Nuclear Medicine, Wollongong Hospital, NSW,

Australia. The scans were scheduled once or twice a week depending on the availability of the camera.

Planar and SPECT acquisitions

In each planar scan, six planar views were acquired in a 256 x 256 matrix: anterior (A), posterior (P), left anterior oblique (LAO), left posterior oblique (LPO), right posterior oblique (RPO) and right anterior oblique (RAO). The planar perfusion scans were acquired at the 140 keV photopeak. The planar perfusion image set was then printed on x-ray film and stored electronically on the hospital PACS.

In each SPECT scan, a step-and-shoot protocol of 12 s/3°step for a total of 60 views per camera head was used. Images were collected at the 140keV energy window. Lung SPECT image sets were reconstructed using a HERMES workstation (Hermes Medical Solutions, Stockholm, Sweden). Reconstruction of coronal (from anterior to posterior), sagittal (from right to left) and transverse (from head to feet) slices were done using FBP with a Butterworth cut off value of 0.4. The images were stored in digital format on the hospital PACS. SPECT images are viewed on the HERMES workstation and also printed on x-ray film.

A close-ended Likert-scale survey

A small scale close-ended Likert-scale survey was conducted to obtain a snapshot of Nuclear Medicine physicians' opinions on the atlas to be used

as a reference resource and a teaching material to interpret lung perfusion and ventilation scans. The survey (Appendix E) was sent to ten Nuclear Medicine physicians at various institutions[19]. The survey was conducted on a paper-based format and on an online-based format[20]. The Nuclear Medicine physicians were requested to score each question with the score value listed in *Table 6.1*. The score values were re-modelled score values used by Heikkinen et al. in their published article (101).

Table 6.1: Nuclear Medicine physicians were required to score each question using the four-points Likert-scale as shown in the table

Score	Image Quality	Specification
1	Poor	Not adequate for clinical application[21]
2	Average	Barely adequate for limited clinical application
3	Good	Adequate for clinical application
4	Excellent	Excellent for clinical application

The survey pack was divided into three parts:

1. Introduction (includes: summary of the anatomical lung phantom; objectives of the survey);
2. The lung perfusion imaging atlas;
3. A series of close-ended questions.

[19] The institutions are: Wollongong Hospital, Australia, St Vincent's Private Hospital, Australia, Peter McCallum Cancer Care Centre, Australia, Theranostics Centre for Molecular Radiotherapy and Molecular Imaging, Germany, Hospital Universiti Sains Malaysia, Malaysia, Hospital Kuala Lumpur, Malaysia, and Pusat Perubatan Universiti Malaya, Malaysia.

[20] http://booroo.com/app/rendersurvey.asp?sid=bj5jya9iebg5xg031784

[21] Clinical application means aiding material to help Nuclear Medicine physicians interpret lung perfusion and ventilation scans for pulmonary embolism diagnosis.

The close-ended survey's questions were:

1. As an experienced Nuclear Medicine Physician, how do you rate the atlas' suitability to be used as a reference resource and teaching aid for new Nuclear Medicine physicians to develop experience in interpreting lung V/Q mismatch defects for PE diagnosis?

2. What is your opinion on the atlas' suitability to be used as a reference (a reference material to experienced Nuclear Medicine physicians) for anatomical bronchopulmonary segmental size and structure (scintigraphic and tomographic) in PE diagnosis by lung perfusion and ventilation scans?

3. What is your opinion on the atlas as an aid to interpret lung perfusion and ventilation scans for PE diagnosis? We propose Nuclear Medicine physicians use the atlas as an aid together with standard interpretation criteria (the revised PIOPED criteria, the Hull criteria or the Gestalt interpretation).

In this study, Nuclear Medicine physicians were informed that all the visible lung perfusion defects were in fact V/Q mismatch defects with associated with a normal chest x-ray (in the region of perfusion abnormality).

6.4 Results

All the planar and SPECT images were gathered together to comprise the lung perfusion imaging atlas (see *Figure 6.1* to *Figure 6.18*). The atlas only contains single segmental lung perfusion defects images (planar and SPECT) of 18 bronchopulmonary segments.

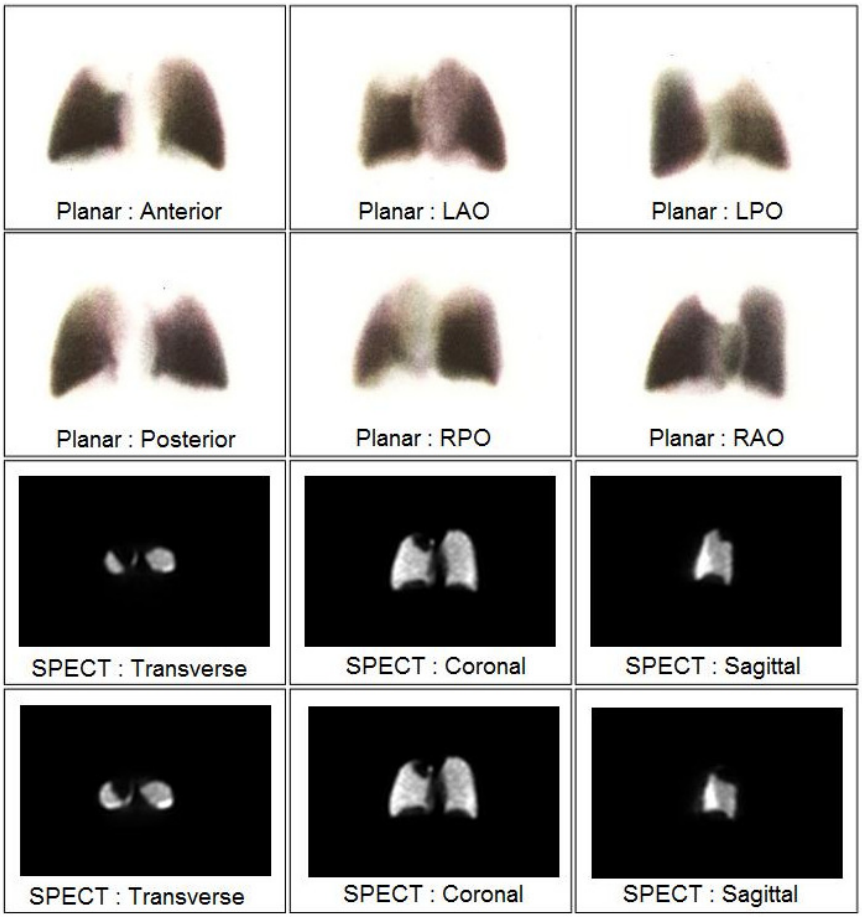

Figure 6.1: Planar and SPECT images of a perfusion defect within the apical segment of the right upper lobe.

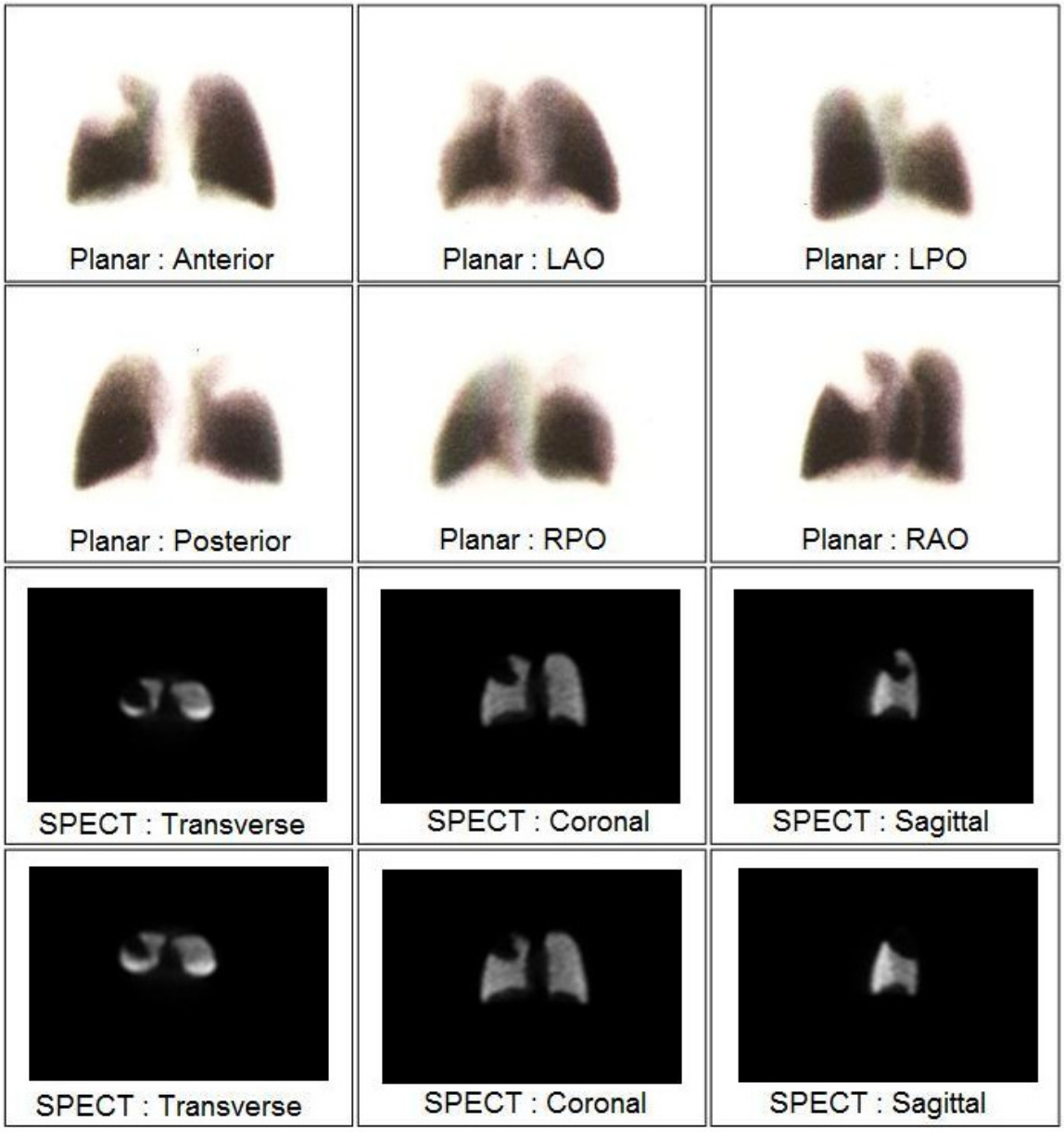

Figure 6.2: Planar and SPECT images of a perfusion defect within the posterior segment of the right upper lobe.

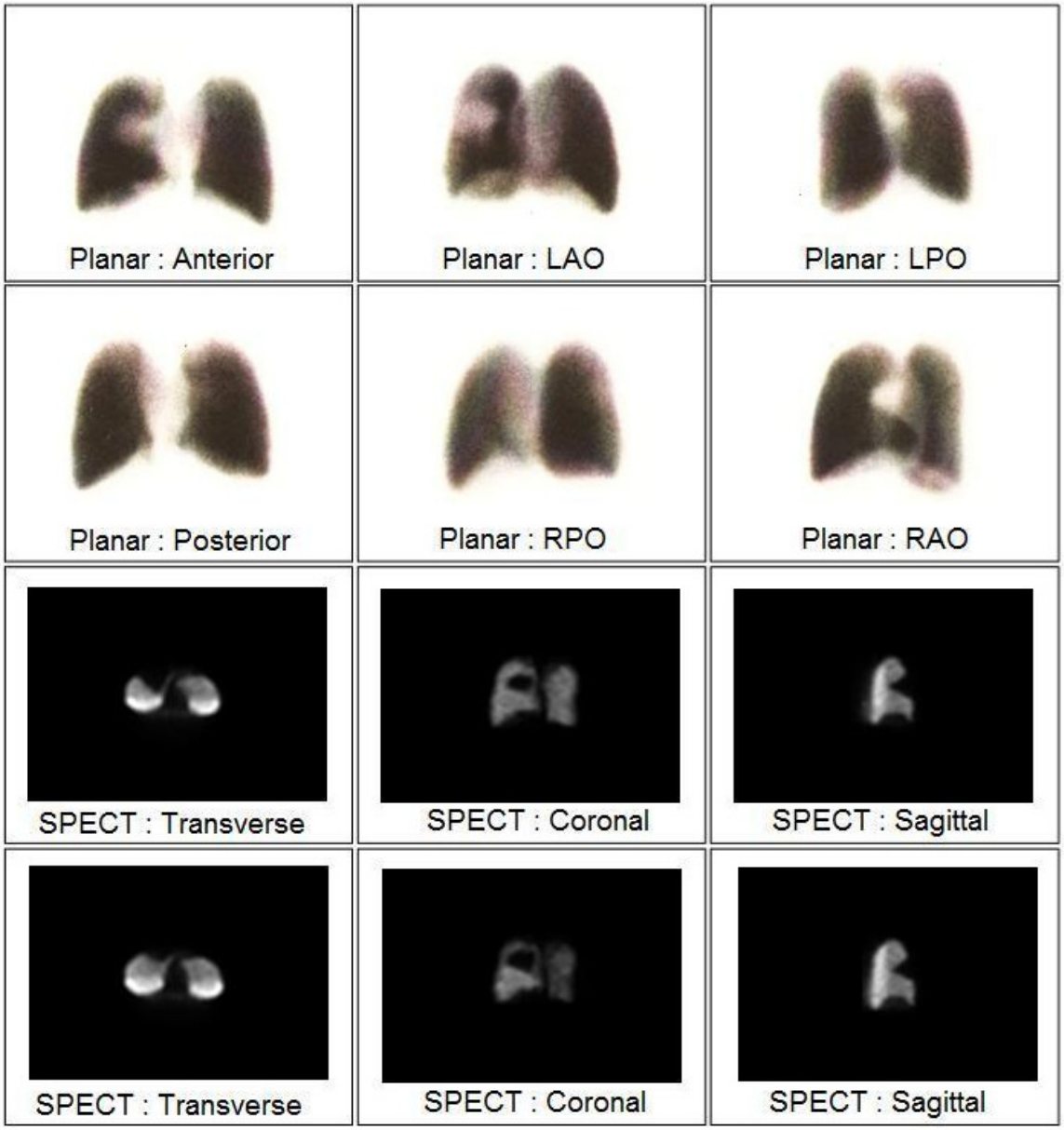

Figure 6.3: Planar and SPECT images of a perfusion defect within the anterior segment of the right upper lobe.

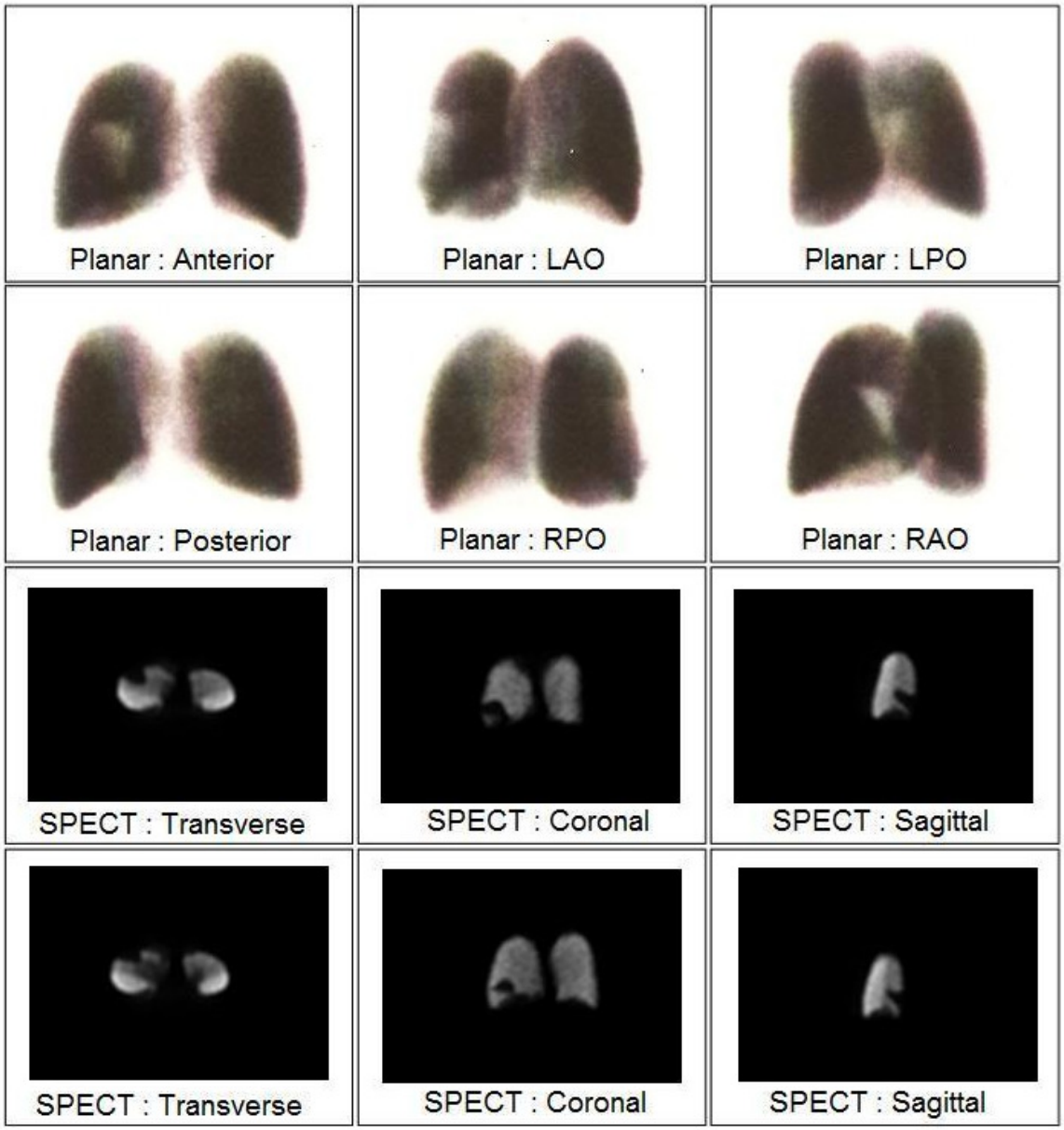

Figure 6.4: Planar and SPECT images of perfusion defect within the lateral segment of the right middle lobe.

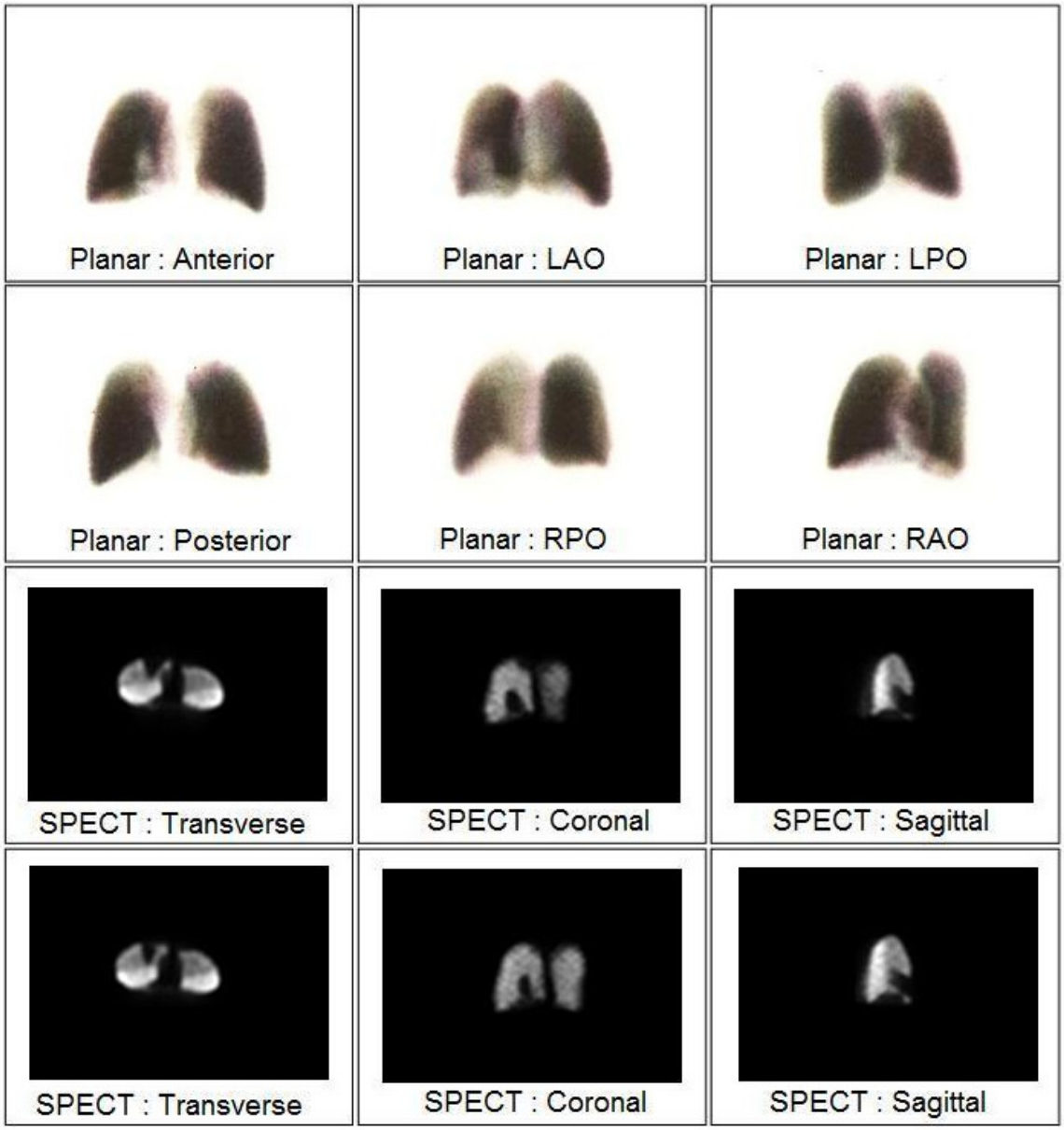

Figure 6.5: Planar and SPECT images of a perfusion defect within the medial segment of the right middle lobe.

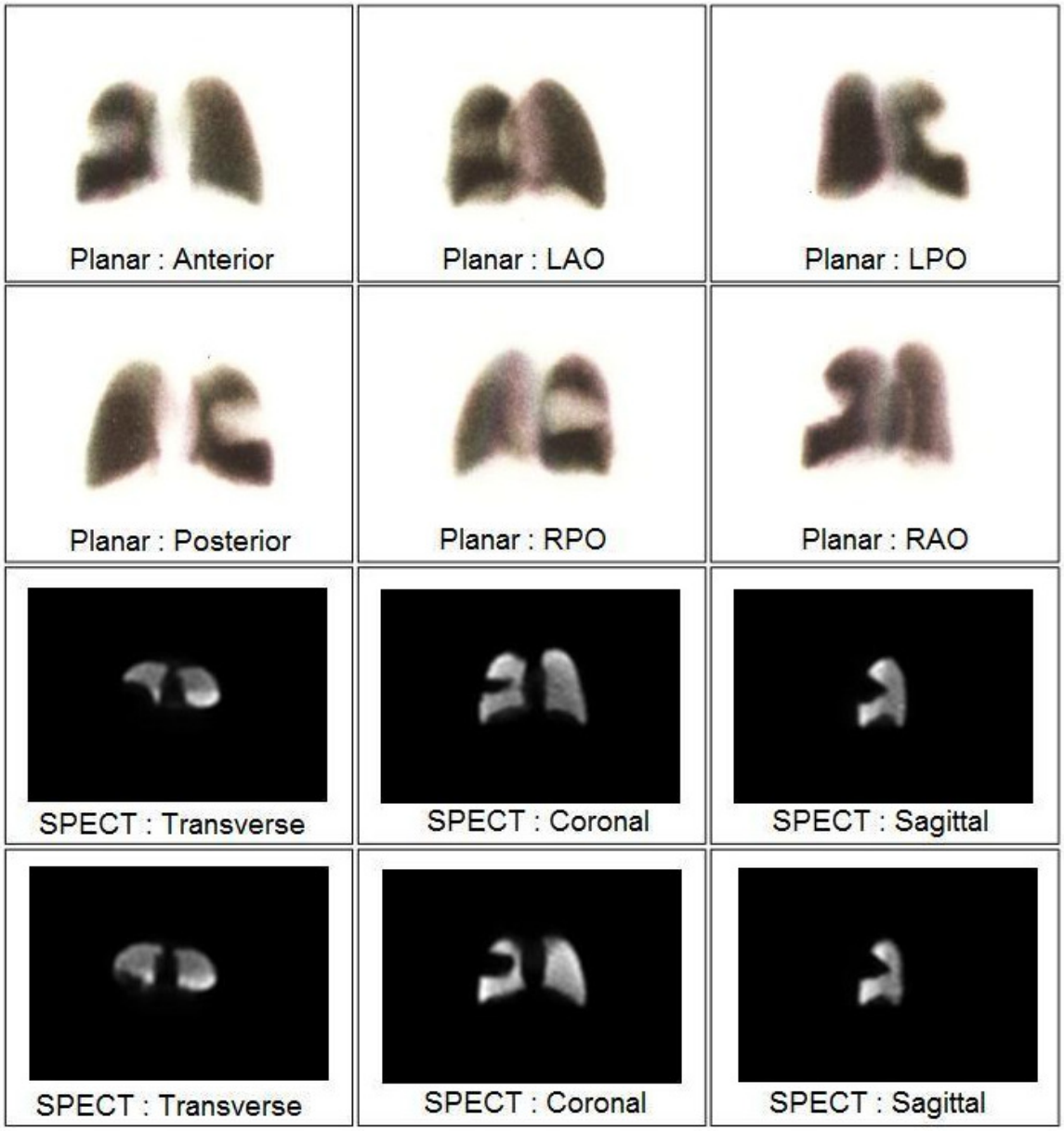

Figure 6.6: Planar and SPECT images of a perfusion defect within the superior segment of the right lower lobe.

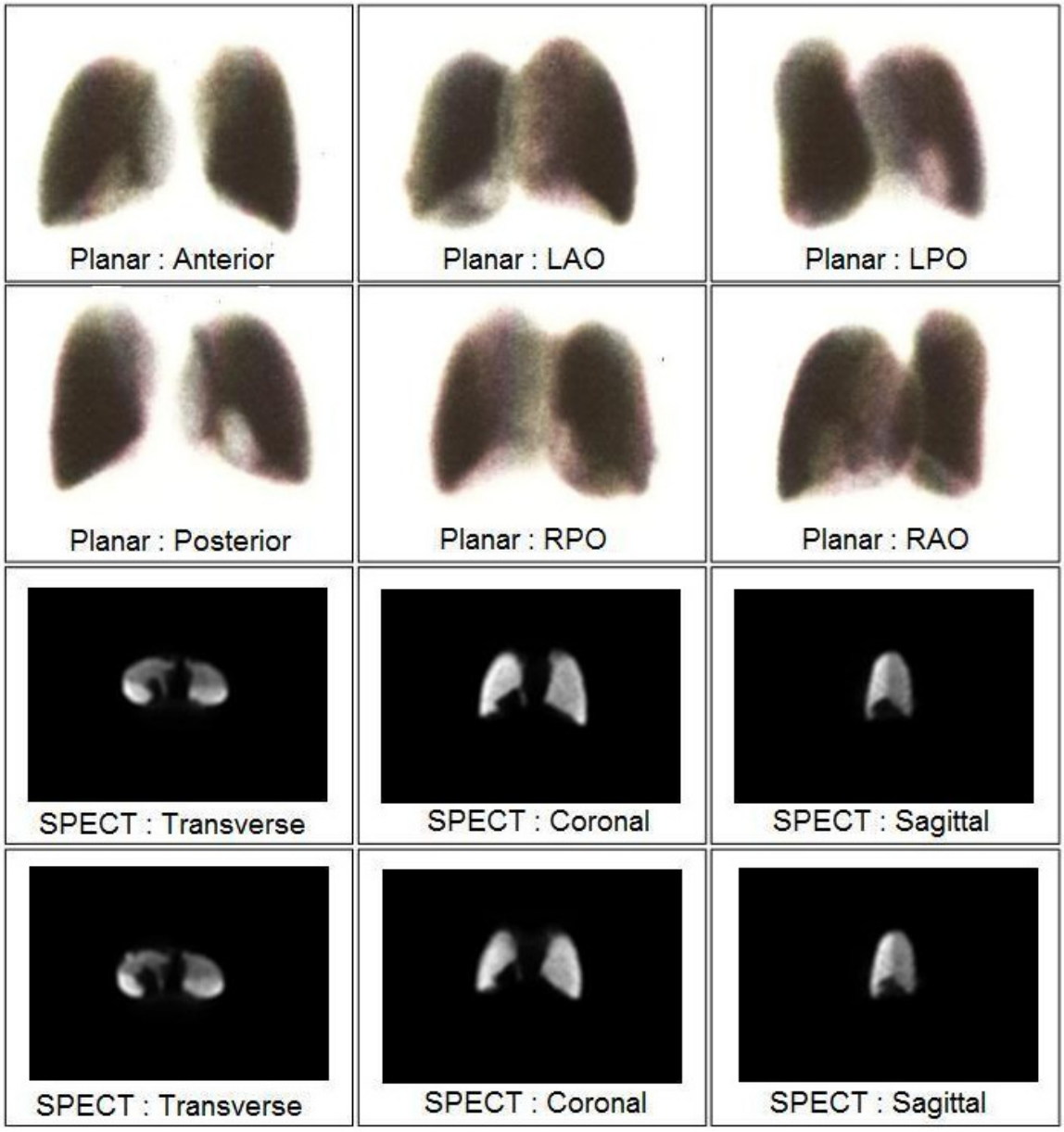

Figure 6.7: Planar and SPECT images of a perfusion defect within the medial basal segment of the right lower lobe.

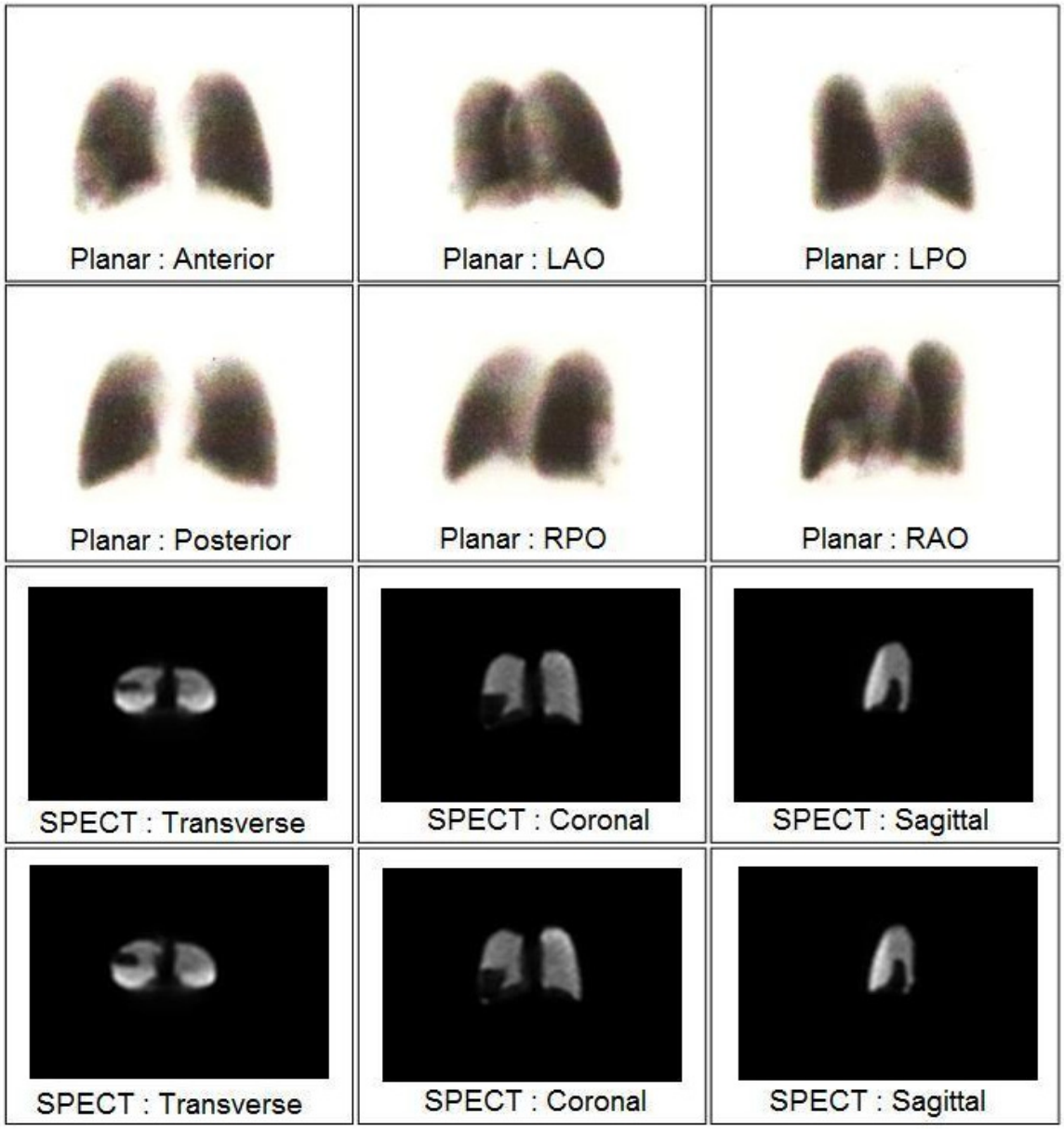

Figure 6.8: Planar and SPECT images of a perfusion defect within the anterior basal segment of the right lower lobe.

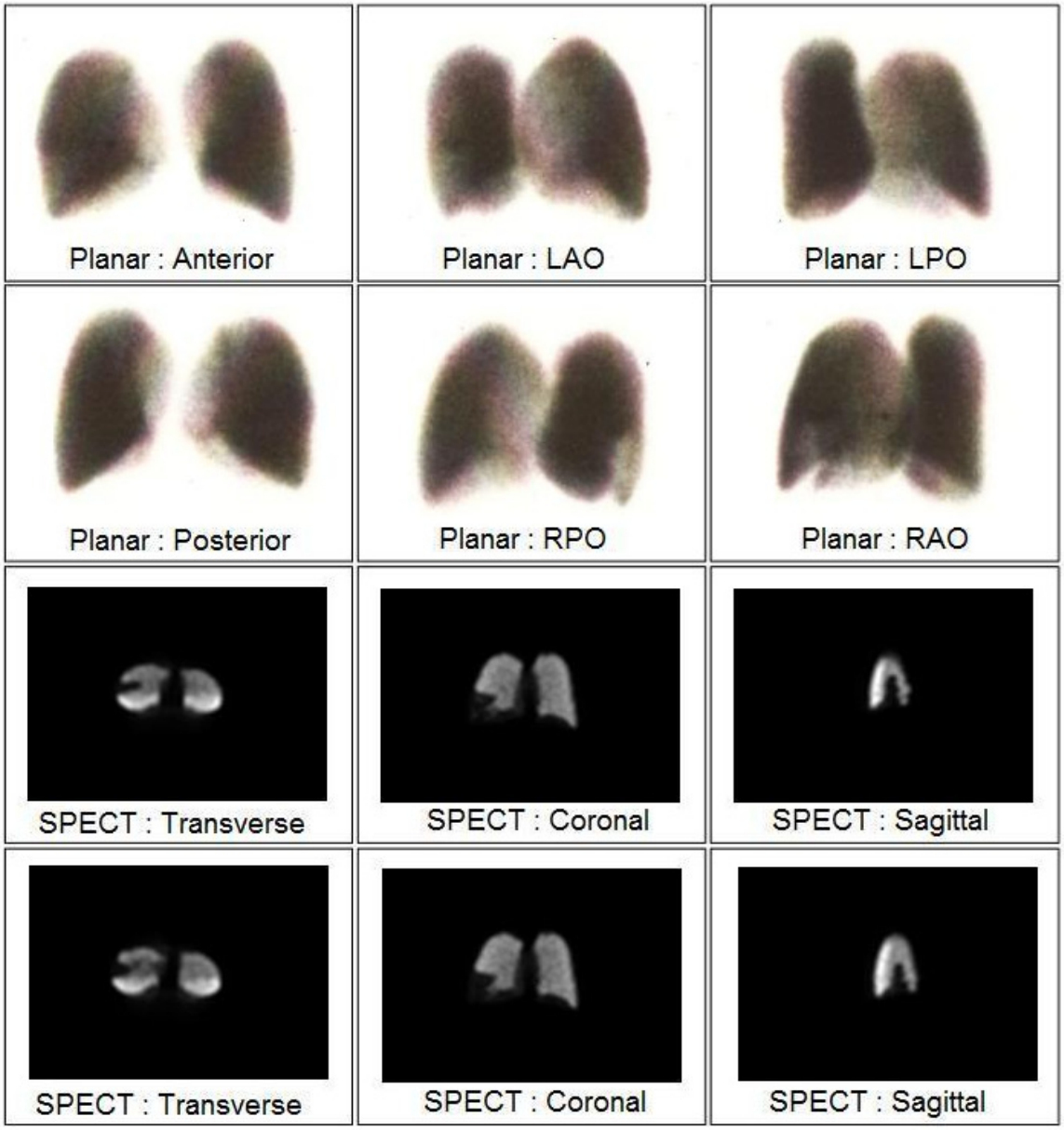

Figure 6.9: Planar and SPECT images of a perfusion defect within the lateral basal segment of the right lower lobe.

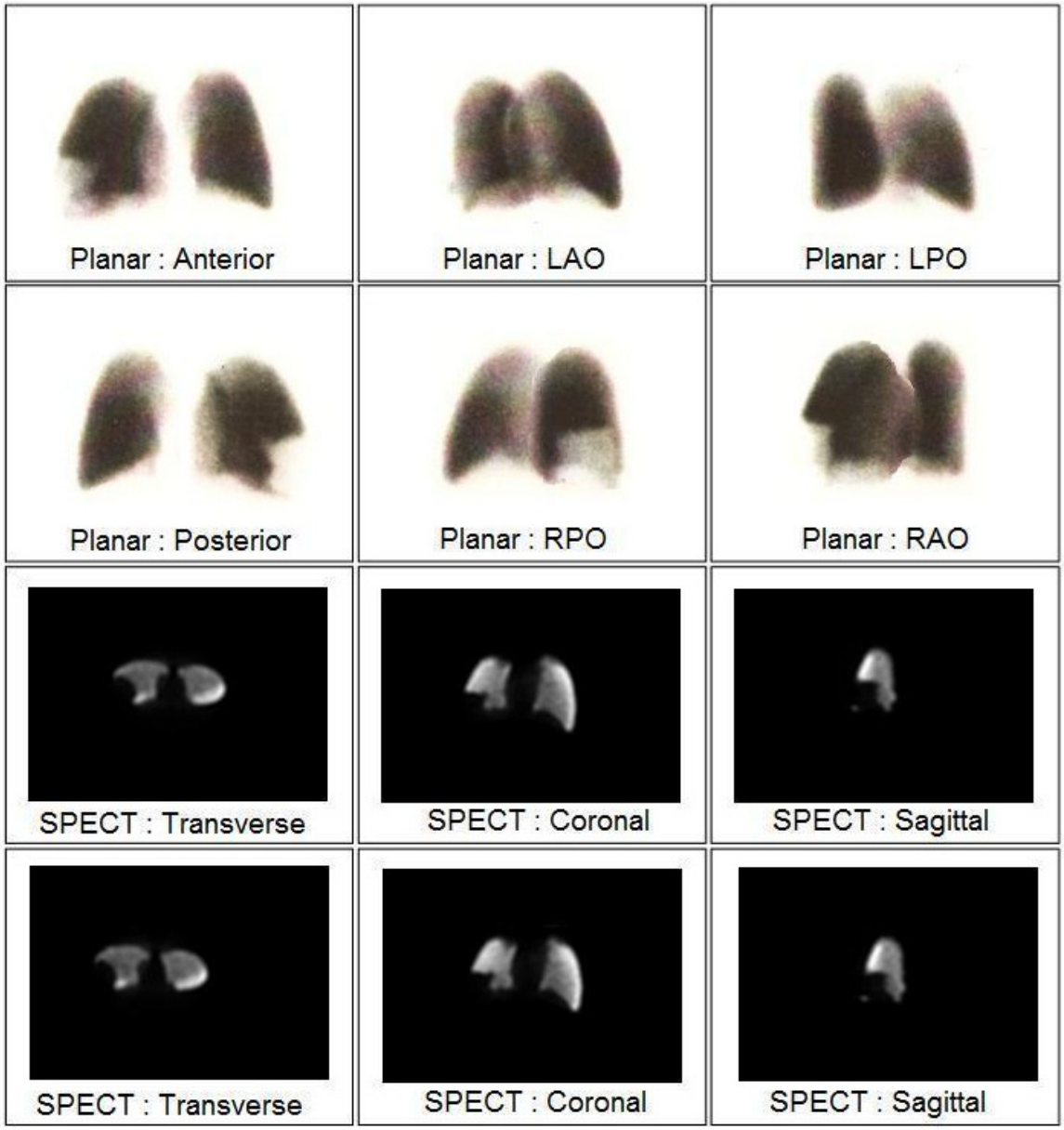

Figure 6.10: Planar and SPECT images of a perfusion defect within the posterior basal segment of the right lower lobe.

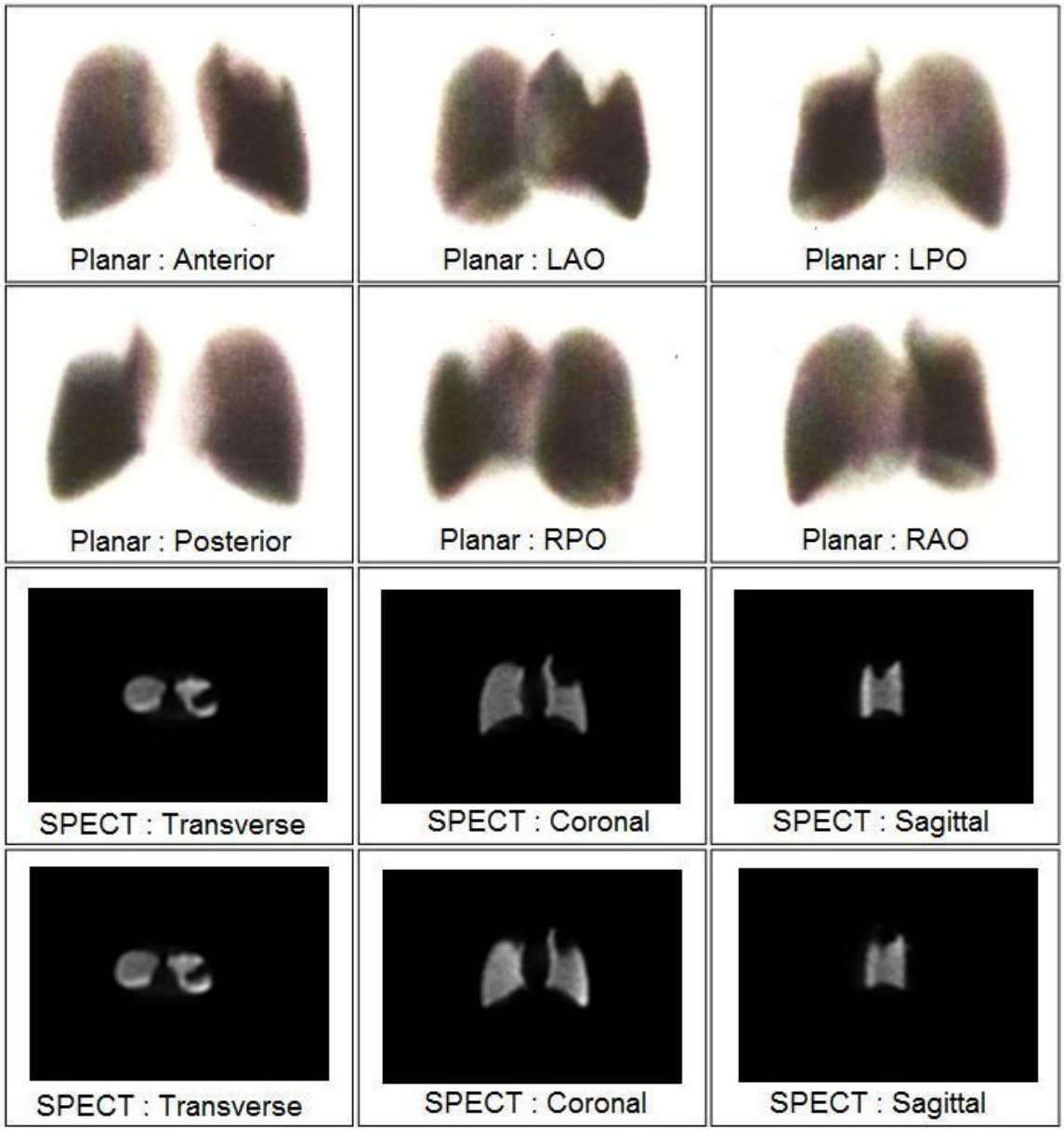

Figure 6.11: Planar and SPECT images of a perfusion defect within the apical and posterior segment of the left upper lobe.

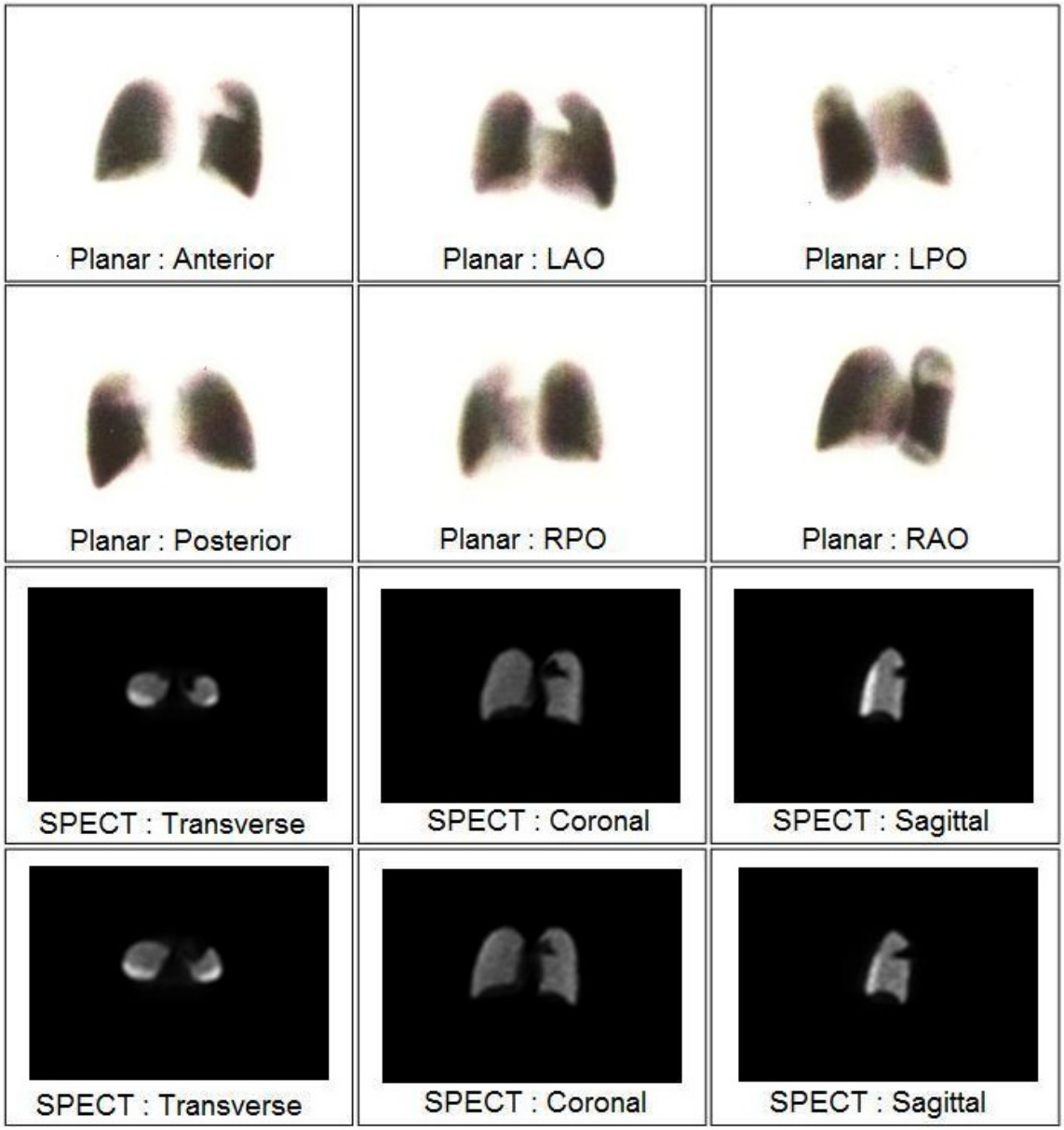

Figure 6.12: Planar and SPECT images of a perfusion defect within the anterior segment of the left upper lobe.

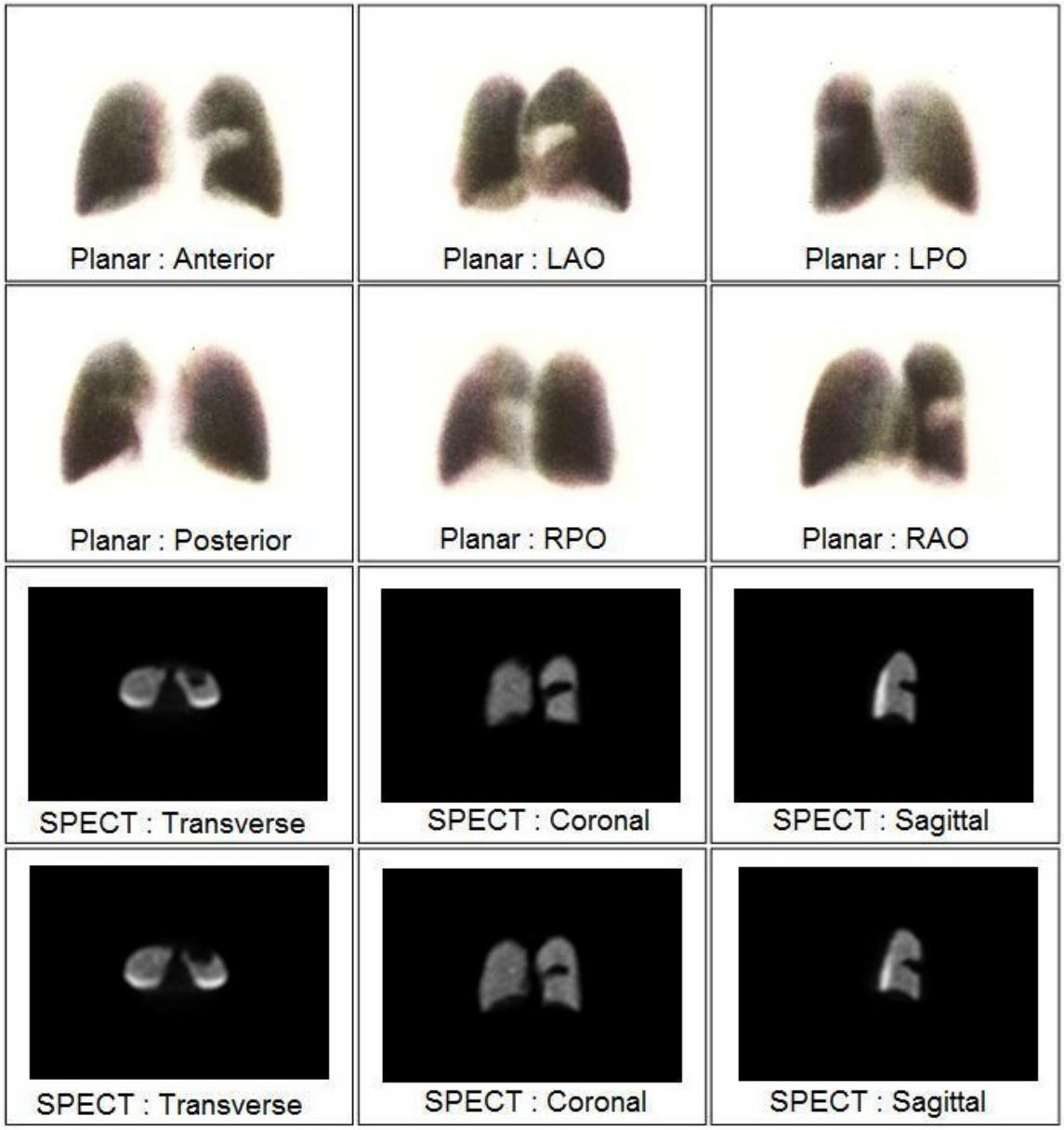

Figure 6.13: Planar and SPECT images of a perfusion defect within the lingular superior segment of the left upper lobe.

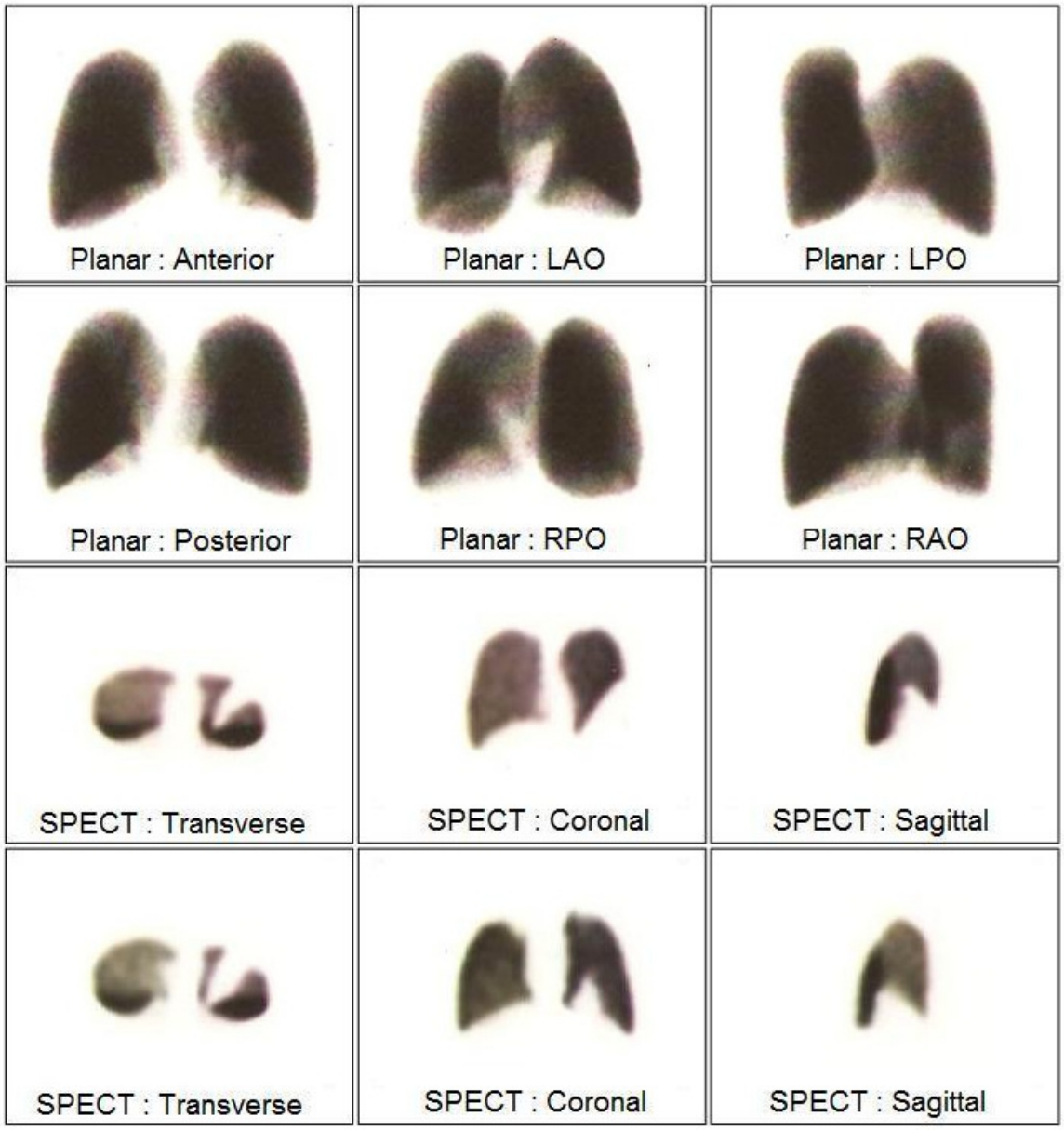

Figure 6.14: Planar and SPECT images of a perfusion defect within the lingular inferior segment of the left upper lobe.

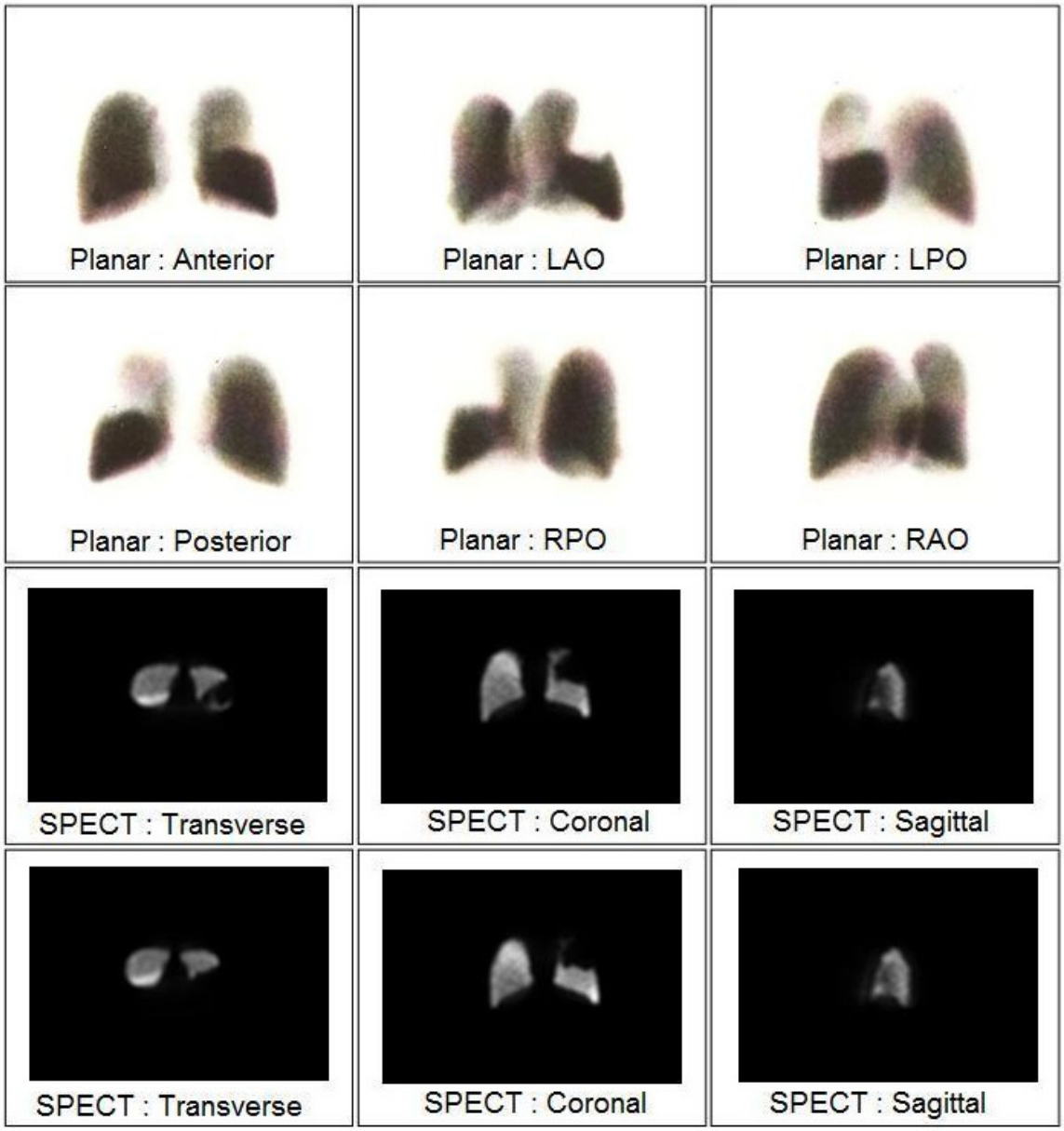

Figure 6.15: Planar and SPECT images of a perfusion defect within the superior segment of the left lower lobe.

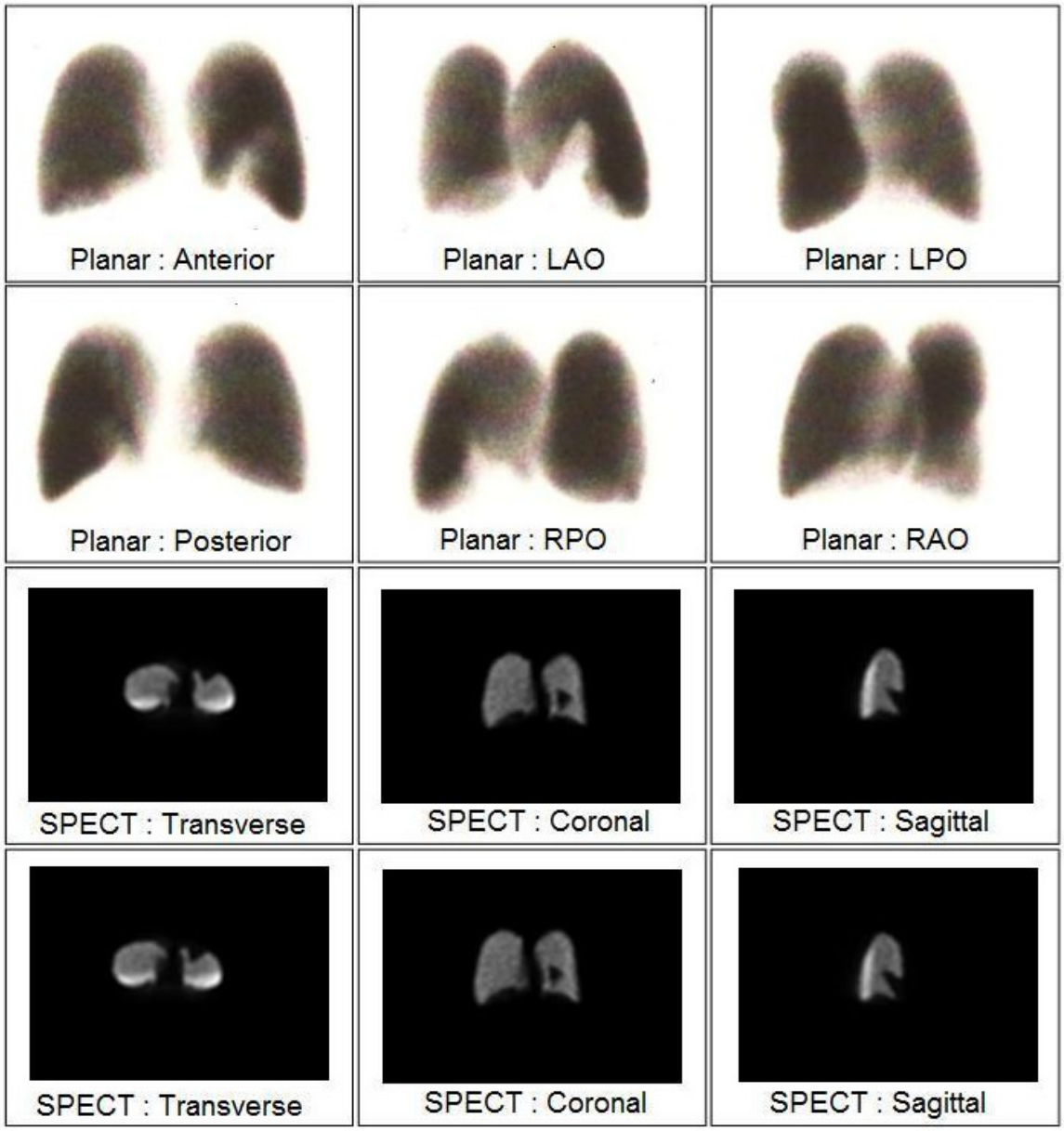

Figure 6.16: Planar and SPECT images of a perfusion defect within the medial and anterior basal segment of the left lower lobe.

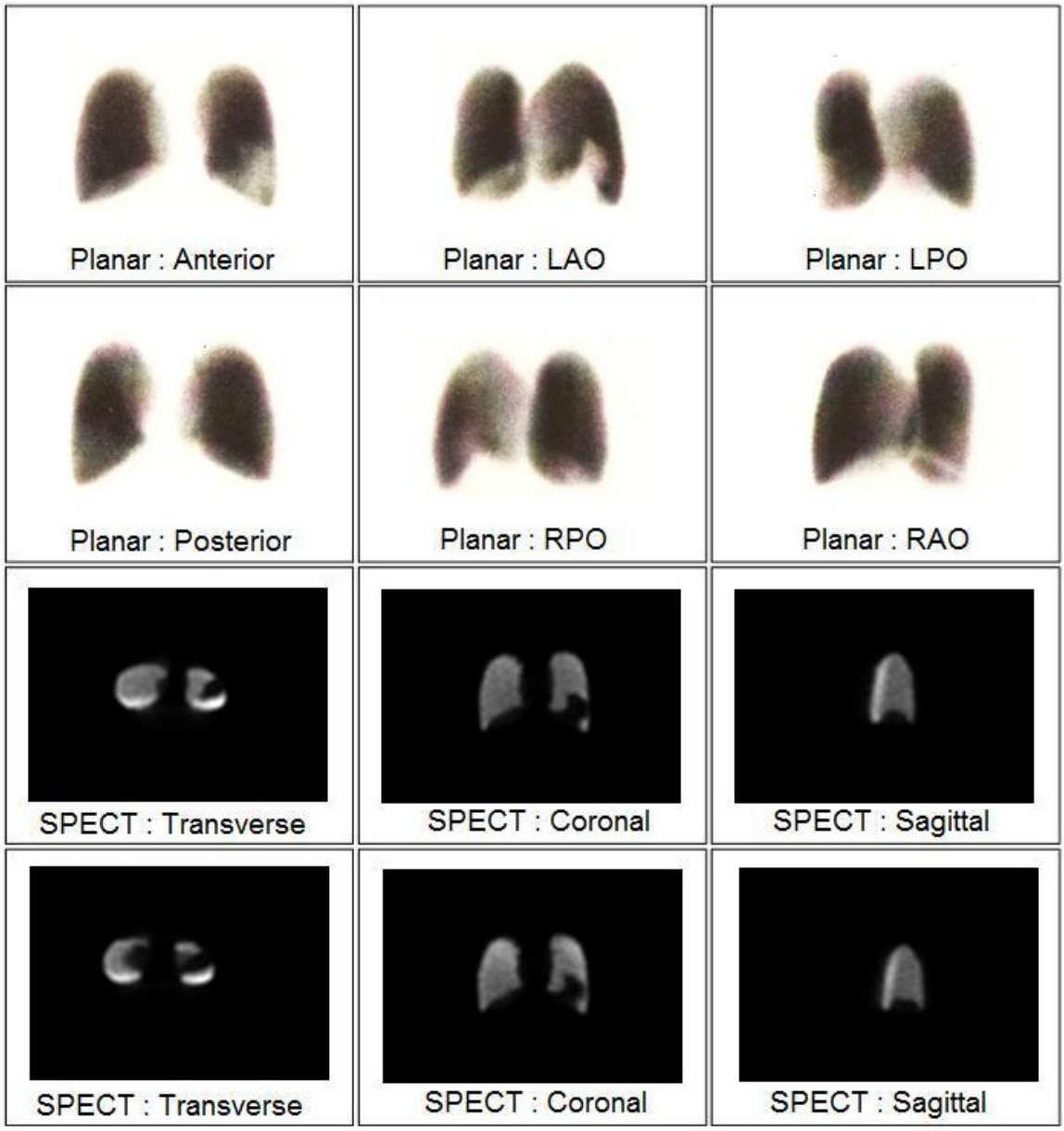

Figure 6.17: Planar and SPECT images of a perfusion defect within the lateral basal segment of the left lower lobe.

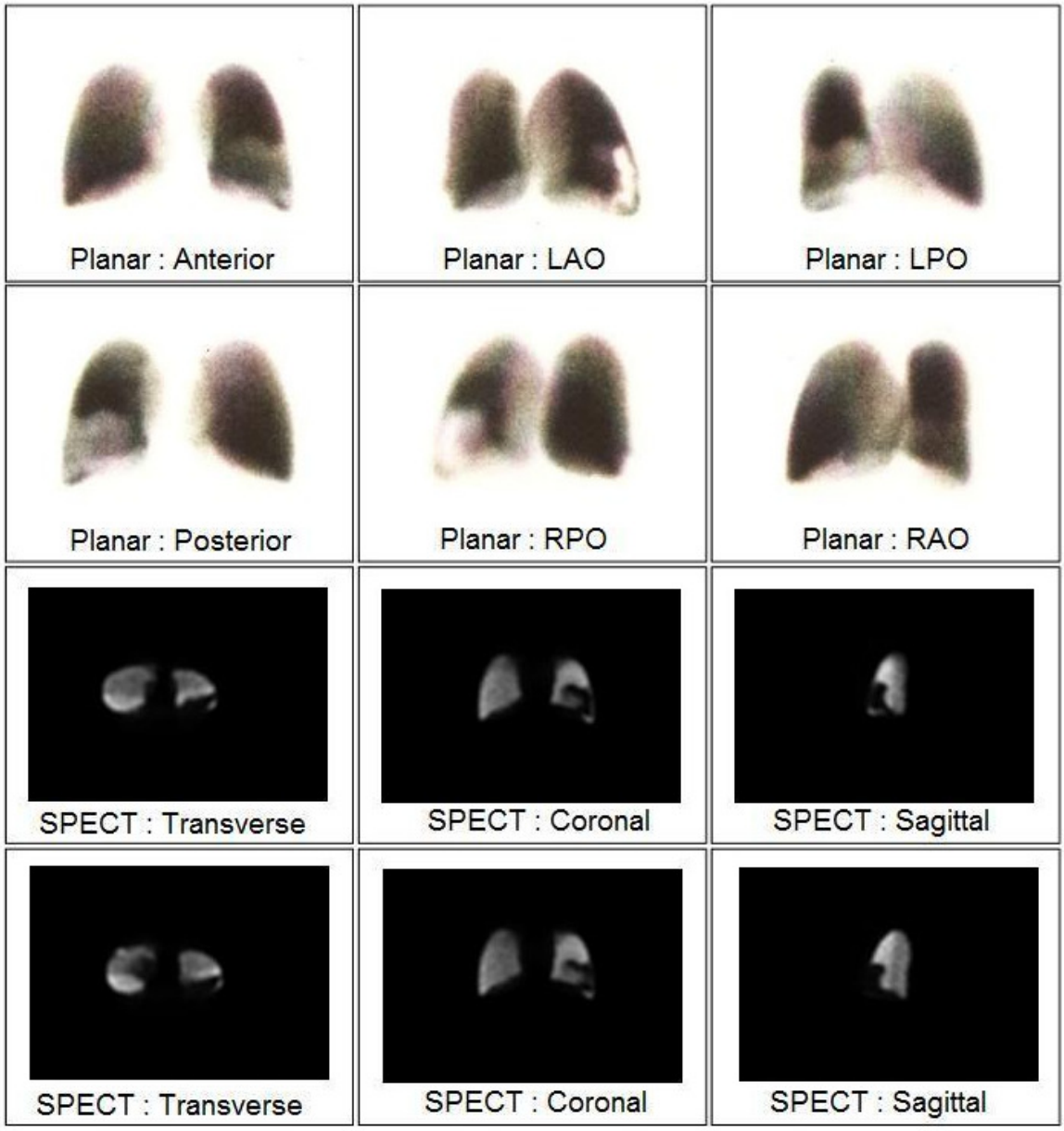

Figure 6.18: Planar and SPECT images of a perfusion defect involving the posterior basal segment of the left lower lobe.

The survey results

This is a small scale survey with a small sample size (SS = 10). As described earlier (see Section 4.5), a conclusion of a small sample size study is unclear with wide uncertainty (103). A small sample size generates large margin of error (104-105). However, the total number of physicians participated in this study is considered acceptable as the project was not designed as a clinical study. The aim of the study was to investigate the clinical value of the atlas to a small group of experienced Nuclear Medicine physician. The following chart (*Figure 6.19*) shows the mode score of the survey study.

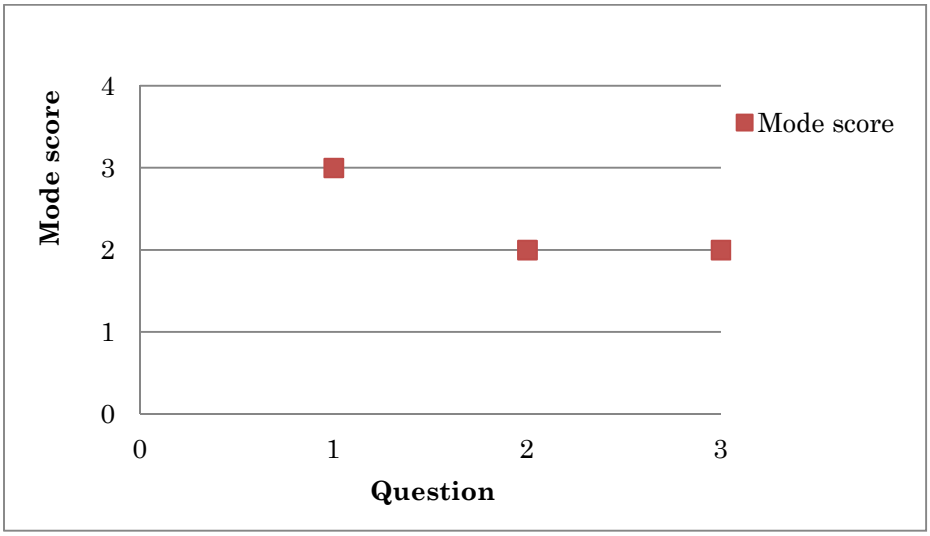

Figure 6.19: The chart shows mode scores of the survey.

As described earlier in Section 4.5, Likert-type rating scales fall within the ordinal level of measurement (102). Median or mode shall be used as a 'measure of central tendency' of ordinal data (102). In this study, the mode scores have been used as a measure of central tendency.

The MS of the Question 1 was 3. The higher the mode score of Question 1, the higher the quality of the information carried by the atlas for new Nuclear Medicine physicians. The result shows that the atlas is of good reference quality for new Nuclear Medicine physicians.

The MS of the Question 2 was 2. The higher the mode score of Question 2, the higher the quality of anatomical information carried by the atlas for experienced Nuclear Medicine physicians. The result shows that the atlas supplies mediocre anatomical information to Nuclear Medicine physicians.

Finally, the MS of Question 3 was 2. The higher the mode score of Question 3, the higher the suitability of the atlas as an aid to interpret lung perfusion and ventilation scan. The result shows that the atlas is an unsuitable aid to interpret lung perfusion and ventilation scans for PE diagnosis.

6.5 Discussion

The lung perfusion imaging atlas

A number of models representing human lung segmental anatomy have been developed over the years. These models were based upon various sources: phantom; volunteer subjects; and virtual models using Monte Carlo simulation. Each model was developed with a specific aim and purpose.

In this study, the lung perfusion imaging atlas represents a comprehensive segmental anatomy of the human lungs in three tomographic planes and in planar views. The aim of the atlas development was to aid Nuclear Medicine physicians in interpreting lung perfusion and ventilation scans. Tomographic images were included in the atlas because many recent publications have claimed that SPECT is superior to planar imaging for the diagnosis of PE (57, 130-132).

Magnussen et al. developed a virtual model of the segmental anatomy of the human lung. In that study 18 single segmental and 47 subsegmental defects were simulated using Monte Carlo simulation. The defects were displayed in tomographic planes and in eight planar views. Their model of the segmental anatomy of a human lung was developed in order to investigate the sensitivity of detection (planar versus SPECT), and accuracy of estimation of defect size (55).

The tomographic images presented in our study are of similar quality compared to the tomographic images simulated by Magnussen et al. Their publication does not contain all the 18 single segmental defects of a typical bronchopulmonary segment of the human lungs. In contrast, the present study offers a complete segmental anatomy of a human lung in tomographic planes and in planar views. Presenting the complete segmental anatomy of the human lungs is the main objective of this study,

in order to assist Nuclear Medicine physicians in their interpretation of lung perfusion and ventilation scans.

Morrell et al., demonstrated appearances of known lobar and segmental defects on lung scans (133). Their study, using healthy volunteers, was carried out to suggest optimal positioning for visualization of a defect. They successfully defined 18 segmental defects in a lung scan. Not all the segmental defects' images were included in their article which mainly focussed on planar scintigraphy (133). In contrast, the lung perfusion imaging atlas in the current study offers planar and SPECT images of all 18 single segmental defects of the human lungs.

Carbonell et al. constructed a lung-thorax phantom to aid lung scintigraphic interpretation. The phantom was made of polyester (thorax) and polyurethane (lung tissue). The segmental defects of the phantom do not resemble true anatomic features of the human lungs (134). The lung phantom used in the present study, as described in Kabir et al [48], was exclusively designed to model single segmental defects of the human lungs. The perfusion defect inserts carry true anatomical features of the human lungs (48).

The survey results

The chart in *Figure 6.19* (Question 1) shows that all nuclear medical physicians agree that the atlas is a good reference for new Nuclear

Medicine physicians. Although the anatomical representations of the atlas is clinically limited, it is still a valuable material to inexperienced Nuclear Medicine physicians that are developing experience in interpreting lung perfusion images of lung perfusion and ventilation scans.

The survey's results in *Figure 6.19* (Question 2) confirm that the atlas carries minimal anatomical information to aid experienced Nuclear Medicine physicians in interpreting lung perfusion scans for PE diagnosis.

Finally, respondents were asked to score the atlas ability in assisting Nuclear Medicine physicians to interpret lung perfusion and ventilation scans for PE diagnosis (Question 3). The atlas was proposed to be used as an aid material together with the standard interpretation criteria (the revised PIOPED criteria, the Hull criteria and Gestalt interpretation) (60-61, 135). The chart in *Figure 6.19* shows that the atlas is an unsuitable aid for Nuclear Medicine physicians to interpret lung perfusion and ventilation scans for PE diagnosis.

6.6 Conclusion

According to survey study, experienced Nuclear Medicine physicians confirmed that the atlas is a valuable reference resource and teaching material for inexperienced Nuclear Medicine physicians. However, the atlas has limited valuable anatomical information and barely benefits

experienced nuclear medicine physician to diagnose PE on lung perfusion and ventilation images.

The survey was conducted on a small scale with ten respondents. Therefore, the statistical power of the survey is certainly low. However, the survey's results represent a valuable snapshot overview of the atlas, from the perspective of experienced Nuclear Medicine physicians.

7. WATER BATH ATTENUATION EFFECTS ON LUNG PHANTOM PLANAR ACQUISITION

7.1 Introduction

Realistic models of the human body have to take into account tissue attenuation (136). The attenuation of gamma radiations in human tissue is a critical factor during imaging (137). Currently available thoracic SPECT phantoms were studied to initiate the development of a simulated thoracic attenuation phantom for the anatomical lung phantom.

The importance of a thoracic cavity for a lung phantom has been demonstrated by Heikkinen et al. (21). The researchers developed a lung phantom to simulate a clinical ventilation-perfusion situation. The lung phantom was inserted inside a physical chest cavity, to simulate the thorax in any planar or SPECT scans. The lung phantom (not including perfusion defect inserts) and the chest cavity are fully tissue equivalent. The attenuation properties of the phantom closely resemble actual clinical attenuation.

Doshi et al. reported the effects of the thorax background in breast cancer scan simulations using Positron Emission Tomography (PET). Three experimental designs were setup to study the role of object scatter and attenuation property in defining image signal-to-noise ratio. The

experimental setups were: the breast phantom (with lesions) was scanned without the thorax cavity; the breast phantom (with lesions) was scanned with the thorax cavity filled with water without radioisotope; the breast phantom (with lesions) was scanned with the thorax cavity filled with realistic activity concentrations. The breast phantom when scanned with the thoracic cavity filled with realistic activity was the closest achievable simulation of breast cancer patient. The simplified phantom (breast phantom scanned without the thorax cavity) does not provide a realistic activity distribution, scatter or attenuation properties (138).

The thoracic cavity is recognised as an important part of the anatomical lung phantom to provide better attenuation properties of any lung perfusion scans. However, the thoracic cavity was neglected in the design of our phantom. The justifications of not using thoracic background in this thesis were:

1. to minimise the time taken to complete the research;
2. to minimise the cost of the research;
3. the preliminary lung perfusion scan simulations using the phantom have been published in a peer reviewed journal and presented in peer reviewed scientific meetings. These show that lung perfusion images generated using the phantom (without the thoracic cavity) are acceptable scientific studies;
4. experienced Nuclear Medicine physicians that participated in one of the snapshot surveys confirmed that the lung perfusion images

generated using the phantom are at of a medium quality. The physicians also confirmed that the quality of lung perfusion images generated using the phantom are suitable for any clinical studies.

The visual effects of a thoracic background on the lung phantom were studied. A practical and economical non-radioactive thorax cavity was developed to be used together with the lung phantom. A water-filled container was chosen to simulate the thorax attenuation properties for the lung phantom. In this study, the dimensions of an actual thoracic cavity were not taken into account. Time and cost were two factors that limited the development of a better thorax cavity for this study. However, the water-filled container was still able to simulate the attenuation medium in thoracic cavity.

Many researchers have used water to simulate thoracic cavity in their radiology phantom studies. Sandborg et al. (139) in their published article reported that water is a soft tissue equivalent material for test phantoms in diagnostic-radiology. In an experiment by Doshi et al. (140), a thoracic phantom was filled with cold water to simulate thoracic (background) attenuator properties. Celler et al. (136) used a plastic cylinder (25 cm high and 24.5 cm diameter) filled with as a substitute thorax for quantitative dynamic functional imaging for SPECT.

7.2 Materials and methods

An experimental setup was designed to add attenuation medium effects on the lung phantom scans (see *Figure 7.1*). The water bath was considered as the thorax attenuation medium for 140 keV ^{99m}Tc gamma rays.

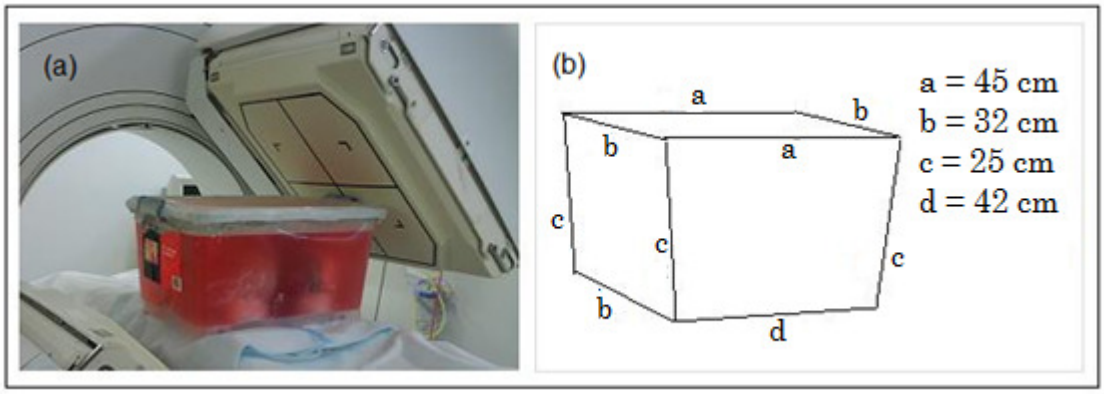

Figure 7.1: ***a*** *Experimental set-up: the anthropomorphic lung phantom submerged in water (red) on the gamma camera bed.* ***b*** *Dimensions of the water bath.*

Firstly, the left lung upper lobe superior perfusion defect insert was installed into the phantom. The phantom was scanned with the planar imaging protocol according to Kabir et al. (48).

Secondly, the phantom was placed in a rectangular container. The container was then filled with water. The water was dyed red to easily monitor leakage in the camera room (see *Figure 7.1*). Then, the phantom was scanned with the planar imaging protocol according to Kabir et al. (48).

7.3 Results

The planar perfusion images of the phantom are shown in *Figure 7.2*. The posterior view was chosen as it shows the perfusion defect at its largest.

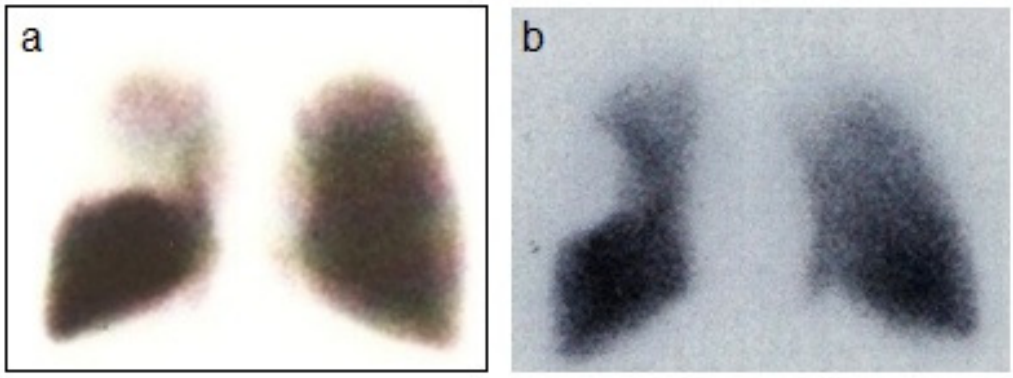

Figure 7.2: ***a*** *The planar posterior view of the anatomical lung phantom scanned without the water bath.* ***b*** *The planar posterior view of the anatomical lung phantom scanned with the water bath.*

The intensity of the gray value of pixels around the edge of images in *Figure 7.2* were analysed using the ImageJ software. A selection tool of the software was used to create region of interest (ROI) around the edges of images (see *Figure 7.3*). The ROI of the planar perfusion image when the lung phantom was scanned without the water bath was named ROI1; and was named ROI2 for planar perfusion image when the lung phantom was scanned with the water bath. The frequency distribution (histogram) of pixel values (0-255) in ROI1 and ROI2 are shown in *Figure 7.3*b and *Figure 7.3*c respectively.

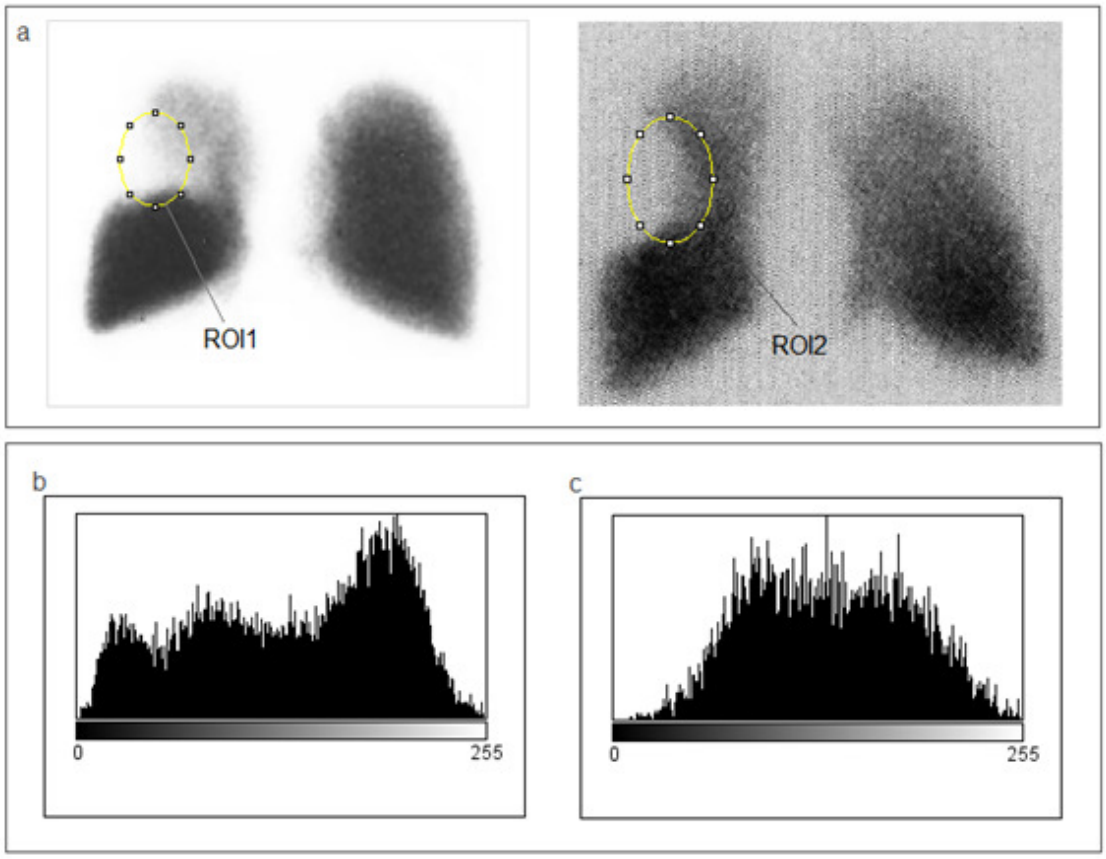

Figure 7.3: ***a*** *ROI1 is the edge of planar perfusion image of the lung phantom without water-filled container. ROI2 is the edge of planar perfusion image of the lung phantom with water-filled container.* ***b*** *Frequency distribution of pixel value intensities (0-255) in ROI1.* ***c*** *Frequency distribution of pixel value intensities (0-255) in ROI2.*

In *Figure 7.3b* the mean is 133.8 and standard deviation is 63.8. The mean is 134.9 and standard deviation is 49.6 respectively in *Figure 7.3c*. A much smaller standard deviation recorded in *Figure 7.3c* means the pixel intensity values in ROI2 lie closer around its mean value compared to ROI1. The ROI2 perfusion defect edges are much softer compared to the ROI1.

7.4 Discussion

In *Figure 7.1*, the aqueous solution of ^{99m}Tc in the lung phantom emits 140 keV gamma radiations as it decay. The gamma radiation interacted with; **i** the aqueous solution of ^{99m}Tc in the lung phantom, and **ii** water in the bath. The gamma radiation interacts with water by photoelectric and Compton scattering mechanisms (see Section 2.7). For energies between 50 keV to 550 keV, Compton scattering is the dominant interaction in material with lower atomic number; for example soft human tissues (atomic number = 7.5) (63). The combined effects of the Compton scattering (dominant interaction) and photoelectric is termed attenuation (63).

Perfusion defect in lung perfusion scans are normally seen as areas of decreased, rather than absent, (141-143), The edges of perfusion defect region when the lung phantom scanned with the water bath (*Figure 7.2*b) are softer, while the edges of the perfusion defect region when the lung phantom scanned without the water bath (*Figure 7.2*a) are sharp. The added attenuation medium generated planar perfusion images that more closely resemble patients' scintigraphic images.

7.5 Conclusion

In this thesis, the water bath was not included as part of the anatomical lung phantom in Chapters 3 to 6. All the planar and SPECT acquisitions

were done without the thoracic background attenuation material (water bath).

The findings in this chapter provide a positive indication that the image quality of lung perfusion images closely resemble lung perfusion image of a patient when the lung phantom was scanned with the water bath. Based on the positive results in this chapter, the development of a tissue equivalent thoracic cavity for the lung phantom is highly recommended in future studies.

8. CONCLUSION

8.1 Review of the thesis

The thesis has successfully demonstrated a method to design and to develop a novel anatomical lung phantom. The lung phantom was exclusively designed to model lung perfusion conditions of suspected PE patients via planar or SPECT imaging. Initial studies showed that the lung phantom was able to model clinical images of suspected PE phantom via planar and SPECT imaging.

The lung phantom has a higher HU values compared to the human lungs. The attenuation property of the lung phantom was compromised to permit high quality anatomical structure of the phantom, as described in Chapter 3. The accuracy of anatomical representations of the lung phantom is a crucial factor in this thesis. The physical material used to model lung perfusion defects (lung bronchopulmonary segments) was able to closely represent the shapes of the human lung. The distribution of ^{99m}Tc radionuclide was analysed, and confirmed to be homogenous throughout the lung phantom. The anatomical lung phantom was able to reproduce planar perfusion images at of a medium reproducibility quality.

A small scale quality assurance study was conducted with the lung phantom used as the main tool. The results showed occasionally Nuclear Medicine physicians make incorrect diagnosis of pulmonary embolism on planar lung perfusion images using the revised PIOPED criteria.

A comprehensive lung perfusion imaging planar and SPECT atlas was included in Chapter 6 of the thesis. Via a survey form, Nuclear Medicine physicians were asked to comment on the efficacy of the atlas. Whilst the statistical power of the study is low (due to small sample size), the results are still considered as a valuable snapshot opinions (opinions on the atlas) of experienced physicians. The physicians agreed that the atlas is a useful reference resource and teaching material to inexperienced Nuclear Medicine physicians.

Finally, use of a uniform water bath revealed the change in attenuation affects the quality of lung planar perfusion images modelled using the lung phantom. However, the water bath was not included in the research project. Justifications for the decision were described in Chapter 7.

On the whole, this thesis has successfully addressed the main objective and other minor objectives of the research.

8.2 Future work

Following the thesis completion, the author plans to continue a number of related projects related to the research including:

1. Remodel the lung bronchopulmonary segments (lung perfusion defect inserts) using tissue equivalent materials. A further literature study is needed to find a tissue equivalent material that is able to better hold the anatomical shapes of human lung.
2. Design an attenuation-correct thoracic cavity that encloses the anatomical lung phantom. The thoracic cavity shall provide background attenuation property to the lung phantom.
3. Reconduct all the survey studies at a larger sample size in order to produce statistically significant conclusions to the studies.
4. Develop more quality assurance studies concerning lung perfusion and ventilation scans using the revised PIOPED criteria.
5. Compare the sensitivity of planar and SPECT imaging on lung perfusion and ventilation scans for PE diagnosis using the anatomical lung phantom.

9. REFERENCES

1. Segars WP, Sturgeon G, Mendonca S, Grimes J, Tsui BMW. 4D XCAT phantom for multimodality imaging research. Medical Physics. 2010;37(9):4902-15.

2. Branham T. Phantom testing. Medical Physics. 2007;34(6):2578-.

3. Di Francia G, Scafè R, De Vincentis G, La Ferrara V, Iurlaro G, Nasti I, et al. Porous silicon phantoms for high-resolution scintillation imaging. Nuclear Inst and Methods in Physics Research, A. 2006;569(2):197-200.

4. Walker GC, Berry E, Smye SW, Brettle DS. Materials for phantoms for terahertz pulsed imaging. Physics in Medicine and Biology. 2004;49(21):N363-N9.

5. SabbirAhmed ASM, Demir M, Kabasakal L, Uslu I. A dynamic renal phantom for nuclear medicine studies. Medical Physics. 2005;32(2):530-8.

6. Heikkinen JO. Physical phantom for renography. Journal of Nuclear Medicine. 2001;42(5):102P-P.

7. Als C, Bräutigam P, Mirzaei S. Sweet nuclear medicine phantoms for scintigraphic sentinel lymph node detection: a cooking recipe. European Journal of Nuclear Medicine and Molecular Imaging. 2005;32(5):623.

8. Park M-A, Zimmerman RE, Taberner A, Kaye MW, Moore SC. Design and Fabrication of Phantoms Using Stereolithography for Small-Animal Imaging Systems. Molecular Imaging and Biology. 2008;10(5):231-6.

9. Hunt DC, Easton H, Caldwell CB. Design and construction of a quality control phantom for SPECT and PET imaging. Medical Physics. 2009;36(12):5404-11.

10. Aubert-Broche B, Evans AC, Collins L. A new improved version of the realistic digital brain phantom. NeuroImage. 2006;32(1):138-45.

11. Chicco P, Magnussen JS, Mackey DW, Murray IP, van der Wall H. Recognition of subsegmental scintigraphic defects in virtual lung scintigraphy. Nuclear Medicine Communications. 1997;18(8):728-33.

12. Kramer GH, Crowley P. An improved virtual torso phantom. Radiation Protecttion Dosimetry. 2000;88(3):233-7.

13. Kramer GH, Capello K, Sung J. The LLNL voxel phantom: comparison with the physical phantom and previous virtual phantoms. Health physics. 2007;93(6):696-700.

14. Hart G. A UK survey of nuclear medicine imaging performance using the TransBone anthropomorphic phantom. Nuclear Medicine Communications. 1997;18(7):668-72.

15. Cannon LM, King DM, Browne JE. The Role of Anthropomorphic Phantoms in Diagnostic Ultrasound Imaging for Disease Characterization (abstract). AIP Conference Proceedings. 2009(Journal Article).

16. Chris C, John C, Larry D, Margaret L. Development of radiographic chest phantoms. Medical Physics. 1986;13(6):917.

17. Schläger M. Comparison of various anthropomorphic phantom types for in vivo measurements by means of Monte Carlo simulations. Radiation Protection Dosimetry. 2011;144(1-4):384-8.

18. Kovtun AN, Puzikov AG, Sokolov IA, Kozheurov VP, Degteva MO. Anthropomorphic phantom with strontium-90 incorporated in the skeleton. Radiation Protection Dosimetry. 2000;89(3-4):301-4.

19. Carton A-K, Bakic P, Ullberg C, Derand H, Maidment ADA. Development of a physical 3D anthropomorphic breast phantom. Medical Physics. 2011;38(2):891-6.

20. Harrison KM, Mathematical UoNSo, Sciences P. A novel anthropomorphic pelvic phantom designed for multicentre level III dosimetry intercomparison: University of Newcastle; 2009.

21. Heikkinen JO, Kuikka JT, Rautio PJ. Interdepartmental audit with an anatomically realistic lung phantom. Journal of nuclear medicine technology. 2006;34(1):34.

22. Rojano K, Kwok L, Dale L, James B. Technical note: A deformable phantom for dynamic modeling in radiation therapy. Medical Physics. 2007;34(1):199-201.

23. Yoon S, Henry RW, Bouley DM, Bennett NR, Fahrig R. Characterization of a novel anthropomorphic plastinated lung phantom. Medical Physics. 2008;35(12):5934-43.

24. William U, Amanda S. Lung phantoms now available. Journal of Nuclear Medicine. 2000;41(3):19N-N.

25. Wood KE. A History of Pulmonary Embolism and Deep Venous Thrombosis. Critical Care Clinics. 2009;25(1):115-31.

26. Muckart D. Pulmonary embolism. CME: Your SA Journal of CPD. 2010;28(6):293.

27. Blann AD, Ebrary. Deep vein thrombosis and pulmonary embolism: a guide for practitioners. Cumbria, CA: M&K Update; 2009.

28. Partridge MR, Ebrary. Understanding Respiratory Medicine: A Problem-Oriented Approach. New York: Thieme Medical Publishers, Incorporated [Distributor]; 2006.

29. Weinberger SE, Cockrill BA, Mandel J. Principles of pulmonary medicine. Philadelphia: Saunders/Elsevier; 2008.

30. Galson SK. Prevention of deep vein thrombosis and pulmonary embolism. Public health reports (Washington, DC : 1974). 2008;123(4):420-1.

31. Brian P. Pulmonary Embolism. JAMA: The Journal of the American Medical Association. 2001;285(6):836-.

32. Goldhaber SZ. Pulmonary embolism. The New England Journal of Medicine. 1998;339(2):93-104.

33. Palla A, Di Ricco G, Giuntini C, Melillo E, Marini C. Pulmonary embolism: epidemiology. Chest. 1995;107(1 Suppl):3.

34. McRae S. Pulmonary embolism. Australian Family Physician. 2010;39(6):462.

35. Cardin T, Marinelli A. Pulmonary embolism. Critical care nursing quarterly. 2004;27(4):310.

36. Stein PD, Matta F. Acute pulmonary embolism. Current Problems in Cardiology. 2010;35(7):314-76.

37. Stein PD, Hull RD, Patel KC, Olson RE, Ghali WA, Alshab AK, et al. Venous thromboembolic disease: comparison of the diagnostic process in men and women. Arch Intern Med. 2003;163(14):1689-94.

38. 2008 AE. The Burden of Venous Thromboembolism in Australia: The Australia and New Zealand Working Party on the Management and Prevention of Venous Thromboembolism 2008 May.

39. Mark P. Pulmonary embolism: A lung attack. Emergency. 1998;30(2):32.

40. Ritesh A, Subhash V. Acute pulmonary embolism. Eastern Journal of Medicine. 2009;14(2):57.

41. Bajc M, Neilly JB, Miniati M, Schuemichen C, Meignan M, Jonson B. EANM guidelines for ventilation/perfusion scintigraphy : Part 2.

Algorithms and clinical considerations for diagnosis of pulmonary emboli with V/P(SPECT) and MDCT. European Journal of Nuclear Medicine and Molecular Imaging. 2009;36(9):1528-38.

42. Hogg K, Dawson D, Mackway-Jones K. Outpatient diagnosis of pulmonary embolism: the MIOPED (Manchester Investigation Of Pulmonary Embolism Diagnosis) study. Emergency medicine journal : EMJ. 2006;23(2):123-7.

43. The PI. Value of the Ventilation/Perfusion Scan in Acute Pulmonary Embolism: Results of the Prospective Investigation of Pulmonary Embolism Diagnosis (PIOPED). JAMA: The Journal of the American Medical Association. 1990;263(20):2753.

44. Kuriakose J, Patel S. Acute pulmonary embolism. Radiologic clinics of North America. 2010;48(1):31-50.

45. Anderson DR, Rodger MA, Wells PS. Excluding Pulmonary Embolism With Computed Tomographic Pulmonary Angiography or Ventilation-Perfusion Lung Scanning--Reply. JAMA: The Journal of the American Medical Association. 2008;299(14):1664-5.

46. Criner GJ, D'Alonzo GE. Pulmonary pathophysiology: Fence Creek Publishing; 1999.

47. Fitzpatrick JM, Sonka M. Handbook of Medical Imaging: Medical Image Processing and Analysis: SPIE; 2000.

48. Kabir NA, Harvey SB, Rosenfeld A. Design and fabrication of pulmonary embolism phantom for planar and SPECT V/Q imaging quality assurance. Australasian Physical & Engineering Sciences in Medicine. 2010;33(3):271-7.

49. Postmus PE, Hoekstra OS, Stokkel MPM, Hagen PJ, Hartmann IJC, Prins MH, et al. Comparison of observer variability and accuracy of different criteria for lung scan interpretation. JOURNAL OF NUCLEAR MEDICINE. 2003;44(5):739-44.

50. Palmer J, Jonson B, Bajc M, Bitzén U, Division V, Lund U, et al. Comprehensive ventilation/perfusion SPECT. JOURNAL OF NUCLEAR MEDICINE. 2001(Journal Article).

51. Marsh S, Barnden L, O'Keeffe D. Validation of co-registration of clinical lung ventilation and perfusion SPECT. Australasian Physical & Engineering Sciences in Medicine. 2011;34(1):63-8.

52. Collart JP, Gillet JB, Roelants V, De Coster P, Trigaux JP, Vanpee D, et al. Is a lung perfusion scan obtained by using single photon emission computed tomography able to improve the radionuclide diagnosis of

pulmonary embolism? Nuclear Medicine Communications. 2002;23(11):1107-13.

53. Magnussen JS, Chicco P, Palmer AW, Bush V, Mackey DW, Storey G, et al. Single-photon emission tomography of a computerised model of pulmonary embolism. European Journal of Nuclear Medicine and Molecular Imaging. 1999;26(11):1430-8.

54. Bajc M, Neilly JB, Miniati M, Schuemichen C, Meignan M, Jonson B. EANM guidelines for ventilation/perfusion scintigraphy : Part 1. Pulmonary imaging with ventilation/perfusion single photon emission tomography. European Journal of Nuclear Medicine and Molecular Imaging. 2009;36(8):1356-70.

55. Magnussen JS, Chicco P, Palmer AW, Bush V, Mackey DW, Storey G, et al. Single-photon emission tomography of a computerised model of pulmonary embolism. European Journal Of Nuclear Medicine. 1999;26(11):1430-8.

56. Stein PD, Freeman LM, Tapson VF, Woodard PK, Matta F, Bailey DL, et al. SPECT in Acute Pulmonary Embolism. Journal of Nuclear Medicine. 2009;50(12):1999-2007.

57. Weinmann P, Moretti J-L, Brauner M. Usefulness of Tomographic Versus Planar Lung Scintigraphy in Suspectd Pulmonary Embolism in a daily Practice. The Open Medical Imaging Journal. 2008;2:49-55.

58. Harris B, Bailey DL, Roach PJ, Schembri GP, Hoshon I, Chicco P, et al. A clinical comparison between traditional planar V/Q images and planar images generated from SPECT V/Q scintigraphy. Nuclear Medicine Communications. 2008;29(4):323-30.

59. Stein PD, Ebrary. Pulmonary embolism. Malden, Mass: Blackwell Futura; 2007.

60. Gottschalk A, Sostman HD, Coleman RE, Juni JE, Thrall J, McKusick KA, et al. Ventilation-Perfusion Scintigraphy in the PIOPED Study. Part II. Evaluation of the Scintigraphic Criteria and Interpretations. J Nucl Med. 1993 July 1, 1993;34(7):1119-26.

61. Hull RD, Coates G, Gill GJ, Raskob GE, Leclerc JR, Jay RM, et al. Diagnostic value of ventilation-perfusion lung scanning in patients with suspected pulmonary embolism. Chest. 1985;88(6):819.

62. Hartmann LJC, Hoekstra OS, Teule GJJ, Stokkel MPM, Hagen PJ, Prins MH, et al. How to use a gestalt interpretation for ventilation-perfusion lung scintigraphy. Journal of Nuclear Medicine 2002;43(10):1317-23.

63. Powsner RA, Powsner ER, Ebrary. Essential nuclear medicine physics. Malden, Mass: Blackwell Pub; 2006.

64. Low FH. Radioisotope measurement in nuclear medicine. University of Michigan: Nuclear Division, Picker X-Ray Corp.; 1960.

65. Pant GS, Ebrary. Basic Physics and Radiation Safety in Nuclear Medicine. New Delhi: ebrary, Incorporated [Distributor]; 2008.

66. Turner JE, Ebooks C. Atoms, radiation, and radiation protection. Weinheim: Wiley-VCH; 2007.

67. Podgorsˇak EB, Ebooks C. Radiation physics for medical physicists. New York: Springer; 2006.

68. Allison W, Ebrary. Fundamental physics for probing and imaging. Oxford: Oxford University Press; 2006.

69. Pant GS, Ebrary. Advances in Diagnostic Medical Physics. New Delhi: ebrary, Incorporated [Distributor]; 2006.

70. Del Guerra A, Ebrary. Ionizing radiation detectors for medical imaging. Hackensack, NJ: World Scientific Pub; 2004.

71. Brant WE, Helms CA, Ovid. Fundamentals of diagnostic radiology. Philadelphia: Lippincott, Williams & Wilkins; 2007.

72. Saha GB. Physics and radiobiology of nuclear medicine. New York: Springer-Verlag; 1993.

73. Cherry SR, Sorenson JA, Phelps ME. Physics in nuclear medicine. Philadelphia, PA: Saunders; 2003.

74. Rashband WS. ImageJ. National Institute of Health, Bethasda, Maryland, USA.

75. Abstracts. Internal medicine journal. 2009;39:A105-A35.

76. Abstracts. Internal medicine journal. 2010;40:1-36.

77. Castellani M, Vanoli M, Calì G, Bacchiani G, Origgi L, Reschini E, et al. Ventilation-perfusion lung scan for the detection of pulmonary involvement in Takayasu's arteritis. European Journal Of Nuclear Medicine. 2001;28(12):1801-5.

78. Rhoades R, Tanner GA. Medical physiology. Philadelphia: Lippincott Williams & Wilkins; 2003.

79. Clemente CD. Anatomy, a regional atlas of the human body. Baltimore: Urban & Schwarzenberg; 1981.

80. Dail DH, Tomashefski JF, Hammar SP, Cagle PT. Dail and Hammar's Pulmonary Pathology: Nonneoplastic lung disease: Springer; 2008.

81. Boyes J. The Effect of Atomic Number and Mass Density on the Attenuation of X-rays. Queen's Helath Sciences Journal. 2003;6(2):23.

82. Bushberg JT. The essential physics of medical imaging. Philadelphia: Lippincott Williams & Wilkins; 2002.

83. Parker J. SNM Procedure Guideline for General Imaging. http://interactivesnmorg/docs/General_Imaging_Version_60pdf. 2010;6.

84. Miller WS. The lung. 1947.

85. Benseler JS, Ebrary. The Radiology Handbook: A Pocket Guide to Medical Imaging. Athens: Chicago Distribution Center [Distributor]; 2006.

86. Lee WG. Principles of CT: Multislice CT. Journal of nuclear medicine technology. 2008;36(2):57.

87. Soejima K, Yamaguchi K, Kohda E, Takeshita K, Ito Y, Mastubara H, et al. Longitudinal follow-up study of smoking-induced lung density changes by high-resolution computed tomography. American journal of respiratory and critical care medicine. 2000;161(4 Pt 1):1264-73.

88. Kalef-Ezra J, Karantanas A, Tsekeris P. CT Measurement of Lung Density. Acta Radiologica. 1999;40(3):333-7.

89. Manier G, Duclos M, Arsac L, Moinard J, Laurent F. Distribution of lung density after strenuous, prolonged exercise. Journal of applied physiology (Bethesda, Md : 1985). 1999;87(1):83-9.

90. Camm AJ, Lüscher TF, Serruys PW. The ESC textbook of cardiovascular medicine: Blackwell Pub.; 2006.

91. Ritt P, Vija H, Hornegger J, Kuwert T. Absolute quantification in SPECT. European Journal of Nuclear Medicine and Molecular Imaging. 2011;38(1):69-77.

92. Matusiak K, Wasilewska-Radwanska M, Stepien A. Dynamic heart phantom for the quality control of SPECT equipment. Physica medica : PM : an international journal devoted to the applications of physics to medicine and biology : official journal of the Italian Association of Biomedical Physics (AIFB). 2008;24(2):112-6.

93. Kim JS, Dailey R, Ebrary. Biostatistics for oral healthcare. Ames, Iowa: Blackwell Munksgaard; 2008.

94. Gil-Monte PR, Olivares Faúndez VE. Psychometric properties of the "Spanish Burnout Inventory" in Chilean professionals working to physical disabled people. The Spanish journal of psychology. 2011;14(1):441-51.

95. Miles J, Shevlin M. Applying regression & correlation: a guide for students and researchers. London: SAGE; 2000.

96. McCluskey A, Lalkhen AG. Statistics II: Central tendency and spread of data. Continuing Education in Anaesthesia, Critical Care & Pain. 2007;7(4):127-30.

97. Peat JK, Barton B. Medical statistics: a guide to data analysis and critical appraisal. Malden, Mass: Blackwell Pub; 2005.

98. Jacobson DR. A Quality Assurance Phantom for Diagnostic Radiology. Radiation Protection Dosimetry. 1993;49(1-3):53-4.

99. Guatelli S, Mascialino B, Pia MG, Pokorski W, editors. Geant4 Anthropomorphic Phantoms 2006: IEEE.

100. Snyder WS, Fisher JHL, Ford MR, Warner GG. Estimates of absorbed fractions for monoenergetic photon sources uniformly distributed

in various organs of a heterogeneous phantom. Journal of nuclear medicine : official publication, Society of Nuclear Medicine. 1969(Journal Article):Suppl 3:7.

101. Heikkinen J, Ahonen A, Kuikka JT, Rautio P. Quality of myocardial perfusion single-photon emission tomography imaging: multicentre evaluation with a cardiac phantom. European Journal Of Nuclear Medicine. 1999;26(10):1289-97.

102. Jamieson S. Likert scales: how to (ab)use them. Medical Education. 2004;38(12):1217-8.

103. Carlin JB, Doyle LW. Sample size. Journal of Paediatrics and Child Health. 2002;38(3):300-4.

104. Crewson PE, Sunshine JH. Diagnostic Radiologists' Subspecialization and Fields of Practice. American Journal of Roentgenology. 2000 May 1, 2000;174(5):1203-9.

105. Fritz S. What is a Survey? American Statistical Association. 2004.

106. Suna K, Franc JTW, Yi-Hwa L. Validation of the Yale circumferential quantification method using (201)T1 and (99m)Tc: A phantom study. The Journal of Nuclear Medicine. 2000;41(8):1436.

107. Hirsh J, Hoak J. Management of deep vein thrombosis and pulmonary embolism. A statement for healthcare professionals. Council on Thrombosis (in consultation with the Council on Cardiovascular Radiology), American Heart Association. Circulation. 1996;93(12):2212.

108. Suga K, Kawakami Y, Koike H, Iwanaga H, Tokuda O, Okada M, et al. Lung ventilation-perfusion imbalance in pulmonary emphysema: assessment with automated V/Q quotient SPECT. Annals of nuclear medicine. 2010;24(4):269-77.

109. Riedel M. Diagnosing pulmonary embolism. Postgraduate Medical Journal. 2004;80(944):309-19.

110. Fletcher J, MacLellan D, Fisher C, Gibbs H, Matthews G, Stacey M, et al. Diagnosis and Treatment of Venous Thromboembolism: The National Working Party on the Management and Prevention of Venous Thromboembolism

111. Alistair F, Charles H, Ella M. Pulmonary embolism: identification, clinical features and management. Nursing Standard. 2009;23(28):49.

112. Mountain D. Diagnosing pulmonary embolism: A question of too much choice? Emergency Medicine. 2003;15(3):250-62.

113. Weiser JC, Drummond KT, Evans BD, Shock DJ, Frick MP. Quality assurance for digital imaging. Journal of digital imaging : the official journal of the Society for Computer Applications in Radiology. 1997;10(3 Suppl 1):7-8.

114. National Council on Radiation P, Measurements. Quality assurance for diagnostic imaging equipment : recommendations of the National Council on Radiation Protection and Measurements. United States1988.

115. Alfaro D, Levitt MA, English DK, Williams V, Eisenberg R. Accuracy of Interpretation of Cranial Computed Tomography Scans in an Emergency Medicine Residency Program. Annals of emergency medicine. 1995;25(2):169-74.

116. Magnussen JS, Chicco P, Palmer AW, Mackey DW, Magee M, Murray IP, et al. Enhanced accuracy and reproducibility in reporting of lung scintigrams by a segmental reference chart: 1. Journal of nuclear medicine : official publication, Society of Nuclear Medicine. 1998;39(6):1095-9.

117. Kumar AM, Parker JA. Ventilation/Perfusion Scintigraphy. Emergency Medicine Clinics of North America. 2001;19(4):957-74.

118. Gray HW, Bessent RG. Pulmonary embolism exclusion: a practical approach to low probability using the PIOPED data. European Journal Of Nuclear Medicine. 1998;25(3):271-6.

119. The PI. Value of the Ventilation/Perfusion Scan in Acute Pulmonary Embolism: Results of the Prospective Investigation of Pulmonary Embolism Diagnosis (PIOPED). JAMA: The Journal of the American Medical Association. 1990;263(20):2753-9.

120. Morrell NW, Nijran KS, Jones BE, Biggs T, Seed WA. The underestimation of segmental defect size in radionuclide lung scanning. Journal of nuclear medicine : official publication, Society of Nuclear Medicine. 1993;34(3):370-4.

121. Jackson CL. Segmental bronchi and the bronchopulmonary segments. American journal of surgery. 1955;89(2):319-23.

122. Swensen SJ, Olson EJ, Ryu JH, Pellikka PA. Diagnosis of pulmonary embolism with use of computed tomographic angiography. Mayo Clinic proceedings Mayo Clinic. 2001;76(1):59-65.

123. Murchison JT, Gavan DR, Reid JH. Clinical utilization of the non-diagnostic lung scintigram. Clinical Radiology. 1997;52(4):295-8.

124. Magnussen JS, Chicco P, Palmer AW, Mackey DW, Magee M, Murray IP, et al. Variability of perceived defect size in virtual lung scintigraphy. Journal of nuclear medicine : official publication, Society of Nuclear Medicine. 1998;39(2):361-5.

125. Brunswick JE, Ilkhanipour K, Seaberg DC, McGill L. Radiographic interpretation in the emergency department. The American journal of emergency medicine. 1996;14(4):346-8.

126. ANZSNM – POSTERS PRESENTATIONS. Internal medicine journal. 2011;41:20-45.

127. Kimberly B. Misdiagnosis in the emergency department: A review of five major conditions. Physician Assistant. 2000;24(12):38.

128. Howarth DM, Booker JA, Voutnis DD. Diagnosis of pulmonary embolus using ventilation/perfusion lung scintigraphy: more than 0.5 segment of ventilation/perfusion mismatch is sufficient. Internal medicine journal. 2006;36(5):281-8.

129. Miniati M, Scoscia E, Dainelli A, Formichi B, Di Ricco G, Prediletto R, et al. A diagnostic strategy for pulmonary embolism based on standardised pretest probability and perfusion lung scanning: a management study. European Journal of Nuclear Medicine and Molecular Imaging. 2003;30(11):1450-6.

130. Zutic H, Kucukalic-Selimovic E, Skopljak-Beganovic A, Begic A, Begic A. Screening of pulmonary embolism by ventilation / perfusion tomography-SPECT and comparation with planar scintigraphy--our experiences. Medicinski arhiv. 2008;62(4):220.

131. Reinartz P, Nowak B, Wildberger JE, Mahnken AH, Buell U, Schaefer W. Tomographic imaging in the diagnosis of pulmonary embolism: A comparison between V/Q lung scintigraphy in SPECT technique and multislice spiral CT. Journal of Nuclear Medicine. 2004;45(9):1501-8.

132. Petersen CL, Kristoffersen US, Kjaer A, Mortensen J, von der Recke P, Gutte H, et al. Comparison of V/Q SPECT and planar V/Q lung scintigraphy in diagnosing acute pulmonary embolism. Nuclear Medicine Communications. 2010;31(1):82-6.

133. Morrell NW, Roberts CM, Jones BE, Nijran KS, Biggs T, Seed WA. The anatomy of radioisotope lung scanning. Journal of nuclear medicine : official publication, Society of Nuclear Medicine. 1992;33(5):676-83.

134. Carbonell AM, Landis GA, Miale JA, Moser KM. Construction and testing of a thorax-lung phantom to aid in scintiphotograph interpretation. Investigative radiology. 1969;4(4):275.

135. Hagen PJ, Hartmann IJC, Hoekstra OS, Stokkel MPM, Postmus PE, Prins MH, et al. Comparison of observer variability and accuracy of

different criteria for lung scan interpretation. Journal of nuclear medicine : official publication, Society of Nuclear Medicine. 2003;44(5):739-44.

136. Celler A, Farncombe T, Harrop R, Lyster D. Dynamic heart-in-thorax phantom for functional SPECT. IEEE Transactions on Nuclear Science. 1997;44(4):1600-5.

137. Saha GB, Broga D. Basics of PET Imaging, Physics, Chemistry, and Regulations, 2nd Edition. Medical Physics. 2011;38(2):1124.

138. Doshi NK, Basic M, Cherry SR. Evaluation of the detectability of breast cancer lesions using a modified anthropomorphic phantom. Journal of nuclear medicine : official publication, Society of Nuclear Medicine. 1998;39(11):1951-7.

139. Sandborg M, Carlsson GA, Persliden J, Dance DR, Centrum för medicinsk bildvetenskap och visualisering C, Kirurgi- och o, et al. Comparison of different Materials for Test Phantoms in Diagnostic-Radiology. Radiation Protection Dosimetry. 1993;49(1-3):345-7.

140. Doshi NK, Basic M, Cherry SR. Evaluation of the detectability of breast cancer lesions using a modified anthropomorphic phantom: 1. Journal of nuclear medicine : official publication, Society of Nuclear Medicine. 1998;39(11):1951-7.

141. Bailey DL, Schembri GP, Harris BE, Bailey EA, Cooper RA, Roach PJ. Generation of planar images from lung ventilation/perfusion SPECT. Annals of nuclear medicine. 2008;22(5):437-45.

142. Kluge A, Dill T, Ekinci O, Hansel J, Hamm C, Pitschner HF, et al. Decreased pulmonary perfusion in pulmonary vein stenosis after radiofrequency ablation: assessment with dynamic magnetic resonance perfusion imaging. Chest. 2004;126(2):428-37.

143. Pickhardt PJ, Fischer KC. Unilateral hypoperfusion or absent perfusion on pulmonary scintigraphy: differential diagnosis. AJR American journal of roentgenology. 1998;171(1):145-50.

10. APPENDIXES

Appendix *A*

Lung Perfusion Image Evaluation 1: Anatomical properties

Introduction:

1. This survey contains questions relating to lung perfusion images of a lung phantom.
2. The phantom was manufactured for research purposes. The main objective of the research is to investigate Nuclear Medicine Physician interpretive performance in evaluating lung perfusion images based on the revised PIOPED criteria. This current survey was developed solely to seek Nuclear Medicine Physician opinion on the phantom's representation of lung perfusion imaging of patients with suspected pulmonary embolism.
3. The images are simulated scintigraphic images of a human lung perfusion scan with and without lung segmental perfusion defects, and mimic a lung perfusion scan for suspected lung thrombolism patients. All perfusion defects are assumed as V/Q mismatch defects.
4. In a normal clinical lung V/Q scan, a perfusion defect appears as reduced or subsegmental perfusion. However, the images generated by the manufactured phantom appear as absent lung perfusion defects.
5. The evaluation survey is divided into two parts.
    i. In the first part, a set of question are presented regarding three sets of lung perfusion images.
    ii. The second part, a blind test for Nuclear Medicine physicians, who are required to identify five different segmental defects in lung perfusion images.

Instruction:

Please score/answer all questions based on criteria given in Table A.

Table A

Score	Image quality	Specification
1	Poor	Not adequate for clinical application.
2	Average	Barely adequate for limited clinical application.
3	Satisfactory	Adequate for clinical but not for exact scientific application.
4	Good	Adequate for clinical and exact scientific application.
5	Excellent	Excellent for clinical and scientific application.

Part 1

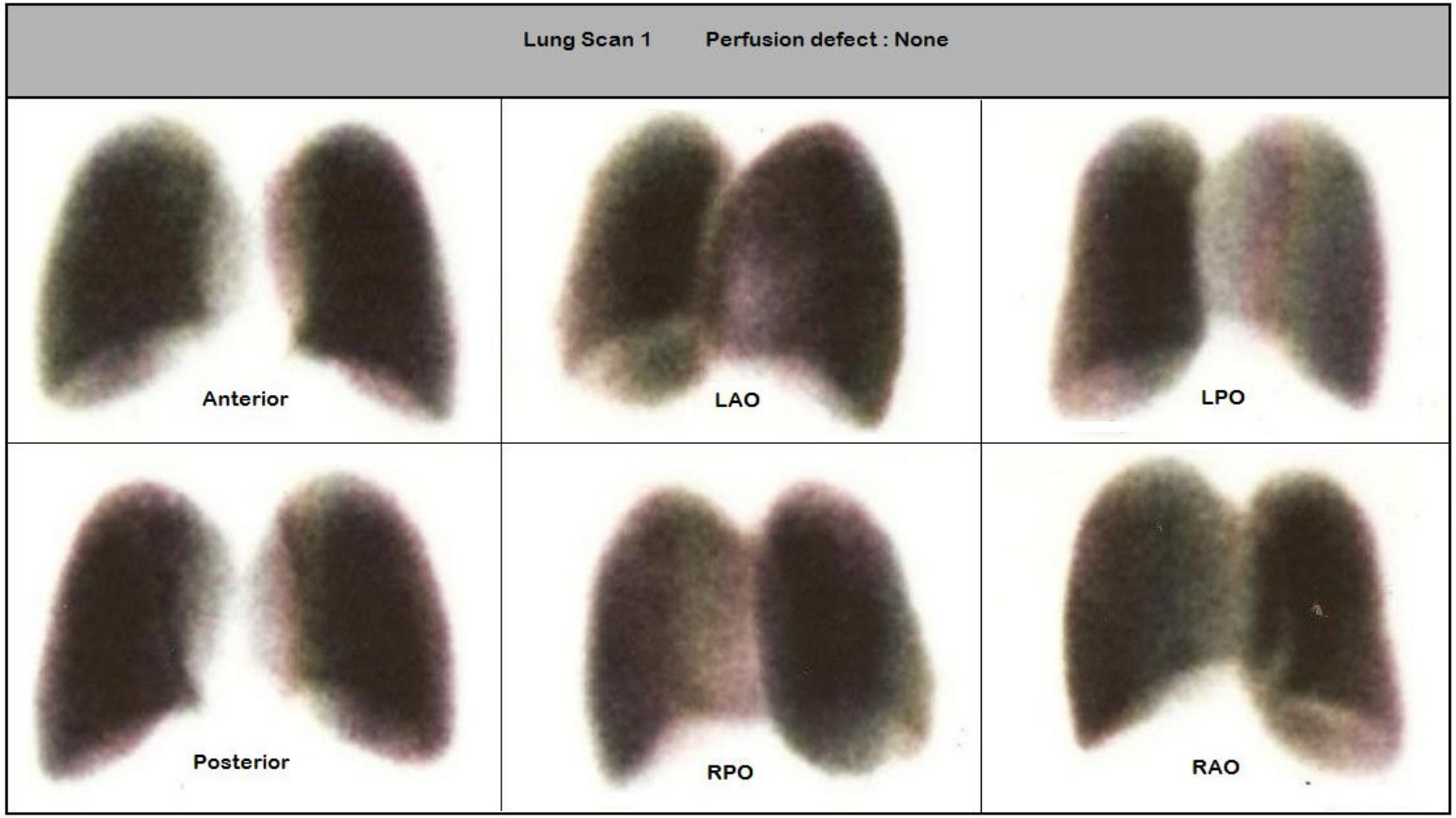

Figure 1

	Questions – Figure 1	**Score**				
		1	2	3	4	5
1	How well does the lung perfusion image set in Figure 1 represent the **anatomical orientation** of a lung perfusion image set of a suspected pulmonary embolism patient with the indicated clinical condition?	o	o	o	o	o
2	How well does the lung perfusion image set in Figure 1 represent the **anatomical location** of a lung perfusion image set of a suspected pulmonary embolism patient with the indicated clinical condition?	o	o	o	o	o
3	How well does the lung perfusion image set in Figure 1 represent the **anatomical shape** of a lung perfusion image set of a suspected pulmonary embolism patient with the indicated clinical condition?	o	o	o	o	o
4	How do you rate the overall ability of the image set in Figure 1 to represent a planar lung perfusion image set of a patient having suspected pulmonary embolism?	o	o	o	o	o

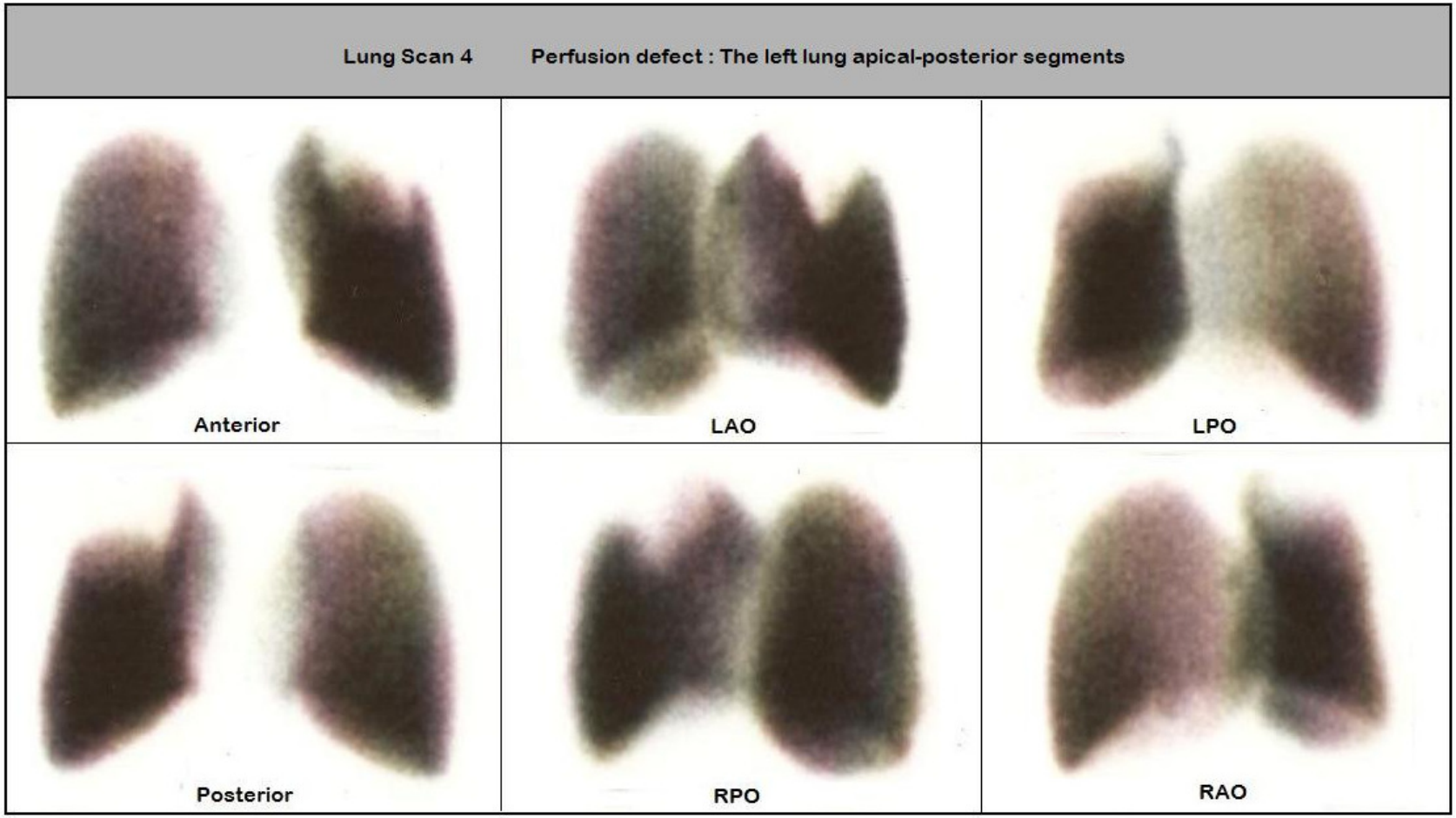
Lung Scan 4
Perfusion defect : The left lung apical-posterior segments
Anterior
LAO
LPO
Posterior
RPO
RAO

Figure 2

	Questions – Figure 2	**Score**				
		1	2	3	4	5
1	How well does the lung perfusion image set in Figure 2 represent the **anatomical orientation** of a lung perfusion image set of a suspected pulmonary embolism patient with the indicated clinical condition?	o	o	o	o	o
2	How well does the lung perfusion image set in Figure 2 represent the **anatomical position/location** of a lung perfusion image set of a suspected pulmonary embolism patient with the indicated clinical condition?	o	o	o	o	o
3	How well does the lung perfusion image set in Figure 2 represent the **anatomical shape** of a lung perfusion image set of a suspected pulmonary embolism patient with the indicated clinical condition?	o	o	o	o	o
4	How do you rate the overall ability of the image set in Figure 2 to represent a planar lung perfusion image set of a patient having suspected pulmonary embolism?	o	o	o	o	o

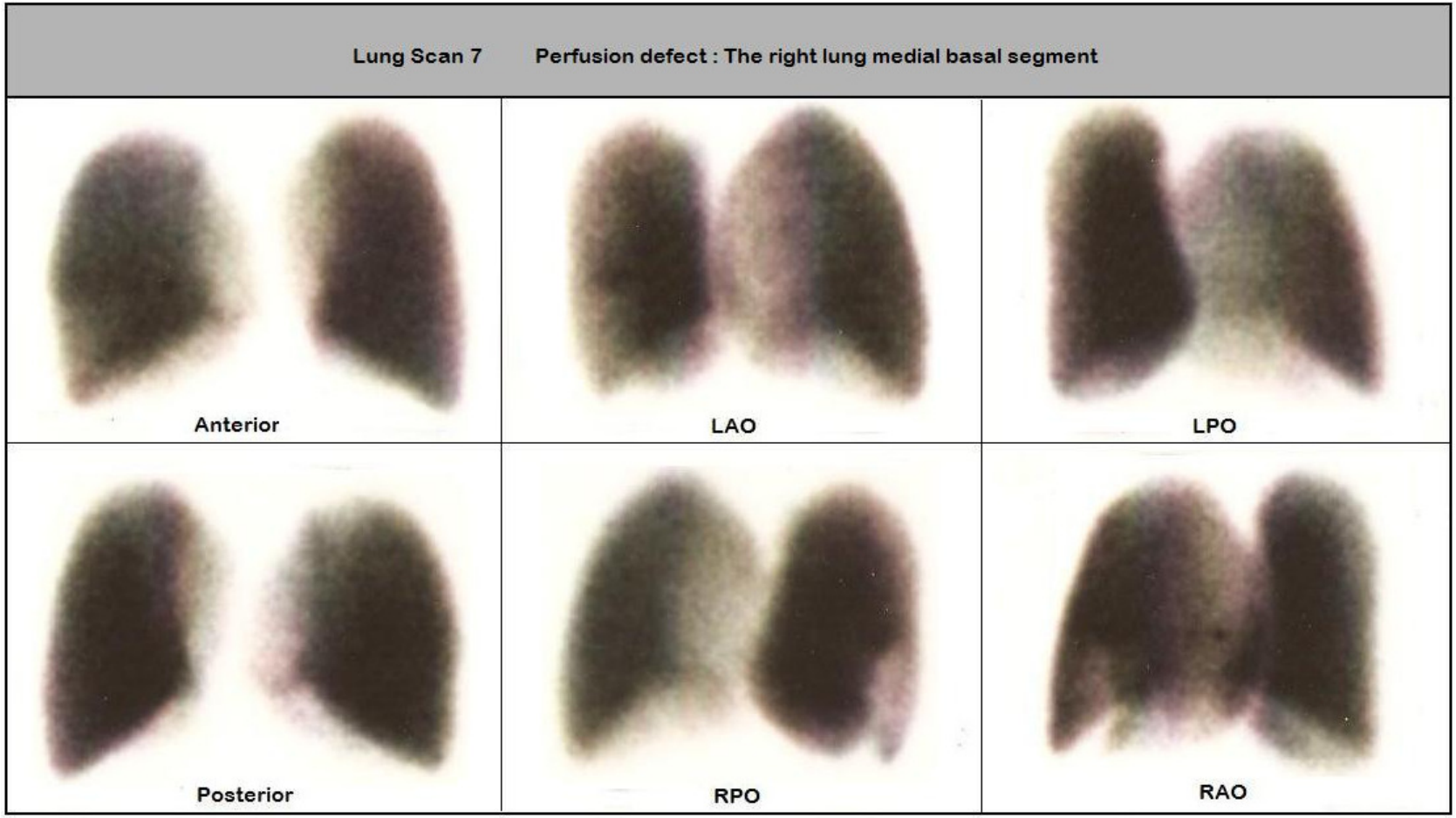
Lung Scan 7
Perfusion defect : The right lung medial basal segment
Anterior
LAO
LPO
Posterior
RPO
RAO

Figure 3

	Questions – Figure 3	**Score**				
		1	2	3	4	5
1	How well does the lung perfusion image set in Figure 3 represent the **anatomical orientation** of a lung perfusion image set of a suspected pulmonary embolism patient with the indicated clinical condition?	o	o	o	o	o
2	How well does the lung perfusion image set in Figure 3 represent the **anatomical position/location** of a lung perfusion image set of a suspected pulmonary embolism patient with the indicated clinical condition?	o	o	o	o	o
3	How well does the lung perfusion image set in Figure 3 represent the **anatomical shape** of a lung perfusion image set of a suspected pulmonary embolism patient with the indicated clinical condition?	o	o	o	o	o
4	How do you rate the overall ability of the lung perfusion image set in Figure 3 to represent a planar lung perfusion image set of a patient having suspected pulmonary embolism?	o	o	o	o	o

Part 2

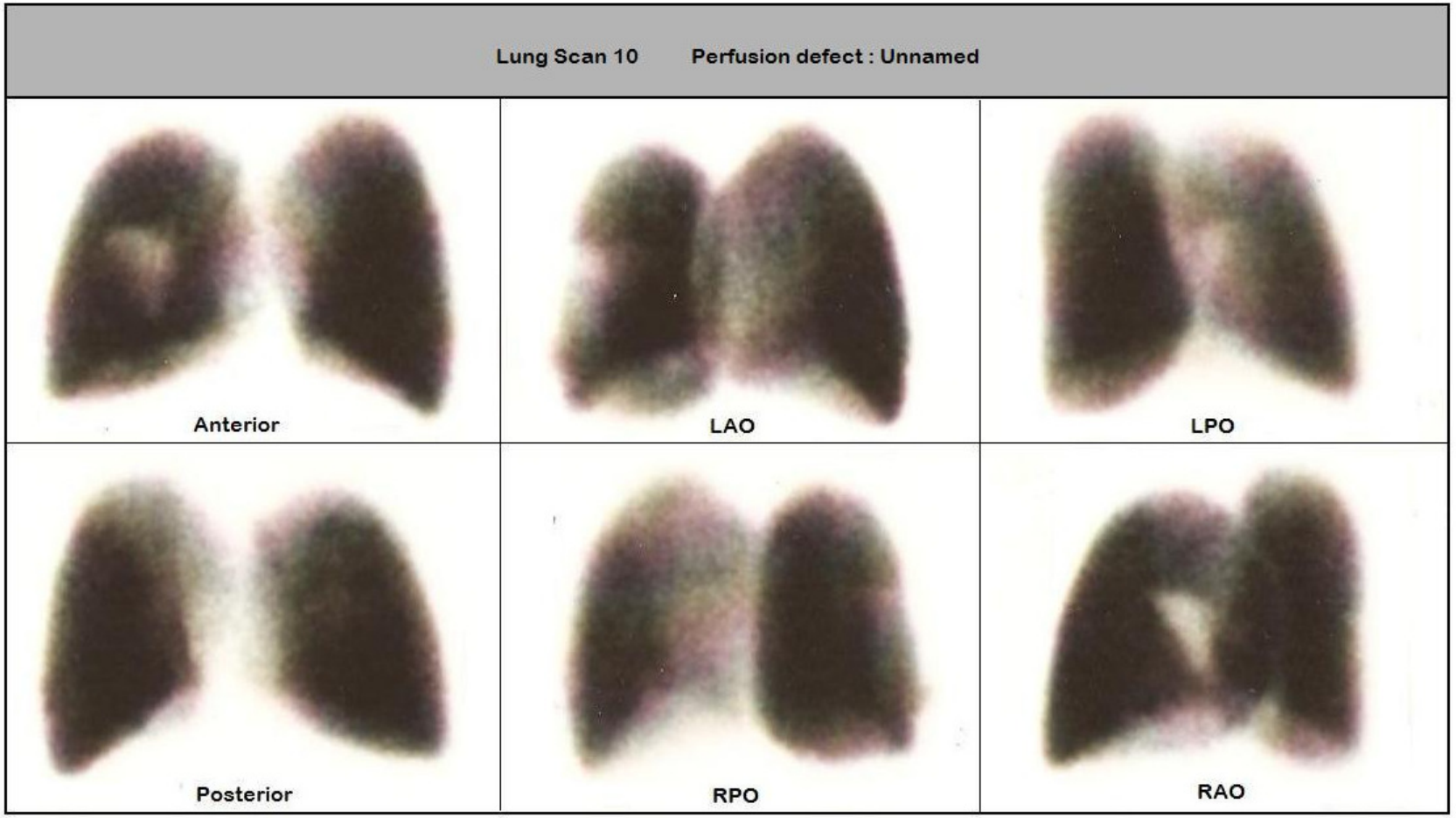

Figure 4

	Questions – Figure 4	**Answer**				
1	Figure 4 simulates a segmental lung perfusion defect in a patient with suspected pulmonary embolism. Please specify the name of the defect segment.	…….....				
2	How do you rate the overall ability of the lung perfusion image set in Figure 4 to represent a planar lung perfusion image set of a patient with suspected pulmonary embolism?	Score				
		1 o	2 o	3 o	4 o	5 o

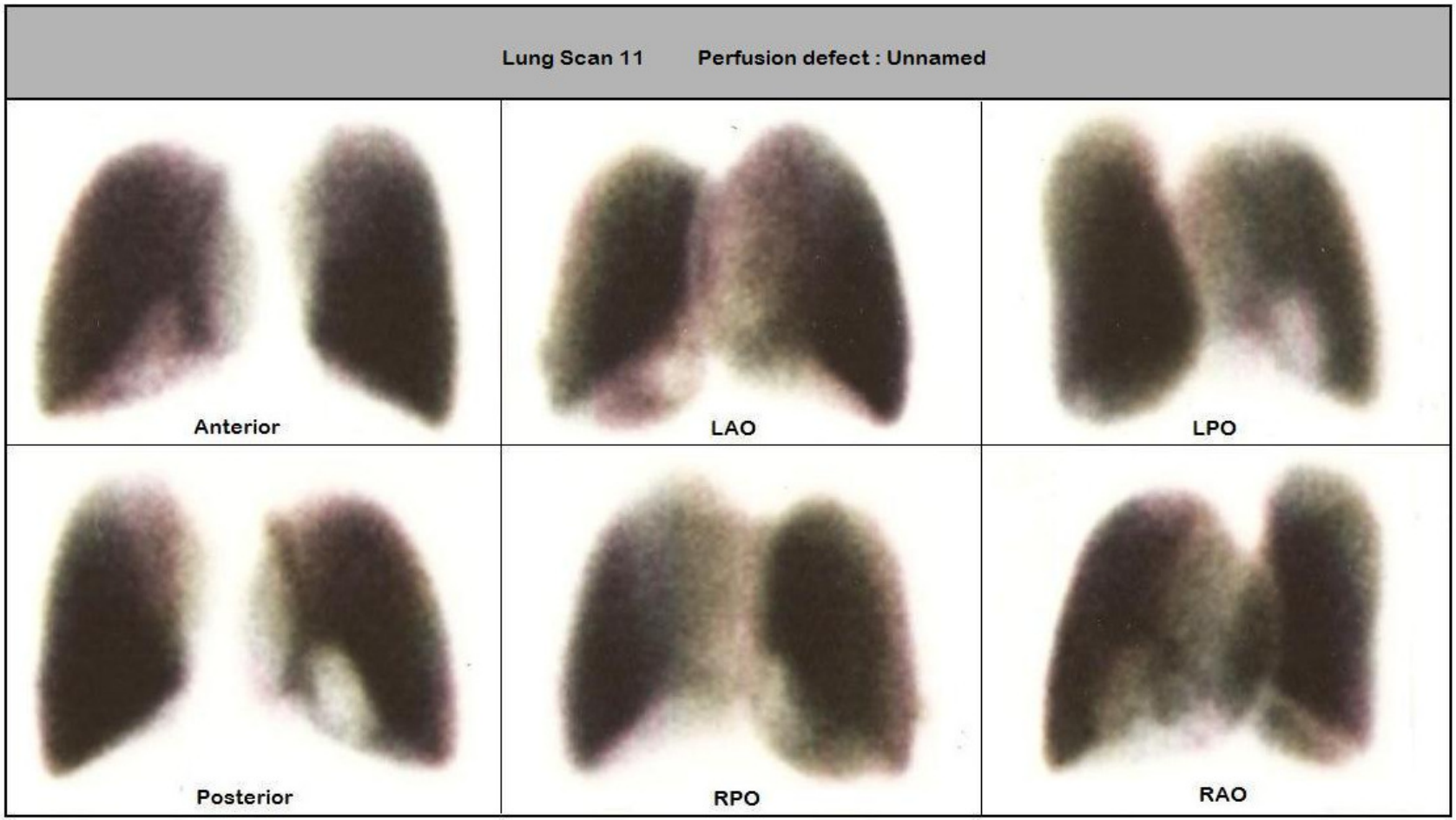
Lung Scan 11
Perfusion defect : Unnamed
Anterior
LAO
LPO
Posterior
RPO
RAO

Figure 5

	Questions – Figure 5	**Answer**				
1	Figure 5 simulates a segmental lung perfusion defect in a patient with suspected pulmonary embolism. Please specify the name of the defect segment.	…….....				
2	How do you rate the overall ability of the lung perfusion image set in Figure 5 to represent a planar lung perfusion image set of a patient with suspected pulmonary embolism?	Score				
		1 o	2 o	3 o	4 o	5 o

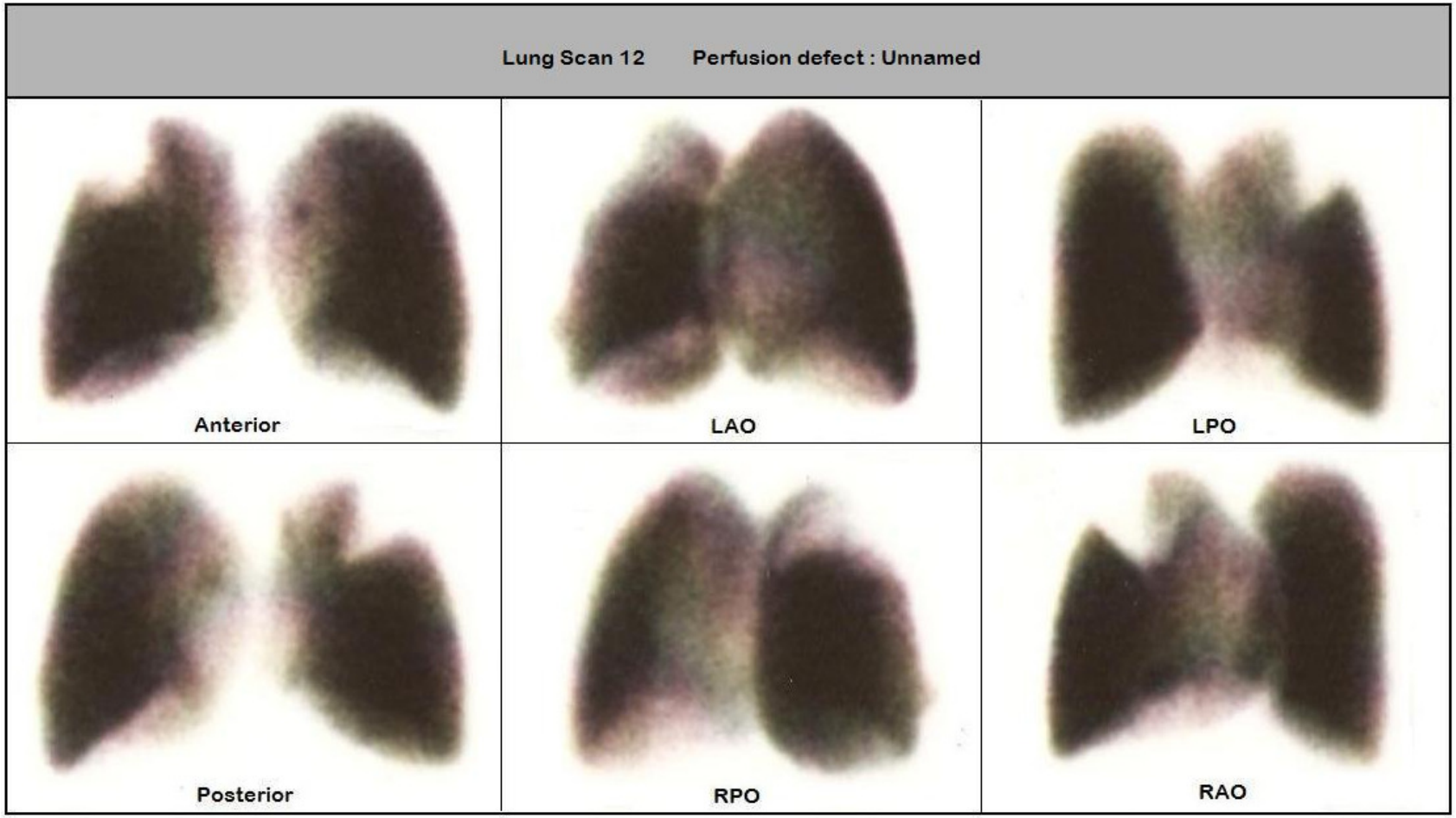
Lung Scan 12 Perfusion defect : Unnamed
Anterior
LAO
LPO
Posterior
RPO
RAO

Figure 6

	Questions – Figure 6	**Answer**				
1	Figure 6 simulates a segmental lung perfusion defect of a patient with suspected pulmonary embolism. Please specify the name of the defect segment.	…….....				
2	How do you rate the overall ability of the lung perfusion image set in Figure 6 to represent a planar lung perfusion image set of a patient with suspected pulmonary embolism?	Score				
		1 o	2 o	3 o	4 o	5 o

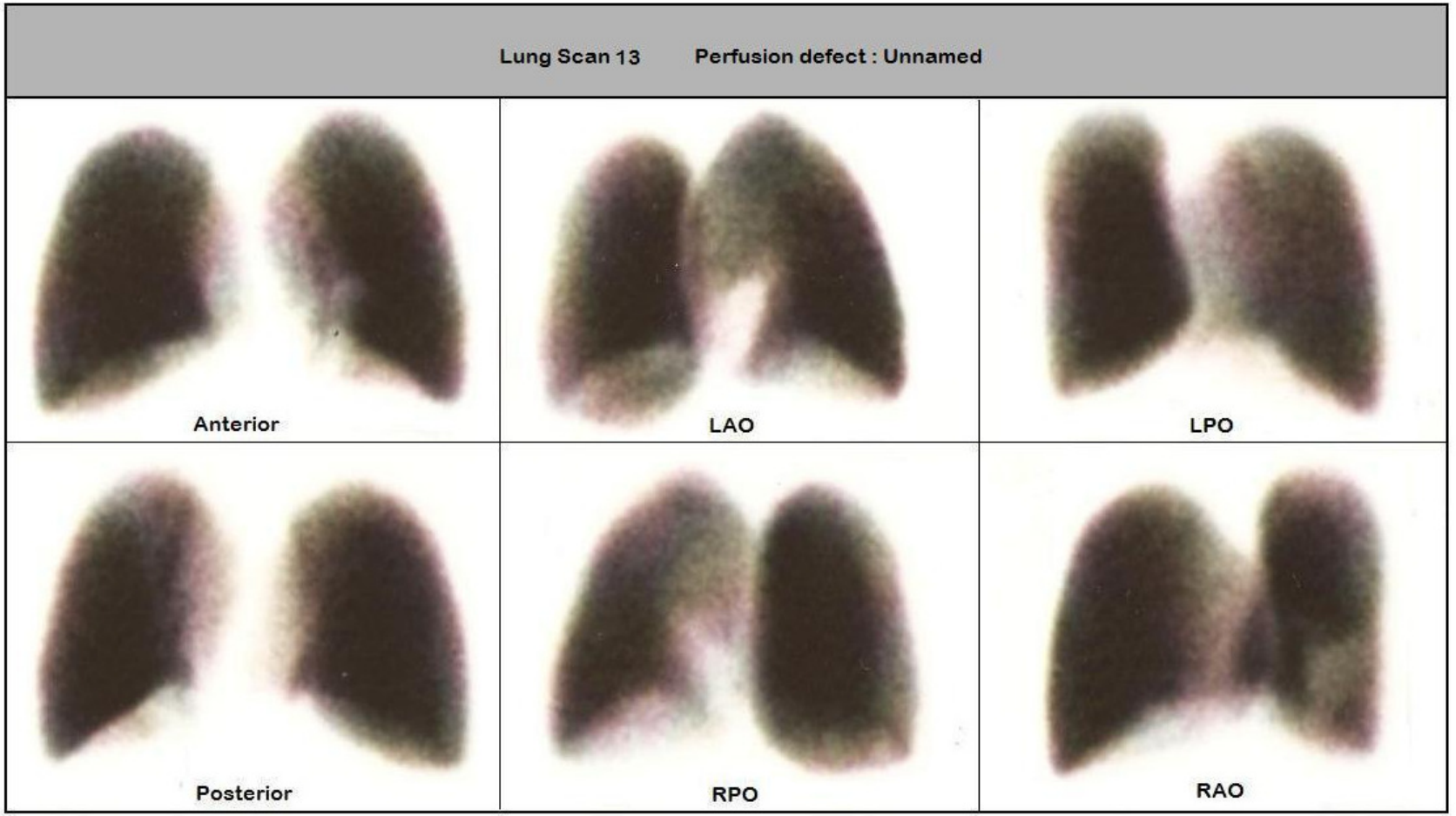
Lung Scan 13
Perfusion defect : Unnamed
Anterior
LAO
LPO
Posterior
RPO
RAO

Figure 7

	Questions – Figure 7	**Answer**				
1	Figure 7 simulates a segmental lung perfusion defect in a patient with suspected pulmonary embolism. Please specify the name of the defect segment.	…….....				
2	How do you rate the overall ability of the lung perfusion image set in Figure 7 to represent a planar lung perfusion image set of a patient with suspected pulmonary embolism?	Score				
		1 o	2 o	3 o	4 o	5 o

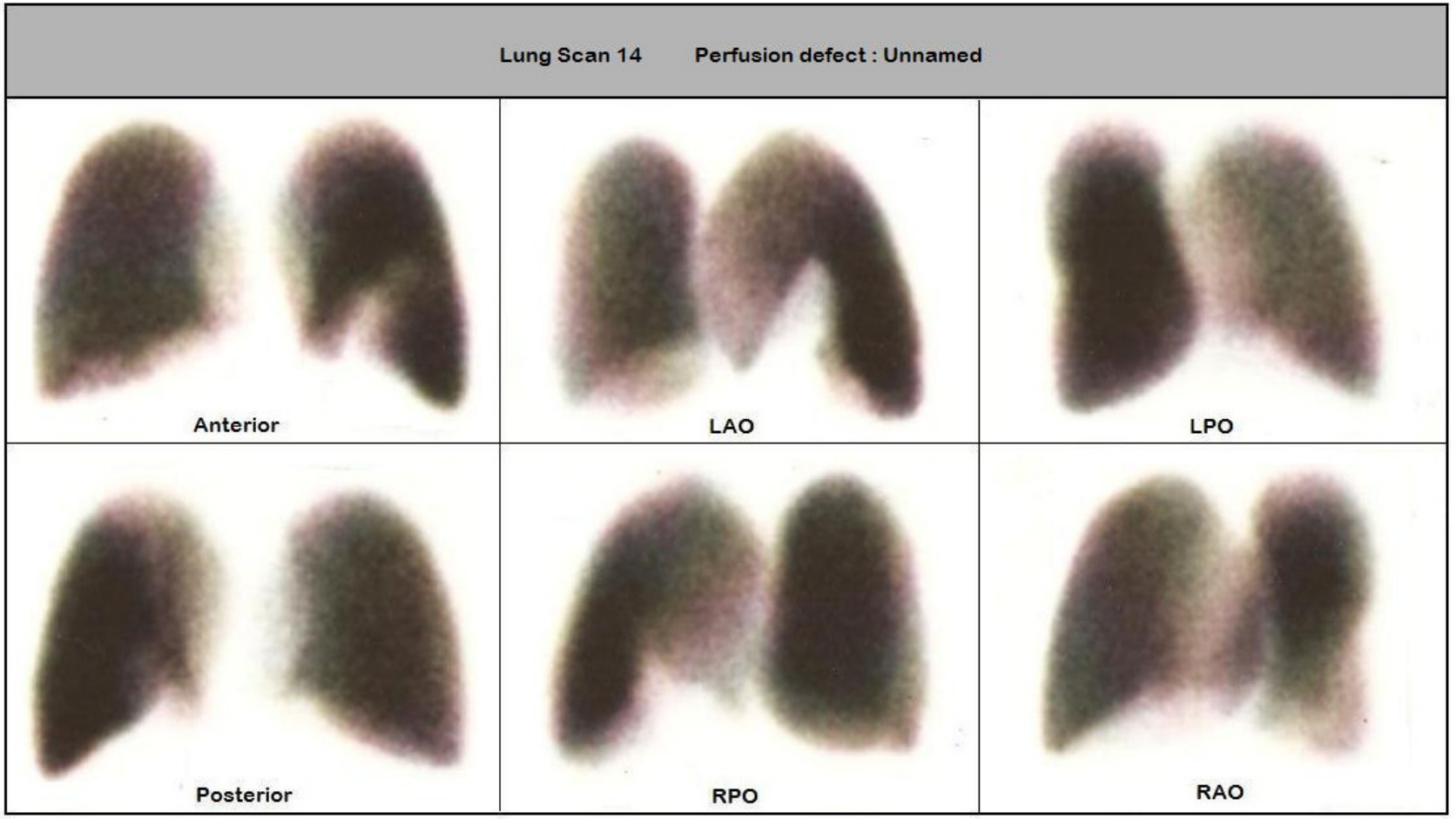
Lung Scan 14 Perfusion defect : Unnamed
Anterior
LAO
LPO
Posterior
RPO
RAO

Figure 8

	Questions – Figure 8	**Answer**				
1	Figure 8 simulates a segmental lung perfusion defect of a patient with suspected pulmonary embolism. Please specify the name of defect.	…….....				
2	How do you rate the overall ability of the lung perfusion image set in Figure 8 to represent a planar lung perfusion image set of a patient with suspected pulmonary embolism?	Score				
		1 o	2 o	3 o	4 o	5 o

Appendix B

Lung Perfusion Image Evaluation 2: Reproducibility

Instructions:

1. This survey was developed to characterise the phantom's ability to reproduce the same lung perfusion image sets.
2. These lung perfusion image sets demonstrate three simulated lung perfusion defect events of patients suspected of having pulmonary embolism. All perfusion defects are assumed **VQ mismatch defects**.
3. Please score/answer all questions based on criteria given in Table B

Table B

Score	Image quality	Specification
1	Poor	The results show an inadequate reproducibility standard of lung perfusion imaging for lung perfusion scan QA assessment.
2	Average	The results show an acceptable reproducibility standard of lung perfusion imaging for lung perfusion scan QA assessment.
3	Satisfactory	The results illustrate an adequate reproducibility standard of lung perfusion imaging for lung perfusion scan QA assessment.
4	Good	The results show a precise reproducibility standard of lung perfusion imaging for lung perfusion scan QA assessment.
5	Excellent	The results show an outstanding reproducibility quality of lung perfusion imaging for lung perfusion scan QA assessment.

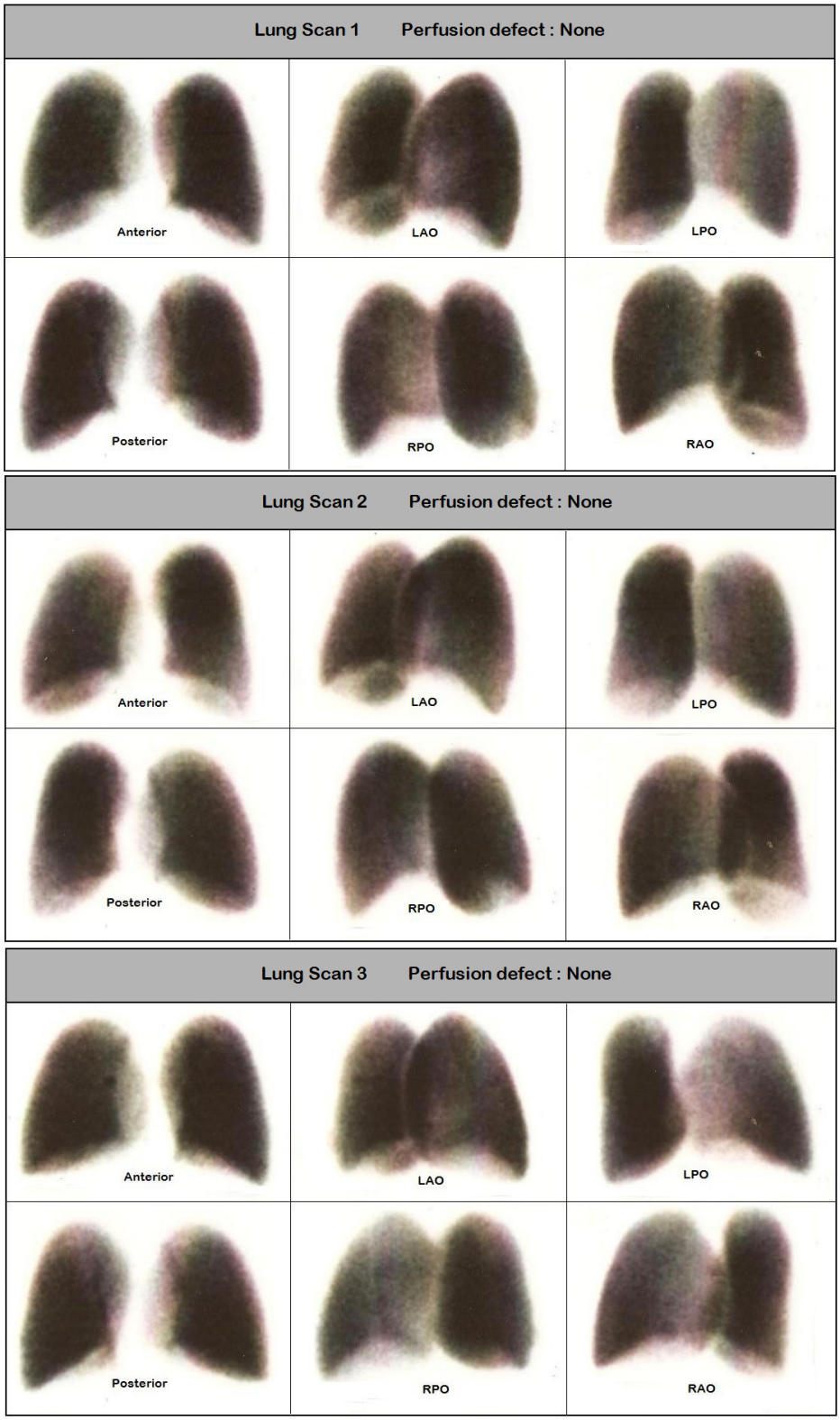
Lung Scan 1 Perfusion defect : None
Anterior
LAO
LPO
Posterior
RPO
RAO
Lung Scan 2 Perfusion defect : None
Anterior
LAO
LPO
Posterior
RPO
RAO
Lung Scan 3 Perfusion defect : None
Anterior
LAO
LPO
Posterior
RPO
RAO

Figure 1

Question – Figure 1	**Score**				
	1	2	3	4	5
To evaluate reproducibility, three separate scans were obtained for a given state of lung perfusion. The lung perfusion image sets are displayed in Figure 1. How do you rate the phantom's reproducibility performance?	o	o	o	o	o

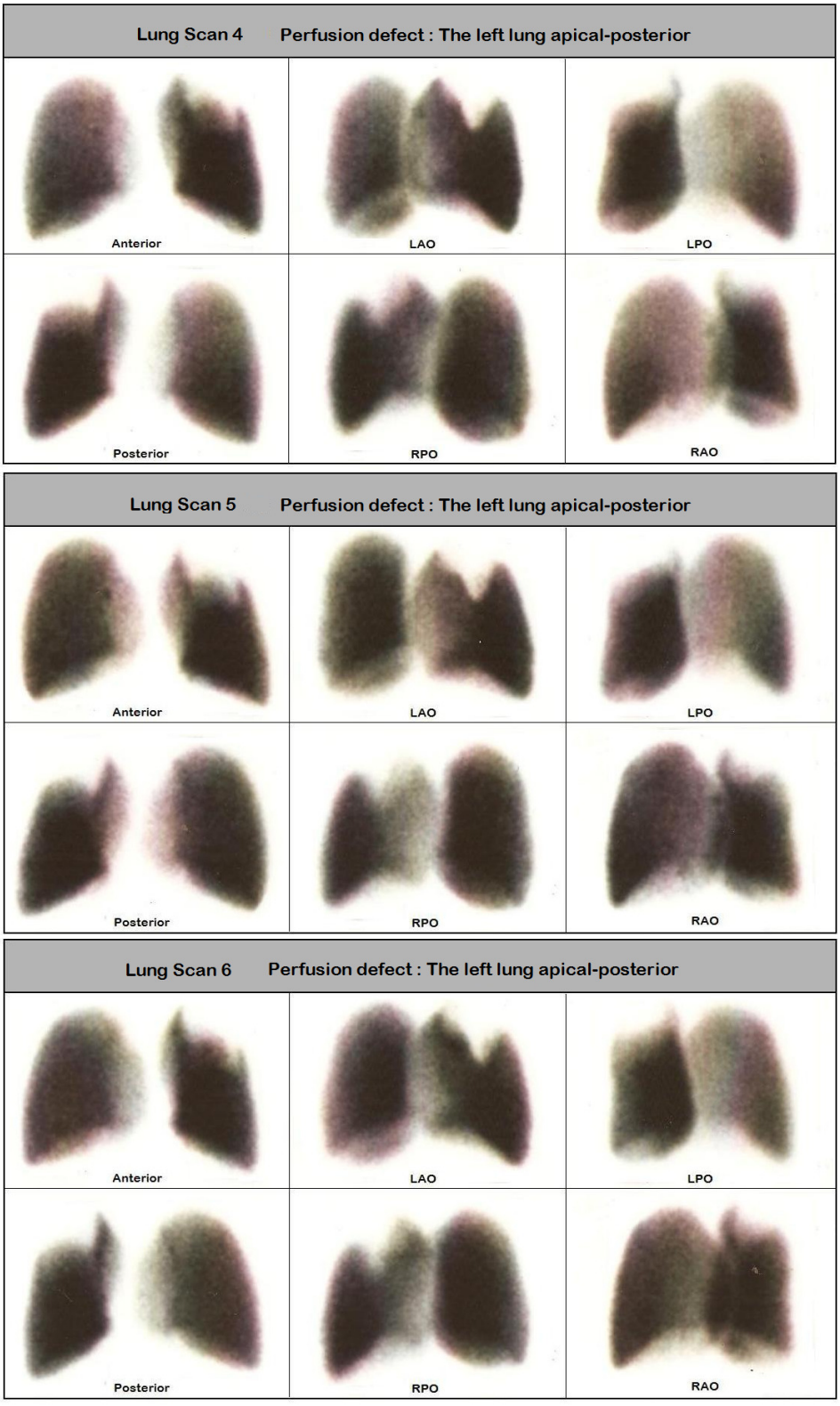
Lung Scan 4
Perfusion defect : The left lung apical-posterior
Anterior
LAO
LPO
Posterior
RPO
RAO
Lung Scan 5
Perfusion defect : The left lung apical-posterior
Anterior
LAO
LPO
Posterior
RPO
RAO
Lung Scan 6
Perfusion defect : The left lung apical-posterior
Anterior
LAO
LPO
Posterior
RPO
RAO

Figure 2

Question – Figure 2	**Score**				
	1	2	3	4	5
To evaluate reproducibility, three separate scans were obtained for a given state of lung perfusion. The lung perfusion image sets are displayed in Figure 2. How do you rate the phantom's reproducibility performance?	o	o	o	o	o

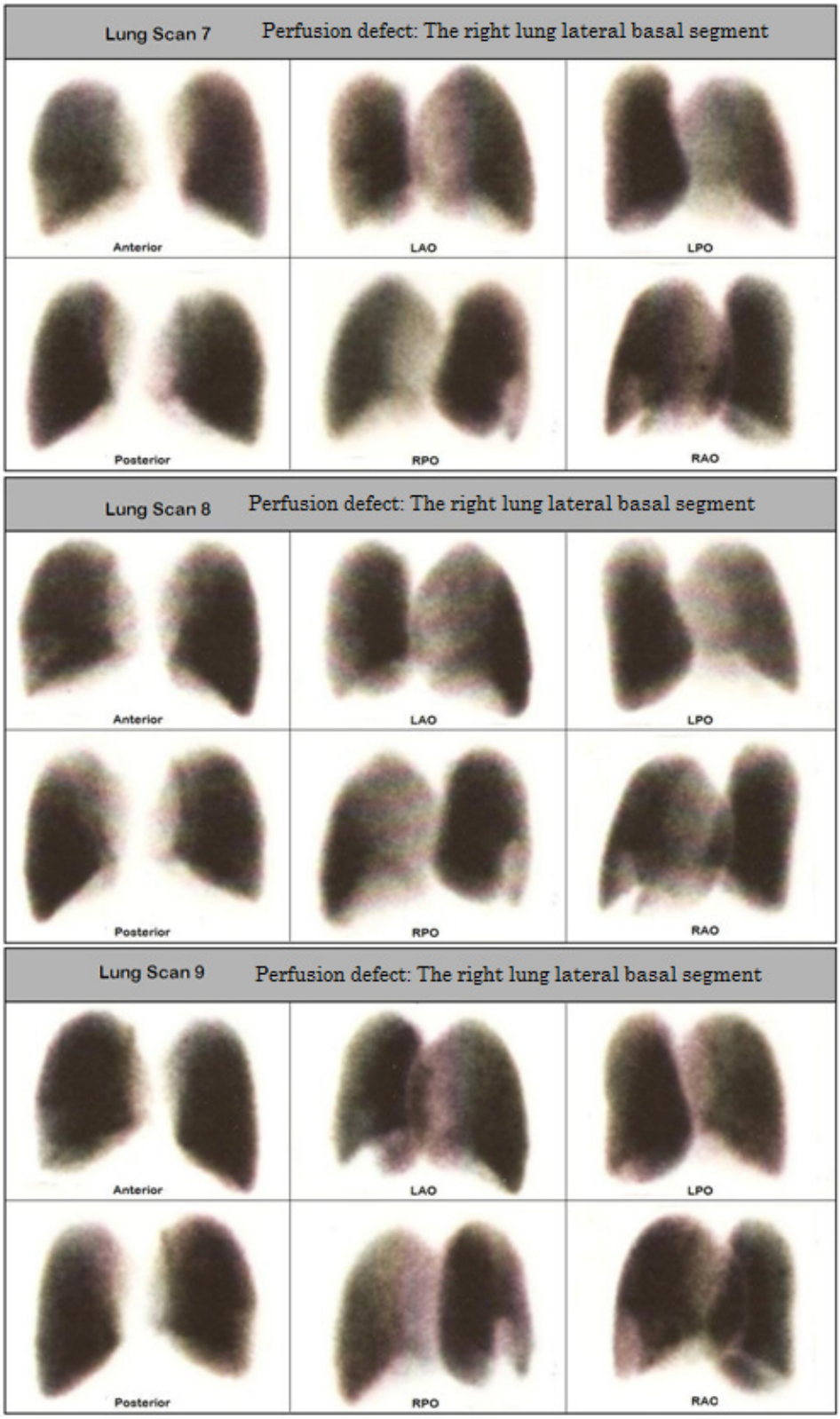
Lung Scan 7
Perfusion defect: The right lung lateral basal segment
Anterior
LAO
LPO
Posterior
RPO
RAO
Lung Scan 8
Perfusion defect: The right lung lateral basal segment
Anterior
LAO
LPO
Posterior
RPO
RAO
Lung Scan 9
Perfusion defect: The right lung lateral basal segment
Anterior
LAO
LPO
Posterior
RPO
RAO

Figure 3

Question – Figure 3	**Score**				
	1	2	3	4	5
To evaluate reproducibility, three separate scans were obtained for a given state of lung perfusion. The lung perfusion image sets are displayed in Figure 3. How do you rate the phantom's reproducibility performance?	o	o	o	o	o

Appendix C

Lung Perfusion Image Blind Test 1: VQ mismatch defect size

1. This test was developed to identify Nuclear Medical Physician accuracy in identifying percentage (size) of perfusion/ventilation VQ mismatch of planar lung perfusion images.
2. The percentage of VQ mismatch in a planar lung perfusion images is crucial to identify the probability of pulmonary embolism according to the revised PIOPED criteria.[1] Incorrect identification of VQ mismatch defects' size leads to misdiagnosis of planar lung perfusion images for pulmonary embolism diagnosis.
3. According to the revised PIOPED criteria, **I.** small VQ mismatch = less than 25% segmental VQ mismatch, **ii.** Moderate VQ mismatch = 25-75% segmental VQ mismatch and **iii.** Large VQ mismatch = more than 75% segmental VQ mismatch.
4. Please categorise the mismatch defects' size based on the revised PIOPED criteria given in the table on the next page.

The revised PIOPED criteria: [1]

High probability	≥ 2 large VQ mismatches
	or
	1 large VQ and ≥2 moderate mismatches
	or
	≥ 4 moderate VQ mismatches
Intermediate probability	1 large ± 1 moderate VQ mismatch
	or
	1-3 moderate VQ mismatches
	or
	Difficult to categorize as low or high
Low probability	≥ 1 perfusion defect with smaller chest radiograph defect in region of perfusion defect
	or
	Perfusion defects due to pleural effusion, cardiomegaly, enlarged aorta, hilum, mediastinum and elevated diaphragm.
	or
	≥ 1 small perfusion defect with normal chest radiograph
	or
	≥ 2 VQ matches with normal chest radiograph
Normal probability	No perfusion defect. Perfusion outline exactly the shape of the lung as seen on the chest radiograph.

[1]Gottschalk A, Sostman HD, Coleman RE *et al*. Ventilation-perfusion scintigraphy in the PIOPED study. Part II. Evaluation of the scintigraphic criteria and interpretations. *J Nuc Med* 1993; **34**: 1119-1126

Question 1

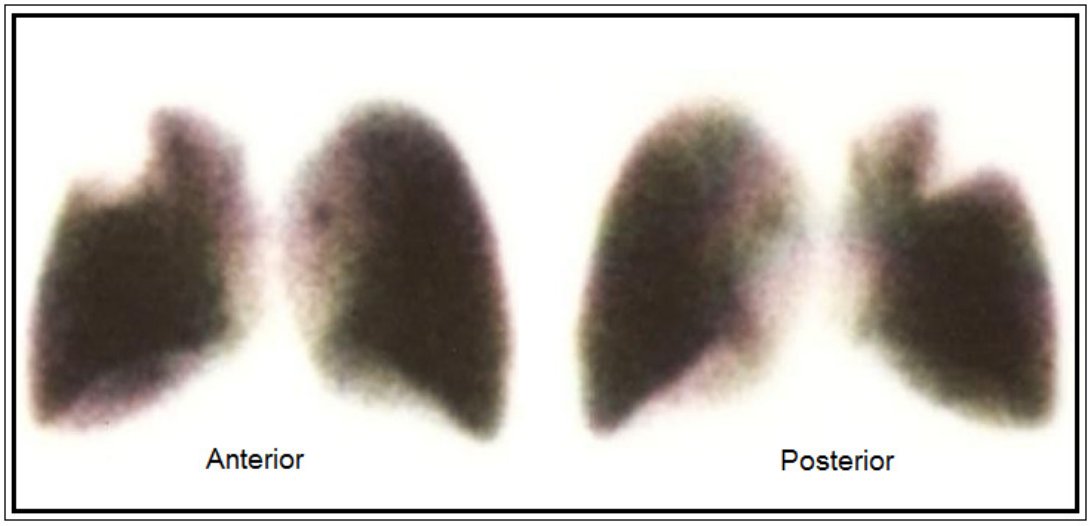

Figure 1: Lung planar perfusion images with a V-Q mismatch defect

Question Figure 1	**VQ mismatch defect size**		
	Small (size < 25%)	Moderate (25% < size < 75%)	Large (size ≥ 25%)
Please specify the VQ mismatch defect size in the lung perfusion images in Figure 1 based on the revised PIOPED criteria.	o	o	o

Question 2

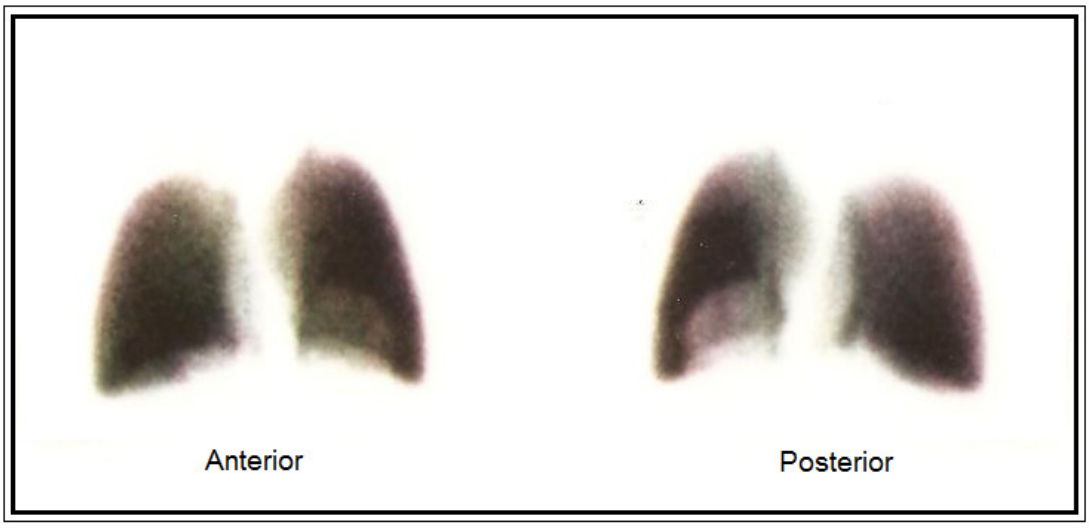

Figure 2 : Lung planar perfusion images with a V-Q mismatch defect

Question – Figure 2	**VQ mismatch defect size**		
	Small (size < 25%)	Moderate (25% < size < 75%)	Large (size ≥ 25%)
Please specify the VQ mismatch defect size in the lung perfusion images in Figure 2 based on the revised PIOPED criteria.	o	o	o

Question 3

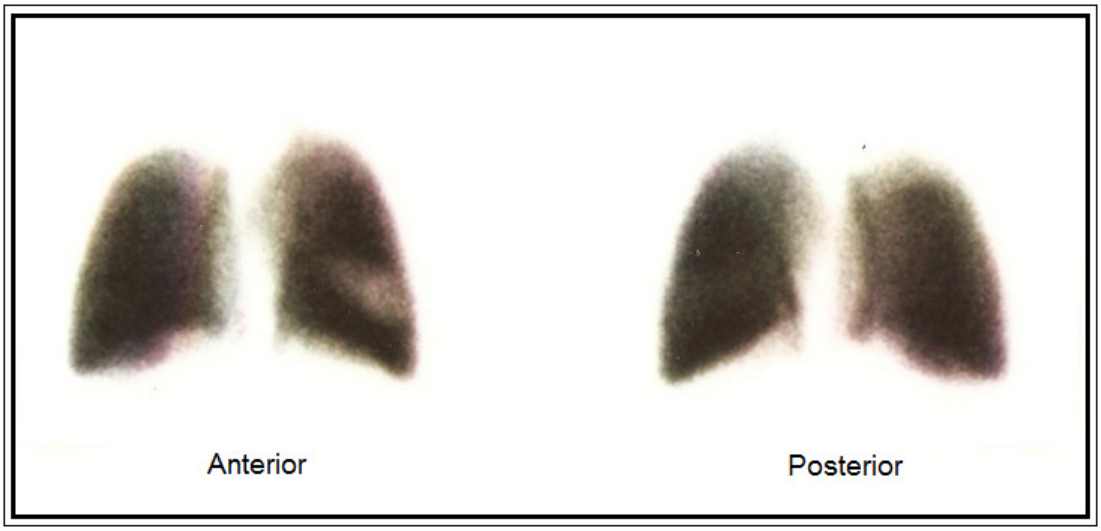

Figure 3: Lung planar perfusion images with a V-Q mismatch defect

Question – Figure 3	**VQ mismatch defect size**		
	Small (size < 25%)	Moderate (25% < size < 75%)	Large (size ≥ 25%)
Please specify the VQ mismatch defect size in the lung perfusion images in Figure 3 based on the revised PIOPED criteria.	o	o	o

Question 4

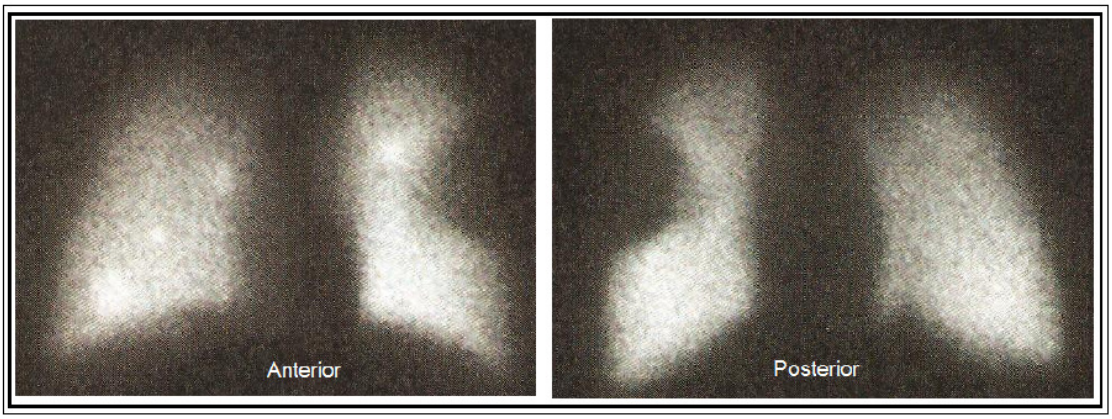

Figure 4 : Lung planar perfusion images with a V-Q mismatch defect

Question – Figure 4	**VQ mismatch defect size**		
	Small (size < 25%)	Moderate (25% < size < 75%)	Large (size ≥ 25%)
Please specify the VQ mismatch defect size in the lung perfusion images in Figure 4 based on the revised PIOPED criteria.	o	o	o

Question 5

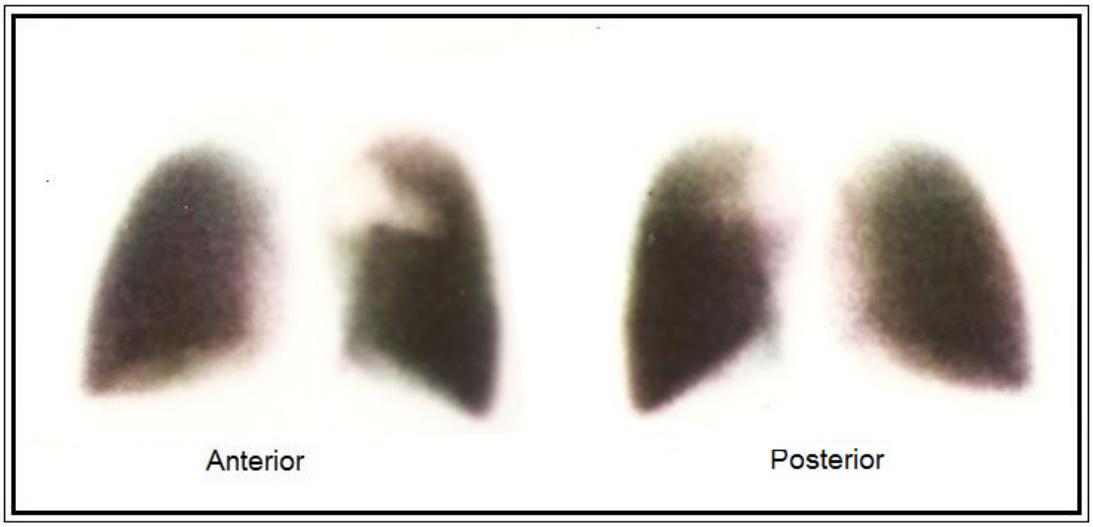

Figure 5: Lung planar perfusion images with a V-Q mismatch defect

Question – Figure 5	**VQ mismatch defect size**		
	Small (size < 25%)	Moderate (25% < size < 75%)	Large (size ≥ 25%)
Please specify the VQ mismatch defect size in the lung perfusion images in Figure 5 based on the revised PIOPED criteria.	o	o	o

Question 6

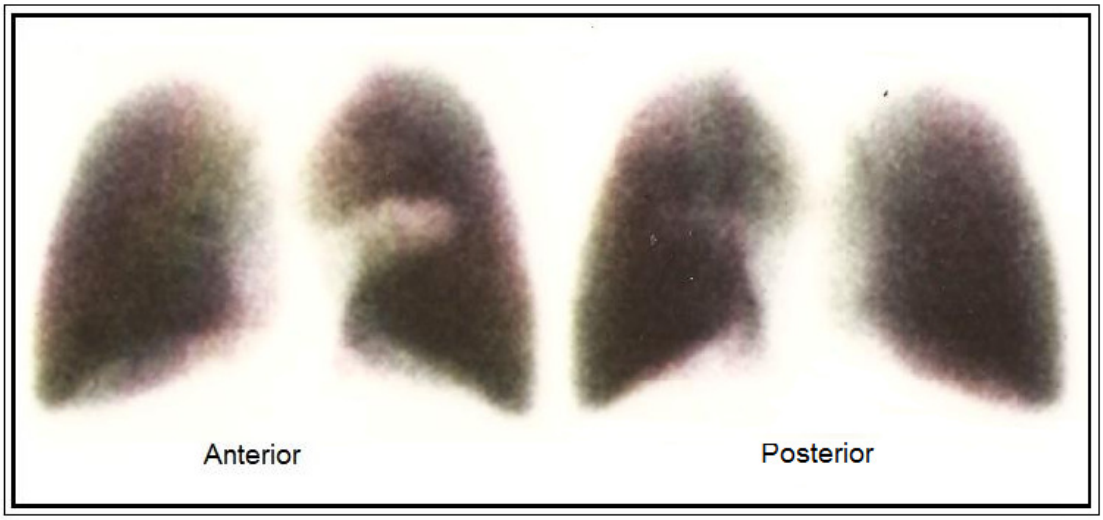

Figure 6: Lung planar perfusion images with a V-Q mismatch defect

Question – Figure 6	**VQ mismatch defect size**		
	Small (size < 25%)	Moderate (25% < size < 75%)	Large (size ≥ 25%)
Please specify the VQ mismatch defect size in the lung perfusion images in Figure 6 based on the revised PIOPED criteria.	o	o	o

Appendix D

Lung Perfusion Image Blind Test 2: Probability of Pulmonary Embolism

Instructions:

1. This test was developed to evaluate and compare lung perfusion scan interpretation by a Nuclear Medicine Physician.
2. The lung perfusion image sets demonstrate six simulated lung perfusion defect events of patients suspected of having pulmonary embolism. All perfusion defects are assumed to be **mismatch defects**.
3. Please fill in the answer sheet provided based on the revised PIOPED criteria given in the table below.

PIOPED revised criteria.[1]

High probability	≥ 2 large VQ mismatches
	or
	1 large VQ and ≥2 moderate mismatches
	or
	≥ 4 moderate VQ mismatches
Intermediate probability	1 large ± 1 moderate VQ mismatch
	or
	1-3 moderate VQ mismatches
	or
	Difficult to categorize as low or high
Low probability	≥ 1 perfusion defect with smaller chest radiograph defect in region of perfusion defect
	or
	Perfusion defects due to pleural effusion, cardiomegaly, enlarged aorta, hilum, mediastinum and elevated diaphragm.
	or
	≥ 1 small perfusion defect with normal chest radiograph
	or
	≥ 2 VQ matches with normal chest radiograph
Normal probability	No perfusion defect. Perfusion outline exactly the shape of the lung as seen on the chest radiograph.

[1]Gottschalk A, Sostman HD, Coleman RE *et al*. Ventilation-perfusion scintigraphy in the PIOPED study. Part II. Evaluation of the scintigraphic criteria and interpretations. *J Nuc Med* 1993; **34**: 1119-1126

Definitions:

VQ mismatch = normal ventilation and normal chest radiograph in region of perfusion defect
or
perfusion is more than ventilation/chest radiograph in region of perfusion defect

small VQ mismatch = less than 25% segmental VQ mismatch
moderate VQ mismatch = 25-75% segmental VQ mismatch
large VQ mismatch ≥ 75% segmental VQ mismatch

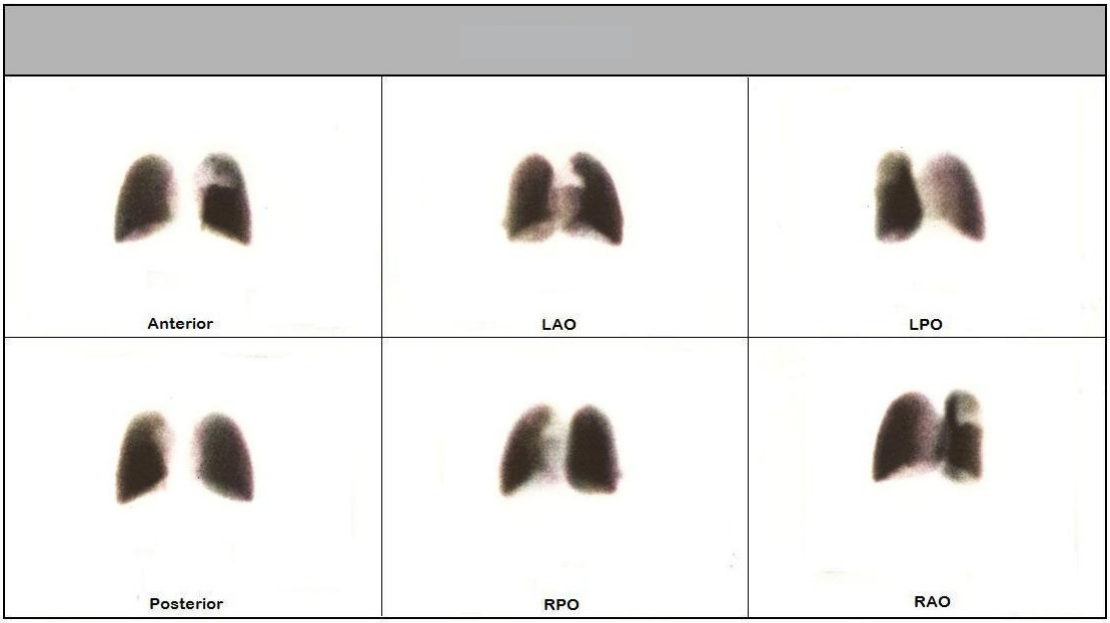

Figure C1

Question – Figure C1	**Probability**			
	High	Intermediate	Low	Normal
Please specify the probability of PE in the lung perfusion images in Figure C1 based on the revised PIOPED criteria.	o	o	o	o

Please specify the reason for your answer

……

……

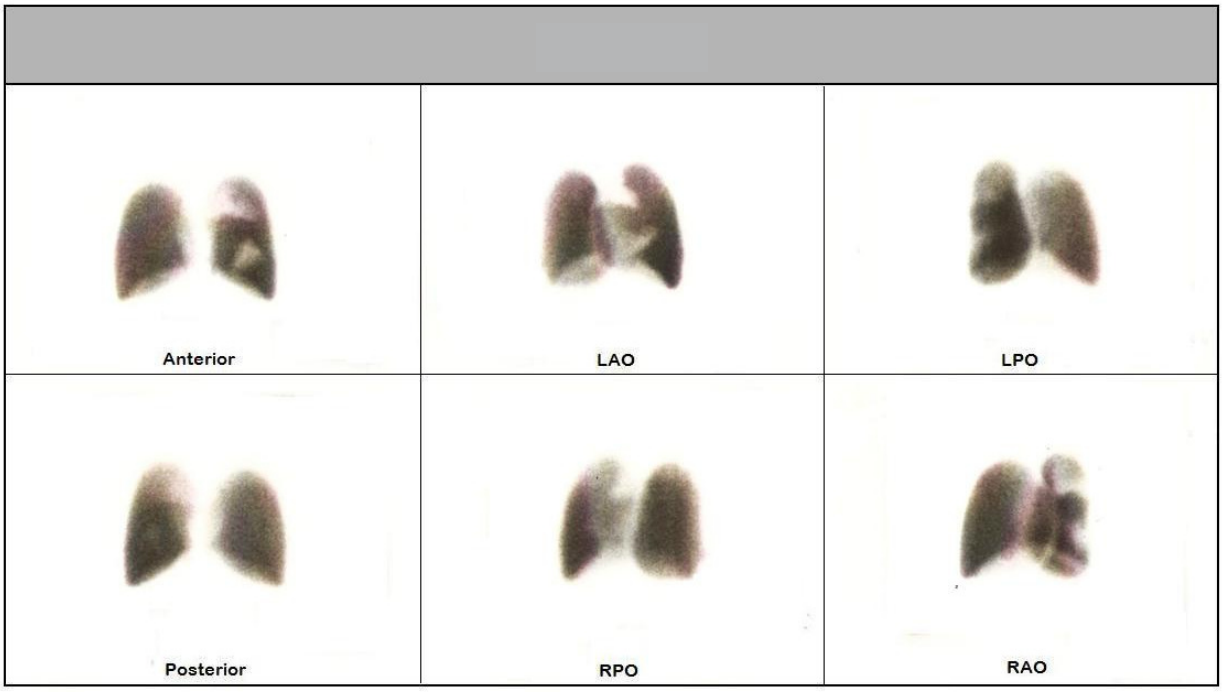

Figure C2

Question – Figure C2	**Probability**			
	High	Intermediate	Low	Normal
Please specify the probability of PE in the lung perfusion images in Figure C2 based on the revised PIOPED criteria.	o	o	o	o

Please specify the reason for your answer

……

……

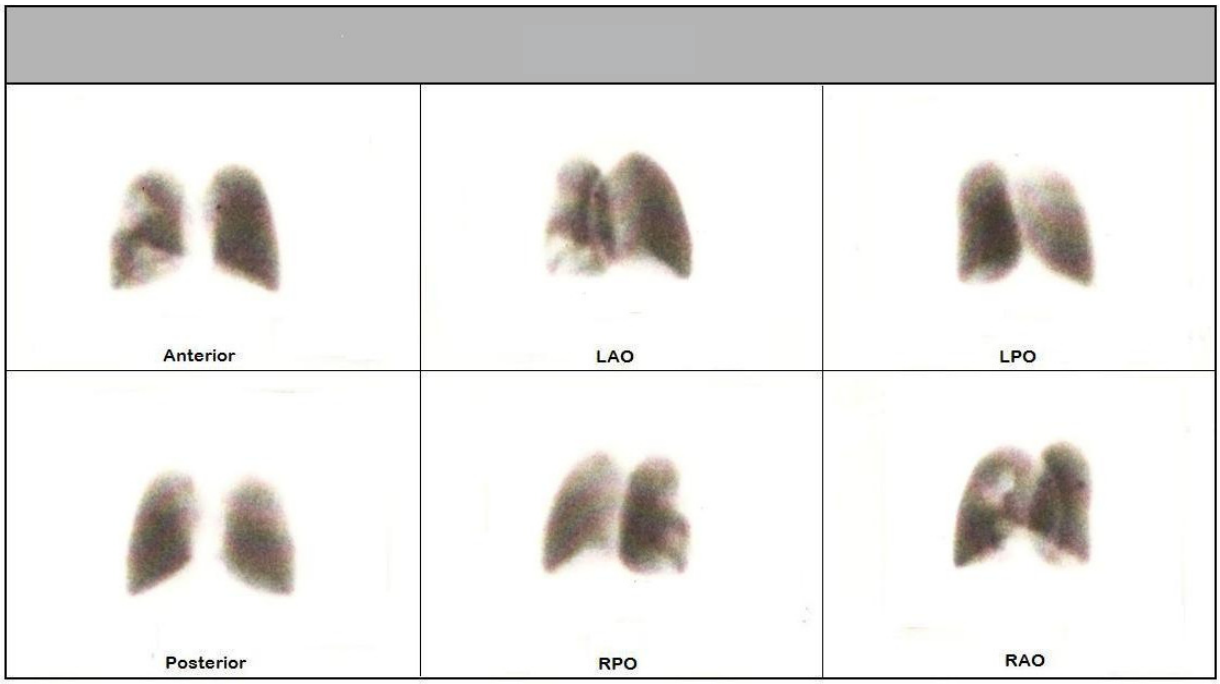

Figure C3

Question – Figure C3	**Probability**			
	High	Intermediate	Low	Normal
Please specify the probability of PE in the lung perfusion images in Figure C3 based on the revised PIOPED criteria.	o	o	o	o

Please specify the reason for your answer

……

……

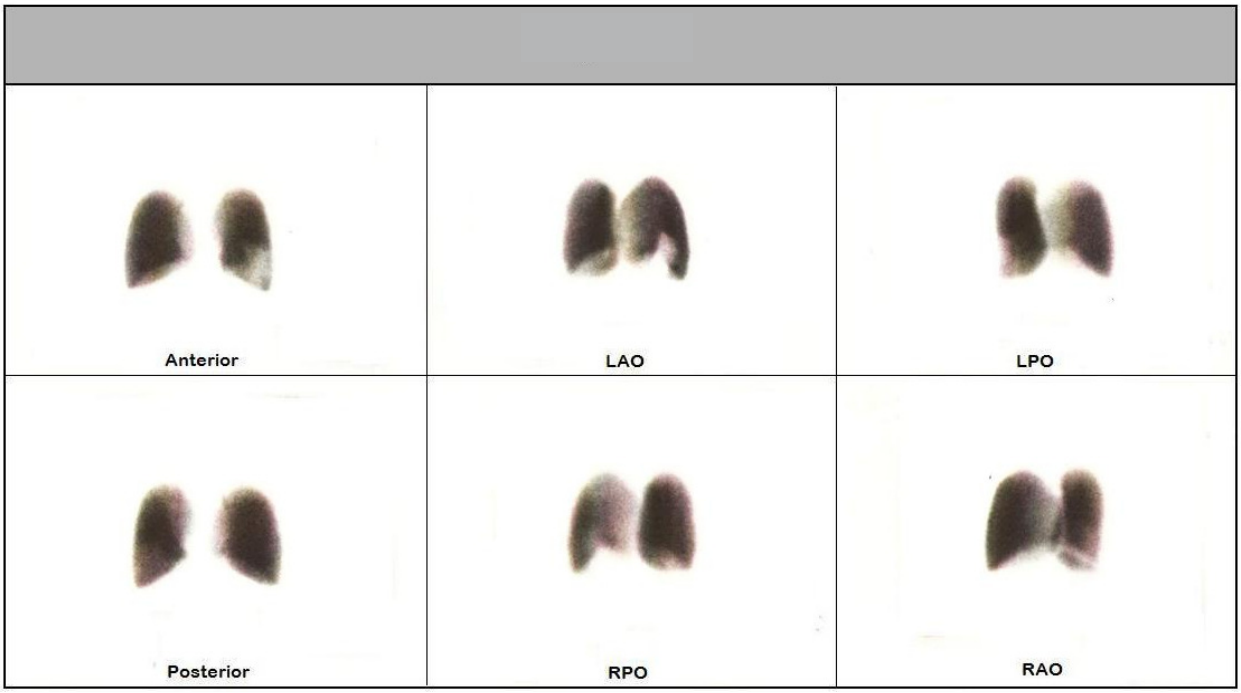

Figure C4

Question – Figure C4	**Probability**			
	High	Intermediate	Low	Normal
Please specify the probability of PE in the lung perfusion images in Figure C4 based on the revised PIOPED criteria.	o	o	o	o

Please specify the reason for your answer

……

……

Figure C5

Question – Figure C5	**Probability**			
	High	Intermediate	Low	Normal
Please specify the probability of PE in the lung perfusion images in Figure C5 based on the revised PIOPED criteria.	o	o	o	o

Please specify the reason for your answer

……

……

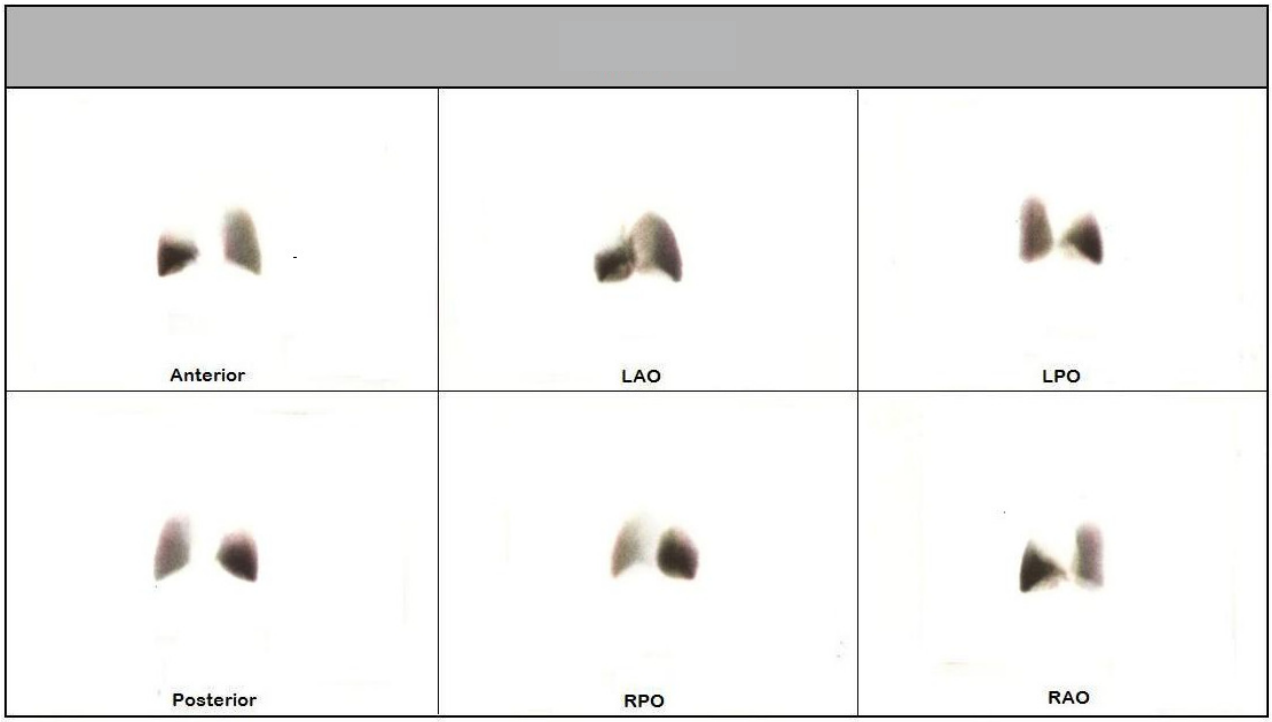

Figure C6

Question – Figure C6	**Probability**			
	High	Intermediate	Low	Normal
Please specify the probability of PE in the lung perfusion images in Figure C6 based on the revised PIOPED criteria.	o	o	o	o

Please specify the reason for your answer

……

……

Appendix E

Lung Perfusion Image Evaluation 3 - Lung scintigraphy atlas

Introduction and instructions:

1. This survey contains questions related to a lung scintigraphy atlas for pulmonary embolism (PE) diagnosis. The atlas was developed to be introduced as an aiding material whilst interpreting lung V/Q scans in diagnosing PE.
2. In this study, an anthropomorphical lung phantom with 18 separable lung segments manufactured at the University of Wollongong, NSW was used to simulate lung perfusion scans. Planar and SPECT images of single segmental perfusion defects depict in lung perfusion scans were simulated for all 18 bronchopulmonary segments of the human lungs. All planar and SPECT image sets were combined to create the lung scintigraphic atlas.
3. In this study, 8 of the left lung and 10 of the right lung bronchopulmonary segments perfusion deficiencies were simulated via planar and SPECT imaging. The simulation images are shown in Figure 1-18. The whole simulated images (Figure 1-18) are named as a **lung scintigraphy atlas**. The atlas represents perfusion segmental defects of each bronchopulmonary segment of the human lungs.
4. Please answer the following questions based on your experience as a nuclear medicine physician.

LUNG SCINTIGRAPHY ATLAS

Figure 1-18: Simulated lung perfusion planar (top) and selected SPECT (bottom) images of the lung bronchopulmonary segments. All defects are presumed mismatch defects. The defects are large in size (100% of a segment according to the revised PIOPED criteria).

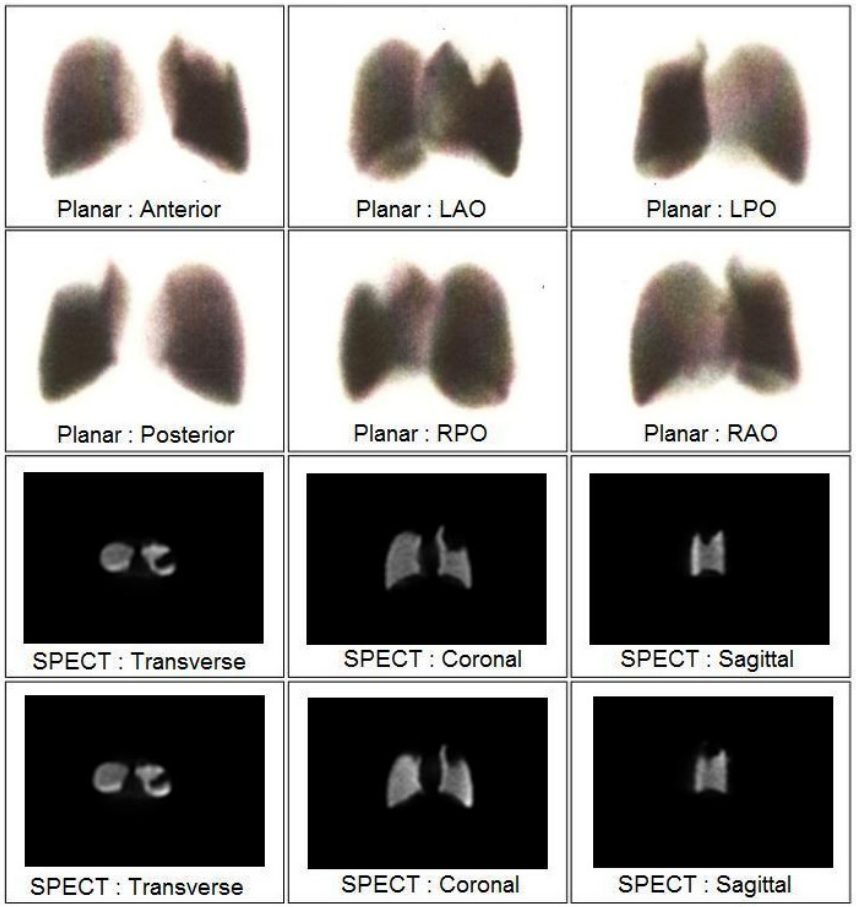

[Figure 1]

Planar and SPECT images of a perfusion defect involving the apical and posterior segment of the left lung.

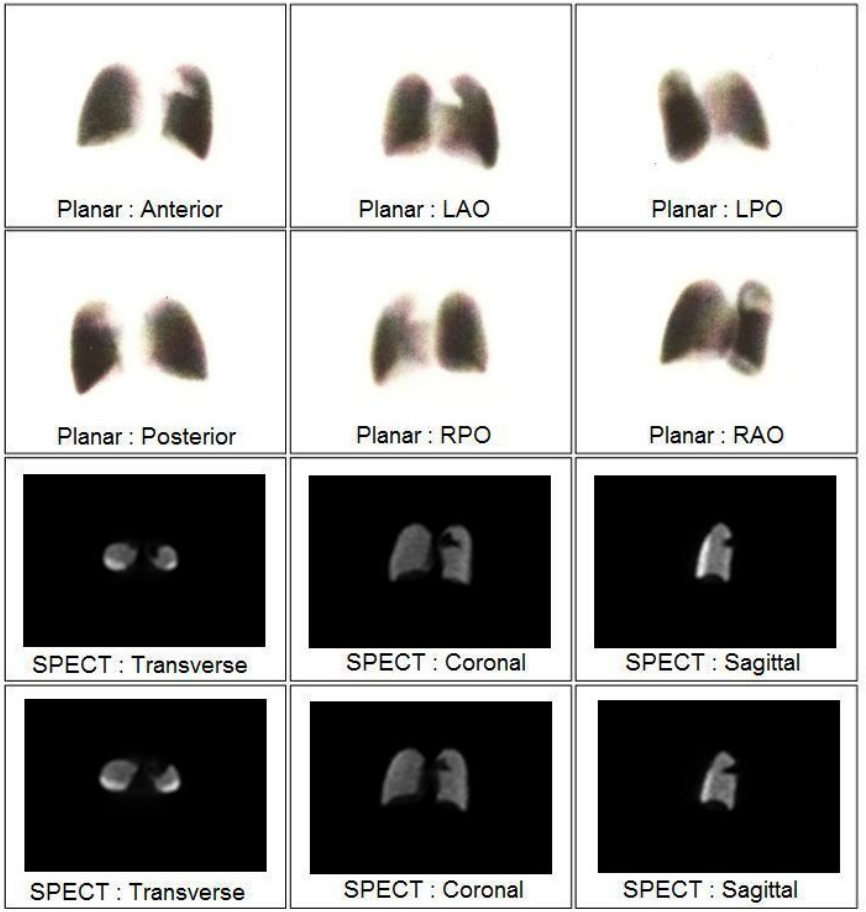

[Figure 2]

Planar and SPECT images of a perfusion defect involving the anterior segment of the left lung.

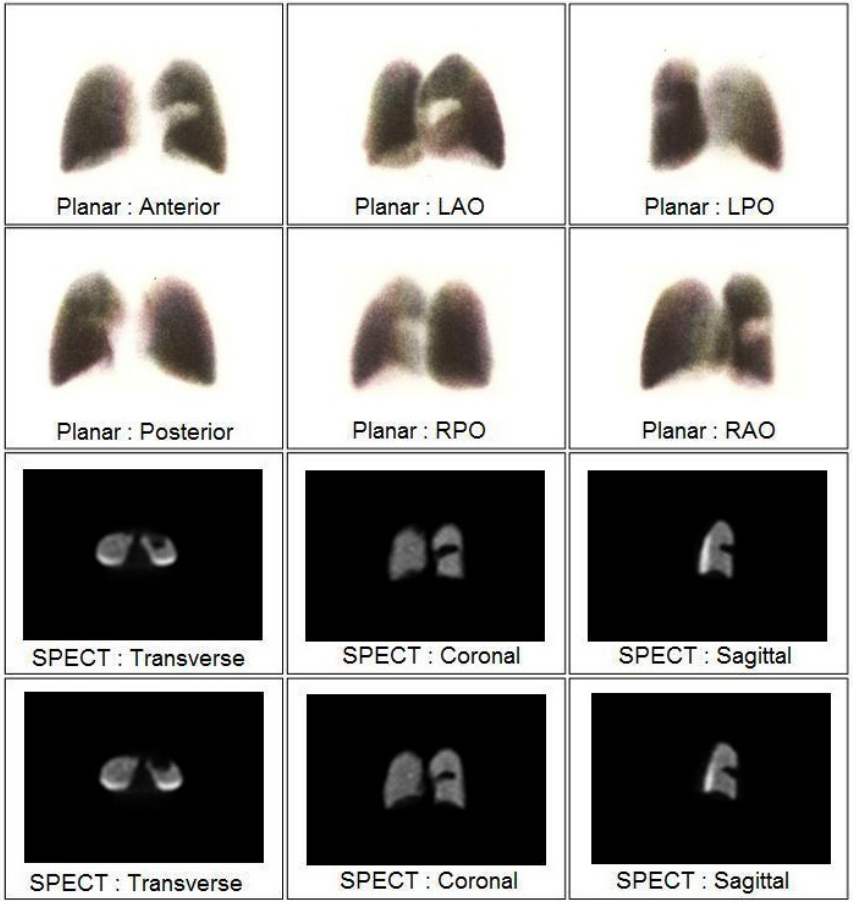

[Figure 3]

Planar and SPECT images of a perfusion defect involving the lingular superior segment of the left lung.

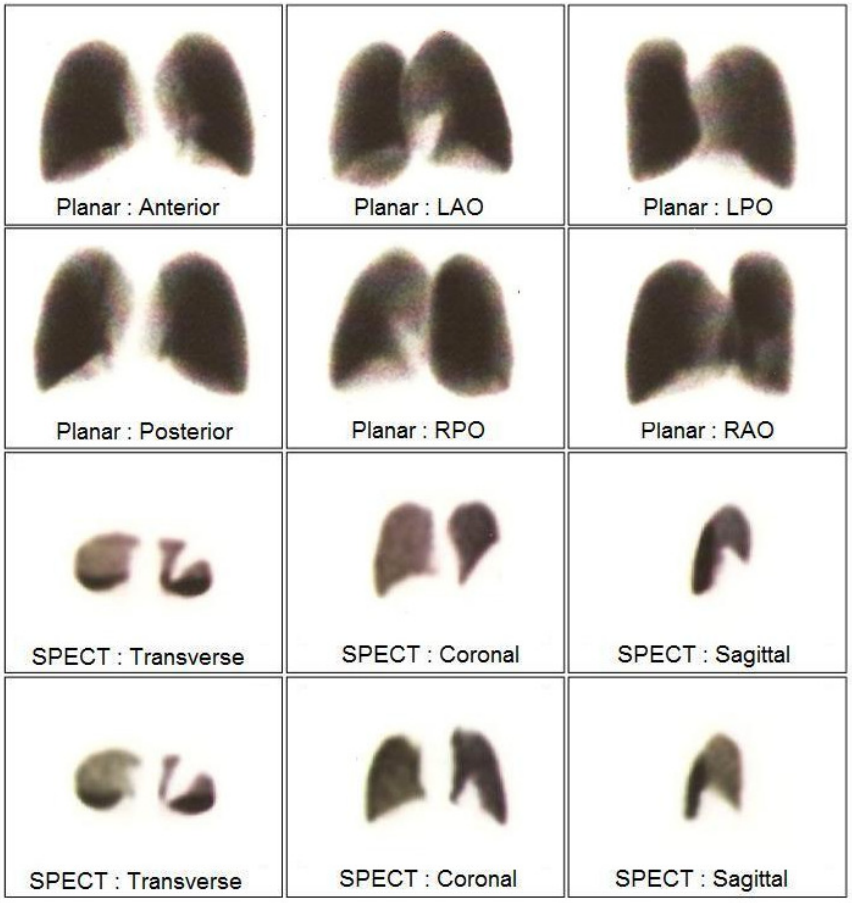

[Figure 4]

Planar and SPECT images of a perfusion defect involving the lingular inferior segment of the left lung.

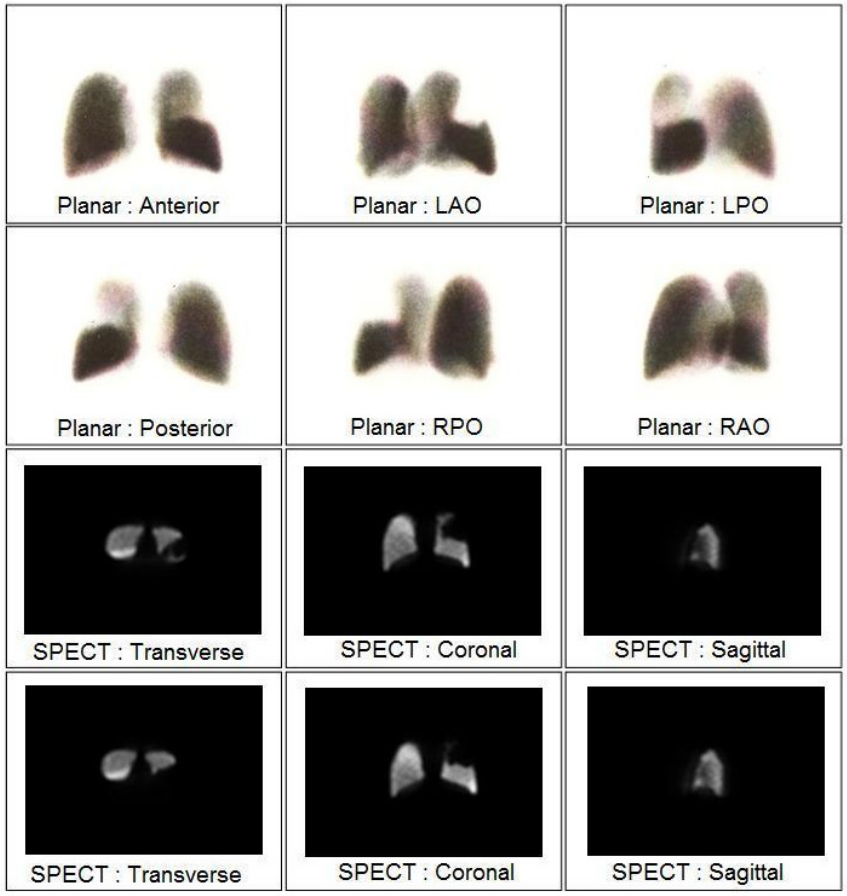

[Figure 5]

Planar and SPECT images of a perfusion defect involving the superior segment of the left lung.

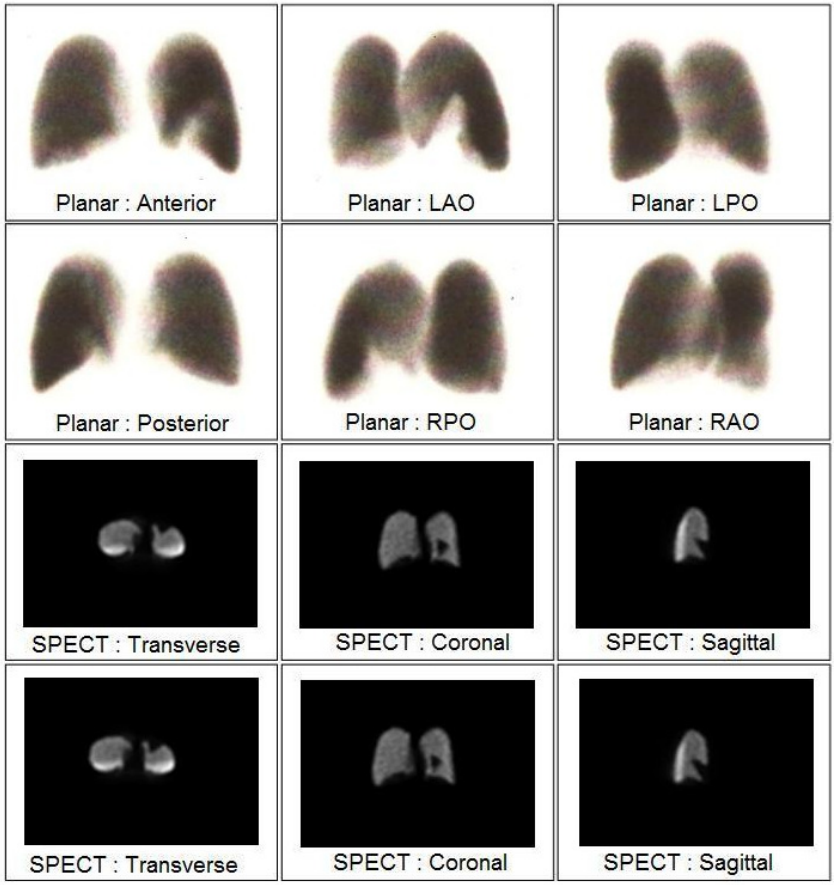

[Figure 6]

Planar and SPECT images of a perfusion defect involving the medial and anterior basal segment of the left lung.

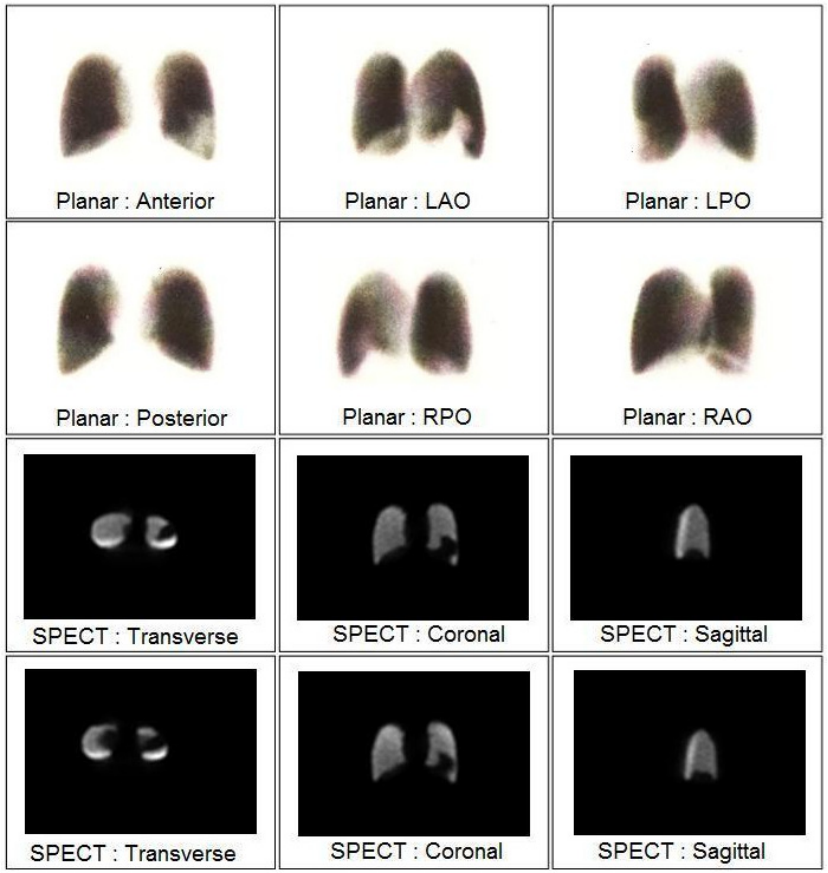

[Figure 7]

Planar and SPECT images of a perfusion defect involving the lateral basal segment of the left lung.

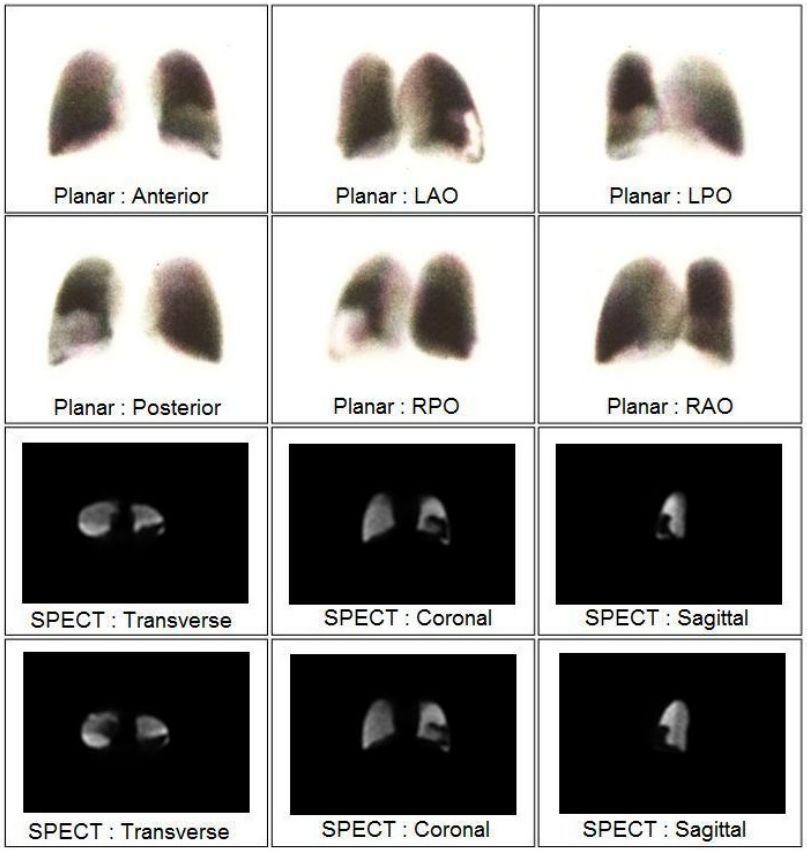

[Figure 8]

Planar and SPECT images of a perfusion defect involving the posterior basal segment of the left lung.

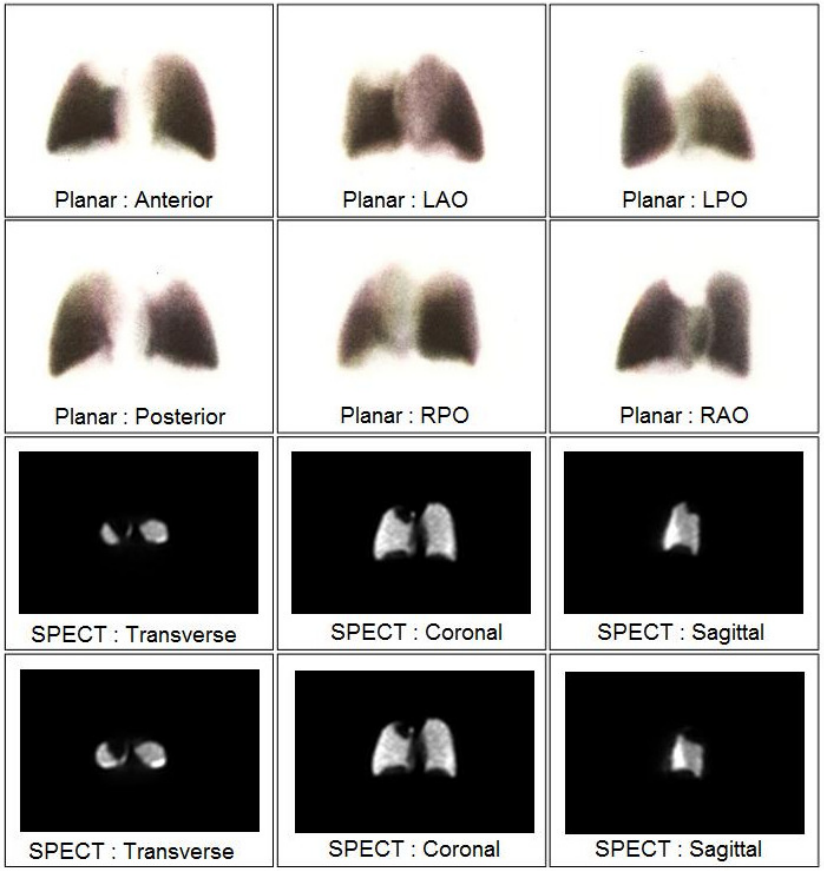

[Figure 9]

Planar and SPECT images of a perfusion defect involving the apical segment of the right lung.

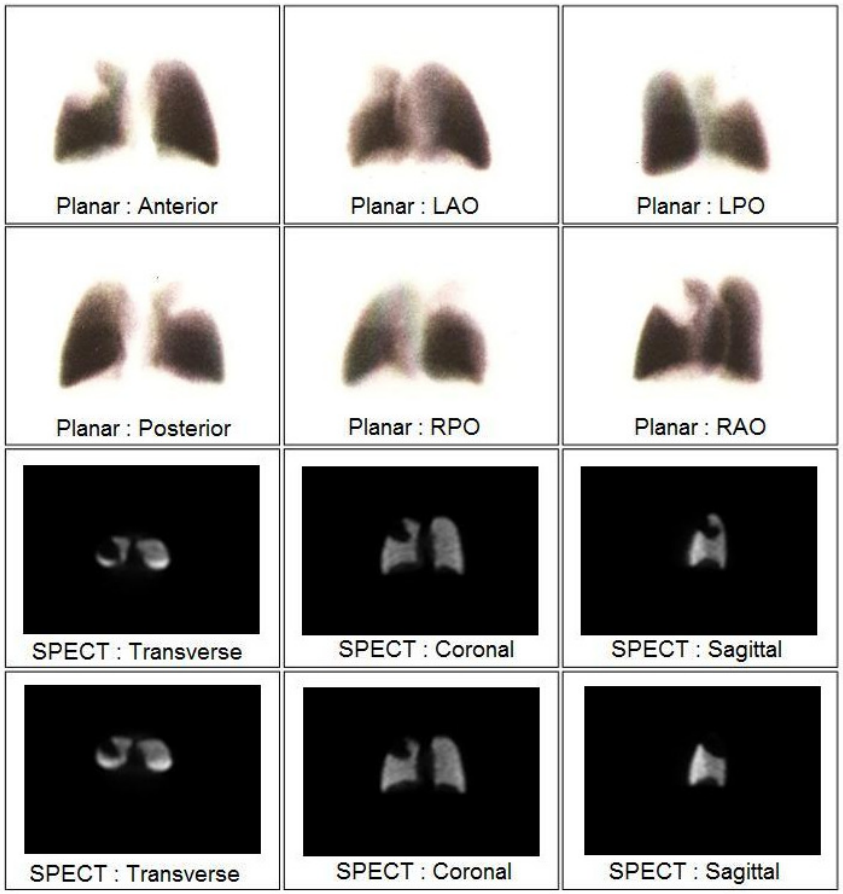

[Figure 10]

Planar and SPECT images of a perfusion defect involving the posterior segment of the right lung.

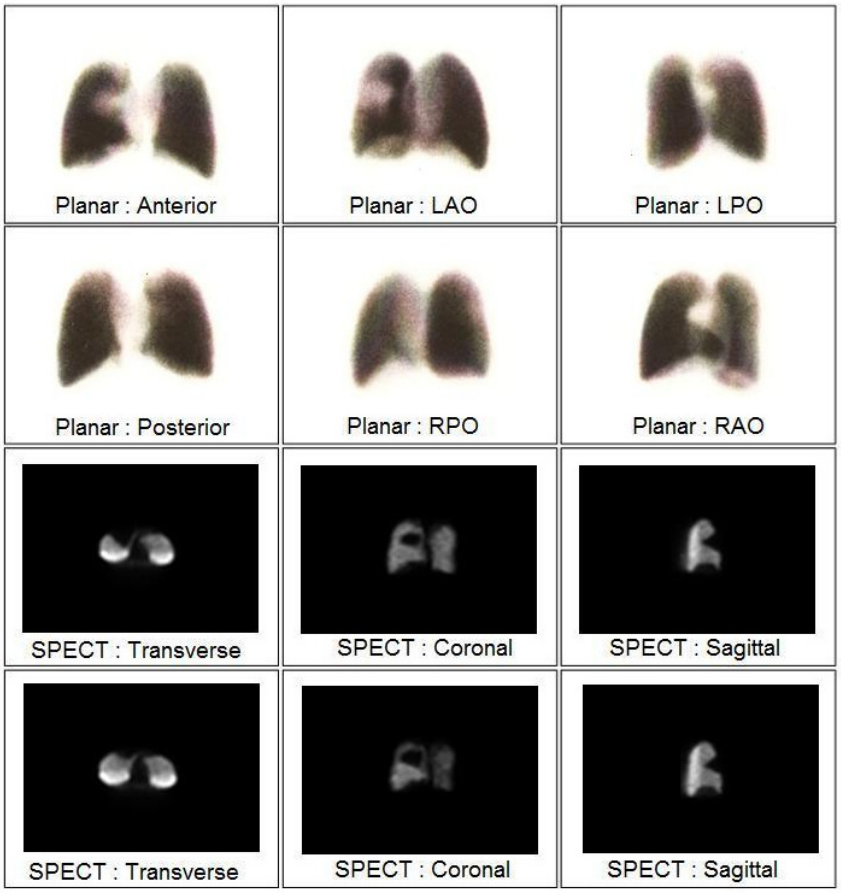

[Figure 11]

Planar and SPECT images of a perfusion defect involving the anterior segment of the right lung.

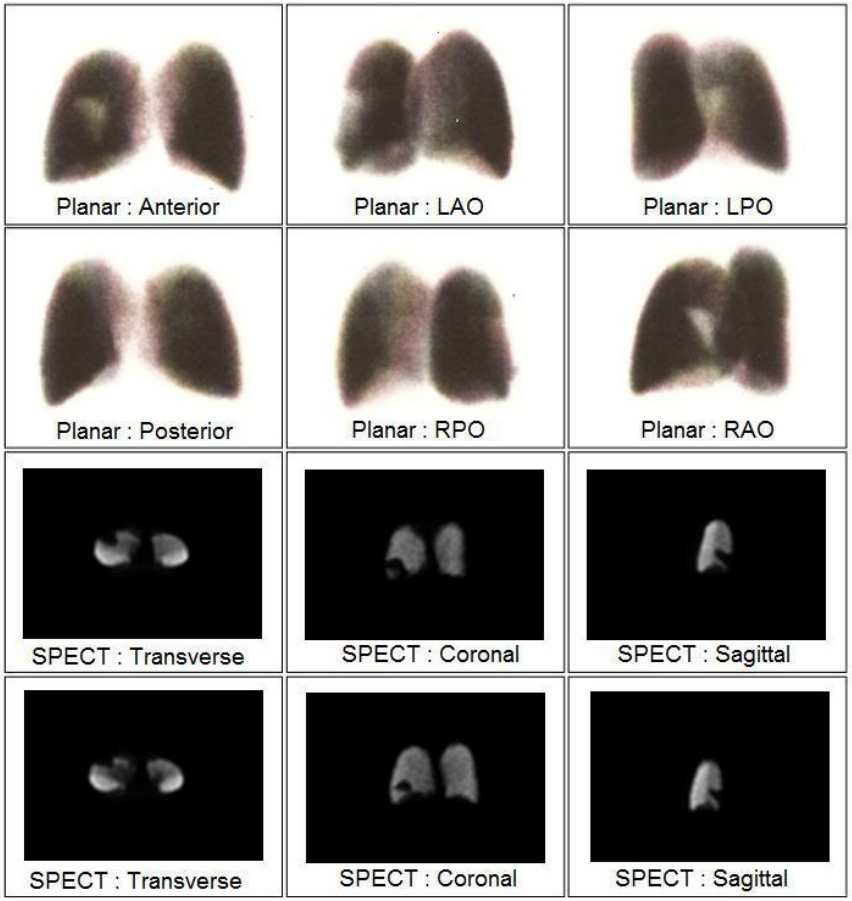

[Figure12]

Planar and SPECT images of perfusion defect involving the lateral segment of the right lung.

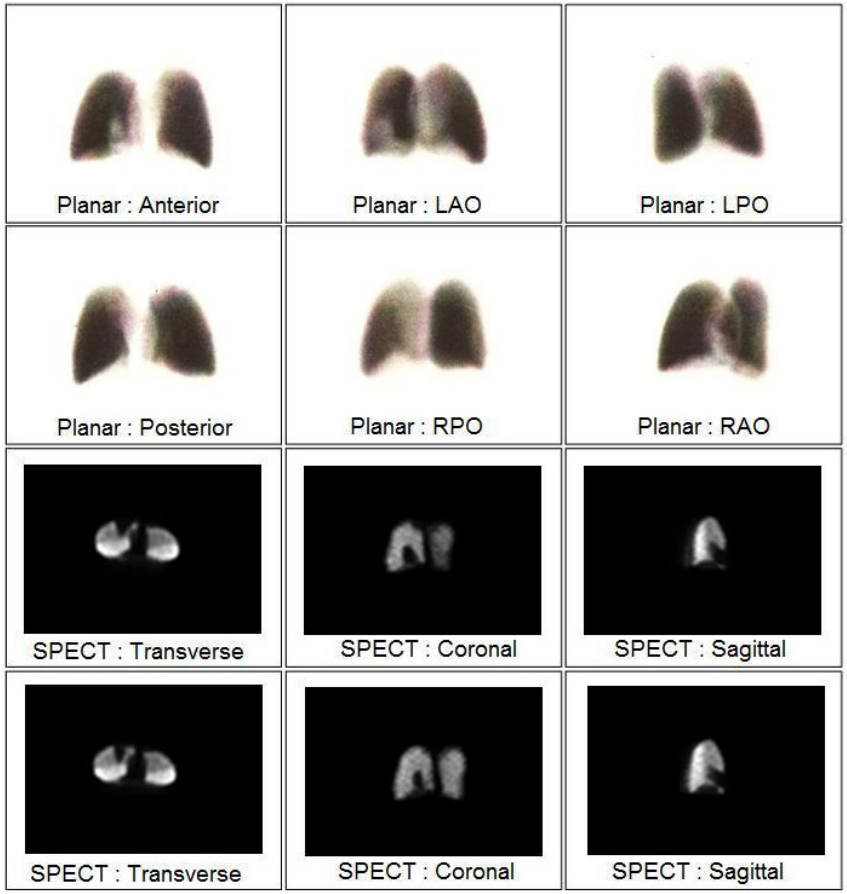

[Figure 13]

Planar and SPECT images of a perfusion defect involving the medial segment of the right lung.

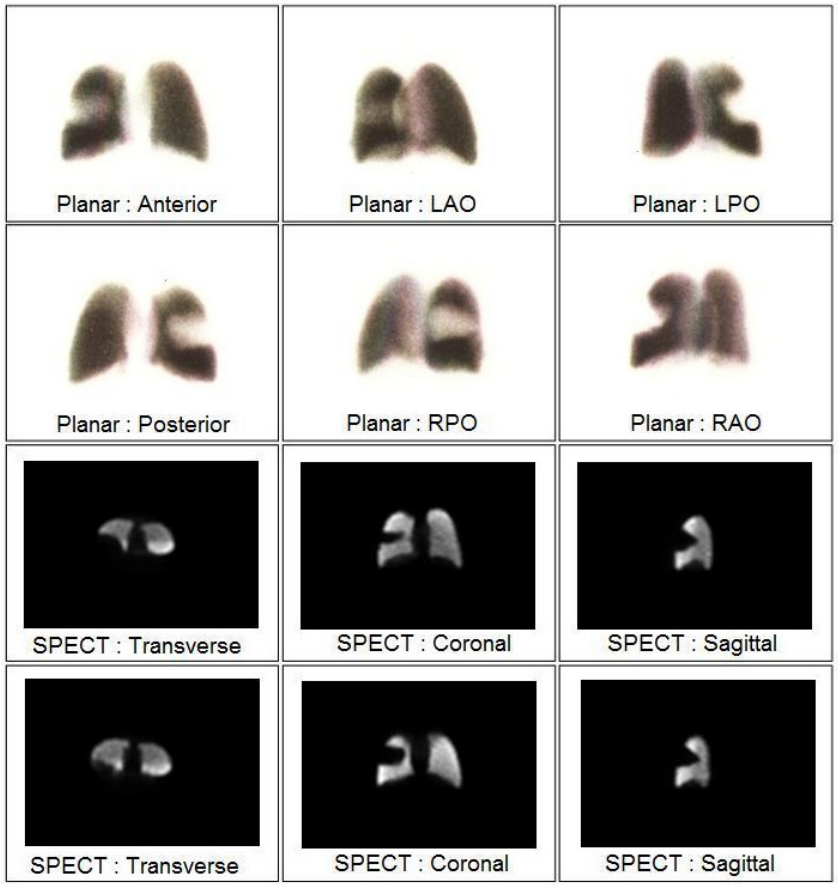

[Figure 14]

Planar and SPECT images of a perfusion defect involving the superior segment of the right lung.

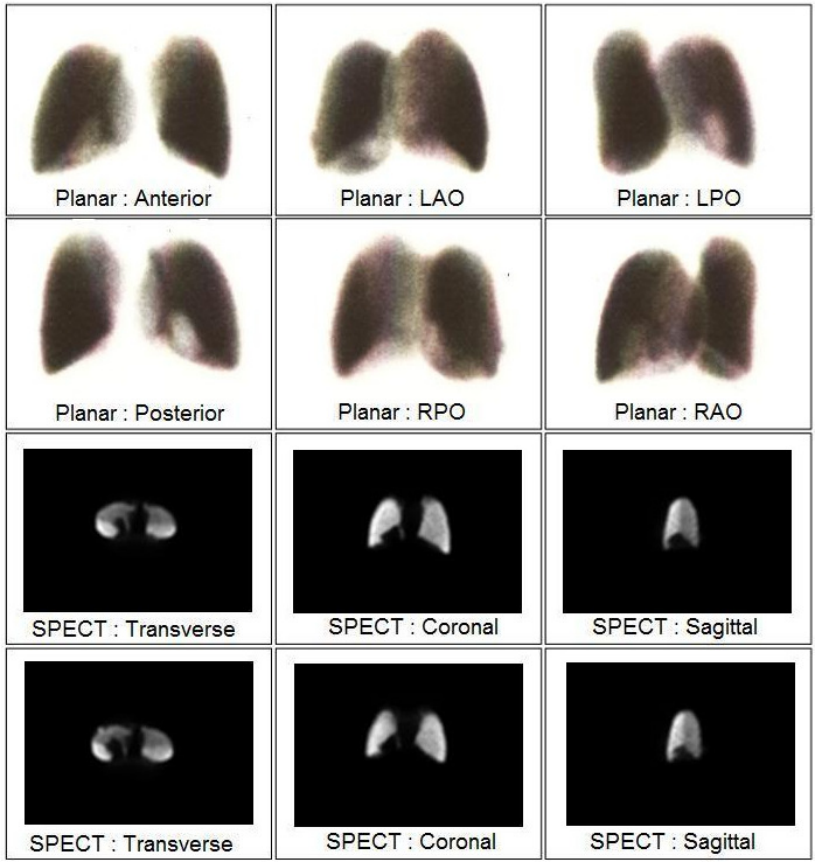

[Figure 15]

Planar and SPECT images of a perfusion defect involving the medial basal segment of the right lung.

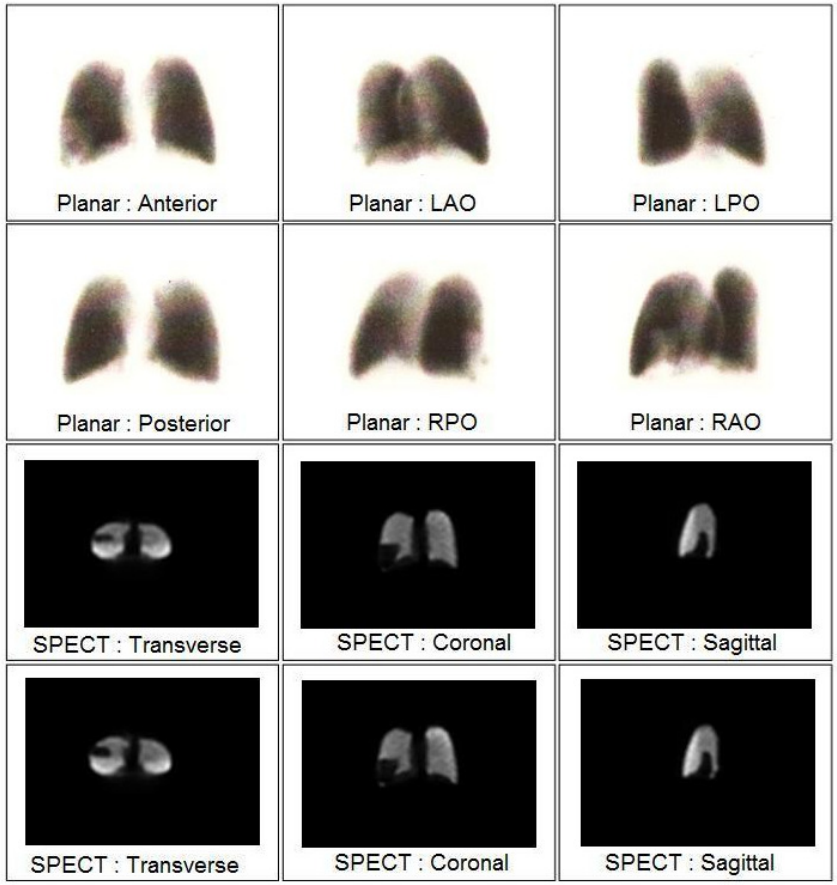

[Figure 16]

Planar and SPECT images of a perfusion defect involving the anterior basal segment of the right lung.

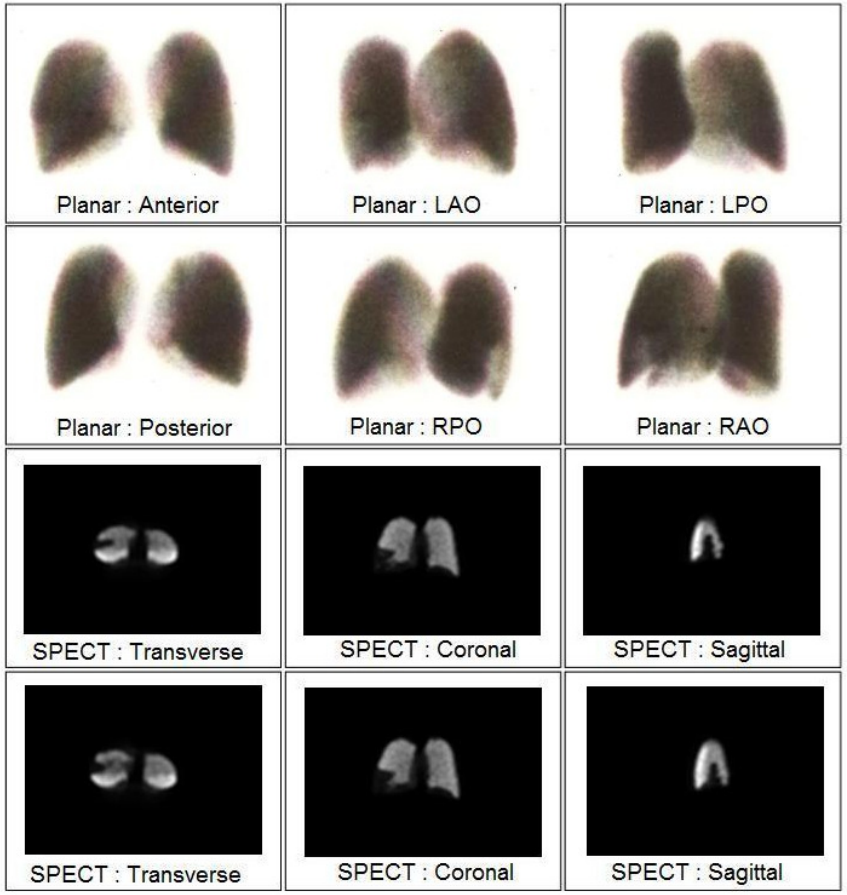

[Figure 17]

Planar and SPECT images of a perfusion defect involving the lateral basal segment of the right lung.

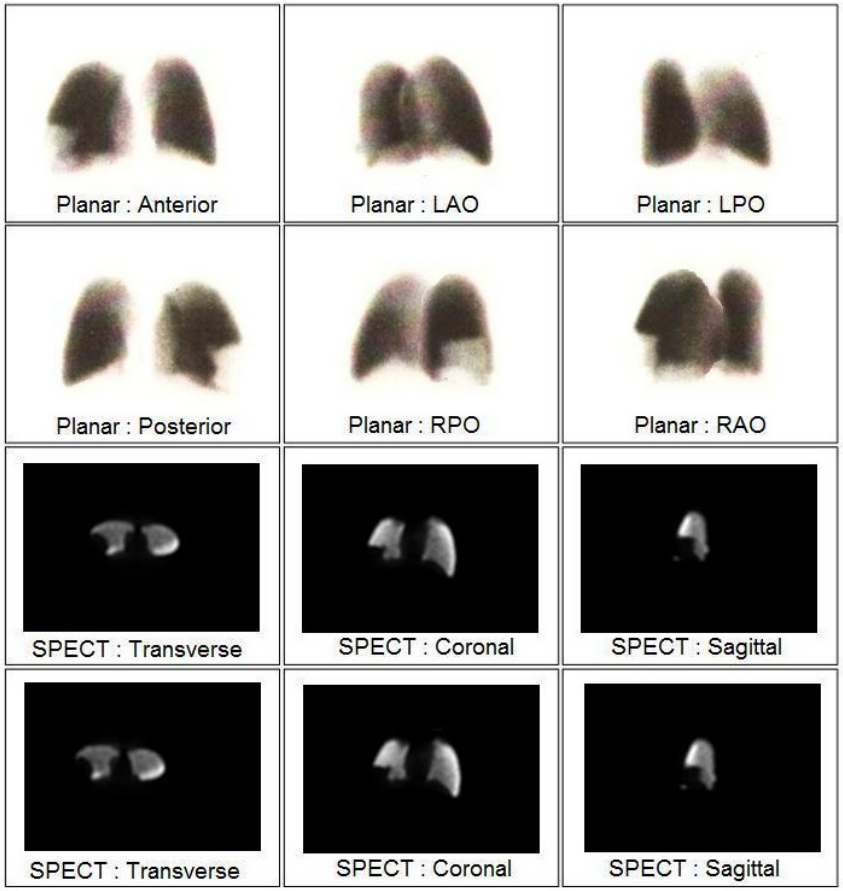

[Figure 18]

Planar and SPECT images of a perfusion defect involving the posterior basal segment of the right lung.

Please score/answer the following questions based on criteria given in the following table.

Score	Image quality	Specification
1	Poor	Not adequate for clinical application.
2	Average	Barely adequate for limited clinical application.
3	Good	Adequate for clinical application.
4	Excellent	Excellent for clinical application.

	Questions	**Score**			
		1	2	3	4
1	As an experienced Nuclear Medicine Physician, how do you rate the atlas' suitability to be used as a reference resource and teaching aid for new Nuclear Medicine physicians to develop experience in interpreting lung V/Q mismatch defects for pulmonary embolism diagnosis?	o	o	o	o
2	What is your opinion on the atlas' suitability to be used as a reference (a reference material to experienced Nuclear Medicine physicians) for anatomical bronchopulmonary segmental size and structure (scintigraphic and tomographic) in pulmonary embolism diagnosis by lung perfusion and ventilation scans?	o	o	o	o
3	What is your opinion on the atlas as an aid to interpret lung perfusion and ventilation scans for pulmonary embolism diagnosis? We propose Nuclear Medicine physicians use the atlas as an aid together with standard interpretation criteria (the revised PIOPED criteria, the Hull criteria or the Gestalt interpretation).	o	o	o	o